

**The importance of efflux transporters in CNS exposure to avermectin
insecticides: studies in human and mouse neuroblastoma cell lines.**

Abigail M Dalzell

**Epithelial Research Group
Institute for Cell & Molecular Bioscience
Medical School Newcastle University
NE2 4HH UK**

PhD Thesis

2012



Sponsored by



Table of Contents.....	I
List of Figures.....	VIII
List of Tables.....	XIV
Acknowledgements.....	XVI
Abbreviations.....	XVII
Abstract.....	XVIII

Table of Contents	Page
Chapter 1: Introduction.....	1
Summary.....	1
1.1. The importance of avermectin insecticides and therapeutics.....	2
<i>Ivermectin.....</i>	<i>4</i>
<i>Emamectin benzoate.....</i>	<i>4</i>
<i>Abamectin.....</i>	<i>4</i>
<i>Other avermectins and the milbemycins.....</i>	<i>5</i>
1.2. ABC Transporters in the Blood-Brain Barrier and CNS.....	6
<i>MDR1 Efflux Transporter.....</i>	<i>8</i>
<i>MRP Efflux Transporter.....</i>	<i>10</i>
<i>BCRP Efflux Transporter.....</i>	<i>11</i>
1.3. Animal sensitivity to avermectins.....	13
1.4. Transport data for avermectins.....	14
1.5. Effects of MDR1 polymorphisms on avermectin exposure in humans and cell line studies.....	15
<i>MDR1 polymorphisms in humans.....</i>	<i>15</i>
<i>Association studies.....</i>	<i>16</i>
<i>Functional studies in vivo.....</i>	<i>18</i>
<i>Functional studies in vitro.....</i>	<i>20</i>

1.6. SH-SY5Y human cells as a model for evaluating neurotoxicity.....	23
1.7. N2a mouse cells as a model for evaluating neurotoxicity.....	24
1.8. Aims of the study.....	26
Chapter 2: Methods.....	27
2.1 Materials.....	27
2.2 Methods.....	27
Cell Culture.....	27
<i>SH-SY5Y human neuroblastoma cells.....</i>	<i>27</i>
<i>N2a mouse neuroblastoma cells.....</i>	<i>27</i>
Total RNA extraction.....	28
<i>For analysis of constitutive transporter mRNA expression (Chapter 3).....</i>	<i>28</i>
<i>For analysis of transporter mRNA expression in avermectin-treated cells (Chapter 6)..</i>	<i>28</i>
End-point and qRT-PCR.....	28
<i>qPCR Arrays.....</i>	<i>29</i>
Immunocytochemical staining of cells for transporter protein expression.....	29
Assays for efflux transporter activity.....	30
<i>Krebs' Buffer used in Transport and MTT assays.....</i>	<i>30</i>
<i>Assay Principles.....</i>	<i>31</i>
<i>H33342 Dye Retention Assay Background (Chapter 4).....</i>	<i>32</i>
<i>H33342 Dye Retention Assay Method (Chapter 4).....</i>	<i>32</i>
<i>H33342 dye retention assay data analysis.....</i>	<i>34</i>
<i>Adaptations to H33342 assay used in this study.....</i>	<i>34</i>
<i>Measures of transporter affinity for H33342 in the dye retention assay.....</i>	<i>35</i>
<i>Inhibition of BCRP/bcrp- mediated H33342 efflux by KO-143.....</i>	<i>36</i>

<i>CMFDA Assay Background (Chapter 5)</i>	36
<i>CMFDA Retention Assay Method (Chapter 5)</i>	37
<i>CMFDA dye retention assay data analysis</i>	38
<i>MTT Assay Background (Chapter 6)</i>	38
<i>MTT Assay Method (Chapter 6)</i>	39
<i>MTT Assay data analysis</i>	40
Neurite Outgrowth Studies with N2a Cells (Chapter 6)	40
<i>Visualisation of neurites</i>	41
Chapter 2 Methods Figures	42
Chapter 3: Efflux Transporter mRNA and protein expression in SH-SY5Y and N2a cells	43
3.1 Summary	43
3.2 Introduction	43
<i>Role of transporters in protection from neurotoxicity</i>	43
3.3 Methods	44
RNA Extractions and PCR	44
Protein Expression	45
3.4 Results	45
qPCR array	45
Constitutive efflux transporter expression in SH-SY5Y and N2a cells	46
Independent qPCR assays	47
<i>Human SH-SY5Y cells</i>	47
<i>Mouse N2a cells</i>	47

Protein Expression of MDR1/mdr1a and BCRP/bcrp.....	48
<i>MDR1 and mdr1 expression.....</i>	<i>48</i>
<i>BCRP and bcrp expression.....</i>	<i>49</i>
3.5 Discussion	49
Expression of human drug transporters in qPCR array.....	49
Expression of efflux transporter proteins in SH-SY5Y and N2a cells.....	51
Chapter 3: Figures.....	52
Summary Conclusions from Chapter 3.....	71
Chapter 4: Measurement of the interaction of avermectin insecticides with efflux transporters using the H33342 fluorescent dye retention assay.....	72
4.1 Summary.....	72
4.2 Introduction.....	73
4.3 Results.....	73
H33342 dose-response curves.....	73
Efflux modulation by CSA.....	74
Inhibition of BCRP- and bcrp- mediated H33342 efflux by KO-143.....	75
Functional assay of MDR1 and mdr1a activity in SH-SY5Y and N2a cells exposed to avermectins.....	75
<i>Abamectin.....</i>	<i>76</i>
<i>Emamectin benzoate.....</i>	<i>76</i>
<i>Ivermectin.....</i>	<i>77</i>
4.4 Discussion.....	78
<i>Potential role of other transporters in avermectin handling.....</i>	<i>82</i>

Chapter 4: Figures.....	84
Summary Conclusions from Chapter 4.....	99
Chapter 5: Measurement of the interaction of avermectin insecticides with multidrug resistance proteins using a CMFDA fluorescence dye retention assay.....	100
5.1 Summary.....	100
5.2 Introduction.....	101
5.3. Results.....	102
CMFDA dose-response curves.....	102
Efflux modulation by MK571 and CSA.....	103
Functional inhibition of CMFDA efflux through MRP/mrp transporters by avermectins.....	104
<i>Abamectin.....</i>	<i>104</i>
<i>Emamectin benzoate.....</i>	<i>105</i>
<i>Ivermectin.....</i>	<i>105</i>
5.4 Discussion.....	106
Chapter 5: Figures.....	110
Summary Conclusions from Chapter 5.....	118
Chapter 6: Cell proliferation and markers of avermectin exposure.....	119
6.1 Summary.....	119
6.2. Introduction.....	119
<i>MTT assay of cell viability.....</i>	<i>119</i>
<i>Chemokines in the CNS.....</i>	<i>120</i>

<i>Neurite outgrowth</i>	120
<i>Modulation of MDR1 and MRP1 expression by avermectins</i>	121
<i>Aims</i>	121
6.3 Results	121
MTT Assay	121
Chemokine and chemokine receptor gene expression after avermectin exposure	122
Neurite outgrowth	123
Modulation of MDR1 and MRP gene expression by avermectins	123
6.4 Discussion	124
MTT assay	124
Chemokines and receptors as potential biomarkers of avermectin exposure	124
Neurite outgrowth	125
Modulation of MDR1 and MRP mRNA expression by avermectins	126
Chapter 6 Figures	127
Summary Conclusions from Chapter 6	141
Chapter 7: General discussion, conclusions and future work	142
<i>Other avermectins and the milbemycins</i>	145
Conclusions	145
Future work	146

Chapter 8: References.....	147
Appendices.....	158-192
Appendix A Primer Sequences.....	158
Appendix B primer alignments.....	159
Human MDR1.....	159
Human BCRP.....	162
Human MRP1.....	164
Mouse mdr1a.....	167
Mouse BCRP.....	170
Appendix C PAHS-070F Human Drug Transporter qPCR array (SABiosciences).....	172
Appendix D PAHS-022F Human Chemokines and Receptors qPCR Array.....	182

List of Figures	Page
Chapter 1	
Figure 1.1: Structures of the avermectins used in the study.....	3
Figure 1.2: Major transporters expressed on the BBB in human and mouse and their substrates.....	7
Chapter 2	
Figure 2.1 Principle of fluorescence dye efflux assays with substrate dyes H33342 for MDR1/mdr1 and BCRP/bcrp or CMFDA for MRP/mrp efflux transporters.....	31
Figure 2.2 H33342 chemical structure	33
Figure 2.3 “ Concentration–response curves for XR9577 in A2780adr cells obtained with the standard Hoechst assay and the new Hoechst assay.....	35
Equation 2.1 The Cheng-Prusoff Equation for Calculating Ki values.....	36
Figure 2.4 Conversion of CMFDA to a fluorescent MRP/mrp substrate by esterases and conjugation with glutathione inside cells.....	37
Figure 2.5 Dose-response curve to CSA read in MRX Fluorimeter.....	42
Figure 2.6 Dose-response curve to CSA read in BMG Labtech Fluorimeter.....	42
Chapter 3	
Figure 3.1 A-H SH-SY5Y Drug Transporter qPCR Array.....	52-55
Figure 3.2 End point PCR gel of SH-SY5Y RNA samples expressing MDR1.....	58
Figure 3.3 End point PCR of N2a RNA samples expressing mdr1a.....	59

Figure 3.4 (A) End-point PCR for mouse bcrp with cDNA from MDCKII-bcrp cells and N2a cells.....	60
Figure 3.4 (B) End-point PCR for mouse gapdh with cDNA from mouse N2a cells.....	60
Figure 3.5 Expression of mRNA for MDR1 from total RNA of SH-SY5Y cells.....	63
Figure 3.6 Expression of mRNA for MRP1 in SH-SY5Y cells.....	63
Figure 3.7 SH-SY5Y and N2a cells grown as an 80% confluent monolayer.....	64
Figure 3.8 SH-SY5Y cells stained for MDR1 protein with MRK-16 antibody.....	65
Figure 3.9 N2a cells stained for mdr1 protein with C219 antibody.....	66
Figure 3.10 N2a cells stained for mdr1 protein with MRK-16 antibody.....	67
Figure 3.11 MDCKII-BCRP cells stained for BCRP protein by BXP-21 antibody.....	68
Figure 3.12 SH-SY5Y cells stained for BCRP protein by BXP-21 antibody.....	69
Figure 3.13 Mouse N2a cells stained for bcrp protein by BXP-21 antibody.....	70
 Chapter 4	
Figure 4.1 Hoechst 33342 dose-response curve (0 - 15 μM) in SH-SY5Y cells.....	84
Figure 4.2 Hoechst 33342 dose-response curve (0 - 15 μM) in N2a cells.....	84
Figure 4.3 Hoechst 33342 dye efflux assay to determine CSA-sensitive transporter expression in SHSY5Y cells at least 1 day after seeding.....	85
Figure 4.4 Dose-response for the ability of CSA (0-10μM) to inhibit transporter-mediated efflux of 1μM H33342 in SH-SY5Y cells.....	85
Figure 4.5 Dose-response curve for the ability of CSA (0-10μM) to inhibit transporter-mediated efflux of 1μM H33342 in SH-SY5Y cells.....	86
Figure 4.6 Dose-response curve for the ability of CSA (0-10μM) to inhibit transporter-mediated efflux of 1μM H33342 efflux in N2a cells.....	86

Figure 4.7 Dose-response curve for the ability of CSA (0-10μM) to inhibit transporter-mediated H33342 efflux in N2a cells, with an H33342 concentration of 1μM.....	87
Figure 4.8 Dose-response curve for the ability of KO-143 (0-5μM) to inhibit BCRP-mediated efflux of 1μM H33342 in SH-SY5Y cells.....	87
Figure 4.9 Dose-response curve for the ability of KO-143 (0-5μM) to inhibit bcrp-mediated efflux of 1μM H33342 in N2a cells.....	88
Figure 4.10 Dose-response curve for the ability of KO-143 (0-5μM) to inhibit BCRP-mediated efflux of 1μM H33342 in MDCKII-BCRP cells.....	88
Figure 4.11 Dose-response curve for the ability of abamectin (0-7μM) to inhibit MDR1-mediated efflux of 1μM H33342 in SH-SY5Y cells.....	89
Figure 4.12 Dose-response curve for the ability of abamectin (0-7μM) to inhibit MDR1-mediated efflux of 1μM H33342 in SH-SY5Y cells.....	89
Figure 4.13 Dose-response curve for the ability of abamectin (0-7μM) to inhibit mdr1a-mediated efflux of 1μM H33342 in N2a cells.....	90
Figure 4.14 Dose-response curve for the ability of abamectin (0-7μM) to inhibit mdr1a-mediated efflux of 1μM H33342 in N2a cells.....	90
Figure 4.15 Dose-response curve for the ability of emamectin benzoate (0-7μM) to inhibit MDR1-mediated efflux of 1μM H33342 in SH-SY5Y cells.....	91
Figure 4.16 Dose-response curve for the ability of emamectin benzoate (0-7μM) to inhibit MDR1-mediated efflux of 1μM H33342 in SH-SY5Y cells.....	91
Figure 4.17 Dose-response curve for the ability of emamectin benzoate (0-7μM) to inhibit mdr1a-mediated efflux of 1μM H33342 in N2a cells.....	92
Figure 4.18 Dose-response curve for the ability of emamectin benzoate (0-7μM) to inhibit mdr1a-mediated efflux of 1μM H33342 in N2a cells.....	92
Figure 4.19 Dose-response curve for the ability of ivermectin (0-7μM) to inhibit MDR1-mediated efflux of 1μM H33342 in SH-SY5Y cells.....	93.

Figure 4.20 Dose-response curve for the ability of ivermectin (0-7μM) to inhibit MDR1-mediated efflux of 1μM H33342 in SH-SY5Y cells.....	93
Figure 4.21 Dose-response curve for the ability of ivermectin (0-7μM) to inhibit mdr1a-mediated efflux of 1μM H33342 in N2a cells.....	94
Figure 4.22 Dose-response curve for the ability of ivermectin (0-7μM) to inhibit mdr1a-mediated efflux of 1μM H33342 in N2a cells.....	94
 Chapter 5	
Figure 5.1 Concentration dependence of intracellular GSMF fluorescence after treatment with CMFDA (0-1.5μM) in SH-SY5Y cells \pm 10μM MK-571.....	110
Figure 5.2 Concentration dependence of intracellular GSMF fluorescence after treatment with CMFDA (0-1.5μM) in N2a cells \pm 10μM MK571.....	110
Figure 5.3 Concentration-dependence of MK571 (0-15μM) for the ability of to inhibit transporter-mediated efflux of 1μM CMFDA in SH-SY5Y cells.....	111
Figure 5.4 Concentration dependence of MK-571 (0-15μM) for ability to inhibit transporter-mediated efflux of 1μM CMFDA in N2a cells.....	111
Figure 5.5 Inhibition of transporter-mediated efflux of 1μM CMFDA efflux by 5μM abamectin, 10μM MK571 or 5μM CSA in SH-SY5Y cells compared to control.....	112
Figure 5.6 Inhibition of transporter-mediated efflux of 1μM CMFDA efflux by 5μM abamectin, 10μM MK571 or 5μM CSA in N2a cells compared to control.....	112
Figure 5.7 Dose-response curve for the ability of abamectin (0-6μM) to inhibit MRP-mediated efflux of 1μM CMFDA in SH-SY5Y cells.....	113
Figure 5.8 Dose-response curve for the ability of abamectin (0-6μM) to inhibit MRP-mediated efflux of 1μM CMFDA in N2a cells.....	113
Figure 5.9 Dose-response curve for the ability of emamectin benzoate (0-6μM) to inhibit MRP-mediated efflux of 1μM CMFDA in SH-SY5Y cells.....	114

Figure 5.10 Dose-response curve for the ability of emamectin benzoate (0-6μM) to inhibit mrp-mediated efflux of 1μM CMFDA in N2a cells.....	114
Figure 5.11 Dose-response curve for the ability of ivermectin (0-6μM) to inhibit MRP-mediated efflux of 1μM CMFDA in SH-SY5Y cells.....	115
Figure 5.12 Dose-response curve for the ability of ivermectin (0-6μM) to inhibit mrp-mediated efflux of 1μM CMFDA in N2a cells.....	115
Chapter 6	
Figure 6.1 SH-SY5Y cells were exposed to a range of concentrations of Triton-X100..	127
Figure 6.2 N2a cells were exposed to a range of concentrations of Triton-X100.....	127
Figure 6.3 SH-SY5Y cells grown to a sub-confluent monolayer were exposed to abamectin at a concentration range 0-10μM for 1 hr.....	128
Figure 6.4 N2a cells grown to a sub-confluent monolayer were exposed to abamectin at a concentration range 0-10μM for 1 hr.....	129
Figure 6.5 SH-SY5Y cells grown to a sub-confluent monolayer were exposed to emamectin benzoate at a concentration range 0-10μM for 1hr.....	130
Figure 6.6 N2a cells grown to a sub-confluent monolayer were exposed to emamectin benzoate at a concentration range 0-10μM for 1hr.....	131
Figure 6.7 SH-SY5Y cells grown to a sub-confluent monolayer were exposed to ivermectin at a concentration range 0-10μM for 1hr.....	132
Figure 6.8 N2a cells grown to a sub-confluent monolayer were exposed to ivermectin at a concentration range 0-10μM for 1hr.....	133
Figure 6.9 A-D Chemokine and chemokine receptor mRNA expression was detected in a 96 well qPCR array in RNA from SHSY5Y cells after exposing them to 1μM emamectin benzoate or ivermectin for 18 hours.....	134-137
Figure 6.10 Neurite outgrowths in N2a cells visualised by confocal microscopy (A-D) and light contrast microscopy (E-F) at x63 magnification.....	139

Figure 6.11 MDR1 mRNA expression in SH-SY5Y cells after exposure to 1 μ M abamectin, emamectin benzoate, ivermectin or solvent control for 18 hours in the absence of serum, normalised to GAPDH expression.....140

Figure 6.12 Expression of MRP1 mRNA in SH-SY5Y cells after exposure to 1 μ M abamectin, emamectin benzoate, ivermectin or solvent control for 18 hours in the absence of serum, normalised to GAPDH expression.....141

List of Tables	Page
Chapter 1	
Table 1.1: Selected substrates of human MDR1 and mouse <i>mdr1</i>	9
Table 1.2: Polymorphisms of MDR1 investigated <i>in vivo</i> by genotyping.....	17
Table 1.3: MDR1 polymorphisms studied <i>in vivo</i>	20
Table 1.4 Table 1.4 Selected MDR1 polymorphisms studied <i>in vitro</i>	22
Chapter 3	
Table 3.1 (A) Summary of Drug Transporters in SH-SY5Y cells, CNS Neurons and the Human Blood-Brain Barrier.....	56
Table 3.1 (B) Summary of Drug Transporters in SH-SY5Y cells, CNS Neurons and the Human Blood-Brain Barrier.....	57
Table 3.2 Expression of mRNA BCRP, MDR1, MRP1 and GAPDH in SH-SY5Y cells.....	61
Table 3.3 Messenger RNA expression of <i>mdr1a</i> and <i>gapdh</i> in mouse N2a cells.....	62
Chapter 4	
Table 4.1 Affinity constants (EC_{50} values) for H33342 in human SH-SY5Y and mouse N2a neuroblastoma cells.....	95
Table 4.2 K_i values for avermectin treatments in human and mouse neuroblastoma cells.....	95
Table 4.3 Mean K_i values of avermectins for MDR1-mediated efflux of H33342 in SH-SY5Y cells, analysed by One-Way ANOVA with Dunnett's post test.....	96
Table 4.4 Mean K_i values of avermectins for <i>mdr1a</i> -mediated efflux of H33342 in N2a cells, analysed by One-Way ANOVA with Dunnett's post test.....	96

Table 4.5 Summary of EC₅₀ values for H33342 (0-15 μ M) CSA in SH-SY5Y cells and N2a cells.....97

Table 4.6 Summary of IC₅₀ and K_i values and Mean \pm SEM of data for the effect of selected avermectins and CSA on MDR1-mediated H33342 efflux in SH-SY5Y cells.....97

Table 4.7 Summary of IC₅₀ and K_i values and mean \pm S.E.M. of data for the effect of selected avermectins and CSA on mdr1a-mediated H33342 efflux in N2a cells.....98

Chapter 5

Table 5.1 IC₅₀ values for interaction of the avermectin insecticides Abamectin, Emamectin benzoate and Ivermectin with human MRP transporters and mouse mrp transporters in the CMFDA assay.....116

Table 5.2 Mean IC₅₀ values for interaction of the avermectin insecticides with MRP transporters in SH-SY5Y cells in the CMFDA assay.....116

Table 5.3 IC₅₀ values for interaction of the avermectin insecticides Abamectin, Emamectin benzoate and Ivermectin with mouse mrp transporters in the CMFDA assay.....117

Acknowledgements

I would like to thank my supervisors, Dr Colin Brown and Professor Faith Williams, for their guidance, support, great patience, and confidence in me over the course of this project. Problems that at times seemed insurmountable have always been overcome with reference to one person or the other, and I cannot thank them both enough for imparting their experience and knowledge throughout. Dr. Pratibha Mistry and Dr. Jayne Wright from Syngenta have been my industrial supervisors, and I thank them for the opportunity and funding to undertake the project, as well as for their lasting belief in the study through its ups and downs.

With regard to help and support in the laboratory, my thanks are due to Dr. Amy Kennedy for instructing and supporting me through my first year, to Dr. Alison Howard and my contemporary Dr Catherine Mowbray for some pertinent advice and help with PCR- any mistakes made are entirely due to my failings as I could not have had better help.

Dr Maxine Geggie keeps the tissue culture facility running like clockwork and I think no-one could really do without her. Dr. Trevor Booth gave me much practical help and guidance with confocal work and was very patient as I learnt how to focus on the cells; Dr Georgina Carr was also kind enough to give sage advice when necessary.

Dr. Alison Howard and Professor Nick Simmons gave me some very useful advice during my yearly assessments, for which I am very grateful.

I am lucky to have met so many friendly and supportive people in the lab environment and I am proud to call them my friends.

Last and most importantly, I thank my parents, Linda and Malcolm Dalzell, for their support through some tough times, their belief in me, and endless love. I would not have become the person I am without them; I am a very fortunate daughter.

Abbreviations

ABC transporter.....	ATP- Binding Cassette transporter
AIMP1.....	aminoacyl tRNA synthetase complex-interacting multifunctional protein 1
BBB.....	Blood-Brain Barrier
BCRP.....	Breast Cancer Resistance Protein
bcrp.....	mouse breast cancer resistance protein
BDNF.....	brain-derived neurotrophic factor
BMEC.....	Brain Microvessel Endothelial Cell
cDNA.....	complimentary DNA
CNS.....	Central Nervous System
CSA.....	Cyclosporin A
CX3CL1.....	chemokine (C-X3-C motif) ligand 1
GAPDH.....	glyceraldehyde-3-phosphate dehydrogenase
hCMEC/D3 cell.....	human blood-brain barrier endothelial cell line
MDCK II-BCRP cell.....	Madin-Darby Canine Kidney II cell transfected with BCRP
MDR1.....	MultiDrug Resistance transporter1, a.k.a human P-glycoprotein
mdr1a/1b.....	multidrug resistance transporter 1a / 1b, expressed in mouse
MRP.....	human multidrug resistance protein(s) 1-9
mrp.....	mouse multidrug resistance protein(s) 1-9
mRNA.....	messenger RNA
N2a cell.....	Neuro-2-A mouse neuroblastoma cell line
OCT/OAT.....	Organic Cation/ Anion Transporter
qPCR.....	quantitative real time PCR
RT-PCR.....	reverse transcription PCR
SDF2.....	stromal cell-derived factor 2
SH-SY5Y cell.....	human SH-SY5Y neuroblastoma cell line

Abstract

Avermectins are macrocyclic lactones insecticides, used as antihelminthics in humans and animals, since they have low human toxicity. There is a clear role for the efflux transporter *mdr1* controlling CNS exposure to avermectins in polymorphic animal models, but the role of MDR1 in limiting human avermectin exposure is less well defined, although no such knockout MDR1 polymorphisms have been identified to date. The aim of this study was to characterise the kinetics of avermectin interactions with efflux transporters in the human SH-SY5Y neuroblastoma cell line, and compare them with mouse isoforms expressed in N2a cells to determine the relevance of mouse data to human avermectin exposure.

Protein and mRNA expression of human MDR1, MRP and mouse *mdr1a* were identified in the cell lines, similar to the blood-brain barrier except BCRP and *bcrp* were absent. K_i values for inhibition of MDR1 or MRP substrate efflux by avermectins did not differ significantly between human and mouse cells ($P > 0.05$); abamectin (MDR1 $K_i = 0.95 \pm 0.08\mu\text{M}$; *mdr1a* $K_i = 0.77 \pm 0.25\mu\text{M}$), emamectin benzoate (MDR1 $K_i = 0.60 \pm 0.07\mu\text{M}$; *mdr1a* $K_i = 0.56 \pm 0.02\mu\text{M}$) and ivermectin (MDR1 $K_i = 0.24 \pm 0.08\mu\text{M}$; *mdr1a* $K_i = 0.18 \pm 0.02\mu\text{M}$), but ivermectin has the highest affinity for inhibition of MDR1- and *mdr1a*-substrate efflux. Cytotoxicity was apparent for emamectin benzoate above $6\mu\text{M}$, which is 100-fold higher than peak exposure concentrations, but not for abamectin or ivermectin. Expression levels of the chemokine genes SDF-2, AIMP1 and BDNF are candidates for biomarkers of avermectin exposure. These data show that SH-SY5Y cells are a good model in which to investigate avermectin exposure and to compare to mouse cells and have confirmed the involvement of MDR1 and MRP transporters. Avermectins are of global importance, so a greater understanding of mechanisms of human exposure is pertinent.

Chapter 1: Introduction

Summary:

1.1. The importance of avermectin insecticides and therapeutics

ivermectin

emamectin benzoate

abamectin

1.2 ABC transporters in the blood-brain barrier and CNS

Transporters in the BBB

MDR1 Efflux Transporter

MDR1 substrates

MRP transporters

BCRP

1.3 Animal sensitivity to avermectins

1.4 Transport data for the avermectins

1.5 Effects of MDR1 polymorphisms on avermectin exposure in animal models and humans

MDR1 polymorphisms in humans

Association studies

Functional studies in vivo

Functional studies in vitro

1.6 SH-SY5Y human cells as a model for evaluating neurotoxicity

1.7 N2a mouse cells as a model for evaluating neurotoxicity

1.8 Aims of the study

1.1. The importance of avermectin insecticides and therapeutics

The avermectins are macrocyclic lactone compounds related to avermectin b1 (abamectin), which was isolated from the soil microorganism *Streptomyces avermitilis*. Molecular structures are given in Figure 1. Ivermectin is the semi-synthetic dihydro-derivative of avermectin b1, used as an anti-parasitic in humans and animals, where abamectin is the most abundant natural product (B1a isoform). Its semi-synthetic relatives, including emamectin benzoate, are used as agricultural insecticides. Avermectins act by binding to invertebrate neuronal GABA receptors and GABA-gated ion channels, causing net chloride influx leading to paralysis and death (Macdonald & Gledhill, 2007). They are efficiently eliminated from the CNS of mammals, and degrade rapidly in light and moisture, so they do not persist in the environment and are relatively non-toxic, with the exceptions of the *mdr1*-deficient animal models discussed below (Campbell, 1989). Figure 1.1 displays the structures of the avermectins used in the current study.

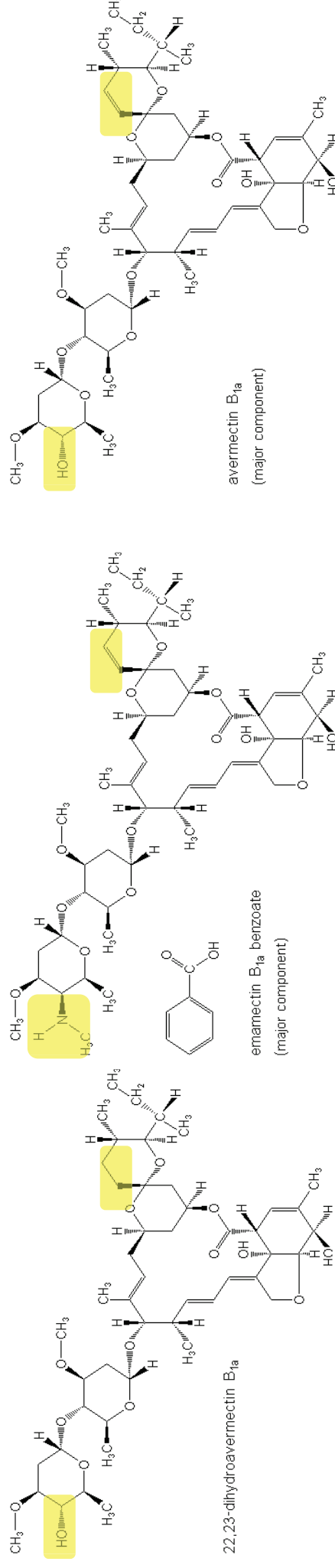
**ivermectin****emamectin benzoate****abamectin**

Figure 1.1: Structures of the avermectins used in the study. Structures are obtained from data sheets available online at:

<http://www.alanwood.net/pesticides/ivermectin.html>; <http://www.alanwood.net/pesticides/derivatives/emamectin%20benzoate.html> and

<http://www.alanwood.net/pesticides/abamectin.html>, checked 24.10.2011. Regions where the structure varies are highlighted using information

from Chapter 1: Chemistry (Fisher & Mrozick) in Campbell, (1989). B1a is the major isoform in each compound, and each is marketed as a mixture of not less than 80% of B1a and not more than 20% of B1b. The two isoform types are considered of equal potency in their antiparasitic action.

Ivermectin

Ivermectin was first identified in 1981 as 22, 23-dihydroavermectin B1, the most active derivative form of a natural compound produced by the soil-dwelling organism *Streptomyces avermitilis*, found to be active against a large number of gastrointestinal and endo-parasites in horses, dogs, cattle and sheep including *Strongylus vulgaris*, hookworm, *Haemonchus* species including *Haemonchus contortus*, and *Toxocara canis* with usual doses of 0.2-0.3mg/kg bodyweight depending upon the species, and maximal doses being 1-2mg/kg (Barragry, 1987) . Due to the presence of active efflux pumps and the tight junction structure of the blood-brain barrier, detailed below, avermectins are restricted from entry into the mammalian CNS, so symptoms of neurotoxicity did not ensue in laboratory studies of toxicity until doses 10-fold higher than therapeutic concentrations were administered, that is 20-30mg/kg bodyweight (Barragry, 1987).

In humans, ivermectin is widely used to treat parasitic infections endemic in Africa, namely lymphatic filariasis, at a dose of 100–200 µg/kg for reduction of micro filaraemia, and onchocerciasis (African River Blindness) at doses from 150 µg/kg en masse once a year and to sufferers, including children who weigh 15 kg or more, every 3-6 months (Taylor *et al.*, 2010).

Emamectin benzoate

Emamectin benzoate is an important treatment for sea-lice infestations in farmed salmon, administered orally at 50µg/kg bodyweight daily for 7 days (Armstrong *et al.*, 2000; Lees *et al.*, 2008). It is also used at low concentrations (6g per acre) on vegetable crops for the control of Lepidoptera species (Wise *et al.*, 1997; Liguori *et al.*, 2010).

Abamectin

Abamectin is the major (B1) component of the natural fermentation of *Streptomyces avermitilis*. It was active against arthropods in preliminary studies and is used against phytophagous mites and insect pests on ornamental plants, citrus, cotton, pears and vegetable crops as a spray in the range of 5 to 27 grams abamectin per hectare

(Lasota & Dybas, 1990). It undergoes rapid photodegradation, with a half-life of 4-6 hours in the presence of light (Campbell, 1989), and thus does not accumulate in the environment. Kokoz *et al.* (1999) investigated the toxic effects of the natural aversectin C complex from *Streptomyces avermitilis*, which is a mixture of 8 constituent avermectins A1a, A1b, A2a, A2b, B1a, B1b, B2a and B2b, on neuroblastoma B103 cells from rat brain. They found that aversectin C was selectively toxic to proliferating cells above density 40×10^3 cells/cm² but not to non-proliferating cells at 20×10^3 cells/cm², and that from the aversectin C complex, components B1 abamectin and its dihydro-derivative ivermectin were not cytotoxic, but rather the A1 constituents were responsible. The effect of the constituents of aversectin C on firing frequency of neurones from rat brain frontal cortex was examined. Aversectin C and the GABA_α receptor activator nembutal both suppressed neuronal firing frequency, and this effect GABA-dependent of aversectin C was narrowed down to abamectin B₁ and B₂.

Other avermectins and the milbemycins

Selamectin, doramectin and the structurally related milbemycins, lacking a sugar substitution on Carbon-13, are chemically modified forms of the naturally-occurring avermectins that have been reported to have higher potency for some applications, e.g. moxidectin has been proposed as an alternative to ivermectin for the treatment of lymphatic filariasis (Taylor *et al.*, 2010). Lower affinity of moxidectin for MDR1 than either selamectin or ivermectin has been observed, and selamectin was reported to accumulate at lower levels in the brains of *mdr1*-deficient mice and to be equipotent with ivermectin in the inhibition of *mdr1* efflux (Griffin *et al.*, 2005). Selamectin also had a wider safety margin in ivermectin sensitive collies; dogs sensitive to 200 µg/kg ivermectin could be safely dosed with a single topical 40mg/kg selamectin. The normal recommended dose range for selamectin is a single dose of 6-12mg/kg per month (Novotny *et al.*, 2000).

Doramectin and the structurally-related milbemycin nemadectin both inhibited MDR1-mediated efflux of rhodamine-123 in the adriamycin-resistant MCF-7/adr human breast carcinoma cell line and showed low cytotoxicity similar to abamectin,

emamectin benzoate and ivermectin, with 8 μ M doramectin having no effect on cell survival as measured in the MTT after 48hr exposure (Gao *et al.*, 2010).

1.2. ABC Transporters in the Blood-Brain Barrier and CNS

Exposure to agricultural insecticides including the avermectins has been associated with toxicity to the Central Nervous System (CNS). CNS exposure to these agents is limited by the activity of efflux transporters expressed at the blood brain barrier (BBB), in mammals and in insects that develop resistance to the pesticides. Important transporters at the BBB include the multidrug resistance transporter (MDR1), the multidrug resistance proteins (MRP 1, 2, 4-6), and breast cancer resistance protein (BCRP). These are all members of the ATP-Binding Cassette (ABC) superfamily of transporters, that actively transport substrates across biological membranes by binding and hydrolysing ATP in conserved intracellular nucleotide binding domains (NBDs) (Leslie *et al.*, 2005).

The low CNS toxicity of the avermectin insecticides in mammals is due to efficient elimination from the CNS by MDR1 (Schinkel *et al.*, 1995; Pouliot *et al.*, 1997). When MDR1 is absent, as in mutant strains of the mouse (Schinkel *et al.*, 1995; Lankas *et al.*, 1997) and collie dog (Mealey *et al.*, 2001), CNS penetration of ivermectin increases, leading to symptoms of neurological toxicity including tremors, ataxia and coma. A number of polymorphisms of the MDR1 gene, ABCB1, have been identified in humans, although there are none so far identified that result in the ablation of *mdr1* function present in the mouse and collie dog models described above. There is conflicting evidence as to whether these mutations affect MDR1 activity or substrate specificity, however. It is possible that mutations which compromise MDR1 function and the interaction of substrates that compete for MDR1-transport may increase intracellular concentrations of substrate insecticides, leading to increased toxicity in animals and man. Figure 1.2 depicts important transporters expressed in the BBB.

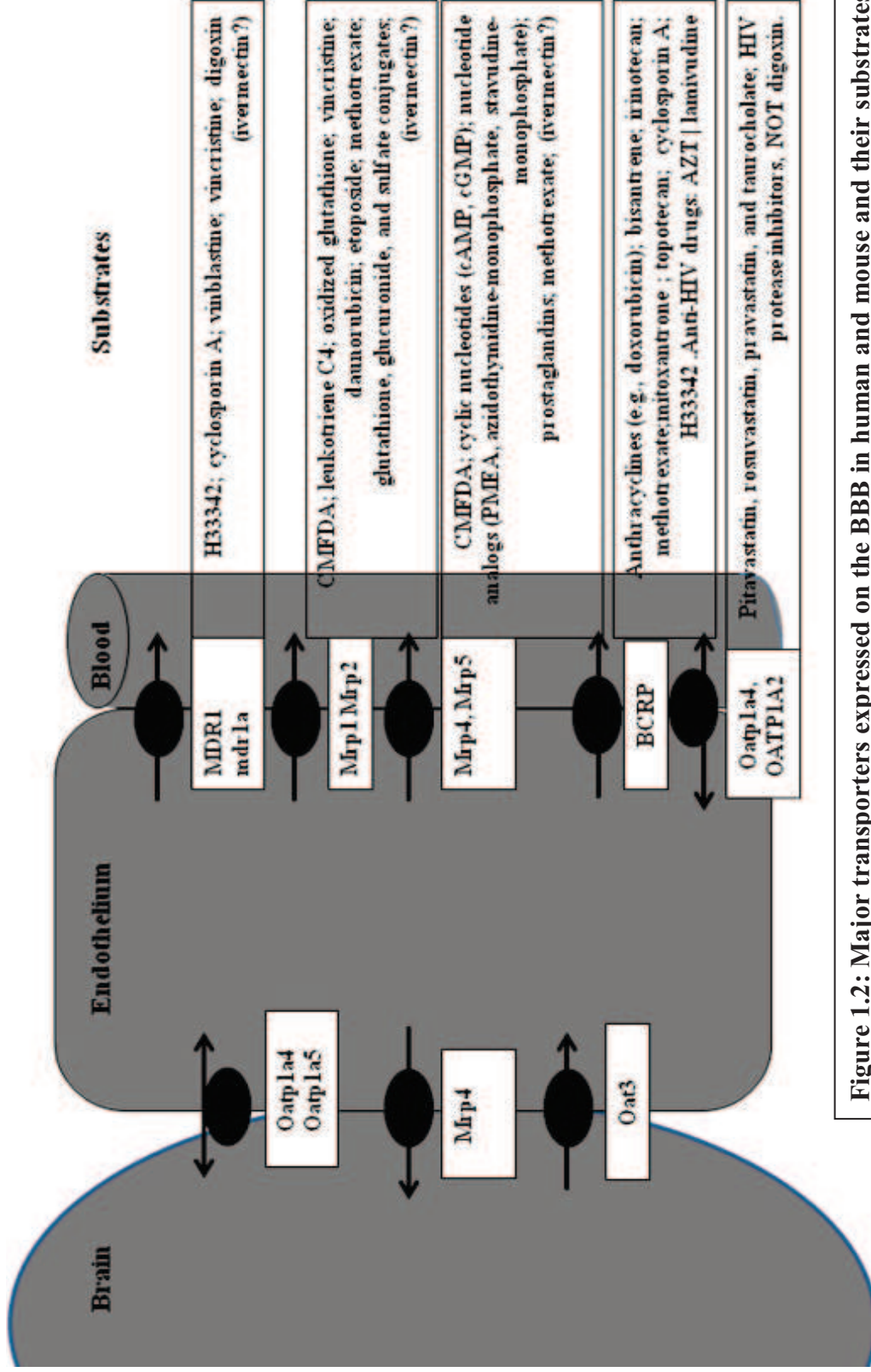


Figure 1.2: Major transporters expressed on the BBB in human and mouse and their substrates.
Adapted from *Figure 1* in Miller, 2010 with reference to Leslie *et al.* 2005; Dallas *et al.* 2006; Löscher & Potschka 2005; Matsson *et al.* 2009.

MDR1 Efflux Transporter

MDR1 is a well-characterised member of the ABC-transporter superfamily, first identified by Juliano and Ling in 1976 as a 170 kDa surface glycoprotein selectively expressed on the surface of colchicine-resistant Chinese hamster ovary cells, where higher levels of MDR1 expression were associated with increased drug resistance. In addition to its overexpression in drug-resistant tumour cells (Korystov *et al.*, 2004), MDR1 is constitutively expressed on the apical surface of cells in the lung, liver, kidney (Leslie *et al.*, 2005), jejunum, colon, pancreatic ductules, diffusely throughout the adrenal gland (Thiebaut *et al.*, 1987), and on the apical surface of capillary endothelial cells at the blood-brain and blood-testes barriers (Cordon-Cardo *et al.*, 1989). Both Thiebaut and co-workers (1987) and Cordon-Cardo *et al.* (1989) proposed that the localisation of MDR1 to apical surfaces of excretory compartments and barrier sites indicate that it has an important role in removing toxins from these tissues, by excreting toxins into the lower gut in bile and by limiting the entry of drugs and toxins into sensitive organs such as the brain. MDR1 is a 12-transmembrane transporter analogous in structure to bacterial multidrug resistance transporters with two binding sites with affinity for either Hoechst 33342 or rhodamine 123 (Loo & Clarke, 2005; Müller *et al.*, 2007).

MDR1 substrates

Substrates of MDR1 are structurally diverse hydrophobic molecules of molecular weight >300kDa (Leslie *et al.*, 2005), Review; Table 1). Ivermectin was confirmed as an *mdr1* substrate by Schinkel *et al.* in 1995. Pouliot and co-workers showed that the steady-state accumulation of [³H]-ivermectin was lower in drug-resistant cells than drug-sensitive human lymphoma cells in a similar manner to the known MDR1 substrate [³H]-vinblastine, that the efflux of both drugs was energy-dependent, and that this efflux can be inhibited by the presence of cyclosporin A or unlabelled ivermectin in molar excess. Schinkel *et al.*, (1995) provided evidence of MDR1-mediated transport of ivermectin, cyclosporin A and digoxin, in a basal to apical direction in bidirectional transfer experiments in porcine kidney epithelial cells transfected with human MDR1 or mouse *mdr1a*. Radiolabelled digoxin and cyclosporin A accumulated at significantly higher levels (35-fold and 17-fold, respectively) in brains of *mdr1a* (-/-) null mice than *mdr1a* (+/+) mice 4 hours after

injection. Both drugs were eliminated more slowly from plasma in the *mdr1a* null mice (Schinkel *et al.*, 1995). Table 1.1 lists selected substrates of MDR1 or *mdr1a*.

Table 1.1: Selected substrates of human MDR1 and mouse *mdr1a*. Fluorescent substrates are in italics; ‘potent’ = good substrate, ‘medium’ or ‘weak’ as described by the research groups. N.B. Cell lines and experimental methods differ between research groups.

Compound	Reference	MDR1 substrate?	<i>mdr1a</i> substrate?
Ivermectin	Schinkel <i>et al.</i> , (1995); Pouliot <i>et al.</i> , (1997)	potent	potent
Selamectin	Griffin <i>et al.</i> , (2005); Geyer <i>et al.</i> , (2009)	potent	potent
Abamectin	Lankas <i>et al.</i> , (1997); Brayden & Griffin, (2008)	potent	potent
cyclosporin a	Schinkel <i>et al.</i> , 1995	potent	potent
digoxin		potent	potent
dexamethasone		medium	medium
morphine		weak	weak
domperidone		medium	potent
phenytoin		weak	weak
budipine	Uhr <i>et al.</i> , (2005)	unknown	medium
odansetron	Schinkel <i>et al.</i> , (1996)	medium	potent
loperamide		medium	potent
amitryptiline	Laika <i>et al.</i> , (2006); Uhr <i>et al.</i> , (2007)	medium	medium
doxorubicin	Bain & LeBlanc, (1996)	potent	potent
vinblastine	Taub <i>et al.</i> , (2005); Jutabha <i>et al.</i> , (2010)	potent	potent
vincristine	Schaefer <i>et al.</i> , (2006); Balayssac <i>et al.</i> , (2005)	potent	potent
verapamil	Takano <i>et al.</i> , (2006); Kodaira <i>et al.</i> , (2010)	potent	potent
cypermethrin	Sreeramulu <i>et al.</i> , 2007	In MDR1 from drug-resistant CHO cells	
endosulfan			
fenvalerate			
methyl parathion			
<i>rhodamine123</i>	Lespine <i>et al.</i> , (2007)	potent	
<i>Hoechst 33342</i>	Müller <i>et al.</i> , (2007); Matsson <i>et al.</i> , (2009)	potent	
<i>bodipy-fl-paclitaxel</i>	Kimchi-Sarfaty <i>et al.</i> , (2007)	potent	

Besides MDR1, other ABC-transporters expressed on the blood-brain barrier are the multidrug-resistance proteins (MRPs) 1, 2, 4, and 5, breast cancer resistance-associated protein (BCRP). These transporters have both distinct and overlapping functions and substrates elsewhere in the body, and their co-expression with MDR1 is an important consideration when evaluating the transport kinetics of MDR1 substrates at the BBB (Leslie *et al.*, 2005; Lespine *et al.*, 2006). Their role in the transport of avermectins has not yet been established, although Lespine and co-workers showed that ivermectin binds to MRPs 1 and 2.

MRP Efflux Transporters

Multidrug resistance related proteins, or MRP transporters, are members of the subdivision of the superfamily of ABC-transporters that includes Cystic Fibrosis Transmembrane Conductance Regulator (CFTR). MRP1 was first identified in 1992, imparting a drug resistant phenotype to a human lung cancer cell line, H69AR, which did not overexpress MDR1 (Cole, 1992). MRP transporters 1-9 have distinct but heterogeneous distribution, and several isoforms have been found to contribute to drug resistance in cells, similarly to MDR1 and BCRP. Mutations in MRP proteins can cause disease such as Cystic Fibrosis, anaemia and retinal degeneration (Dallas *et al.* 2006, Review). MRP1, 2, 4 and 5 have been identified in the BBB of human and mouse (Leslie *et al.*, 2005; Löscher & Potschka, 2005; Dallas *et al.*, 2006; Miller, 2010). Mrp1 is the most highly expressed multidrug resistance protein transporter in mouse brain, whereas MRP5 is one of the most highly expressed mRNAs in human brain (Klaassen & Aleksunes, 2010 Review). MRP5 transports both endogenous substrates such as cAMP and cGMP and folate (McAleer *et al.*, 1999), as well as the anti-cancer drug methotrexate (Wijnholds *et al.*, 2000). Reports have identified protein expression of MRP4 and MRP5 on the luminal side of the Blood-Brain Barrier endothelium in humans (Bronger *et al.* 2005) and polarised expression of mrp4 on the basolateral membrane of mouse choroid plexus and the apical membrane of endothelial cells of the mouse blood-brain barrier which mediated resistance to topotecan (Leggas *et al.* 2004). In addition human MRP4 and MRP5 are expressed in subcortical astrocytes and MRP5 in pyramidal neurons (Nies *et al.* 2004). The mouse choroid plexus epithelium expresses mrp1, mrp2 and mrp3 proteins, whereas mouse blood-brain barrier expresses mdrla, mrp1, mrp2 and mrp5 (Soontornmalai *et al.* 2006).

A recent report found MRP1 expressed in the choroid plexus epithelium of human foetuses from early gestation (22-26 weeks) and in large pyramidal cells of the cerebellum in newborns, but, conversely, not in endothelial cells of the blood-brain barrier at any age up to adulthood, in contrast to MDR1 and BCRP (Daood *et al.* 2008). Mice deficient in *mrp1*^{-/-}, *mdr1a*^{-/-} and *mrd1b*^{-/-} (triple knockout) showed a tenfold greater accumulation of etoposide in CSF compared to *mdr1a*^{-/-}*mdr1b*^{-/-} double knockout (Wijnholds *et al.* 2000) indicating that *mrp1* has a role in drug efflux from CSF in the mouse, albeit with overlapping substrates. A naturally occurring *mrp2* deficient rat model, TR⁻, accumulated higher phenytoin concentrations in brain tissue than *mrp2*-expressing rats, suggesting that *mrp2* helps regulate the entry of phenytoin into the brain (Potschka *et al.* 2003). There are currently conflicting reports as to the role of MRP/*mrp* transporters in ivermectin efflux (Brayden & Griffin, 2008; Lespine *et al.* 2007).

BCRP Efflux Transporters

BCRP and *bcrp* mRNA expression has been confirmed in brain microvessel endothelial cells forming the luminal surface of the blood-brain barrier in human, rat, mouse, pig and cow (Cisternino *et al.*, 2004; Yousif *et al.*, 2007; Warren *et al.*, 2009) and protein function; it has been implicated in the efflux transport of mitoxantrone and prazosin at the mouse bbb (Kodaira *et al.*, 2010). *Bcrp* and *mdr1a* appear to have overlapping substrates, since *bcrp* mRNA expression is up-regulated 3-fold in the brain of *mdr1a*^{-/-} mice (Cisternino *et al.* 2004). Human BCRP transports H33342 if present (Matsson *et al.*, 2009) and has been shown to interact with cyclosporin A (Gupta *et al.*, 2006) as well as showing the potential to be up-regulated when MDR1 function is compromised, under conditions of stress e.g. epilepsy, and Alzheimer's Disease (Miller, 2010). Potential roles of BCRP in ivermectin handling are dealt with further in Chapter 4 discussion.

1.3. Animal sensitivity to avermectins

Exceptions to the low toxicity of avermectins in animal models are the *mdr1a*^{-/-} mouse (Schinkel *et al.*, 1994), a subpopulation of CF-1 mice (Lankas *et al.*, 1997) and of the Collie dog (Mealey *et al.*, 2001), all of which exhibit symptoms of neurotoxicity including tremors, ataxia, coma and death at doses far below those considered safe in other animals, and all lack a functional MDR1/*mdr1* efflux transporter. A selection of pesticides with different structures have been shown to interact with human MDR1 (Bain & LeBlanc, 1996; Sreeramulu *et al.*, 2007), including the avermectin insecticides, which are macrocyclic lactones (Lespine *et al.*, 2007). Bain and LeBlanc (1996) demonstrated that pesticides from different chemical classes, differing significantly in structure, can bind to MDR1 and inhibit its efflux transport of doxorubicin in B16/F10 mouse melanoma cells transfected with human MDR1 (B16/hMDR1).

In 1994, Schinkel and co-workers provided strong evidence that *mdr1a* protects the brain from exposure to ivermectin and the anti-cancer agent and *mdr1* substrate vinblastine when they generated homozygous *mdr1a* (-/-) mice that were viable and phenotypically normal except for extreme sensitivity to ivermectin administered topically to treat a mite infestation. Mice of both *mdr1a* (+/+) and (-/-) genotypes ingested the ivermectin during grooming. Subsequently only the *mdr1a* (-/-) mice exhibited symptoms of intoxication including immobilisation, recumbency, tremors and coma/death, whereas the homozygous *mdr1a* (+/+) or heterozygous mice were not affected (Schinkel *et al.*, 1994). The single gene for MDR1 (ABCB1) in humans has two corresponding homologues in mice, *mdr1a* and *mdr1b*, which have different tissue distributions but together perform all the functions undertaken by MDR1 in humans. Mouse *mdr1a* is predominantly expressed in the blood-brain-barrier, intestine, placenta, liver and kidney, whereas *mdr1b* is distributed in the adrenal gland, endometrium, ovary, placenta, liver and kidney (Schinkel *et al.*, 1994, 1995, 1996; Leslie *et al.*, 2005).

Mice with the genotype *mdr1a* (-/-) were consistently 50-100-fold more sensitive to oral ivermectin than were *mdr1a* (+/+) mice. Mdr1 was present on the endothelium of brain capillaries of *mdr1a* (+/+) mice and was absent in those of *mdr1a* (-/-) mice.

Chapter 1: Introduction

Accordingly, accumulation of [³H]-ivermectin was 90-fold greater in brain of *mdr1a* (-/-) mice than in that of *mdr1a* (+/+) mice after 24 hours, and was 8-10-fold raised in other tissues including gall bladder and testis. Mice homozygous for the *mdr1a* null mutation were 3-4 fold more sensitive to vinblastine toxicity than *mdr1a* (+/+) mice (Schinkel *et al.*, 1994). These results suggested that mouse brain was protected from exposure to ivermectin and vinblastine if *mdr1a* was present, but did not provide direct evidence that it transported these compounds.

Lankas *et al.* studied CF-1 mice in 1997, of which a subpopulation (c. 25%) were approximately 80 -100-fold more sensitive to single oral doses of both abamectin and ivermectin than resistant CD-1 mice. Insensitive CF-1 mice could tolerate a single dose of 2.5mg/kg abamectin without symptoms, whereas 0.2mg/kg intoxicated sensitive CF-1 mice. In 16/17 sensitive mice, no *mdr1* was detected in brain by the monoclonal antibody C219. The remaining sensitive mouse expressed very low *mdr1* levels in brain but not jejunum. In contrast, a random sample of 17 CF-1 insensitive mice all expressed levels of *mdr1* in cerebellum and cerebrum comparable to CD-1 mice, none of which exhibited a toxic response to abamectin or ivermectin. Intoxicated CF-1 mice exhibited similar symptoms to *mdr1a*(-/-) mice (Schinkel *et al.*, 1994). These results provided further evidence that the activity of *mdr1 in vivo* in the brain protected it from exposure to the avermectins (Lankas *et al.*, 1997).

Based on previous studies noting that ivermectin-sensitive collies accumulate much higher levels of ivermectin in brain tissue than -insensitive collies or beagle dogs (Daurio *et al.*, 1987), Mealey *et al.* predicted in 2001 that ivermectin sensitive collies might express polymorphic *mdr1* at the blood-brain barrier which is altered in either its expression level or activity. Sequencing of the *mdr1* gene revealed a homozygous 4 base-pair deletion mutation present in 7/7 ivermectin-sensitive collies but heterozygous in 6/6 -insensitive animals. Stop codons were generated early on in the mutant sequence, which generated a severely truncated, non-functional *mdr1* transporter.

These results together strongly suggest that the expression and function of *mdr1* at the blood-brain barrier is essential to protect mammals from CNS exposure to the pesticides ivermectin and abamectin. Wise *et al.*, (1997) found that emamectin benzoate causes developmental neurotoxicity in Sprague-Dawley rat pups at high

doses of 2.5mg/kg/day administered to the dam from gestational day 6 to lactational day 20, with a No Observable Adverse Effect Level (NOAEL) of 0.6mg/kg/day. Administration of 3.5/2.5mg/kg/day to mothers from gestational day 6 to lactational day 20 was associated with significantly decreased body weight gain in pups compared to untreated controls. Hindlimb splay and whole-body tremors were also exhibited by this treatment group, whereas placebo-treated controls were unaffected. Emamectin benzoate is not used in mammals as much as farmed salmon, with administered doses of 50 μ g/kg per day. However, its interactions in mammalian CNS need to be investigated, as new uses for the compound become apparent.

1.4. Transport data for avermectins

Lespine *et al.* (2007) tested the avermectin insecticides ivermectin, abamectin, doramectin, eprinomectin, selamectin and the structurally related milbemycin moxidectin as putative inhibitors of rhodamine123 dye efflux from porcine kidney epithelial cells transfected with either murine *mdr1a* or human MDR1. The cyclosporin A analogue valsopodar was used as a positive control and inhibited rhodamine123 efflux in *mdr1a*-transfected but not untransfected cells, IC₅₀ 0.11 \pm 0.03 μ M. All the avermectins inhibited transport of rhodamine 123 in *mdr1a*-transfected cells. Abamectin inhibited transport by 83 \pm 2%, and ivermectin by 86 \pm 2% of the effect of valsopodar; the compounds returned IC₅₀'s of 0.11 \pm 0.01 μ M and 0.44 \pm 0.07 μ M, respectively, proving them relatively potent inhibitors of the efflux transport of rhodamine123.

The other avermectins had similar effects, but the milbemycin moxidectin was a significantly weaker inhibitor with an IC₅₀ of 4.4 \pm 0.6 μ M (Lespine *et al.*, 2007). Similar trends were observed in the inhibition of the ATPase activity of MDR1, with IC₅₀ values for abamectin and ivermectin at 0.2 and 2.0 μ M for basal-, and 0.02 and 0.05 μ M for verapamil-stimulated ATPase activity, respectively. Abamectin and ivermectin were thus shown to be potent modulators of *mdr1* activity in vitro in LLCK-PK1 *mdr1a*-transfected cells. In LLCK-PK1 cells transfected with human MDR1, ivermectin inhibited rhodamine123 efflux with an IC₅₀ of 1.0 \pm 0.2 μ M.

Griffin *et al.* (2005) investigated transepithelial transport of ivermectin, selamectin and moxidectin across human intestinal epithelial Caco-2 cells. All three were transported preferentially in a basolateral to apical direction, although the milbemycin moxidectin was a weaker MDR1 substrate than the avermectins, since the secretory flux of both ivermectin and selamectin, but not moxidectin, was decreased in the presence of the MDR1 inhibitor verapamil (20 μ M). Ivermectin and selamectin were potent inhibitors of rhodamine-123 secretion, with IC₅₀'s of 0.1 μ M, whereas the IC₅₀ for moxidectin of 10.0 μ M indicates much weaker inhibitory activity (Griffin *et al.*, 2005).

As well as being a substrate for MDR1, Lespine *et al.*, (2006), showed that ivermectin can inhibit the ATPase activity of MRPs 1, 2 and 3, and is transported by MRP1. They suggested that the MRP transporters may influence ivermectin transport as well as MDR1. Brayden and Griffin (2008) transfected MDCK canine kidney epithelial cell lines with either MDR1, MRP-1 or MRP-2. They found significant basal to apical transport of ivermectin and selamectin, similar in all four cell lines including control. They detected canine *mdr1* expression in all four lines and concluded that this was responsible for the transport, which was indeed inhibited by the other MDR1/*mdr1* substrate verapamil, but not by MRP inhibitors. They therefore claimed that MRP transporters have negligible influence if MDR1 is expressed. An awareness of the influence of transporters other than MDR1 is essential though; SH-SY5Y human neuroblastoma cells used in our study are morphologically different from kidney.

1.5. Effects of MDR1 polymorphisms on avermectin exposure in humans and cell line studies

MDR1 polymorphisms in humans

A number of single nucleotide polymorphisms (SNPs) of MDR1 have been identified in humans by haplotype analysis. Some are synonymous, in which a nucleotide base change does not result in an amino acid change, due to the degeneracy of triplet codons. Others result in amino acid changes. The severity of the effect of the amino acid change on function will be influenced by both the type of substitution and the position of the substitution along the sequence; amino acid changes in transmembrane

or nucleotide binding domains of MDR1 may have a more drastic effect on function than substitutions elsewhere in the sequence (Shilling *et al.*, 2006).

Association studies

In view of the demonstrated importance of MDR1 in protecting the CNS from exposure to pesticides and associations of exposure to pesticides other than avermectins with adverse health effects, a number of association studies have been conducted to investigate whether there is a correlation between polymorphic forms of MDR1 and increased risk from pesticide exposure. Risks of significant exposure to pesticides are recognised as living in a rural area, drinking drill-well water or being occupationally exposed (Drożdżik *et al.*, 2003). Table 2 lists MDR1 polymorphisms genotyped in humans. Lee *et al.*, (2004) examined seven SNPs found by genotyping 206 Chinese patients with Parkinson's Disease (PD) and 224 matched normal controls. They found that 1236T, 2677T and 3435T were significantly over-represented in the control group compared to the PD patients. Tan *et al.*, (2005) also studied the MDR1 polymorphisms 2677 and 3435 by multiplex sequencing in a case control study with 185 PD patients and 206 controls. They found that a haplotype containing both SNPs 2677T and 3435T occurred at significantly lower frequency in PD patients than in matched controls ($P < 0.001$), and thus inferred that the polymorphisms 2677T with 3435T protect against PD in ethnic Chinese.

Drożdżik *et al.*, (2003) genotyped Polish patients with PD who had either been significantly exposed to pesticides for longer than 10-15 years or not exposed, compared to healthy controls. They found a significantly higher incidence of the heterozygous 3435T allele in PD patients exposed to pesticides (72.9% of 59 patients) than in non-exposed PD sufferers (47.9% of 48 patients), $P < 0.01$. Drożdżik and colleagues concluded that the risk of developing PD is approx. 5-fold higher in carriers of the 3435T allele (heterozygotes and homozygotes) exposed to pesticides than in carriers who are not exposed, however, these association studies do not specify to which pesticides the individuals have been exposed. The avermectin pesticides have not been linked to the development of neurological disorders in this way.

The data of Drodzik et al. (2003) are in agreement with the observations of Furuno *et al.*, (2002), who performed a case-control association study on 95 Parkinson's Disease (25 early onset, age ≤ 45 years) patients and 106 controls to assess whether there is a link between 'common' MDR1 polymorphisms and Parkinson's Disease (PD). The chosen polymorphisms were 3435C>T, 2677G>T/A and -129T>C. Frequency of the 3535T/T genotype was highest in the early-onset PD group (36.0%), 22.9% in the late onset PD group and 18.9% in the control group, but this trend was not statistically significant ($P=0.08$) The frequency of the 3435C/C genotype was conversely highest in controls (26.4%) and lowest in early onset PD patients (20.0%), again without statistical significance. Together these data suggest that the functional effect of the 3435T/T MDR1 genotype needs investigating further. Table 1.2 shows selected polymorphisms of MDR1 identified by genotyping.

Table 1.2: Polymorphisms of MDR1 investigated *in vivo*

SNP/ Haplotype	Location	Study size control /PD	Association with PD	Reference
1236C>T	Exon12	224/206	C = PD risk	Lee <i>et al.</i> , 2004
2677G/T/A	Exon21		G= PD risk	
3435T/C	Exon26		C= PD risk	
2677T_3435T	e21-e26	206/185	TT= lower risk	Tan <i>et al.</i> , (2005)
1236TT_2677TT_3435TT vs. CC_CC_CC	e12_e21_e26	33 healthy males	No effect	Takano <i>et al.</i> , (2006)
3435T/C	Exon26	103/107	T = PD risk	Drożdżik <i>et al.</i> , (2003)
3435T/C	Exon26	106/95	No significant association	Furuno <i>et al.</i> , (2002)
2677G>T/A	Exon 21			
-129T>C	Exon 1b			
3435C>T	Exon 26	115/200	CC = drug resistance	Siddiqui <i>et al.</i> , (2003)

The statistical power of all these association studies is limited by their small sample size and by the difficulty of examining individual SNPs separately (Macdonald & Gledhill, 2007). The polymorphisms need to be examined by functional studies both *in vivo* and *in vitro*.

Functional studies in vivo

To date, the only identified polymorphisms that result in non-functional human MDR1 similar to that found in collies is T3587G which causes amino acid 1196 to change from isoleucine (non-polar) to serine (polar) and C3583T which results in substitution of tyrosine for histidine at amino acid 1195. These substitution mutations are located in the Walker B domain of the second ATP binding region of MDR1, and I1196S MDR1 was found to be deficient in ATP-binding ability (Mutoh *et al.*, 2006). Of 605 Japanese cancer patients analysed, 2 were heterozygous for one or both mutations, giving a sample frequency of 0.3% for both polymorphisms. Murine fibroblast NIH3T3 cells were stably transfected with T3587G MDR1 that corresponded to I1196S substitution, or wild type MDR1, since they express low levels of endogenous murine *mdr1*. Unlike wild type, I1196S-MDR1 was not expressed at the cell surface, and was also expressed at a much lower level within the cell. NIH3T3 cells transfected with wild type MDR1 were more resistant to vincristine by 22-fold and doxorubicin by 7-fold than untransfected control NIH3T3 cells, whereas I1196S-Pgp transfectants were no more resistant than control. Together, these results indicate loss of functional activity in the I1196S mutant, which is found at very low frequency ($\geq 0.3\%$ of 605 patients) and only so far in heterozygotes (Mutoh *et al.*, 2006).

There is evidence both in support of and contradicting the idea that other identified MDR1 polymorphisms have effects on functionality or expression levels. An example is the synonymous C3435T polymorphism. When homozygous, C3435T has been found to be associated with 2-fold lower MDR1 gene expression and 65-fold lower protein expression and to result in higher plasma levels of digoxin, reflecting reduced activity of MDR1 in the duodenum (Hoffmeyer *et al.*, 2000). Conversely, Brunner *et al.*, (2005) compared ten MDR1 homozygotes for the haplotype (3435T, 1236T and

2677T) to ten controls (3435C, 2677G and 1236C) using [¹¹C]-verapamil (a known MDR1 substrate (Hendrikse *et al.*, 1999)).

Takano *et al.*, (2006) investigated the uptake clearance of [¹¹C]-verapamil over time by PET in individuals homozygous for haplotypes 1236TT/2677TT/3535TT (20 volunteers) vs. 1236CC/2677GG/3435CC (13 volunteers, mean age in both groups 23 years). They injected all subjects with an IV bolus of [¹¹C]-verapamil and measured radioactivity in brain and plasma for 16 minutes after the injection. They found no significant difference in brain/plasma concentrations between the two groups. Likewise, uptake clearance from brain was not significantly different at 0.053 ± 0.011 mL/g/min for the TTT haplotype and 0.051 ± 0.011 mL/g/min for the CCC haplotype. These results suggest that there is no difference in MDR1 function at the BBB between the two haplotypes (Takano *et al.*, 2006). Table 1.3 lists selected *in vivo* studies on functional polymorphisms.

Table 1.3: MDR1 polymorphisms studied in vivo

SNP/Haplotype	Location	AA Effect	Function	Reference
3587T>G	Walker B of 2 nd NBD	1196 isoleucine to serine	Loss of surface expression	Mutoh <i>et al.</i> , 2006
3435C>T	Exon 26	No change	Lower expression in duodenum	Hoffmeyer <i>et al.</i> , (2000)
<i>1236TT_2677TT_3435TT vs. CC_GG_CC</i>	<i>e12_e21_e26</i>	A893T/S	No effect	Brunner <i>et al.</i> , (2005); Takano <i>et al.</i> , (2006)

Functional studies in vitro

A number of studies have been conducted in epithelial cell lines that express endogenous MDR1 at a low level and are then transfected with wild type or polymorphic MDR1, which is over-expressed. These studies have been useful for assessing functional activity of MDR1 within cells and revealing its interactions with individual substrates (Bain & LeBlanc, 1996; Morita *et al.*, 2003; Taub *et al.*, 2005; Kimchi-Sarfaty *et al.*, 2007; Gow *et al.*, 2008).

Gow *et al.*, (2008) transiently transfected HEK293T cells with non-synonymous SNP variants, reference MDR1 and a nucleotide binding domain (NBD) mutant, and measured intracellular accumulation of the established MDR1 substrates BODIPY-FL-paclitaxel and calcein-AM in the presence or absence of 10 μ M cyclosporin A. Using flow cytometry, they found that intracellular calcein levels were similar to wild type for all variants, indicating similar transport activity, except for the NBD mutant, which accumulated a 20-fold higher intracellular calcein concentration than reference, suggesting compromised activity. The variants N21D, R669C and A893S had slightly increased sensitivity to inhibition of calcein transport by cyclosporin A compared to

Chapter 1: Introduction

reference at 100% (136 ± 28 , 139 ± 43 and $130\pm 22\%$, respectively). Intracellular BODIPY-FL-paclitaxel levels were increased in the A893S and V1251I mutants and the (N21D/1236C>T/A893S/3435C>T) haplotype compared to reference at $114\pm 13\%$, $118\pm 12\%$ and $124\pm 13\%$ respectively, indicating slightly reduced efflux transport of this substrate.

The V1251I mutant and the haplotype N21D/1236C/A893S/3435C>T were $65\pm 26\%$ and $53\pm 8\%$ less sensitive to inhibition of BODIPY-FL-paclitaxel transport, respectively, than the wild-type MDR1. Together, these results demonstrate alterations in MDR1-mediated transport in cells by the different variants that are substrate-specific, assuming, as noted by Gow *et al.* (2008), that cellular uptake of substrate is constant, and that differences in substrate accumulation reflect differences in efflux among MDR1 variants.

The idea that the effects of polymorphisms on MDR1 transport are substrate-specific suggests that tests with a single substrate, such as ^{11}C -verapamil, or calcein-AM, would not necessarily highlight defects in structure or function that are relevant to the transport of individual substrate pesticides or therapeutic agents. It follows that tests for the individual substrates and modulators are required for each MDR1 variant (Gow *et al.*, 2008). Of relevance to this concept, a molar excess of verapamil inhibited energy-dependent efflux of [^3H]-ivermectin in vinblastine-resistant human lymphoma cells, restoring intracellular ivermectin levels to that of drug-sensitive cells, but did not have the same effect on intracellular [^3H]-verapamil (Pouliot *et al.*, 1997).

Further support for substrate-dependent effects of polymorphisms came from Shilling *et al.* in 2006, who performed site-directed mutagenesis on amino acids in different regions of MDR1, and were able to demonstrate ‘hotspots’ in which mutations had a greater effect on transport activity, and that some mutations altered the affinity for one substrate but not another. Kimchi-Sarfaty *et al.*, (2007) explored effects of the C3435T polymorphism in 2007 and found that, when included in haplotypes, it altered MDR1 affinity for verapamil, but not rapamycin. Schaefer *et al.*, (2006) assessed MDR1-mediated vincristine transport in High Five insect cells transfected with polymorphic variants 893Ala, 893Ser or 893Thr. They found that vincristine accumulation was lowest for 893Ala (wild-type) and increased up to 3-fold

for the mutants. 893Ser was also less sensitive to inhibition of vincristine transport by digoxin than 893Ala or Thr. It is clear from these studies that MDR1 substrates and modulators interact in distinct ways, so it is necessary to take into account the effect of other therapeutic agents to which the CNS is exposed simultaneously with pesticides. Table 1.4 summarises *in vitro* studies on SNPs in MDR1.

Table 1.4 Selected MDR1 polymorphisms studied *in vitro*

SNP	Location	AA Effect	Cell line	Transport effect	Reference
61	Exon 2	N21D	HeLa	None	Kimchi-Sarfaty <i>et al.</i> , (2007)
307	Exon 5	F103L			
1107	Exon 10	G369P			
1199	Exon 11	S400N			
2677	Exon 21	A893T/S			
2995	Exon 24	A998T			
61A>G	Exon 2	N21D	HEK293T	Increased sensitivity to CSA	Gow <i>et al.</i> , (2008)
1199	Exon 11	S400N		No effect	
2005C>T	?	R669C		S =increased CSA sensitivity, T= increase in calcein transport	
2677G>T/A	Exon 21	A893S/T			
3421T>A	?	S1141T		No effect	
3751G>A	?	V1251I		Increase in calcein transport	
2677G/A/T	Exon 21		LLC-PK1	No effect	Morita <i>et al.</i> , (2003)
3435C/T	Exon 26	none			
2677G>T/A	Exon 21	A893S/T	HighFive insect cells	S/T may compromise vincristine clearance	Schaefer <i>et al.</i> , (2006)

Of further relevance to the substrate specificity of MDR1 transport function proposed by Gow et al. (2008), Taub et al. (2005) examined bidirectional transport of the MDR1 substrates tritiated paclitaxel, -vinblastine and -digoxin in MDCK cells transfected with MDR1, MDCK-wild type and Caco-2 cells. They found that the ratios of verapamil-sensitive, MDR1-mediated, basal-apical/apical-basal transport ratios were approx 4-fold greater ($[^3\text{H}]$ -paclitaxel), 5-fold greater ($[^3\text{H}]$ -vinblastine) and 7-fold greater ($[^3\text{H}]$ -digoxin) in MDCK-MDR1 cells than in MDCK wild type controls. Cyclosporin A at $3\mu\text{M}$ reduced basal-apical apparent permeability (P_{app}) to between 5 and 25% of control for $[^3\text{H}]$ -paclitaxel, $[^3\text{H}]$ -vinblastine and $[^3\text{H}]$ -digoxin, in both MDCK-MDR1 and MDCK wild-type cells, in agreement with its classification as a potent inhibitor of MDR1.

Notably, ketoconazole and loperamide were both significant activators of transport in MDCK-MDR1 cells at $3\mu\text{M}$ for tritiated vinblastine ($164.3\pm 17.2\%$ of control, $P < 0.01$) and -digoxin, ($124.2\pm 4.1\%$ of control, $P < 0.05$) but not significantly for $[^3\text{H}]$ -paclitaxel. Both agents conversely inhibited efflux transport at the 10-fold higher concentration of $30\mu\text{M}$ (Taub *et al.*, 2005). Caco-2 cells were also used as a model of human intestinal epithelial MDR1-expressing cells, and transport of the tritiated substrates was not activated in this cell line by $3\mu\text{M}$ ketoconazole or loperamide. MDCK-MDR1, MDCK wild type and Caco-2 cells demonstrated different sensitivities to inhibition of MDR1 transport by quinidine. For example, $10\mu\text{M}$ quinidine inhibited transport of tritiated vinblastine, paclitaxel and digoxin to 25-50% of control ($P < 0.01$) in MDCK wild type cells, but had no significant effect in MDCK-MDR1 cells. In Caco-2 cells, $10\mu\text{M}$ quinidine inhibited tritiated-paclitaxel and -digoxin transport to 25-50% of control ($P < 0.01$), but, conversely, had no effect on -vinblastine transport (Taub *et al.*, 2005). These studies suggest that modulator concentration- and cell line differences can have effects on MDR1 transport function, which highlights the pressing need for functional studies in a cell line representative of the human CNS, such as SH-SY5Y (Biedler *et al.*, 1973).

1.6. SH-SY5Y human cells as a model for evaluating neurotoxicity

SH-SY5Y cells are a neuroblastic subclone derived from SK-N-SH cells by Biedler and co-workers in 1973. Parent SK-N-SH cells were isolated from a bone marrow

aspiration taken in 1971 from a 4 year-old female neuroblastoma patient (Biedler *et al.*, 1973). Differentiated SH-SY5Y cells were resistant to infection by the HIV type-1 virus (Vesonen *et al.*, 1994). SH-SY5Y cells were successfully differentiated, stained and visualised by Price *et al.*, (2006). After retinoic acid-induced differentiation the cells produced highly branched neurites. Subsequently dibutyryl cAMP was found to induce morphological differentiation in a similar manner to retinoic acid (Kume *et al.*, 2008). Pioglitazone was used to stimulate the PPAR γ receptor in SH-SY5Y cells, and thereby PPAR γ activation was implicated in promoting neurite outgrowth (Miglio *et al.*, 2009a) since nanomolar concentrations of the PPAR γ agonists rosiglitazone and pioglitazone prevented neuronal cell death induced by glucose deprivation and increased dendrite density in differentiated SH-SY5Y cells (Miglio *et al.*, 2009b).

Differentiation of SH-SY5Y cells with RA resulted in resistance to oxidative stress and a decrease in activity of the apoptotic marker caspase-3 compared to undifferentiated control cells after exposure to the neurotoxin 6-Hydroxydopamine (6-OHDA) (Cheung *et al.*, 2009). The environmental pollutant 2,3,7,8-tetrachlorodibenzo-*p*-dioxin (TCDD) was investigated for its ability to induce a neurotoxic response in differentiated SH-SY5Y cells by Jung *et al.*, (2009); these researchers found that 5nM TCDD treatment up to 6 hours after retinoic acid induction was sufficient to significantly decrease the percentage of “neurite-bearing cells” but this effect was no longer significant after 12 or 24 hours.

As a model cell line to investigate neurotoxicity in their undifferentiated state, SH-SY5Y cells were subjected to hypoxia and subsequent reoxygenation, after which MTT cell proliferation assay returned a drop in the proportion of viable cells to 62% of control after 24 hours' hypoxia and both mRNA and protein expression for the amyloid precursor protein cleavage enzyme BACE1 were upregulated, suggesting a mechanistic link between hypoxia and the development of amyloid plaques in Alzheimer's Disease (Li *et al.*, 2010).

1.7. N2a mouse cells as a model for evaluating neurotoxicity

N2a cells were isolated from a brain neuroblastoma in a Strain A albino mouse by Klebe and Ruddle (1969). These cells have been used extensively in studies of

pesticide toxicity, due to their clear morphological change from an epitheloid structure to the expression of a predominance of single, long neurites when grown in induction media containing dibutyryl cyclic AMP (Shea *et al.*, 1991; Flaskos *et al.*, 1998, 1999, 2007). It is widely reported to be easy to image and count, or measure the length of these singly-branched neurites. In 1998, Flaskos *et al.* incubated N2a cells with the organophosphate pesticide tri-o-cresyl phosphate (1 $\mu\text{g}/\text{ml}$) for 24 hours then differentiated them for 2 days in serum-free media containing 0.3mM dibutyryl cAMP. At the end of this period a significant drop in the number of long (>2 cell bodies') axonal outgrowths was observed in N2a cells that had been pre-treated with tri-o-cresyl phosphate compared to control, along with a reduction in the reactivity of neurofilament protein, involved in axonal stability. In 1999, Flaskos *et al.* found similar results with the pesticides carbaryl and trichlorphon.

Lawton *et al.* (2007) investigated the toxicity of methylmercury chloride (1 μM) to N2a cells, and found a significant (55%) reduction in the percentage of neurite outgrowths compared to control after methylmercury treatment for 4 hours during differentiation. The oxon metabolite of the organophosphate pesticide diazinon (DZO) was found to reduce the number of axonal processes in N2a cells after 24hours' differentiation in 0.3mM dibutyryl cAMP and co-treatment with 1, 5 and 10 μM DZO. The same concentrations of DZO reduced acetylcholinesterase activity in N2a cells by approximately 60% after 4 hours' treatment, but this effect was not evident after 24 hours (Sidiropoulou *et al.*, 2009).

Importantly, the avermectin derivatives abamectin and doramectin inhibited the expression of *mdr1a* and cytoskeletal proteins, resulting in inhibition of neurite outgrowth after 48 hours' exposure after induction with 0.3mM dibutyryl cAMP (Sun *et al.*, 2010)

It is notable that Bates and co-workers found that, while inducing cellular differentiation, retinoic acid caused up-regulation of MDR1 mRNA in SH-SY5Y cells over a 4-day period (Bates *et al.*, 1989). In order to avoid any fluctuation in transporter expression that might be brought about by inducing differentiation, cellular assays of mRNA expression, transport and cell proliferation were all performed in undifferentiated SH-SY5Y and N2a cells in the current study.

1.8. Aims of the study

As a prerequisite to understanding the impact of the functional MDR1 polymorphisms already identified, and those at novel sites to be characterised in future, it is important to identify similarities and differences between interactions of these avermectins with endogenous human MDR1 and mouse *mdr1a*, as well as other important CNS efflux transporters, to ascertain how useful data from murine models can be in predicting the consequences of human avermectin exposure.

To this end, the current study proposes to test the hypothesis that, excepting the abnormal CF-1 and *mdr1a*^{-/-} knockout mice, the kinetics of avermectin interactions in *mdr1a*-expressing mouse cells are similar to those in MDR1-expressing human cells, and data from mouse models can therefore be usefully applied in predictions of human CNS toxicity. The current work aimed to characterise transporter expression in SH-SY5Y cells to establish their utility cell models. The efflux activity of these cells was then compared upon exposure to a known substrate and known inhibitor for each transporter type, and the capability of avermectins to inhibit this transport was investigated using fluorescent dye retention assays. It was also of interest to quantify the toxic dose limits of avermectins for these neuroblastoma cells and to identify potential markers of exposure at subtoxic doses.

Chapter 2: Methods

2.1 Materials

All plastics for cell culture were Costar by Corning Life Sciences, obtained from Fisher Scientific, Loughborough, UK. General cell culture reagents and ingredients for Krebs' Buffer were from Sigma, Poole, UK. Abamectin and Emamectin benzoate were supplied as free samples by Syngenta, Bracknell, UK. Ivermectin was bought from ChemService, West Chester, PA. Antibodies and other individual reagents are mentioned where applicable in the methods. All other reagents were of the highest grade commercially available.

2.2 Methods

Cell Culture

SH-SY5Y Human Neuroblastoma Cells

SH-SY5Y cells were maintained in high glucose DMEM, supplemented with 2mM L-Glutamine (1%), 10% Foetal Calf Serum (FCS) and antibiotics; penicillin (10,000units/ml) and streptomycin (10,000 μ g/ml.) Fresh complete media was used within 4 weeks of being made up. Cells were sub cultured every 7 to 9 days. Cell media was removed and cell monolayers rinsed twice with a Ca²⁺-free phosphate buffered saline (PBS). Cell monolayers were then incubated in a small volume PBS with the addition of 0.02% Trypsin/EDTA for 5 minutes at 37°C. Detached cells were collected by centrifugation at 1500 rpm for 3 minutes; the pellet was re-suspended in media and passed x20 through a wide bore needle to generate a single cell suspension. Cell number was assessed using a Coulter Counter Z1™ (Beckman Coulter, Luton, UK.). Cells were seeded onto 96-well plates (Costar) from this culture to achieve 80-90% confluence 3-4 days after seeding (approx 30,000 cells/well). Cells were also subcultured after each passage with 1.5 million cells in a T75 Flask (Costar). Cells were incubated at 37°C in 5% CO₂/95% air. Cells were used from passage 29 – 39 and after these 20 passages the cells were replaced from frozen stock.

N2a Mouse Neuroblastoma Cells

N2a cells were maintained in high-glucose DMEM containing 2mM L-glutamine (1%), 10% Foetal Calf Serum (FCS), 1mM pyruvate, 0.1% v/v Non-essential amino acids and antibiotics; penicillin (10,000units/ml) and streptomycin (10,000 μ g/ml). Fresh complete media was used

within 4 weeks of being made up. Cells were subcultured every 4-6 days by washing twice with pre-warmed Ca^{2+} -free Phosphate Buffered Saline (PBS), then 2ml of Trypsin/EDTA solution was added and incubated for 1-2 minutes. The Trypsin/EDTA solution was neutralised with 7.5ml complete growth media. Detached cells were collected by centrifugation at 1500 rpm for 3 minutes; the pellet was re-suspended in media and passed x20 through a wide bore needle to generate a single cell suspension. Cells were counted using a Coulter Counter Z1TM and seeded into a fresh flask at 40,000 cells/ cm^2 (3 million per T75 flask). For each experiment, cells were seeded in 96-well plates to achieve 80-90% confluence 3-4 days after seeding (approx 20,000 cells/well). Cells were incubated at 37°C in 5% CO_2 /95% air. Cells were used from passage 5-20 and after these 15 passages the cells were replaced from frozen stock, to avoid overgrowth of the epitheloid subpopulation.

Total RNA extraction

For analysis of constitutive transporter mRNA expression (Chapter 3)

Cells grown in complete media to subconfluence in T-75 Tissue Culture Flasks were processed with the RNeasy Midi Kit (Qiagen, Crawley, West Sussex, UK). RNA concentration was analysed and quality confirmed as RNA Integrity Number (RIN) ≥ 8.0 using an Agilent 2100 bioanalyser for RNA and the RNA 6000 Nano Kit (Agilent Technologies, Cheshire, UK).

For analysis of transporter mRNA expression in avermectin-treated cells (Chapter 6)

Cells grown in complete media to 80% confluence over 4 days had media removed and replaced with media free from FCS, containing treatment solutions at concentrations described in the figure legends. Cells were incubated with treatments for 18 hours, after which RNA was extracted using the SV Total RNA Isolation System (Promega, Southampton, UK) as per manufacturer's instructions, quantified and quality controlled with RIN ≥ 8.0 using an Agilent 2100 Bioanalyser, and Agilent RNA 6000 Nano Kit.

End-point and qRT-PCR

Total RNA obtained from cells over 3 independent passages was reverse-transcribed with oligo dT primers and Omniscript RT-Kit (Qiagen, Crawley, UK) or RT enzyme (Promega, Southampton, UK) as available. End point PCR was performed to check identity of transporter

cDNA using GoTaq Green DNA polymerase and compatible buffers and dNTPs from Promega. Custom primers for both end point and qPCR were synthesized and purified by IDT (Glasgow, UK). qRT-PCR experiments were performed using the LightCycler 480 II (Roche, West Sussex, UK) and SYBR Green Master Mix (Applied Biosystems, Paisley, UK) according to the manufacturer's protocol. Sequences for gene-specific primers corresponding to PCR targets were obtained using Primer Design software (Invitrogen.com) and checked against corresponding sequences in the NCBI Genbank database (<http://www.ncbi.nlm.nih.gov/genbank/>). Expression for individual genes was normalised to expression of the human/mouse GAPDH/gapdh housekeeping gene to account for differences in cDNA input concentrations.

qPCR Arrays for endogenous expression of human drug transporters (Chapter 3) and changes in expression of selected chemokines in response to avermectin exposure (Chapter 6).

Control or avermectin treated RNA samples, verified for RNA integrity ≥ 8.0 , were transcribed to cDNA using the RT² First Strand kit (SABiosciences). qPCR was performed as per manufacturer's instructions on 2 independent RNA samples for each condition using array plates PAHS-070F (human drug transporters) and PAHS-022F (chemokines and receptors) and RT² SYBR Green qPCR Master Mix with the Roche LightCycler 480 II.

Immunocytochemical staining of cells for MDR1/mdr1a protein expression and BCRP/bcrp protein expression

Cell monolayers were grown to confluence in 12-well plates on 13mm coverslips pretreated with 0.1% poly-L-lysine (Sigma). When they reached 60% confluence, after 3-4 days in culture were washed 2x in PBS then fixed in a suitable medium according to the primary antibody used. The antibody for MDR1/mdr1a staining, MRK-16 (Kamiya Biomedical Company, USA), required fixing in 3% paraformaldehyde (PFA) for 15 min, to avoid disrupting MDR1 structure, whereas all other antibodies used (BXP21; BXP9 and C219; AbCam, Cambridge, UK) were suitable for fixation in 100% methanol for 5 min. Fixed cells were washed again 3x in PBS, and could be stored in PBS at 4°C overnight. PBS storage buffer was removed from cells and, if cells were fixed in PFA, 0.1% Triton X-100 in water (400µl/well) was added. Cells were shaken for 15 minutes to allow permeabilisation, then washed 3x in PBS. 400ul 3% goat serum diluted in sterile PBS was added and the plates shaken for 1 hour to block non-specific binding.

Primary antibody (MRK16, human monoclonal anti-MDR1 antibody) was diluted 1:20 or 1:50 in goat serum, or BXP-9 (anti-BCRP antibody) or BXP-21 (anti-mouse bcrp were diluted 1:20 or 1:50 in horse serum) Laboratory parafilm was stretched across a new plate. 50 μ L primary antibody was pipetted onto parafilm for each allotted well then the cell layers on coverslips were placed cell-side down into the antibody solution, in order to maximise binding of antibody in minimum volume. The coverslips were incubated overnight at 4°C. Control coverslips with no primary antibody were set up for each condition to detect non-specific binding of the secondary antibody; these were incubated in goat serum overnight at 4°C.

After this time, all coverslips were transferred to fresh wells and washed 3x in PBS, gently rocking the plate to cover the cells. The last PBS wash was removed and 400 μ L 3% rabbit serum was added for 1 hour incubation at room temperature. The rabbit serum was then removed and coverslips were incubated in a solution of AlexaFluor 488-tagged rabbit-anti-mouse IgG secondary antibody against MRK-16 (1:100), or AlexaFluor488-tagged goat-anti-rat IgG antibody against BXP-9 and BXP-21 (1:100) and phalloidin (1:250) at 50 μ L per coverslip for 1hr at room temperature in the dark. Phalloidin was used to counterstain the cell membrane by binding to the actin cytoskeleton. At the end of this time, coverslips were transferred to new wells, washed 3x in PBS as previously and mounted onto slides using Vectashield mounting medium. Slides were wrapped in silver foil to protect them from light and stored at 4°C for confocal imaging up to 24 hours later.

The settings on the Leica TCS SP2 UV confocal microscope were FITC excitation 488nm, emission 500 - 545 nm; TRITC excitation 543nm, emission 550 – 600 nm. Magnification was achieved using a x63 0.5 NA oil immersion lens. Data was analysed using LCS 2.6.1 software (Leica Microsystems, GmbH, Heidelberg).

Assays for Transporter Activity

Krebs' Buffer used in Transport and MTT assays

Krebs; mM: 137 NaCl, 5.4 KCl, 0.99 MgSO₄.7H₂O, 0.34 KH₂PO₄, 0.30 NaH₂PO₄.2H₂O, 10 Glucose, 10 HEPES, 2.8 CaCl₂.2H₂O made up to pH 7.4 with Tris base, at 37°C.

Assay Principles

The general principles of the fluorescence dye retention assays are summarized in Figure 2.1. Specific assays are described in individual sections. All concentrations of abamectin, emamectin benzoate and ivermectin used in the assays were calculated according to the molecular weights of the predominant B1a isoform.

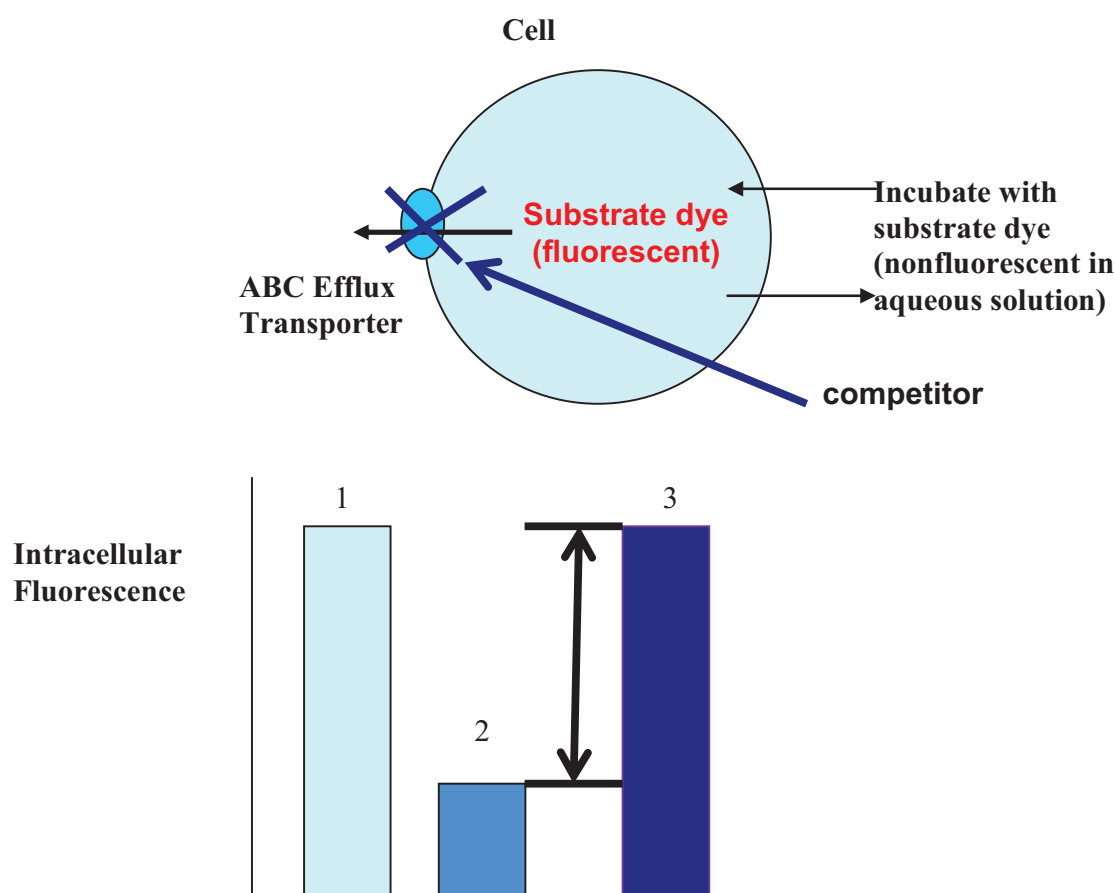


Figure 2.1 Principle of fluorescence dye efflux assays with substrate dyes H33342 for MDR1/mdr1 and BCRP/bcrp or CMFDA for MRP/mrp efflux transporters. In the absence of efflux transporters, dye diffuses through the cell membrane and establishes equilibrium. In an intracellular environment the dye becomes fluorescent, either by association with lipid (H33342; (Crissman & Steinkamp, 1987) or after cleavage by intracellular esterases and subsequent conjugation with glutathione (CMFDA; (Förster *et al.*, 2008) (1). In the presence of functional efflux transporters for which it is a substrate, fluorescent dye is actively effluxed and intracellular fluorescence decreases (2). With the introduction of a competitor, efflux of dye is reduced and intracellular fluorescence rises (3). Observed IC_{50} values are used to measure affinity of the receptor for the competitor.

H33342 Dye Retention Assay Background (Chapter 4)

The Hoechst 33342 dye retention assay was first used by Lalande, Ling and Miller (1981) as a flow cytometric assay, then used as an efflux assay by, among others, Goodell et al (1996) and Shapiro & Ling (1997). The Hoechst 33342 dye retention assay measures efflux activity by exploiting the affinity of Hoechst 33342 dye (Figure 2.3) for the “H”- binding site on MDR1 (Shapiro & Ling, 1997). This dye diffuses easily through cell membranes, and in a lipid-rich environment inside cells, H33342 becomes fluorescent with excitation spectral maxima at 333nm (free dye), 367nm (H33342-dsDNA complex) and 360nm (H33342-poly[A] DNA) and broad emission spectra with maxima at 457 nm (free dye), 460nm (H33342-dsDNA complex) to 495nm (H33342-poly[A] DNA; Kapunski J. 1990). In the absence of efflux transporters MDR1 and BCRP, for both of which H33342 is a substrate, it establishes equilibrium between inter- and extracellular environments (Figure 4.1). If MDR1 or BCRP are present, H33342 is also actively effluxed from the cell by these transporters, causing a drop in intracellular fluorescence levels. This efflux can be inhibited by the introduction of any agent that interferes with the efflux activity of the transporters, resulting in an increase in intracellular fluorescence, whether the agent inhibits ATPase activity, or is a substrate or blocker of the binding sites (Müller *et al*, 2007).

H33342 Dye Retention Assay Method (Chapter 4)

Cell monolayers grown on 96- well plates to 80-90% confluence were aspirated free from media and washed 2x in 200 μ L Krebs' buffer warmed to 37°C, pH 7.4. After removal of the final wash, 200 μ L of the appropriate experimental solution was applied to each well. The composition of the experimental solution is detailed in the appropriate figure; all solutions within each experiment, including the control, contained the same concentration of solvent, $\leq 0.3\%$. Monolayers were incubated in the experimental solution at 37°C, for 30 minutes, protected from light. After this period, the experimental solution was aspirated off and replaced with 200 μ l of the same solution, containing Hoechst 33342 at a final concentration detailed in the relevant figure legend. Cells were incubated with Hoechst 33342 at 37°C for 20 minutes in the absence of light, since 20 min was long enough for levels of intracellular H33342 to peak and plateau in two different cell lines (Morgan *et al*. 1989). At the end of this period, cell monolayers were washed 2x, in ice cold

Krebs' buffer. The final wash was aspirated and 200 μ l Krebs buffer added for reading of cell monolayers in 96-well plates in either a Dynex MFX Microplate Fluorimeter (Dynex Technologies, Chantilly, VA) or a FLUOstar Omega plate reader (BMG Labtech), according to instrument availability. Fluorescence reads for 96-well plates in the Dynatech instrument were excitation wavelength 355 ± 20 nm; emission wavelength 460 ± 20 nm and in the Omega instrument excitation 355 ± 5 nm; emission 480 ± 5 nm. These were chosen following a study by Latt and Stetten (1976); spectral maxima for free H33342 / H33342-DNA were, respectively ex 340/355 nm, em 510/465 nm.

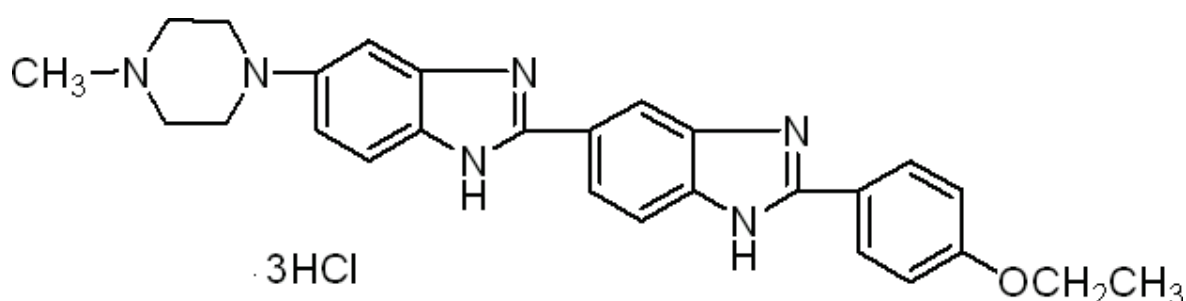


Figure 2.2 H33342 chemical structure (from Sigma-Aldrich website, product B2261).

The magnitude of the raw data obtained differed between instruments due to the differences in measurement parameters, i.e. halogen lamp in the Dynatech instrument versus xenon flash lamps in the Perkin-Elmer and Omega instruments, making it impossible to mean the raw data between experiments. See Figures 2.6 and 2.7 for a comparison of the same plate read in the Dynex and Omega fluorimeters; differences in signal magnitude between machines did not affect IC_{50} or K_i values obtained ($IC_{50} = 0.22 \pm 0.06 \mu\text{M}$ in Figure 2.5 and $0.20 \pm 0.04 \mu\text{M}$ in Figure 2.6). The magnitude of the signal, (V_{max}), is also dependent on the number of transporters present and therefore differed between experiments, but differences in V_{max} should have no influence on K_i which is a measure of dissociation constant of the transporter-inhibitor complex and is independent of both transporter density and of substrate concentrations used (<http://www.graphpad.com/curvefit/inhibitors.htm>). Experimental solutions containing CSA or avermectins at maximal exposure concentrations were read on the instruments; these controls did

not quench the fluorescence signal of 1 μ M H33342 compared to Krebs buffer as a background. All solutions contained vehicle (DMSO and/or methanol) to a final vehicle concentration $\leq 0.3\%$, at a consistent concentration within each experiment, to ensure that measured differences in intracellular fluorescence were due to the test compounds, rather than solvent.

H33342 dye retention assay data analysis

Data are expressed as mean \pm S.E.M., fitted to a non-linear least-squares regression curve (one-site binding, hyperbola) to generate IC₅₀ values. IC₅₀ values were converted to K_i values according to the Cheng and Prusoff method (Cheng and Prusoff, 1973) using Equation 2.1 given below and the mean H33342 EC₅₀ values for MDR1 and mdrla (Table 4.1). Statistical differences were tested using Student's unpaired t-test or a One-Way ANOVA with Dunnett's post-hoc test as appropriate. Statistical significance was assessed as or P < 0.05 or lower. Analysis was performed using Graphpad Prism 4 software (Graphpad, San Diego, CA, USA).

Adaptations to H33342 assay used in this study

The H33342 assay used in this study was decided with reference to Müller *et al* (2007) after observations in the current study that, with three wash steps to remove dye, cells were flushed off the surface of the well at the required confluence of >80%. Müller *et al* (2007) observed that the dye retention of Hoechst is comparable whether the dye is added after incubation with putative inhibitors, then washed off, or whether it is added to a background well without cells and the background fluorescence is subtracted from the reading in the well containing cells, omitting the wash steps. Since the neuroblastoma cells used in this study were relatively loosely attached and washed off easily, eliminating an extra wash step from the assay prevented the loss of cells, and was an advantage; therefore a compromise was adopted. In the current study cells were washed twice to remove FCS proteins present in complete media, pre-incubated with inhibitors, then 1 μ M H33342 was added for 20 min and washed off twice and the cell sample read, In contrast, in the original assay the cells are washed up to 3x and the inhibitor added with no dye, before H33342 dye is added and incubated, then a further 3 washes are performed (Müller *et al*. 2007; Goodell *et al* 1996). Removing a wash step did not significantly affect results in preliminary experiments in our laboratory and in experiments by Müller *et al*. (2007; Figure 2.3).

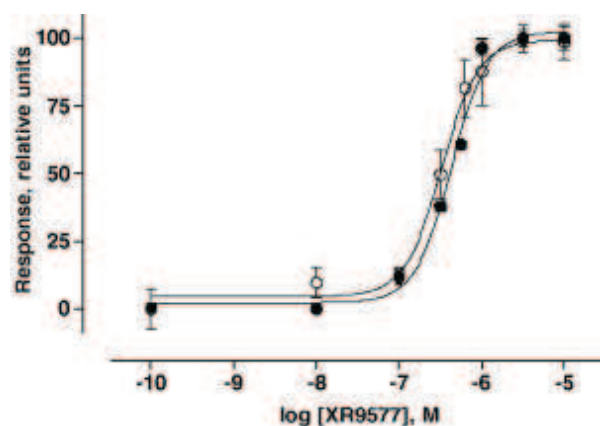


Figure 2.3 “ Concentration–response curves for XR9577 in A2780adr cells obtained with the standard Hoechst assay (open circles) and the new Hoechst assay (closed circles). In comparison to the standard Hoechst assay, the new Hoechst assay avoids three additional washing steps to remove extracellular Hoechst 33342. Data presented are average \pm SE from one typical experiment with three replicates belonging to a series of three independent experiments: standard assay: $pIC_{50} = 6.36 \pm 0.07$, $n_H = 2.27 \pm 0.26$, new assay: $pIC_{50} = 6.49 \pm 0.08$, $n_H = 1.96 \pm 0.53$ ”. Figure and legend from Müller *et al.*, (2007).

Measures of transporter affinity for H33342 in the dye retention assay

The assay chosen is a competition assay for binding of H33342 to transporters for efflux, with and without the presence of a competitor. The competitor used was either CSA or avermectin insecticides. The dye retention data was fitted to a One-site binding Hyperbola by nonlinear regression analyses and IC_{50} values were obtained. IC_{50} values give the concentration of competitor required to inhibit H33342 efflux by 50% of the maximum, and therefore cause 50% maximal increase in intracellular dye fluorescence. These results are better compared between different experiments as K_i (inhibition) values, which are measures of the affinity of the receptor for the competitor. K_i values account for differences in the affinity of the individual receptor for the substrate (in this case MDR1 and *mdr1a*) and also for differences in H33342 substrate concentration used throughout the test assays. Values representing the affinity of each transporter for H33342 are equilibrium dissociation constants, EC_{50} in Table 4.1 and equation 2.1 below. EC_{50} values give the concentration of H33342 substrate dye that resulted in 50% maximal increase in H33342 dye retention. K_i values were converted from IC_{50} values obtained for each competitor, using the Cheng & Prusoff equation (1973) (Equation 2.1 below).and Graphpad Prism’s online guide:

http://www.graphpad.com/curvefit/one_kind_of_receptor.htm.

$$K_i = \frac{IC_{50}}{1 + \frac{[ligand]}{EC_{50}}}$$

Equation 2.1 Cheng & Prusoff's equation (1973) for calculating K_i from EC_{50} values, to take account of differences in affinity for H33342 between transporters. EC_{50} values for each mdr1 receptor were taken from Table 4.1. EC_{50} is the concentration of substrate ligand required to produce 50% maximal increase in efflux transporter activity. IC_{50} is the concentration of inhibitor (for example, CSA or abamectin) required to inhibit this increase in efflux activity by 50%, and thus cause 50% maximal increase in intracellular fluorescence.

Inhibition of BCRP/bcrp- mediated H33342 efflux by KO-143

Although CSA is a known substrate for MDR1, at higher concentrations it can also interact with other transporters and in using it as an internal standard in these dye retention experiments, it was necessary to identify any BCRP-dependent efflux of H33342 for further investigation. For these experiments the BCRP-specific inhibitor KO-143 was used. It is routinely used at 0.1 μ M for effective BCRP inhibition; it has relatively high affinity for inhibition of BCRP, with 90% inhibition (EC_{90}) at approx. 25nM (Allen *et al.*, 2002). In this study it was tested over a concentration range 0-5 μ M, including 5 μ M CSA as standard to compare MDR1 activity.

CMFDA Assay Background (Chapter 5)

CMFDA, 5-chloromethylfluorescein-diacetate, is a non-fluorescent, lipophilic derivative of fluorescein, which easily permeates across the cell membrane (Figure 2.4). Inside the cells it is cleaved by unspecific esterases forming the fluorescent intermediate 5-chloromethylfluorescein (CMF). CMF is hydrophilic and exhibits a very slow permeation across cell membranes. In a second step, the chloromethyl group reacts with intracellular thiol groups, predominantly glutathione. Glutathione methylfluorescein, GSMF, is produced, which is much more hydrophilic. GSMF is a substrate for MRP2 and is actively excreted out of the cells. Interactions of test-compounds with MRP2 result in an increased intracellular fluorescence intensity (Förster *et al.*, 2008).

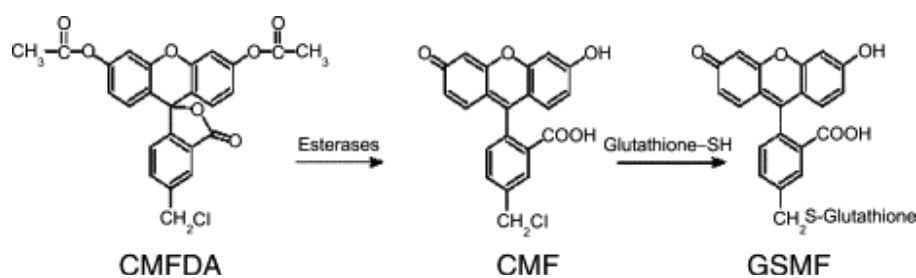


Figure 2.4 Conversion of CMFDA to a fluorescent MRP/mrp substrate by esterases and conjugation with glutathione inside cells. Taken from Forster *et al.*, (2008).

Unlike H33342, the chemical conversion of CMFDA and rapid excretion of GSMF means that intracellular fluorescence decays within a relatively short time period after CMFDA exposure; approx. 30 min (Forster *et al.* 2008). This two-step conversion process might explain why the relationship between CMFDA concentration and intracellular fluorescence was linear over the concentration ranges tested (0 - 1.5 μ M in this study; 0 -10 μ M by others in our laboratory), unlike for H33342 (0 -15 μ M) where intracellular fluorescence had begun to plateau by 10 μ M.

CMFDA Retention Assay Method (Chapter 5)

Cell monolayers grown on 96 well plates to 80-90% confluence were aspirated free from media and washed 2-3 times in Krebs' buffer warmed to 37°C, pH7.4. After removal of the final wash, 200 μ l of the appropriate experimental solution was applied to each well. The composition of the experimental solution is detailed in the appropriate figure. Monolayers were incubated in the experimental solution at 37°C, for 30 minutes, protected from light. After this period, the experimental solution was aspirated off and replaced with 200 μ l of the same solution, containing CMFDA at a final concentration detailed in the relevant figure legend. Cells were incubated with CMFDA at 37°C for 30 minutes in the absence of light. At the end of this period, cell monolayers were washed 3 times, in ice cold Krebs' buffer. The final wash was aspirated and 200 μ l Krebs buffer added for reading of cell monolayers in 96-well plates in a FLUOstar Omega plate reader (BMG Labtech, Aylesbury, UK), Fluorescence reads for CMFDA in the Omega instrument were excitation 480nm \pm 5nm emission 520nm \pm 5nm. The gain was set at the beginning of each experiment for the plate where highest fluorescence was expected and then

kept constant throughout the experiment. The gain was consistently set to 4500 ± 250 units throughout all experiments. All experimental solutions were read on the instrument compared to water background and did not quench the fluorescence signal. All solutions contained vehicle (DMSO and/or methanol) to a final vehicle concentration $\leq 0.3\%$, at a consistent concentration within each experiment, to ensure that measured differences in intracellular fluorescence were due to the test compounds, rather than solvent.

CMFDA dye retention assay data analysis

The readings for cells without dye were subtracted from the raw data and these data were normalised to the average of readings for the solvent control, which was taken to be 100%. Control (100%) was then subtracted and the data were expressed as % increase above control. An analysis with nonlinear least squares regression (One-site binding, Hyperbola) was performed on Graphpad Prism 4 software up to $6 \mu\text{M}$ concentration of the avermectins. Above $6 \mu\text{M}$ there was a consistent drop-off in intracellular fluorescence for all three avermectins tested, which is attributed to cellular toxicity at 7 and $10 \mu\text{M}$ (See Chapter 6). Hence these concentrations were excluded from the analysis, and the V_{max} value of curves was constrained to 20% above the highest mean value, in order to define the plateau of the curve and obtain IC_{50} values. It was not possible to convert IC_{50} values for experiments with CMFDA to K_i values, since EC_{50} values for CMFDA were not obtainable due to the linear relationship between CMFDA concentration and intracellular fluorescence of GSMF.

MTT Assay Background (Chapter 6)

The MTT assay was initially described by Mossman in 1983 as a method of assessing cell viability after exposure to potential toxins. MTT (3-[4,5-dimethylthiazol-2-yl]-2,5-diphenyltetrazolium bromide) is a water soluble tetrazolium salt, which is converted to an insoluble purple formazan by cleavage of the tetrazolium ring by succinate dehydrogenase within the mitochondria. The formazan product is impermeable to the cell membranes and therefore it accumulates in healthy cells (Fotakis and Timbrell, 2006). The spectral maximum of the formazan salt is altered in the presence of media, so Denizot and Lang (1986) proposed the use of phenol red-free media for incubation, and removal of the media before reading the absorbance

of formazan produced. The current study avoids this change in spectral maxima altogether, since incubation for both the transporter and MTT assays can be performed in Krebs buffer. MTT conversion was found to be one of the more sensitive assays after short incubations of 3, 5 and 8 hours (Fotakis and Timbrell, 2006) and it is also suitable to perform in situ where the cells are grown, with the solubilisation of formazan taking place at the end of the assay. As such, the MTT assay was chosen as a suitable assay of gross changes in cell proliferation after avermectin exposure.

MTT Assay Method (Chapter 6)

Cell monolayers at 80-90% confluence were aspirated free from growth media, and the monolayers were washed twice with 200 μ l Krebs' buffer for 96 well plates. (Krebs; mM: 137 NaCl, 5.4 KCl, 0.99 MgSO₄.7H₂O, 0.34 KH₂.PO₄, 0.30 NaH₂PO₄.2H₂O, 10 Glucose, 10 Hepes, 2.8 CaCl₂.2H₂O made up to pH 7.4 with Tris base, at 37°C) To initiate the MTT assay, Krebs' buffer was removed from each well and replaced with experimental solutions dissolved in warm Krebs' buffer; either 200 μ l of experimental solution (96 well plates) or 1000 μ l of experimental solution (24 well plates). Details of the experimental solutions are outlined in the appropriate figure legends. All control solutions included the appropriate amount of vehicle (DMSO and/or methanol). Total vehicle concentration never exceeded 0.3%. Monolayers were incubated with test reagents for 1 hour at 37°C in the absence of light.

At the end of this period, the experimental solutions were aspirated and replaced with either 100 μ l (for 96 well plates) or 750 μ l (for 24 well plates) of a 1mM MTT solution made up in warm Krebs buffer. Monolayers were then incubated in the presence of the MTT at 37°C, for 2 hours in the absence of light.

After 2 hours, the MTT solution was aspirated off, and replaced with either 100 μ l (for 96 well plates) or 250 μ l (for 24 well plates) 100% isopropanol (propan-2-ol). Plates were incubated on a shaker for 15 minutes. The formazan product, solubilized by the incubation with isopropanol, was quantified at 570 nm using a Dynatech MR5000 plate reader.

MTT cell proliferation assay data analysis

Data are mean \pm S.E.M. of $n = 24$ expressed as % control where solvent control = 100% and analysed by One-Way ANOVA with Dunnett's post-hoc test as above. Statistical significance was assessed as $P < 0.05$.

Neurite Outgrowth Studies with N2a Cells (Chapter 6)

To measure neurite outgrowth N2a cells were grown on poly-L- lysine coated cover slips in 6 well plates. Polyglycine coated coverslips were prepared by sterilising glass coverslips with 70% ethanol. After the ethanol evaporated off the coverslips, 200 μ l polyglycine was added to each well containing a cover slip and allowed to evaporate off. Cover slips were then gently washed with 200 μ l PBS. Coverslips were then seeded with N2a cells at a density of 40,000 cells/ well and allowed to adhere to the cover slip overnight. After this the cell media was replaced and the cells grown to approx 50-60% confluence. At this point the growth media was removed and induction media was added (DMEM containing 2mM L-glutamine, 1mM pyruvate, 0.1v/v NEAA and 0.3mM cAMP) for 24 hours or 48 hours. Induction media arrested cell proliferation and induced differentiation to neurite-expressing cells.

To test the impact of test agents on neurite outgrowth, cells were incubated with the agent under test for 1hr at 37⁰C in induction media. At the end of the test period, the media was removed, the cells were rinsed once with 1x PBS and fixed with 0.5ml/well of 100% methanol for 20 mins at -20⁰C. To visualise neurite outgrowth, microtubules were stained using mouse monoclonal anti-acetylated tubulin primary antibody (Sigma, Poole, UK) and Alexa Fluor[®] 488 rabbit anti-mouse IgG (Invitrogen). Nuclei were visualised using propidium iodide to stain the DNA.

After cells were lysed with 100% methanol at -20⁰C, the cells were incubated for 1 hour in the presence of 5% BSA to block non specific binding. Cells were then washed three times with PBS-Tween buffer before being incubated with the primary antibody, mouse monoclonal anti acetylated tubulin antibody (1:1000, Sigma) The primary antibody solution was removed after 1 hour and cells were washed with PBS-T 3x with intervals of 10 minutes for 30 minutes. Cells were then exposed to the secondary antibody, 20 μ g/ml Alexa Fluor[®] 488 rabbit anti-mouse IgG

fluorescein isothiocyanate (FITC) for 1.5 hours. The secondary antibody solution was removed and the cells washed 3x in PBS-Tween buffer. Propidium Iodide staining was carried out for 30 seconds at 1µg/ml diluted in PBS tween. Coverslips were then washed 3x in PBS-tween and mounted on glass slides using Vectashield (Vector Laboratories, Burlingame, CA) sealed with nail varnish and stored at -20°C overnight.

Visualisation of neurites

2-3 fields per treatment were scanned with a Leica TCS SP2 UV confocal microscope using a 63x 0.5 NA lens and 2CS 2.5 software (Leica Microsystems, GmbH, Heidelberg). An argon (488nm) laser was used to excite FITC. Emissions between 510-550nm were collected (FITC peak is 520nm). In experiments to assess the impact of avermectins upon neurite outgrowth, hydrogen peroxide at 0.1mM for 15 minutes was used a positive control for complete inhibition of neural outgrowth in N2a cells.

SH-SY5Y cells were not suitable for neurite outgrowth analysis as they produced highly branched neurites after incubation with cAMP (data not shown).

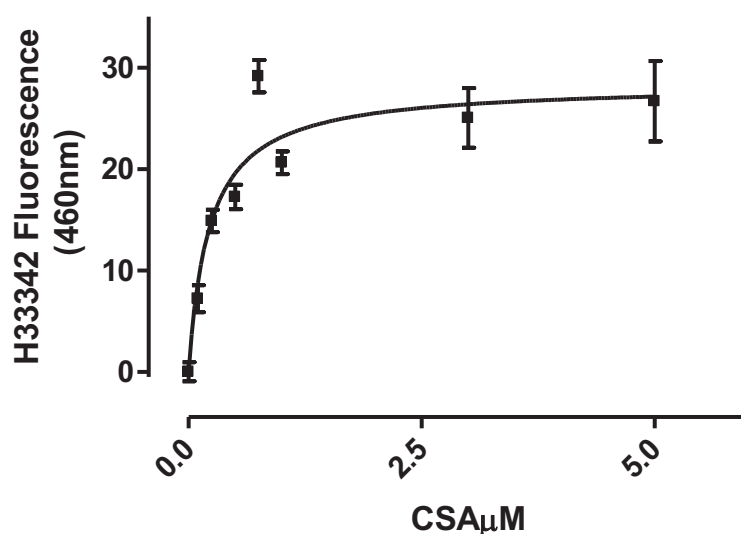


Figure 2.5 Dose-response curve to CSA (0 – 5 μM) in N2a cells to compare reads between machines with H33342 dye kept constant at 1 μM , read in MRX Fluorimeter. Data expressed as mean \pm S.E.M. of 6 wells per concentration in a single experiment. Data were analysed with nonlinear least squares regression analysis. IC_{50} in the above experiment is $0.22 \pm 0.06 \mu\text{M}$.

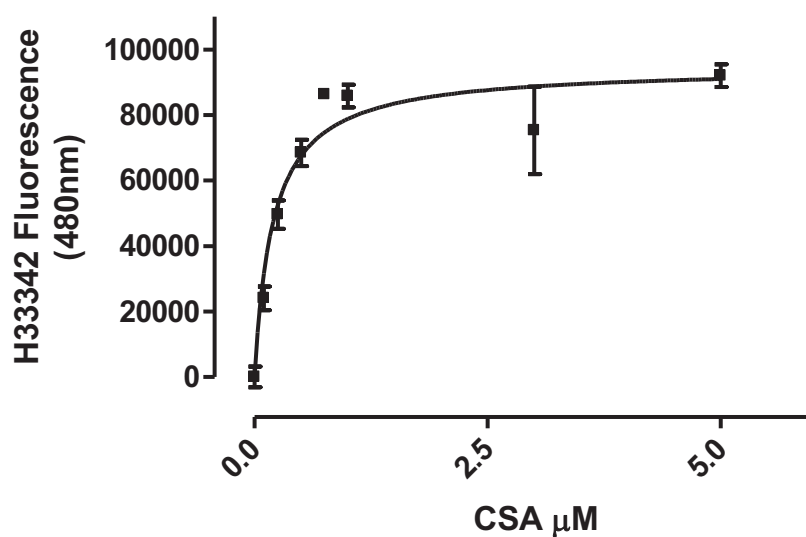


Figure 2.6 Dose-response curve to CSA (0 – 5 μM) in N2a cells to compare reads between machines with H33342 dye kept constant at 1 μM , read in BMG Labtech Omega Multifunction Fluorimeter. Data expressed as mean \pm S.E.M. of 6 wells per concentration in a single experiment. Data were analysed with nonlinear least squares regression analysis. IC_{50} in the above experiment is $0.20 \pm 0.04 \mu\text{M}$.

Chapter 3 Efflux transporter mRNA and protein expression in SH-SY5Y and N2a cells

3.1 Summary

This section of work aims to verify the selected cell lines as models for studying the effects of avermectin exposure by characterising efflux transporter mRNA and protein expression.

- I. SH-SY5Y cells were analysed for uptake- and efflux- transporter mRNA expression by PCR array, and found to express a panel of transporters similar to cells of the human blood-brain barrier and nigrostriatal tract, including the efflux transporters MDR1, MDR6 (a mitochondrial transporter), MRP1, MRP4 and MRP5, but the fluorescence signal for BCRP was not detected above background levels.
- II. In end-point PCR and real time qPCR assays over 3 independent passages, SH-SY5Y cells expressed mRNA for MDR1 and MRP1, but signals for BCRP were not detected above background levels.
- III. In end point PCR, N2a cells expressed mRNA for *mdr1a* but not *bcrp*.
- IV. At the protein level, SH-SY5Y cells immunostained positive for expression of the MDR1 protein with the anti-human MDR1 monoclonal antibody MRK-16 but did not stain for BCRP using the anti BCRP/*bcrp* antibody BXP-21.
- V. N2a cells immunostained stained positive for the presence of *mdr1* protein with MRK-16 but not C219 but did not express *bcrp* as ascertained with the antibody BXP-21.

3.2 Introduction

Role of transporters in protection from neurotoxicity

The efflux transporters MDR1 and *mdr1a* are important in protecting the human and mouse brain, respectively, from toxin exposure. Schinkel et al. demonstrated the essential role of *mdr1* in protection from ivermectin exposure in 1994 with *mdr1a/b* (-/-) mice, who were much more susceptible to ivermectin toxicity than control mice, developing up to 60% higher ivermectin concentrations in the brain. *Mdr1a/b* knockout mice also accumulated higher concentrations of substrates such as vinblastine and digoxin (Schinkel et al. 1994). BCRP/

bcrp is also expressed at the human and mouse blood-brain barrier, along with MRP 1, 2, 4 and 5 (Klaassen & Aleksunes, 2010 Review). Bcrp and mdrla appear to have overlapping substrates, since bcrp expression is up-regulated 3-fold in the brain of mdrla^{-/-} mice (Cisternino *et al.* 2004). Mrp1 is the most highly expressed multidrug resistance protein transporter in mouse brain, whereas MRP5 is one of the most highly expressed mRNAs in human brain (Klaassen & Aleksunes, 2010 Review). MRP5 transports both endogenous substrates such as cAMP, cGMP and folate (McAleer *et al.*, 1999), as well as the anti-cancer drug methotrexate (Wijnholds *et al.* 2000).

In mice, important uptake transporters include oct3 and oat3. Oct3 null mice exhibit more susceptibility to sodium depletion (Vialou *et al.*, 2004). Also, oct3 null mice accumulate higher concentrations of extracellular dopamine in the brain and are more susceptible to striatal nerve damage after methamphetamine dosing (Cui *et al.* 2009 & Klaassen & Aleksunes, 2010 Review). Oat3 takes up xenobiotics from cerebrospinal fluid to the choroid plexus epithelium, and oat3 null mice accumulate lower concentrations of its substrate fluorescein (Sweet *et al.* 2002).

The aim of this part of the study was to identify suitable model cell lines to compare the impact of CNS exposure to pesticides in mouse and man. To do this it was necessary to ascertain which transporters are expressed in SH-SY5Y and N2a cells, and how closely transporter expression in the cell lines resembles that of physiological tissue in the blood-brain barrier and neurons within the brain.

3.3 Methods

RNA extractions and PCR

For control RNA extractions, cells were grown to subconfluence and total RNA was extracted from three independent passages of each cell line after 6-7 days' growth in SH-SY5Y cells and 4-5 days' growth in N2a cells. Samples were reverse transcribed to cDNA as described in methods and end-point PCR was performed with appropriate primers (see Appendix) to check for successful reverse transcription and presence of the target product MDR1/ mdrla. Since cDNA is transcribed from mRNA and is therefore without introns, the two are equivalent, so the cDNA samples directly carry the "message" of expressed mRNA.

Primers were designed and verified using Invitrogen online primer design software and checked for specificity against sequences on the NCBI database. All positive control PCR products used in real-time PCR were identified from end-point PCR products by sequencing and alignment with their respective mRNA sequences on the NCBI database <http://blast.ncbi.nlm.nih.gov/Blast.cgi> (data not shown).

Protein expression

To investigate protein expression, cells were grown to 70-80% confluence on coverslips as described in methods Chapter 2, then fixed and treated with appropriate primary and secondary antibodies and phalloidin counterstain of the actin cytoskeleton. Fixed and treated cells were always visualized within 48 hours to avoid decay of the fluorescent signal.

3.4 Results

To identify and quantitate the expression of MDR1 and other important transporters from messenger RNA, 2 strategies were employed. Two total RNA samples from independent passages of SH-SY5Y cells were applied to a preset real-time PCR array panel of 84 human drug transporters from SABiosciences. A similar panel for the mouse N2a cells was not available. These samples were subsequently analysed for the expression mRNA of key efflux transporters by end point PCR then qPCR.

qPCR Array

Figure 3.1 is a series of bar graphs with expression levels of transporters expressed in SH-SY5Y cells above background levels as detected in the qPCR array. Figure 3.1 A shows that, of the ABC binding cassette transporters, mRNA for MDR1 was expressed at the highest level, along with MDR6, which is expressed within the cell, on the mitochondrial membrane (Krishnamurthy *et al.* 2006). MRP1, MRP4 and MRP5 mRNA were also expressed. Figure 3.1 G shows ABC transporters with an expression level below ($2^{-\Delta Ct}$) = 0.002 including MDR3, MRP3 and MRP6, but BCRP mRNA was not detected above threshold levels. Other notable ABC transporters expressed in both passages above background levels in SH-SY5Y cells are ABCD3 and ABCA12.

Of drug-transporting members of the SLC family of uptake transporters, including the OAT and OATP series, SLC16A1, SLC19A2, SLC29A2, SLC38A2, SLC3A1, SLC7A6, SLC7A7 and GLUT1 (SLC2A1) mRNAs are expressed above background levels (Figures 3.1B (higher level expression) and 3.1H (low level expression). Of the OATs, only OAT4 is expressed at a low level (Figure 3.1H), whereas OATP1A2, OATP3A1 and OATP4A1 are all expressed above background levels (Figure 3.1C). Table 3.1 summarises transporter mRNAs expressed in the SH-SY5Y cells and how these compare with transporters found at the blood-brain barrier or intracerebral neurons.

Constitutive efflux transporter expression in SH-SY5Y and N2a cells

Using total RNA samples isolated from cells under normal growing conditions, the expression of the key efflux transporters MDR1, MRP1 and BCRP were further assayed in both cell lines, initially by end-point PCR and then by quantitative real-time PCR (qPCR).

Figure 3.2 is a representative gel showing the results of end point PCR for MDR1 performed on the reverse-transcribed RNA samples from 5 independent extractions of total RNA from SH-SY5Y cells, at an annealing temperature of 58°C, showing that mRNA for MDR1 was expressed in all reverse transcribed samples at the expected product size of 82bp. The identity of the end-point product of the MDR1 primers was confirmed by sequencing (data not shown).

Figure 3.3 is a representative gel showing the results of end point PCR for *mdr1a* performed on the reverse-transcribed RNA samples from 8 independent extractions of total RNA from N2a cells, at an annealing temperature of 55°C, showing that mRNA for *mdr1a* was expressed in all reverse transcribed samples at the expected product size of 87bp. The identity of the end-point product of the *mdr1a* primers was confirmed by sequencing (data not shown). Figure 3.4A shows the results of end-point PCR assays performed with a positive cDNA sample from MDCKII-*bcrp* cells, and a *bcrp*-negative N2a sample, and Figure 3.4B shows a positive sample for *gapdh*, from mouse N2a- derived mRNA. Thus, both the *bcrp* and *gapdh* primers work in end-point PCR. The identity of the *bcrp* product was confirmed by sequencing.

Independent qPCR assays

SH-SY5Y human cells

The reverse transcribed control SH-SY5Y cDNA samples from 3 separate passages were assayed by qPCR using the BCRP, MDR1 and MRP1 primers, using DNA clones of the target product as positive controls (Summarised in Table 3.1). Samples were compared to GAPDH expression in parallel. In contrast to the MDR1, MRP1 and GAPDH samples, where the Ct values for positive samples are clearly lower than those of the negatives and the melting temperatures of the samples match the positive controls closely, the BCRP sample products returned high C_t values from 37.62-40.00, which did not differ from the negative controls at 37.66-40.00. In contrast the BCRP clone was successfully detected over its standard curve, returning a consistent melting temperature of 75.81. The BCRP product is not expressed above background levels, confirming the PCR array data.

In contrast, mRNA for MDR1 and MRP1 are expressed consistently over the three passages tested in qPCR assays. These data have been expressed in Figure 3.5 (MDR1) and Figure 3.6 (MRP1) as arbitrary concentration units normalized to GAPDH concentration. The Ct reading for each product was applied to a standard curve dilution series of 5 from DNA clones of the respective PCR products to generate concentration units. It should be emphasized that, since the arbitrary concentration values calculated depend on the absolute DNA concentration of each original clone, the absolute units for MDR1 are not comparable to those for MRP1; the expression of MRP1 is not definitively higher than MDR1, although the clones were diluted in the same way. Messenger RNA for both MDR1 and MRP1 is expressed consistently over all three control passages tested.

N2a mouse cells

Similar qPCR assays were conducted for the N2a samples with cDNA samples reverse transcribed on 2 independent occasions, using the primers from end-point PCR (Table 3.3). Samples assayed for *mdr1a* returned Ct values that did not differ from negative controls (24.61-26.90 versus 23.94 and 29.45, respectively). The same was true for the corresponding *gapdh* assay, so this qPCR was unsuccessful.

Protein Expression of MDR1/mdr1a and BCRP/bcrp

Figure 3.7 A and B show live unfixed SH-SY5Y and N2a cells respectively, at x63 magnification, their plasma membranes stained with FITC-conjugated wheatgerm agglutinin to show what the cells look like growing as a sub-confluent monolayer. Wheatgerm agglutinin binds to cell membranes via oligosaccharides containing terminal N-acetylglucosamine or chitobiose, structures which are common to many serum and membrane glycoproteins (Vector Labs product information) without fixation, making it a convenient way to visualize the cells in a state representative of that in which the antibody staining and transport assays were performed.

MDR1 and mdr1 expression

Figure 3.8 confirms expression of MDR1 protein in SH-SY5Y cells after fixation in 3% paraformaldehyde and staining with the anti-MDR1 antibody MRK-16 (1:50) and AlexaFluor488-conjugated rabbit anti-mouse IgG (1:250) since the fluorescence of secondary antibody bound to primary (A) is above the level of background control without the primary antibody (C). The actin cytoskeleton of cells is counterstained by phalloidin (1:450, B and D).

MRK-16 was supposed to be human-specific and would not stain mouse *mdr1* according to the product information, so the MDR1/*mdr1* monoclonal antibody C219 was used as an alternative to stain N2a cells, since it had been used with success, albeit at relatively high concentrations (1:10 or 1:20), to stain mouse and human *mdr1* and MDR1 proteins (Thiebaut et al. 1987).

Figure 3.9 shows the results of staining N2a cells with C219 antibody (1:20) and AlexaFluor 488-conjugated rabbit anti-mouse IgG (1:250) secondary. In this case there was no visible difference between the primary staining (A) and background control (C). Therefore MRK-16 staining was used with on the mouse cells. Although there was a high level of non-specific background staining (Figure 3.10 C), at a 1:20 dilution MRK-16 returns brighter fluorescence than control, indicating expression of *mdr1* protein in N2a cells (Figure 3.10A). This ties in with the positive end-point PCR results for *mdr1a*.

BCRP and bcrp expression

Human and mouse BCRP were detected with the antibody BXP-21, reported to be active against BCRP/bcrp protein from both species. Since it was expected that the two cell lines may be negative for BCRP and bcrp protein, following the PCR results, it was necessary to confirm the reactivity of the anti-BCRP/bcrp antibody chosen. To do this, MDCK-BCRP cells were stained with BXP-21 (Figure 3.11). Figure 3.11A shows that, at a 1:50 dilution, BXP-21 stained cells show much brighter fluorescence than the background control (Figure 3.11 C).

Figure 3.12A shows SH-SY5Y cells treated with anti-BCRP antibody BXP-21 (1:20) and AlexaFluor488-conjugated rabbit anti-mouse IgG (1:200) plus phalloidin (1:450). The fluorescence level of the BXP-21 stained cells appears very slightly above background control, suggestive of potentially very low level BCRP protein expression, however this would contradict the qPCR results and also, in Chapter 4, the transport assay data. It is concluded that BCRP protein is expressed at a negligible level in SH-SY5Y cells. It is also noted that 1:20 is a very high dilution of the primary antibody to use and some non-specific binding may be expected.

N2a cells were likewise stained with BXP21 (1:20), shown in Figure 3.13 (A). In accord with the findings for mRNA expression, fluorescent signal for BCRP protein was not detected above the signal for no primary antibody control (C).

3.5 Discussion**Expression of human drug transporters in qPCR array**

The expression of MDR1 and MDR6 in SH-SY5Y cells corresponds to transporters situated on the cell membrane (Shapiro and Ling, 1997) and mitochondria (Krishnamurthy *et al.* 2006), respectively. The protein expression of MDR1 and MRP1 co-localized with mRNA detected in the PCR array. This data parallels results from an identical PCR array performed on the human blood-brain barrier cell line hCMEC/D3, which is a lentivirus-mediated co-transfect of hTERT (human telomerase catalytic unit) and the SV40 T antigen of primary isolated human brain endothelial cells (Carl *et al.* 2010). The hCMEC/D3 cell line is considered a potential model of the blood brain barrier since it retains functional

characteristics of the human BBB including expression of MDR1, MRP1 and BCRP (Carl *et al.* 2010), similar to SH-SY5Y cells except for the lack of BCRP expression in the latter. BCRP is however a key transporter at the blood brain barrier (Carl *et al.* 2010; Klaassen and Aleksunes, 2010) and has been shown to interact with CSA (Gupta *et al.* 2006). Further to the qPCR array results, there was expression of MDR1 and MRP1 in SH-SY5Y cells and *mdr1a* in N2a cells. In contrast, BCRP was absent. The potential of BCRP to influence avermectin pesticide distribution needs to be investigated independently, therefore, and the hCMEC/D3 cell line is a good prospect.

With regard to other key transporters expressed in SH-SY5Y cells, the following have been identified:

ABCD3 encodes a dimeric half-transporter responsible for import of fatty acids and fatty acyl-CoAs into the intracellular peroxisome (<http://www.ncbi.nlm.nih.gov/gene/5825>). ABCA12 is implicated in lipid transport; mutations in the gene are associated with the congenital skin disorder Harlequin Ichthyosis (Kelsell *et al.* 2005).

SLC16A1 is a monocarboxylate transporter responsible for the transfer of pyruvate and lactate across the plasma membrane. SLC16A2 encodes a transporter of thyroid hormones T3 and T4 and is essential to sufficiency of thyroid function (<http://www.ncbi.nlm.nih.gov/gene/6567>).

SLC19A2 is a high affinity thiamine transporter, mutations in which are associated with thiamine deficiency disorder Roger's syndrome (Guerrini *et al.* 2005). SLC38A2 codes for a high affinity glutamine transporter in neurons within the brain (Blot *et al.* 2009).

SLC3A1 is an activator of cysteine, dibasic and neutral amino acid transport expressed in the intestine and renal tissue. Mutations are associated with cysteinuria, and several splice variants have been identified whose function is unknown (NCBI Gene database –updated 27.08.2011)

The SLC7A6 gene codes for a heterodimeric amino acid transporter known as y(+)LAT2, implicated in the release of arginine from a wide variety of cell types in brain, heart, testis, kidney, small intestine and parotis (Bröer *et al.* 2000).

The human Blood-Brain barrier cell line hCMEC/D3 has a very similar expression profile to the SH-SY5Y cells; it is noted that OCT1, OCT2 and OAT1-4 were not detected (Carl *et al.* 2010), and only OAT4 was detected at low level in SH-SY5Y cells. OAT4 undertakes sodium-dependent excretion of toxic organic anions, mainly in the placenta (NCBI Gene

database), so its low-level expression in neuronal cell types is unexpected. This could be because the origin of the parent cells of SH-SY5Y was not brain but bone marrow (Ross *et al.* 1983).

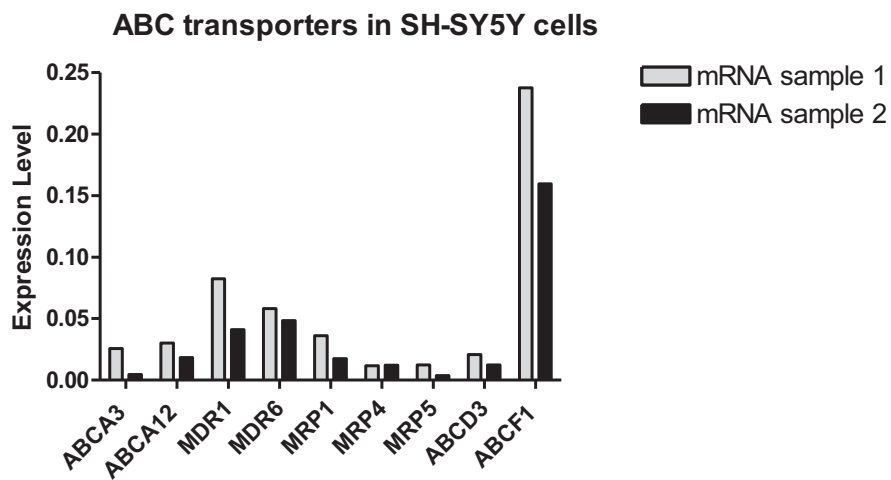
Expression of efflux transporter proteins in SH-SY5Y and N2a cells

Evidence for MDR1/ *mdr1a* and BCRP/*bcrp* mRNA expression is borne out by the protein staining, confirming that SH-SY5Y cells express MDR1 protein but not BCRP. N2a cells likewise express mRNA for *mdr1a* and *mdr1* protein but not *bcrp* as ascertained with BXP-21. Utilisation of the BCRP-transfected MDCKII-BCRP cell line confirmed that the BXP-21 antibody successfully detected the presence of human BCRP.

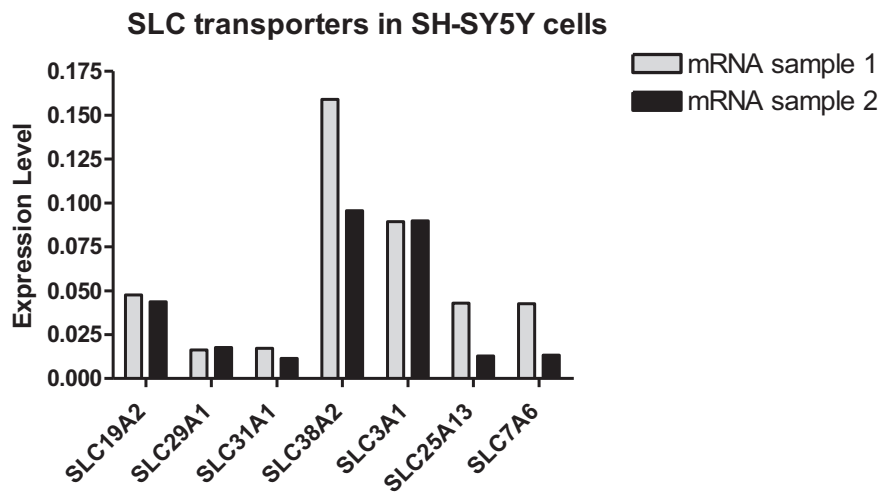
MRK-16 has been used to identify MDR1 distribution in human tissues (Thiebaut *et al.* 1987) and both MRK-16 and C219 were used with success to visualize the localization of *mdr1* in primary and secondary cultures of rat astrocytes (Ronaldson *et al.* 2004). MRK-16 was used at a 1:300 dilution, however, and C219 as high as 1:10. The fact that C219 needed to be so concentrated to obtain cell labelling is interesting and correlates with the lack of C219 cell staining at a 1:20 dilution in this study in mouse N2a cells. It worth noting that C219 returned a clear band in Western Blot at a dilution of 1:100 in the same study (Ronaldson *et al.* 2004) and may simply be unsuitable for immunocytochemistry.

The evidence for expression of MRP transporters in SH-SY5Y cells is strong, both from the qPCR array and from the independent qPCR assays with primers designed for MRP1. It is still necessary to confirm the expression of MRP proteins as appropriate antibodies were not available during these studies.

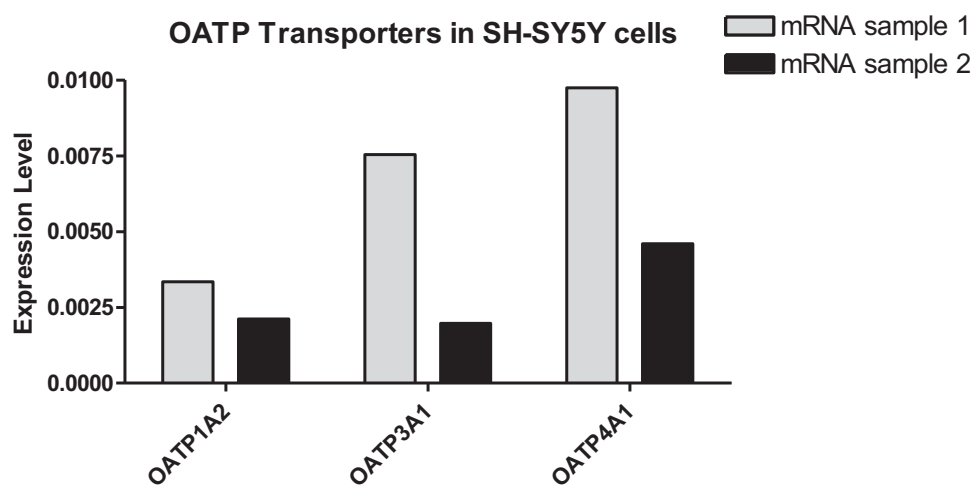
3.1A



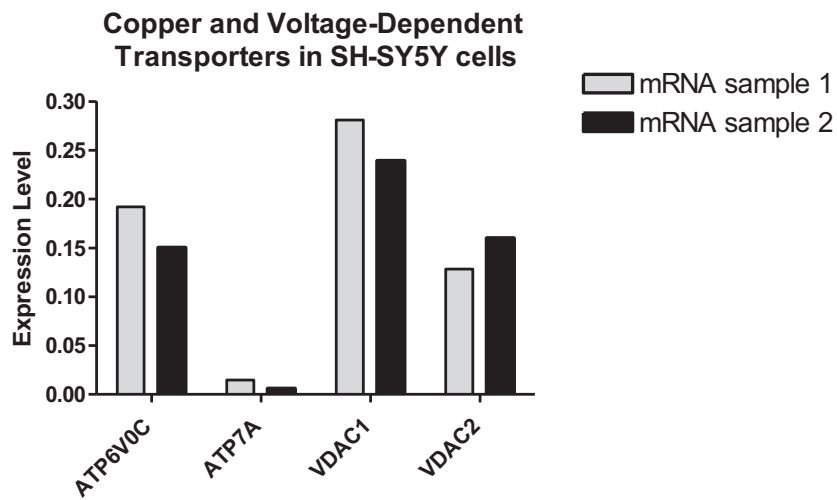
3.1 B



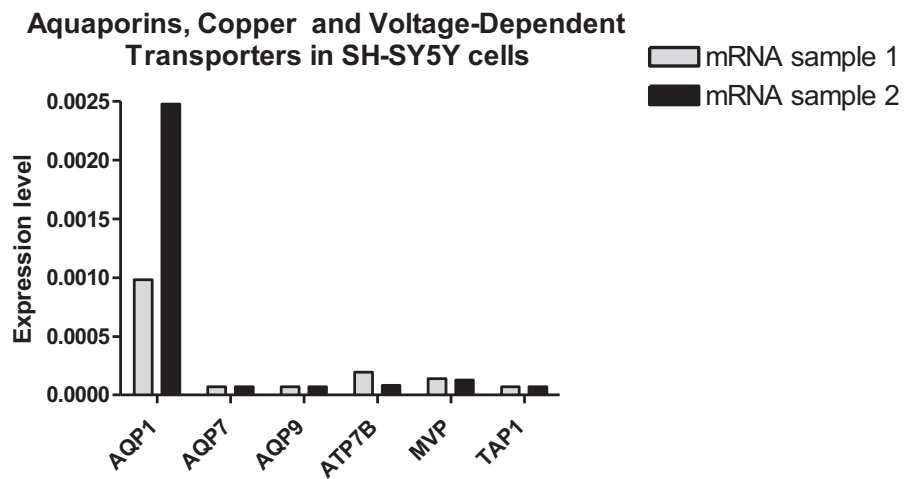
3.1 C



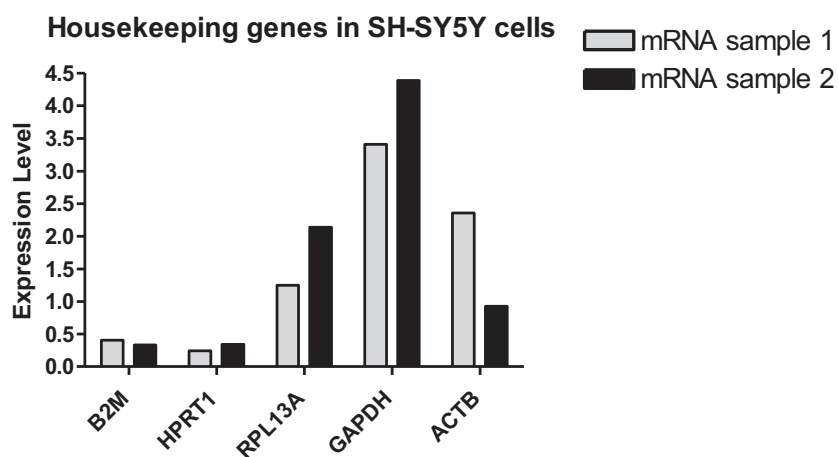
3.1 D



3.1 E



3.1 F



3.1 G

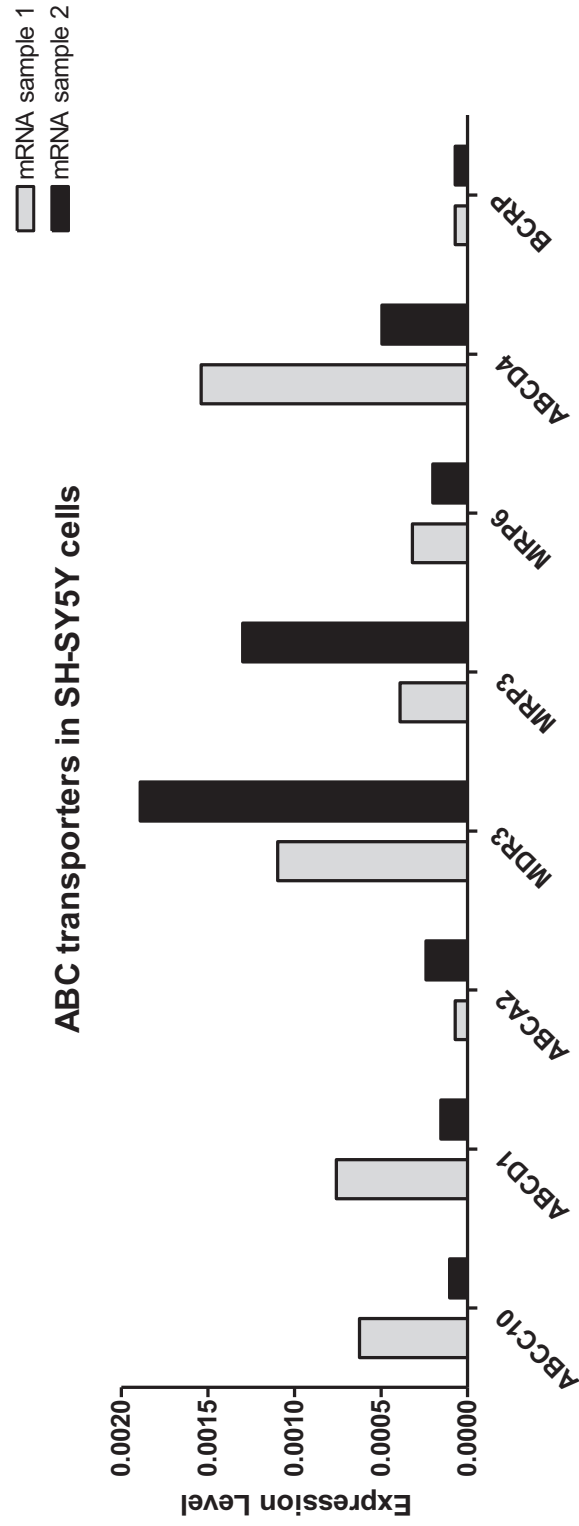


Figure 3.1 SH-SY5Y Drug Transporter qPCR Array.

SH-SY5Y total RNA samples were analysed by qPCR array for expression of mRNA for 84 different drug transporters plus housekeeping genes. Expression levels for transporter whose expression was detected above Ct 35, and housekeeping genes are given in Figure 3.1 A-H below. RNA samples from two independent passages were assayed, and results obtained from <http://www.sabiosciences.com/pcrarraydataanalysis.php> as expression levels ($2^{-\Delta Ct}$). A) ABC transporters with mRNA expressed above ($2^{-\Delta Ct}$) = 0.010; B) SLC transporters with mRNA expressed above ($2^{-\Delta Ct}$) = 0.010; C) SLCO transporters with mRNA expressed above ($2^{-\Delta Ct}$) = 0.0010; D) Copper- and voltage-dependent transporters with mRNA expressed above ($2^{-\Delta Ct}$) = 0.010; E) Aquaporins and voltage-dependent transporters with mRNA expressed below ($2^{-\Delta Ct}$) = 0.0025; F) Housekeeping genes; G) ABC transporters with mRNA expressed below ($2^{-\Delta Ct}$) = 0.0020 H) SLC transporters with mRNA expressed below ($2^{-\Delta Ct}$) = 0.0060.

3.1 H

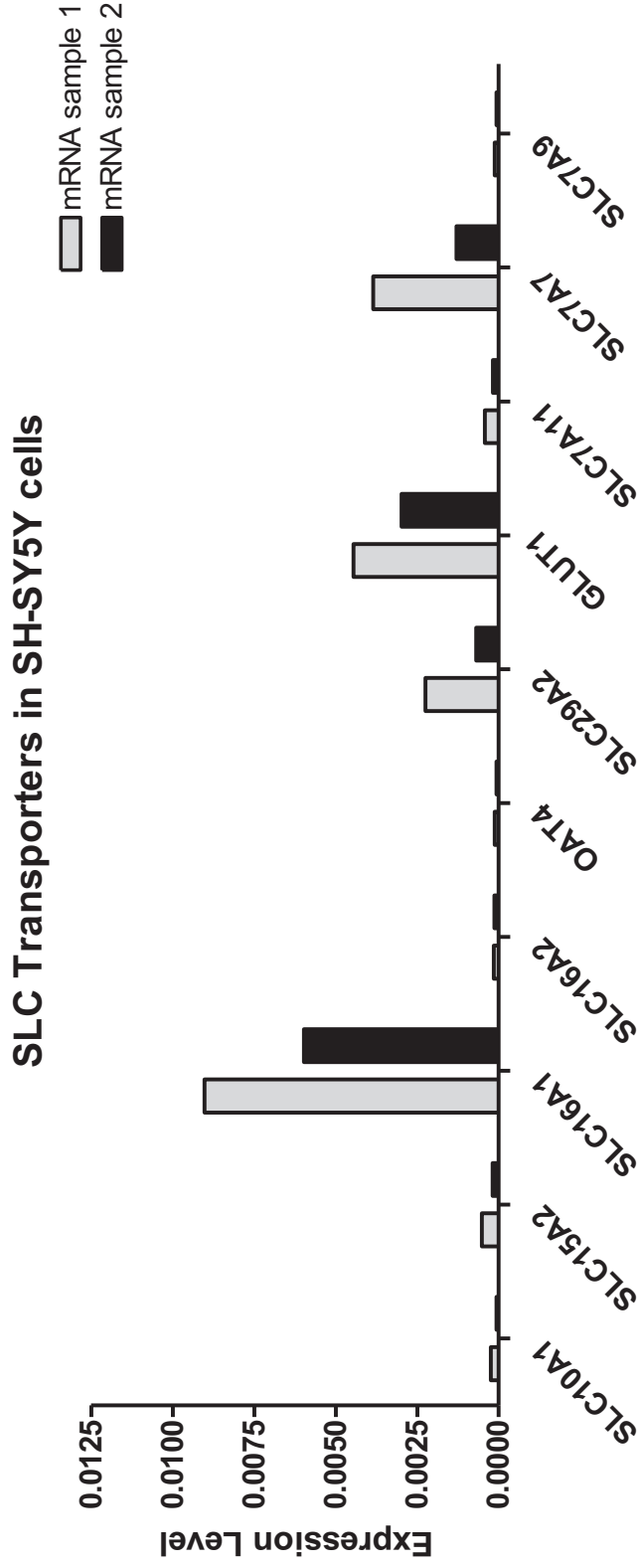


Figure 3.1 SH-SY5Y Drug Transporter qPCR Array.

SH-SY5Y total RNA samples were analysed by qPCR array for expression of mRNA for 84 different drug transporters plus housekeeping genes. Expression levels for transporter whose expression was detected above Ct 35, and housekeeping genes are given in Figure 3.1 A-H below. RNA samples from two independent passages were assayed, and results obtained from <http://www.sabiosciences.com/pcrarraydataanalysis.php> as expression levels ($2^{-\Delta Ct}$). A) ABC transporters with mRNA expressed above ($2^{-\Delta Ct}$) = 0.010; B) SLC transporters with mRNA expressed above ($2^{-\Delta Ct}$) = 0.010; C) SLCO transporters with mRNA expressed above ($2^{-\Delta Ct}$) = 0.0010; D) Copper- and voltage-dependent transporters with mRNA expressed above ($2^{-\Delta Ct}$) = 0.010; E) Aquaporins and voltage-dependent transporters with mRNA expressed below ($2^{-\Delta Ct}$) = 0.0025; F) Housekeeping genes; G) ABC transporters with mRNA expressed below ($2^{-\Delta Ct}$) = 0.0020 H) SLC transporters with mRNA expressed below ($2^{-\Delta Ct}$) = 0.0060.

Table 3.1 (A) Summary of Drug Transporters in SH-SY5Y cells, CNS Neurons and the Human Blood-Brain Barrier.

Expression of mRNA for key drug uptake and efflux transporters in SH-SY5Y cells obtained by PCR array compared to human CNS neurons and human Blood-Brain Barrier as reported in the literature. ND = not detected.

PCR product	SH-SY5Y cells	CNS neurons	Blood-Brain Barrier
MDR1	Present	Present	Present
MDR6	Present	ND	ND
MRP1	Present	Present	Present
MRP2	ND	Present	Present
MRP3	Present	Present	ND
MRP4	Present	ND	Present
MRP5	Present	Present	Present
MRP6	ND	ND	Present
OAT1	ND	Present	ND
OAT2	ND	ND	ND
OAT3	ND	Present	ND
OAT4	Present	Present	ND

Table 3.1 (B) Summary of Drug Transporters in SH-SY5Y cells, CNS Neurons and the Human Blood-Brain Barrier.

Expression of mRNA for key drug uptake and efflux transporters in SH-SY5Y cells obtained by PCR array compared to human CNS neurons and human Blood-Brain Barrier as reported in the literature. ND= not detected.

PCR product	SH-SY5Y cells	CNS neurons	Blood-Brain Barrier
OCT1	ND	ND	ND
OCT2	ND	ND	ND
OCT3	ND	ND	ND
OATP1A2	Present	ND	Present
OATP1B1	ND	ND	ND
OATP1B3	ND	ND	ND
OATP2A1	ND	ND	ND
OATP2B1	ND	Present	Present
OATP3A1	Present	Present	Present
OATP4A1	Present	Present	Present

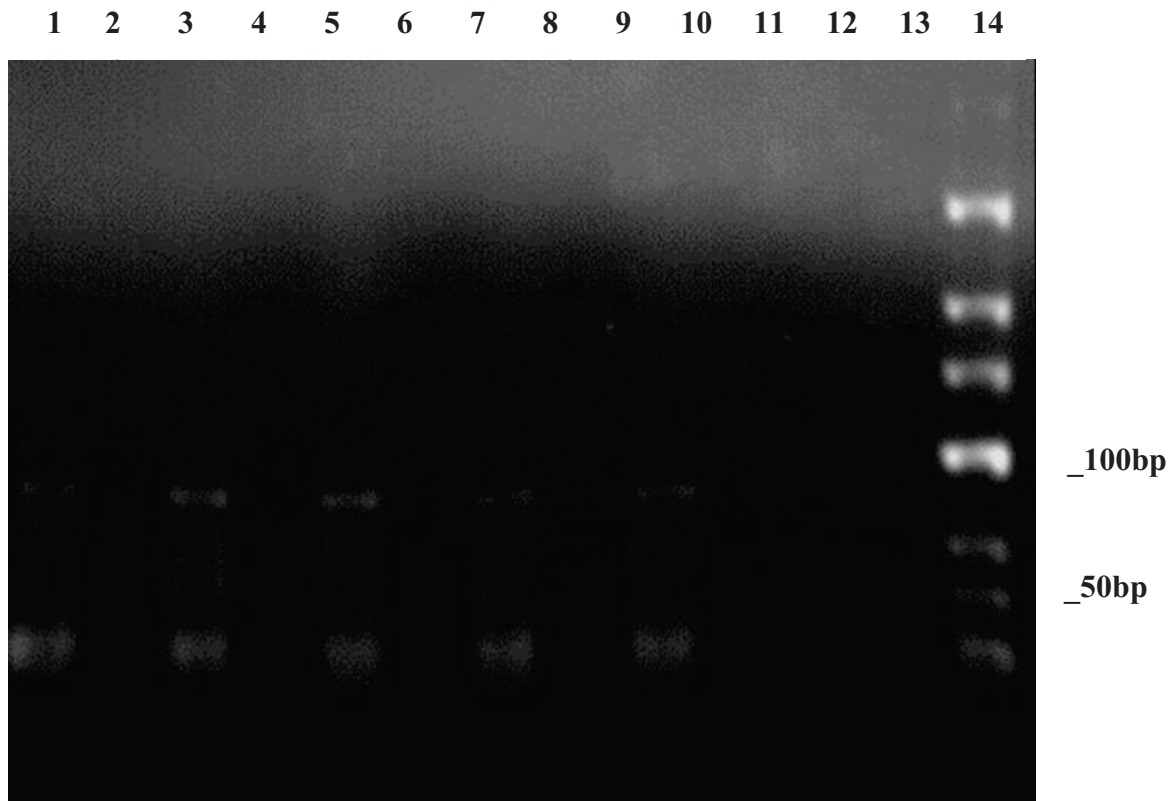


Figure 3.2 End point PCR of SH-SY5Y RNA samples expressing MDR1.

Total RNA Samples 1-5 from 5 independent passages of SH-SY5Y cells were reverse transcribed to cDNA and end-point PCR was performed with MDR1 forward and reverse primers with an annealing temperature of 58°C (see appendix for sequences). The expected product size was 82bp and the product identity was confirmed by sequencing (data not shown). Products were run on a 1% agarose gel in 1 x TBE at 120V for approximately 1 hour, with the expected PCR product alongside the RT enzyme negative control, expected blank (RT Negative). The second diffuse “band” at approx. 25bp is most likely a front of the loading gel. **Lanes:** 1 = Sample 1; 2 = Sample 1 RT negative; 3 = Sample 2; 4 = Sample 2 RT negative; 5 = Sample 3; 6 = Sample 3 RT negative; 7 = Sample 4; 8 = Sample 4 RT negative; 9 = Sample 5; 10 = Sample 5 RT negative; 11 = water blank; 12 = empty; 13 = empty; 14 = 100-1000bp marker.

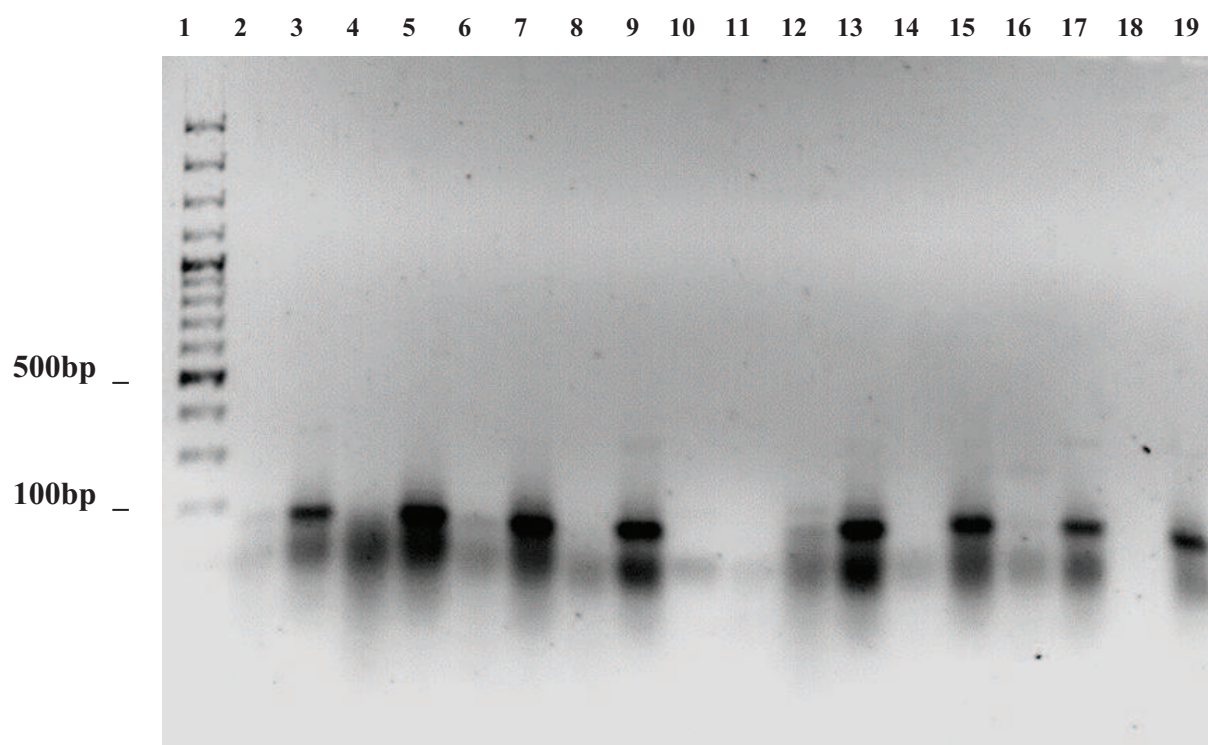


Figure 3.3 End point PCR of N2a RNA samples expressing *mdr1a*.

Total RNA Samples 1-8 from 8 independent passages of N2a cells were reverse transcribed to cDNA and end-point PCR was performed with *mdr1a* forward and reverse primers with an annealing temperature of 55°C (see appendix for sequences). Products were run on a 1% agarose gel in 1 x TBE at 120V for approximately 1 hour. The expected product size was 87bp and the product identity was confirmed by sequencing (data not shown). The additional bands running ahead are due to overloading. The sample product (expected 87bp) was run alongside the RT enzyme negative control (expected blank). **Lanes:** 1 = 1000bp marker; 2 = Sample 1 RT negative; 3 = Sample 1; 4 = Sample 2 RT negative; 5 = Sample 2; 6 = Sample 3 RT negative; 7 = Sample 3; 8 = Sample 4 RT negative; 9 = Sample 4; 10 = water blank; 11 = empty; 12 = Sample 5 RT negative; 13 = Sample 5; 14 = Sample 6 RT negative; 15 = Sample 6; 16 = Sample 7 RT negative; 17 = Sample 7; 18 = Sample 8 RT negative; 19 = Sample 8.

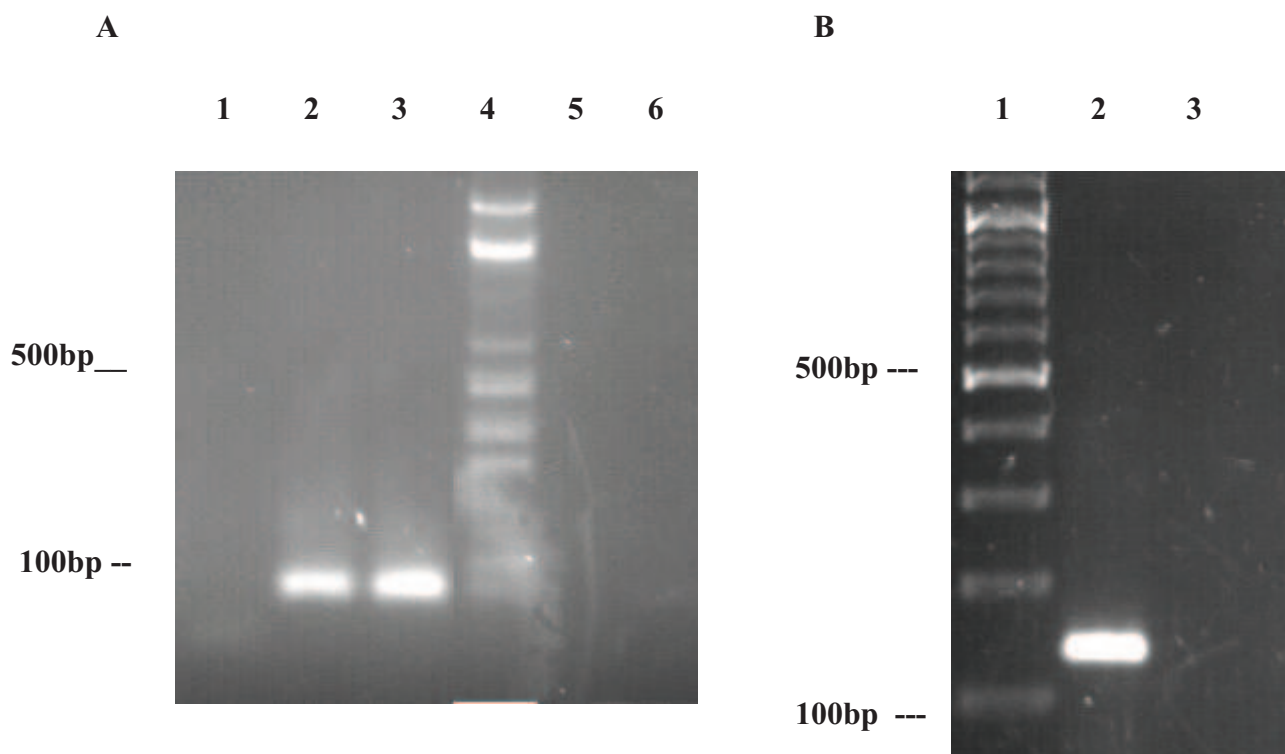


Figure 3.4 (A) End-point PCR for mouse *bcrp* with cDNA from MDCKII-*bcrp* cells and N2a cells.

Expected product size = 86bp. Figure 3.4A shows the results of end-point PCR assays performed with 2 positive cDNA samples from separate passages of MDCKII-*bcrp* cells, confirmed by sequencing (Lanes 2, 3), and a *bcrp*-negative N2a sample (Lane 6). RT negative (lane 5) is a no-enzyme RT control, expected blank. This data confirms that the mouse *bcrp* primers are functional in end-point PCR, detecting the correct mouse *bcrp* product from *bcrp*-expressing cells, and that mouse N2a cells do not express this product in end-point PCR. See appendix for *bcrp* primer sequence. Lane 1 = water blank; 2 = MDCKII-*bcrp* sample 1; 3 = MDCKII-*bcrp* sample 2; 4 = DNA Ladder; 5 = N2a sample 1 RT negative; 6 = N2a sample 1 cDNA.

Figure 3.4 (B) End-point PCR for mouse *gapdh* with cDNA from mouse N2a cells.

Expected product size = 140bp using SABiosciences mouse primers for *gapdh*. Lane 1 = 1000bp DNA ladder; 2 = mouse *gapdh*-positive sample from mRNA isolated from N2a cells; 3 = N2a RT negative control, expected blank. As expected, mRNA for *gapdh* was expressed in the mouse sample therefore the chosen *gapdh* primers are functional in end-point PCR.

Table 3.2 Expression of mRNA BCRP, MDR1, MRP1 and GAPDH in SH-SY5Y cells.

Total RNA samples 1-3 from 3 independent passages of SH-SY5Y cells were assayed by real-time qPCR. The end-point PCR product from each primer set was verified by sequencing (data not shown). Each sample was assayed in triplicate and Ct values for samples have been subtracted from the Ct value for the negative control (NTC) which controlled for the presence of genomic DNA, to give mean delta Ct values. “Positive” melting temperatures of the cloned PCR products are given as comparison to sample T_m. Where the sample product is the same as the clone, the melting temperatures should match. Expression of the GAPDH housekeeping gene was assayed to verify cDNA input quantity.

	Sample	C _t			T _m	positive T _m	NTC C _t	NTC T _m	delta C _t			Mean _d C _t	S.E.M.	n
		38.75	40.00	37.63					37.63	40.00	77.50			
human BCRP	1	38.75	40.00	37.63	77.50	75.81	37.66	75.95	-1.09	-2.34	0.03	-1.13	0.68	3
	2	40.00	40.00	40.00	77.49		40.00	77.93	0.00	0.00	0.00	0.00	0.00	3
	3	37.87	37.62	37.82	75.95		40.00	78.03	2.13	2.38	2.18	2.23	0.06	3
human MDR1	1	21.76	21.71	21.49	79.58	79.49	35.21	80.38	13.45	13.50	13.72	13.56	0.07	3
	2	25.47	25.42	26.27	79.84		40.00	76.66	14.53	14.58	13.73	14.28	0.25	3
	3	24.92	25.04	26.00	79.02		32.60	79.31	7.68	7.56	6.60	7.28	0.29	3
human MRP1	1	22.62	22.45	22.73	87.86	87.90	31.42	81.28	8.80	8.97	8.69	8.82	0.08	3
	2	25.89	25.95	25.90	87.50		32.56	83.76	6.67	6.61	6.66	6.65	0.02	3
	3	24.49	24.46	24.70	87.29		36.16	78.08	11.67	11.70	11.46	11.61	0.07	3
human GAPDH	1	17.57	16.98	17.72	84.12	84.08	32.03	82.68	14.46	15.05	14.31	14.61	0.21	3
	2	20.13	20.93	20.77	84.09		36.50	79.75	16.37	15.57	15.73	15.89	0.09	3
	3	20.02	19.77	19.47	83.58		30.05	83.78	10.03	10.28	10.58	10.30	0.10	3

Table 3.3 Messenger RNA expression of mdr1a and gapdh in mouse N2a cells.

RNA from 5 independent passages of N2a cells was reverse transcribed to cDNA was assayed using mdr1a and gapdh primers detailed in the appendix. The primers used were the same as those in end-point PCR, above (Figures 3.3-3.4). The identity of the mdr1a primer products were verified by sequencing, and the mouse gapdh primer set had been designed and verified by SABiosciences. Each sample was assayed in triplicate and Ct values for samples have been subtracted from the Ct value for the negative control (NTC) which controlled for the presence of genomic DNA, to give mean delta Ct values. "Positive" melting temperatures of the cloned PCR products are given as comparison to sample T_m. Where the sample product is the same as the clone, the melting temperatures should match. Expression of the GAPDH housekeeping gene was assayed to verify cDNA input quantity. Mouse mdr1a or gapdh were not detected above background in 2 separate assays.

	C _t		T _m			positive T _m	positive C _t	NTC C _t	NTC T _m	delta C _t		Mean	SEM	n	
mouse mdr1a	35.71	ND	79.77	ND	ND	80.62	20.47 21.01	34.99	80.12	-0.72	ND			3	
	34.52	33.70	79.73	81.32	80.78			34.25	81.11	-0.27	0.55	0.82	0.37	0.33	3
	34.11	34.72	80.32	80.40	81.86			40.00	84.66	5.89	5.28	5.54	5.57	0.18	3
	35.53	34.57	80.36	82.24	ND			40.00	79.84	4.47	5.43	ND			3
	38.80	34.19	80.13	80.46	ND			34.65	79.73	-4.15	0.46	ND			3
mouse gapdh	40.00	40.00	85.90	87.91	83.18	85.82	9.22	36.16	85.76	-3.84	-3.84	-3.84	0.00	3	
	40.00	40.00	85.69	78.82	79.52			35.54	86.10	-4.46	-4.46	-3.90	-4.27	0.19	3
	36.93	36.68	87.06	85.98	78.82			40.00	79.86	3.07	3.32	2.69	3.03	0.18	3
	36.93	40.00	86.04	83.63	80.11			34.85	85.75	-2.08	-5.15	-5.15	-4.13	1.02	3
	40.00	40.00	84.31	87.25	81.47			39.10	88.71	-0.90	-0.90	-0.90	-0.90	<0.01	3

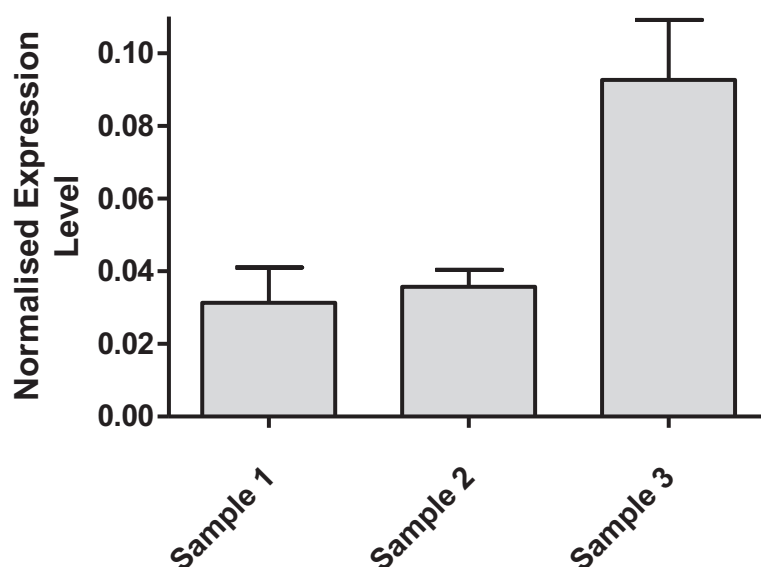


Figure 3.5 Expression of mRNA for MDR1 from total RNA of SH-SY5Y cells.

Data shows MDR1 mRNA concentrations normalised to those of GAPDH, derived from the raw Ct data given in Table 3.2 and read off a standard curve from clones of GAPDH and MDR1. Samples 1-3 are from 3 independent passages of cells and each sample was assayed in triplicate.

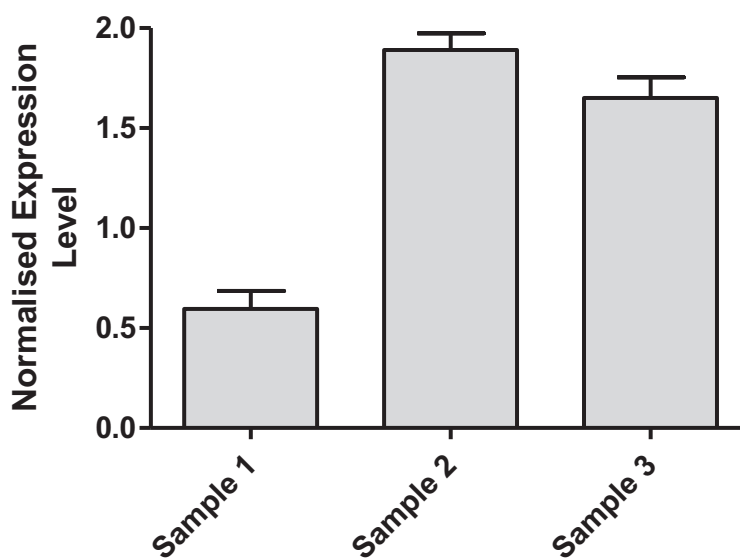


Figure 3.6 Expression of mRNA for MRP1 in SH-SY5Y cells.

Data shows MRP1 mRNA concentrations normalised to those of GAPDH, derived from the raw Ct data given in Table 3.2 and read off a standard curve from clones of GAPDH and MRP1. Samples 1-3 are from 3 independent passages of cells and each sample was assayed in triplicate.

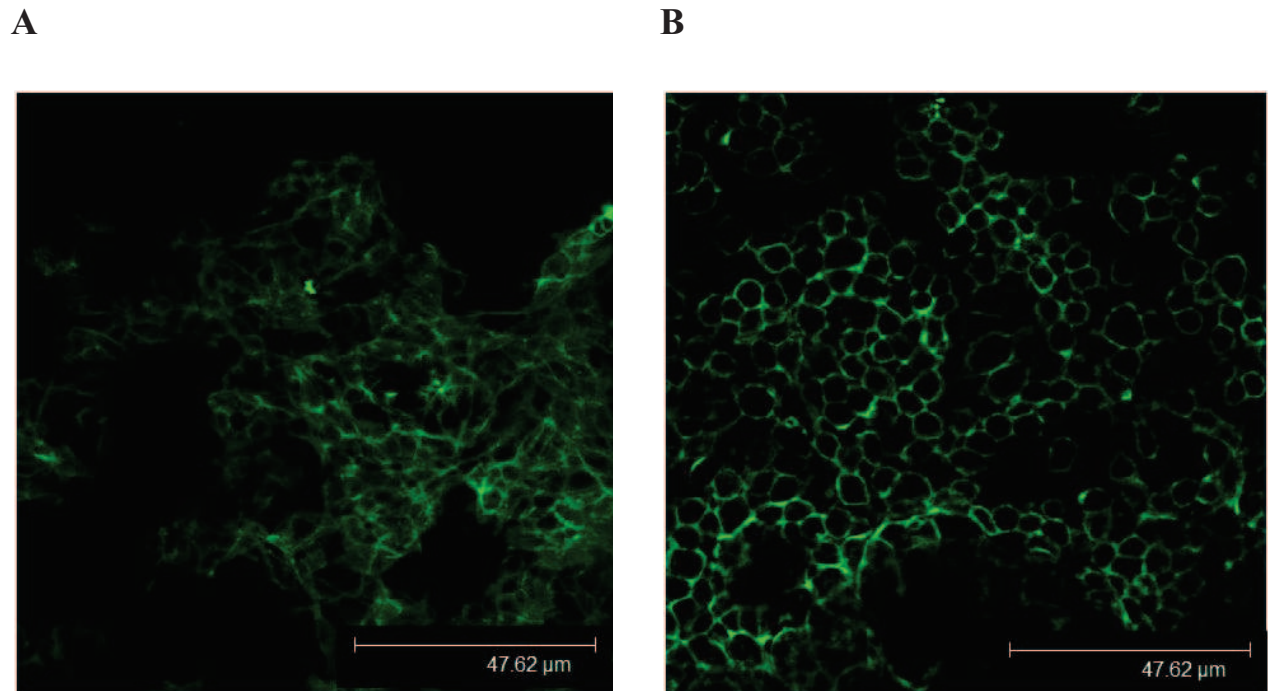


Figure 3.7 SH-SY5Y and N2a cells grown as an 80% confluent monolayer.

(A) SH-SY5Y cells and (B) N2a cells, both live and unfixed, were stained with fluorescein-conjugated wheatgerm agglutinin (1:250) and viewed under a Leica Confocal microscope at x63 magnification. Wheatgerm agglutinin binds to cell membranes via oligosaccharides containing terminal N-acetylglucosamine or chitobiose, structures which are common to many serum and membrane glycoproteins (Vector Labs product information). The field chosen is representative of at least 3 different fields of view for each cell line.

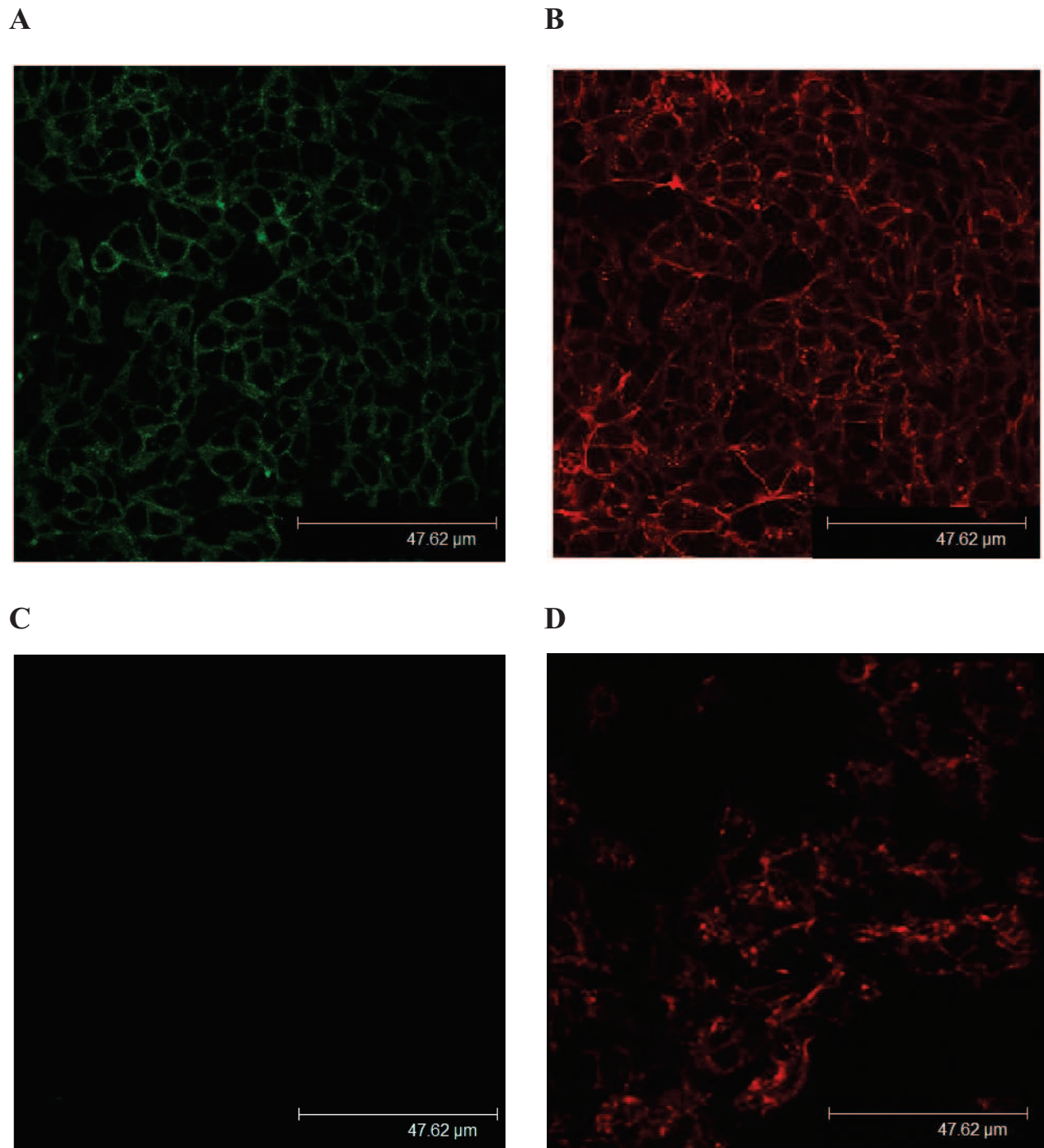


Figure 3.8 SH-SY5Y cells stained for MDR1 protein with MRK-16 antibody.

SH-SY5Y cells, shown at x63 magnification, were fixed in 3% PFA, permeabilised in 0.1% Triton X-100 and stained for MDR1 protein with (A) MRK-16 anti-MDR1 monoclonal primary antibody (1:50) and AlexaFluor488 conjugated rabbit anti-mouse IgG secondary antibody (1:250) and (C) no primary antibody control. The actin cytoskeleton is counterstained with phalloidin at 1:450 dilution ((B) and (D)). The field chosen is representative of at least 3 similar fields of view in each case. Cell samples from 3 separate passages were stained and visualised to confirm MDR1 expression status.

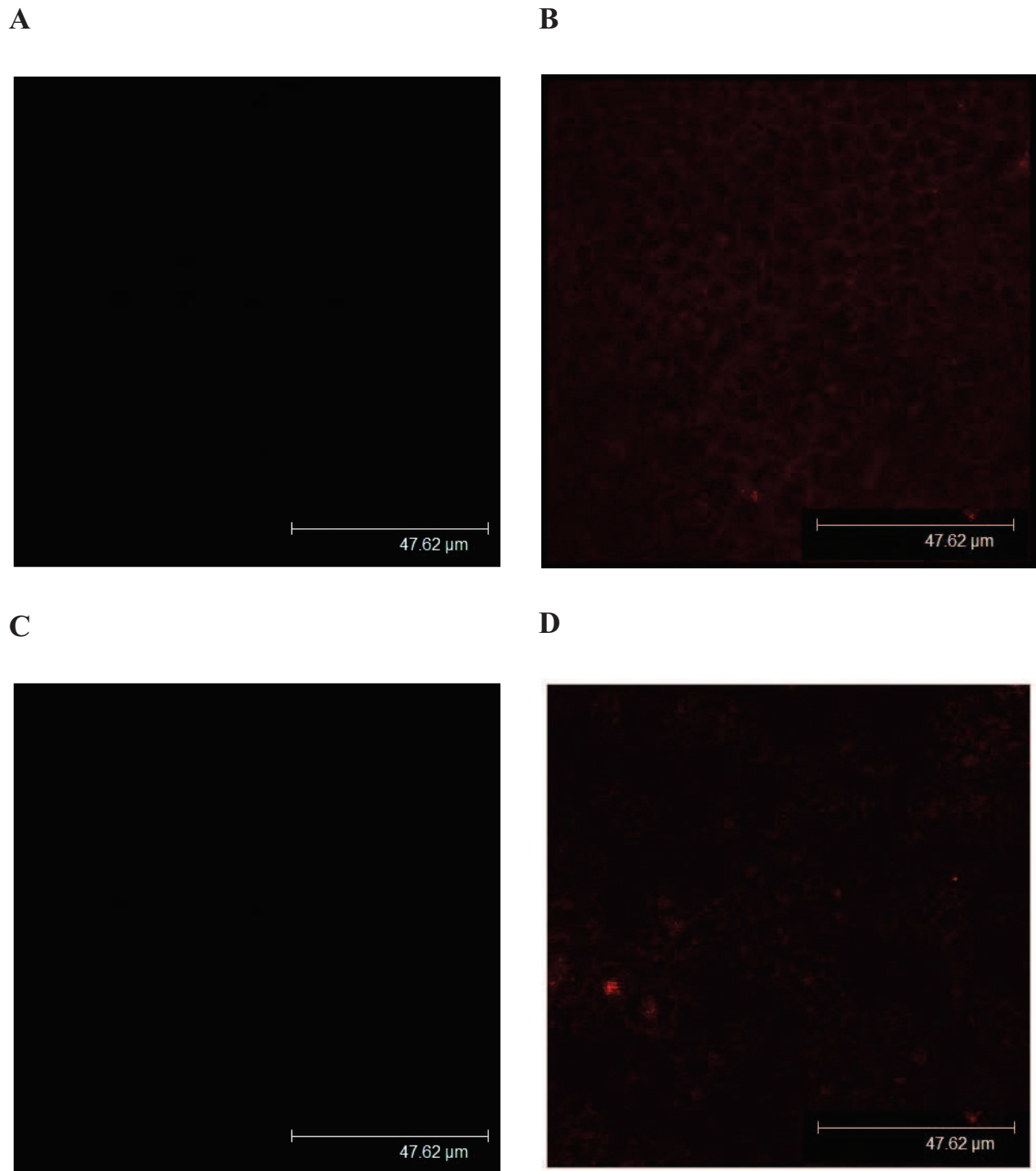


Figure 3.9 N2a cells stained for mdr1 protein with C219 antibody.

N2a cells, shown at x63 magnification, were fixed and permeabilised in 100% methanol, then stained for mdr1 protein with (A) C219 anti-mdr1 monoclonal primary antibody (1:20) and Alexa-Fluor488 conjugated rabbit anti-mouse IgG secondary antibody (1:250) and (C) no primary antibody control. The actin cytoskeleton of the cells is counterstained with red phalloidin at 1:450 dilution, (B) and (D). The field chosen is representative of at least 3 similar fields of view in each case. Cell samples from 3 separate passages were stained and visualised to confirm mdr1 expression status. C219 antibody at 1:20 did not stain N2a cells for mdr1.

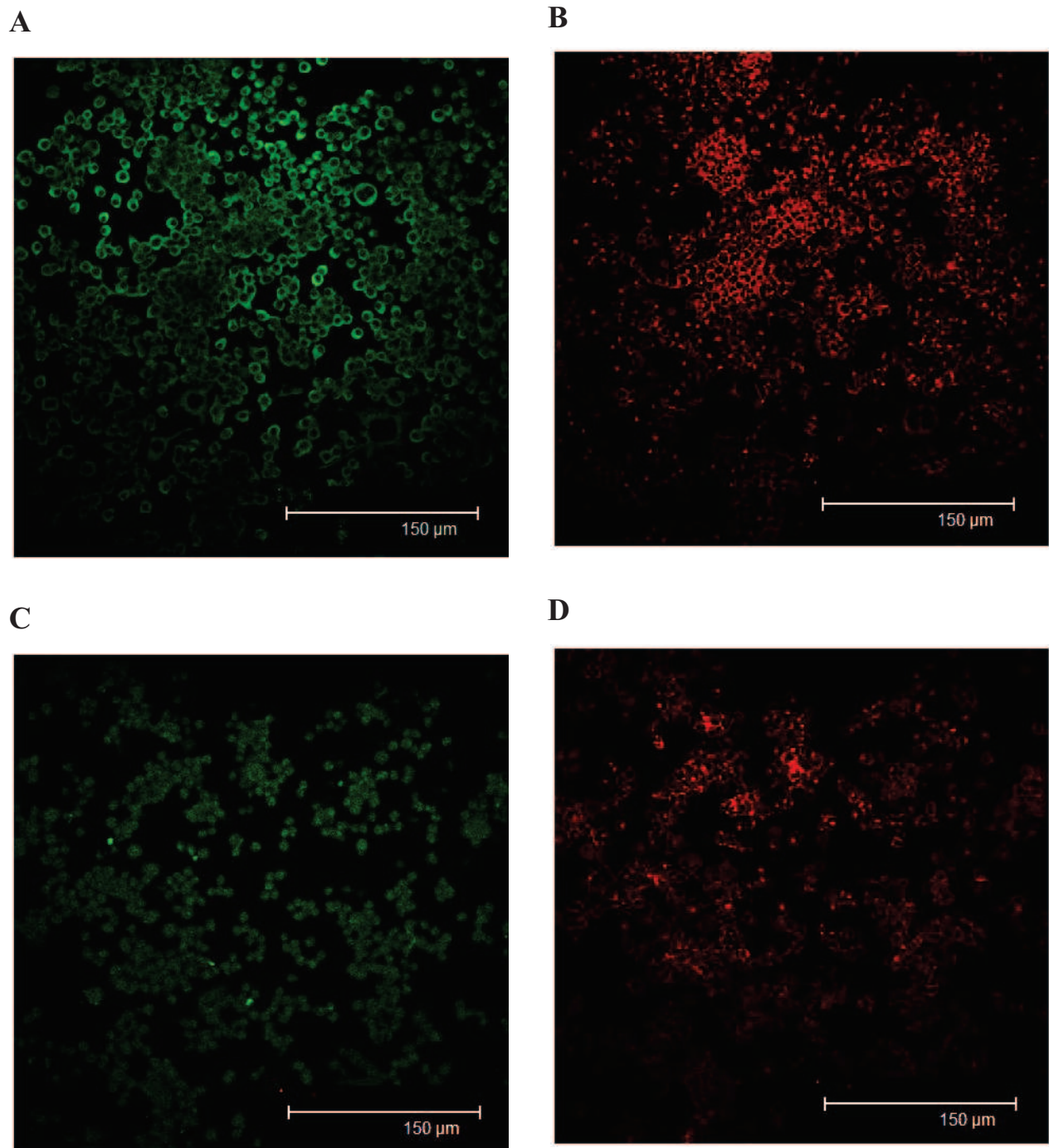


Figure 3.10 N2a cells stained for mdr1 protein with MRK-16 antibody.

N2a cells (x20 magnification) were fixed in 3% PFA, permeabilised in 0.1% Triton X-100 and stained for mdr1 protein with (A) MRK-16 anti-MDR1 monoclonal primary antibody (1:20) and AlexaFluor488 conjugated rabbit anti-mouse IgG secondary antibody (1:250) or (C) no primary antibody control. The actin cytoskeleton is counterstained with red phalloidin (1:450) ((B) and (D)). Since C219 antibody did not distinguish mouse mdr1, human MRK-16 antibody was used with some success, but non-specific binding was expected and is evident in panel C (no primary antibody). Cell samples from 3 separate passages were stained and visualised to confirm mdr1 expression status, and images are representative of at least 3 different fields of view in each case.

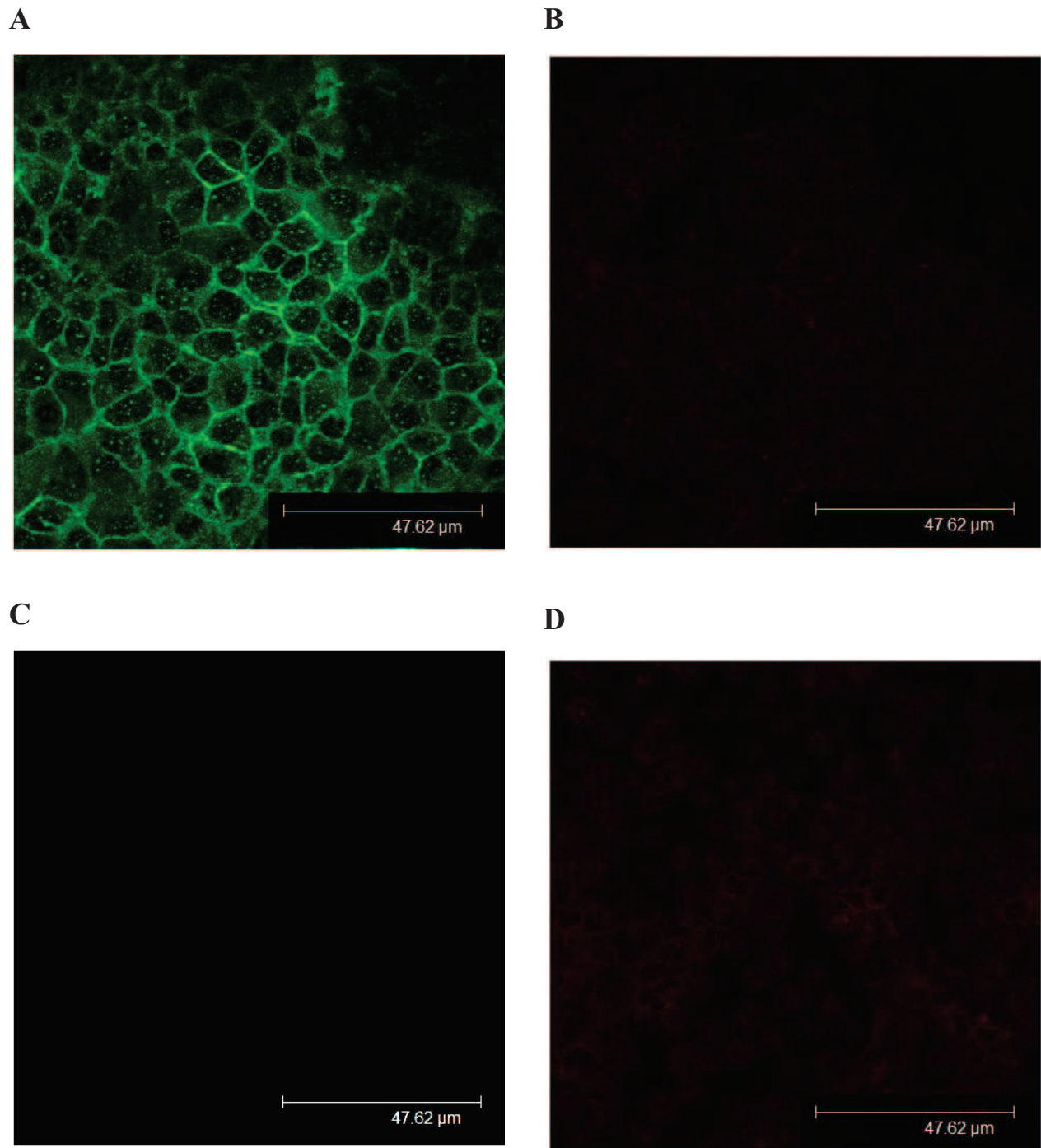


Figure 3.11 MDCKII-BCRP cells stained for BCRP protein by BXP-21 antibody.

MDCKII-BCRP cells ($\times 63$ magnification) were fixed and permeabilised in 100% methanol and stained for BCRP protein with (A) BXP-21 anti-BCRP/bcrp monoclonal primary antibody (1:50) and AlexaFluor488 conjugated rabbit anti-mouse IgG secondary antibody (1:250) or (C) no primary antibody control. The actin cytoskeleton of cell membranes is counterstained with red phalloidin at 1:450 dilution; (B) and (D). The field chosen is representative of at least 3 similar fields of view in each case. Cell samples from 3 separate passages were stained and visualised to confirm BCRP expression status. This data confirms that the BXP-21 antibody is correctly detecting its target, in BCRP-expressing cells.

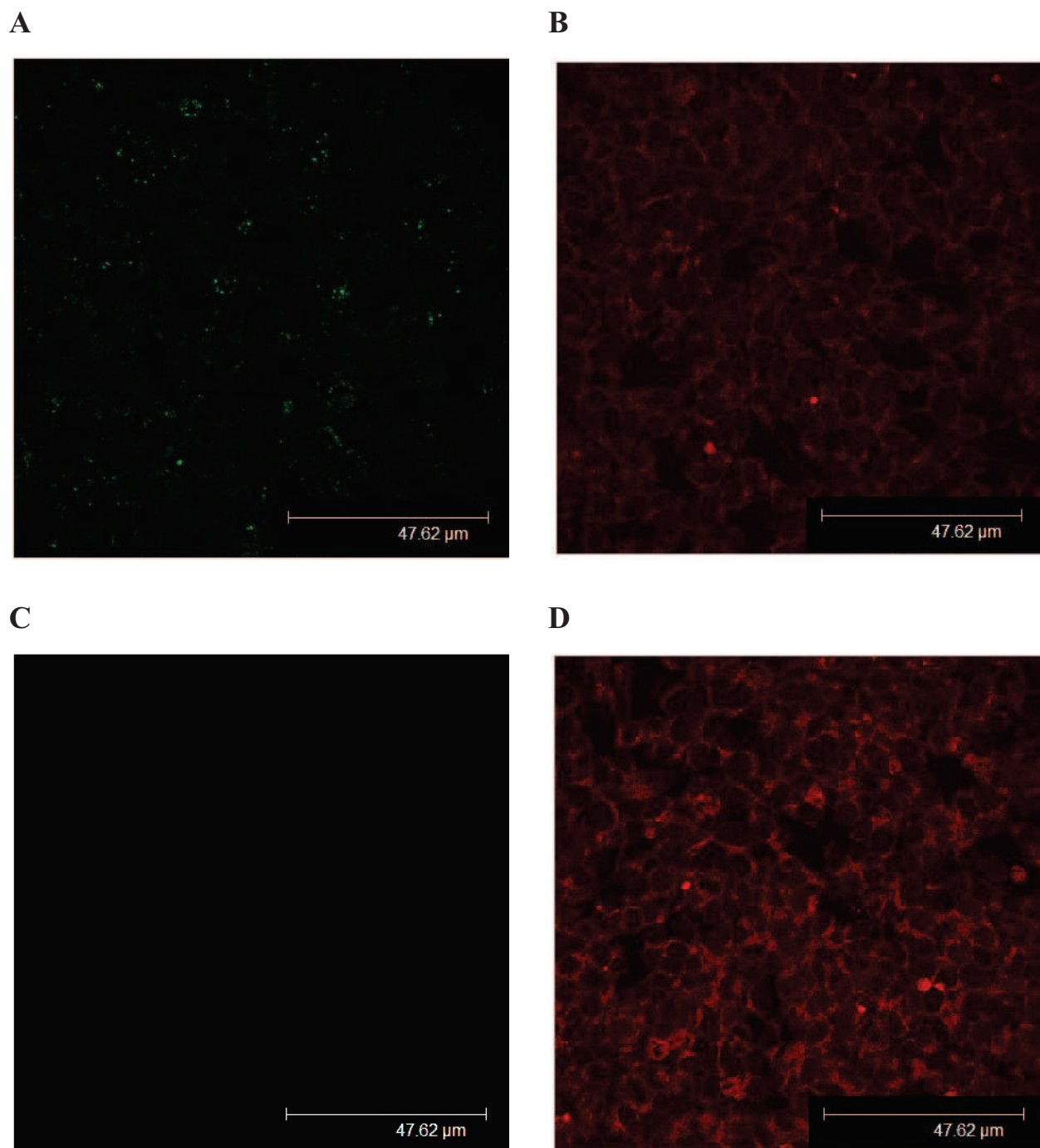


Figure 3.12 SH-SY5Y cells stained for BCRP protein by BXP-21 antibody.

BCRP protein expression in human SH-SY5Y cells was visualised by confocal microscopy at x63 magnification. Immunolocalisation of BCRP protein was determined by primary antibody BXP-21 (1:20) and AlexaFluor488- conjugated rabbit anti-mouse IgG (1:250). BCRP-conjugated fluorescence appears slightly higher in test cells (A) than in background control (C), however 1:20 was a very high dilution of primary antibody and some non-specific binding may be expected. In agreement with the PCR/qPCR data, BCRP expression was detected as negligible or zero in SH-SY5Y cells. Cell membranes were counterstained with red phalloidin diluted 1:450; (B) and (D). Cell samples from 3 separate passages were stained and visualised to confirm BCRP expression status.

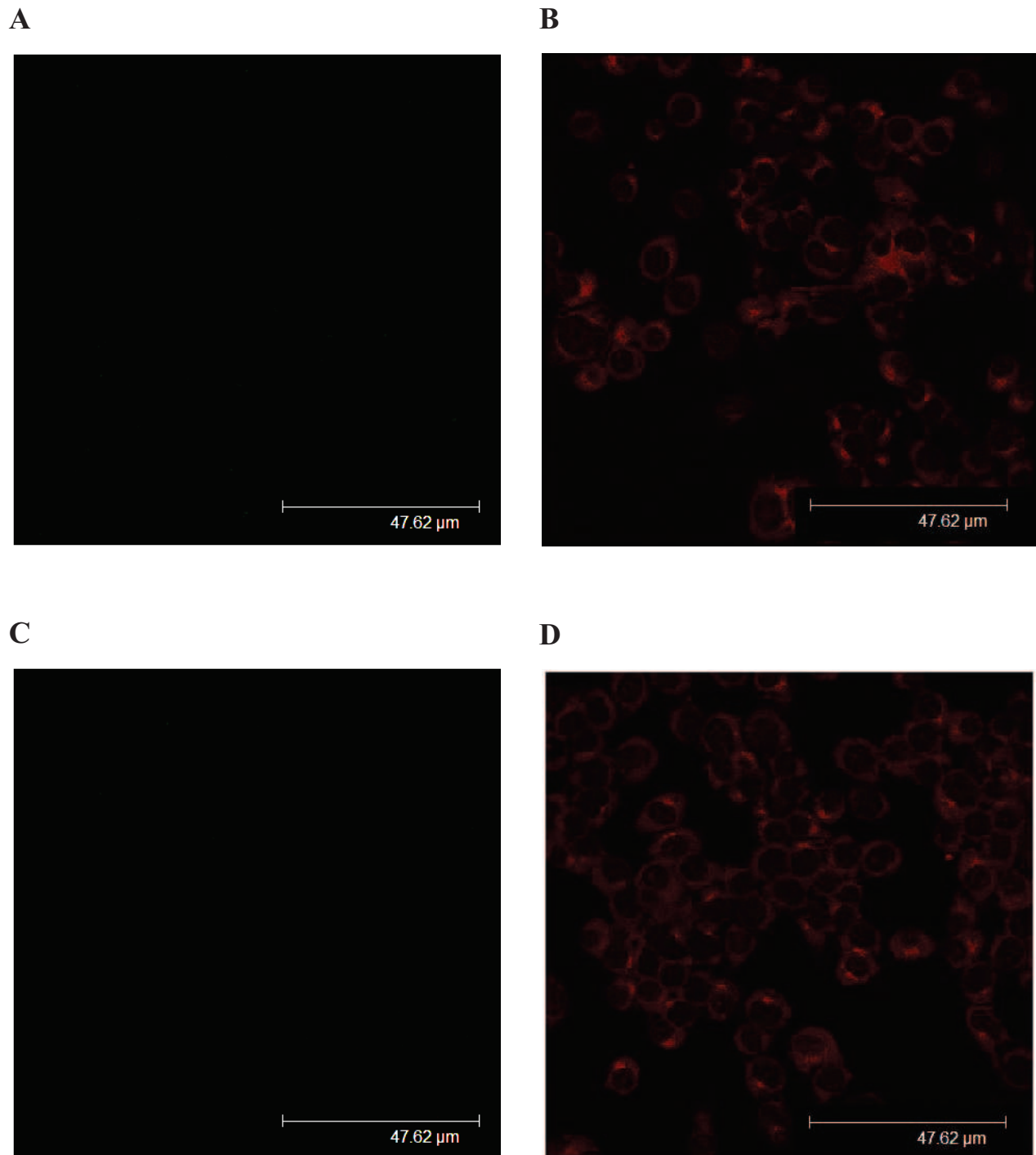


Figure 3.13 Mouse N2a cells stained for bcrp protein by BXP-21 antibody.

Mouse bcrp protein expression in N2a cells was visualised by confocal microscopy at x63 magnification. Cells were fixed and permeabilised in 100% methanol. Immunolocalisation of bcrp protein was determined by the primary antibody BXP-21 (1:20) and AlexaFluor488-conjugated rabbit anti-mouse IgG (1:250). Mouse bcrp was not detected in the N2a cell sample (A) compared to no primary antibody background control (C). Cell membranes were counterstained with red phalloidin; 1:450, (B) and (D). The field chosen is representative of at least 3 similar fields of view in each case. Cell samples from 3 separate passages were stained and visualised to confirm bcrp expression status.

Summary Conclusions from Chapter 3

The aim of this chapter was to characterise efflux transporter mRNA and protein expression in the chosen cell lines SH-SY5Y and N2a to validate the cells as models to study the effects of avermectin exposure. The presented results have shown that the SH-SY5Y cells used expressed MDR1 and MRP1 but not BCRP at the mRNA level, along with expression of related uptake and efflux transporters that mirror transporters at the human blood-brain barrier (BBB); accordingly they were a good model to study BBB transporters. SH-SY5Y cells also expressed MDR1 protein but not BCRP. N2a cells expressed *mdr1a* mRNA and protein but not mouse *bcrp*; they were therefore a good comparative model to study *mdr1a* function.

Chapter 4: Measurement of the interaction of avermectin insecticides with efflux transporters using the H33342 fluorescent dye retention assay

4.1 Summary

This section of work set out to characterise the dependence of intracellular accumulation of the MDR1 and BCRP substrate H33342 dye upon avermectin exposure and to compare kinetics in mouse and human cells for the interactions.

- I.** Initial experiments demonstrated that both human and mouse neuroblastoma cell lines showed a saturable intracellular retention of the fluorescent dye H33342 (0-15 μ M). In SH-SY5Y cells the K_a for H33342 dye retention was $10.30 \pm 3.12 \mu\text{M}$. In N2a cells the K_a for H33342 dye retention was $5.33 \pm 1.18 \mu\text{M}$. Values are mean \pm S.E.M. of 4 separate experiments. There were no significant differences in the EC_{50} values for H33342 dye retention between cell lines ($P > 0.05$).
- II.** Competitive inhibition of H33342 efflux by Cyclosporin A (CSA, 0-10 μ M) was measured at an H33342 dye concentration of 1 μ M. Concentration-dependent increases in intracellular dye retention were found which confirmed CSA-sensitive efflux activity in human SH-SY5Y and mouse N2a cells. K_i values for the ability of CSA to inhibit MDR1/mdr1a were $1.42 \pm 0.29 \mu\text{M}$ (mean \pm S.E.M. $n = 5$) in SH-SY5Y cells and $0.37 \pm 0.10 \mu\text{M}$ (mean \pm S.E.M. $n = 4$) in N2a cells ($P < 0.05$).
- III.** Validation assays with the BCRP/bcrp-inhibitor Ko143 up to 1 μ M demonstrated no significant BCRP/bcrp activity above control in either SH-SY5Y or N2a cell lines, while 5 μ M CSA confirmed activity of MDR1 and mdr1a. In contrast, MDCKII-BCRP transfected cell lines demonstrated concentration-dependent sensitivity to Ko143.
- IV.** Dose-response curves were obtained for each of the avermectin pesticides over the concentration range 0-7 μ M, at an H33342 dye concentration of 1 μ M. K_i values for abamectin were $0.95 \pm 0.08 \mu\text{M}$ in SH-SY5Y cells and $0.77 \pm 0.25 \mu\text{M}$ in N2a cells ($P > 0.05$). K_i values for emamectin benzoate were 0.60

$\pm 0.07 \mu\text{M}$ in SH-SY5Y and $0.56 \pm 0.02 \mu\text{M}$ in N2a cells ($P > 0.05$). K_i values for ivermectin were $0.24 \pm 0.08 \mu\text{M}$ in SH-SY5Y cells and $0.18 \pm 0.02 \mu\text{M}$ in N2a cells ($P > 0.05$). All values are mean \pm S.E.M. of at least 4 independent experiments, each experiment having $n = 6$ wells per condition.

4.2 Introduction

The aim of this section of work was to evaluate the interactions of abamectin, emamectin benzoate and ivermectin with efflux transporters expressed by human neuroblastoma SH-SY5Y cells and mouse neuroblastoma N2a cells and to assess whether there are species differences in interactions of efflux transporters with these avermectins between human and mouse cell-lines. MDR1/mdr1a activity was measured as inhibition of Hoechst 33342 (H33342) dye efflux from the cell by CSA. BCRP/bcrp activity was assessed as the KO-143 sensitive component of H33342 dye efflux, since H33342 is also a substrate of BCRP/bcrp, and CSA can inhibit BCRP/bcrp activity as well as MDR1/mdr1 (Gupta *et al*, 2006; Matsson *et al*, 2009). In Chapter 5, the ability of MK-571 to inhibit CMFDA dye efflux was used to assess activity of the multidrug resistance proteins (MRP/mrp).

In this chapter, transporter efflux activity was examined over a dye concentration range H33342 0-15 μM . Dose response curves for the ability of CSA (0-10 μM), or abamectin, emamectin benzoate and ivermectin (0-7 μM) to inhibit H33342 dye efflux in each cell line were obtained with an H33342 concentration of 1 μM . 5 μM CSA was included in all experiments as an internal control for inhibition of dye efflux. Data were analysed to generate IC₅₀ and K_i values as described in the methods section (Chapter 2).

4.3 Results

H33342 dose-response curves

A single experiment, representative of three other similar experiments, is shown in Figure 4.1, in which SH-SY5Y cells were exposed to a range of H33342 dye concentrations (0-

15 μM). There was a concentration-dependent increase in intracellular fluorescence which begins to plateau at 10 μM H33342, with an EC_{50} of $9.00 \pm 1.00 \mu\text{M}$.

Figure 4.2 depicts a single representative experiment in which N2a mouse cells were exposed to a range of H33342 dye concentrations (0-15 μM). The concentration-dependent increase in intracellular dye retention plateaus at 10 μM H33342, with an EC_{50} of $2.68 \pm 0.34 \mu\text{M}$.

The EC_{50} value for H33342 in SH-SY5Y cells was $10.30 \pm 3.11 \mu\text{M}$ (mean \pm S.E.M. $n = 4$). In N2a cells the EC_{50} value for H33342 was $5.33 \pm 1.17 \mu\text{M}$ (mean \pm S.E.M. $n = 4$). There were no significant differences in mean EC_{50} values for H33342 dye retention ($P > 0.05$) between human and mouse cell lines (Table 4.1 and 4.5). Cells were exposed to a range of H33342 dye concentrations to confirm dye efflux and to determine the lowest practical dye concentration to use to profile putative efflux inhibitors. 1 μM H33342 was selected, as it was on the rising section of the curve, to ensure measurable sensitivity to inhibitors.

Efflux modulation by Cyclosporin A (CSA)

Preliminary experiments in SH-SY5Y cells revealed a significant ($P < 0.01$) concentration-dependent increase in intracellular fluorescence at 1 μM and 10 μM CSA treatments ($42 \pm 8 \%$ and $74 \pm 11 \%$ higher than control, respectively, Figure 4.3). Dose-response curves for the ability of CSA to increase intracellular H33342 dye retention were profiled over the concentration range 0-10 μM , at a constant H33342 dye concentration of 1 μM . Mean K_i values are given in Table 4.2. For IC_{50} and K_i values see Tables 4.6 and 4.7.

Figures 4.4 and 4.5 show a representative experiment for the inhibition of transporter-mediated dye efflux by CSA in SH-SY5Y cells. Dye retention by the cells shows saturation kinetics with an apparent IC_{50} of $0.42 \pm 0.09 \mu\text{M}$. Analysis of the data from 5 independent experiments gave an overall IC_{50} of $1.66 \pm 0.33 \mu\text{M}$. Conversion of the IC_{50} values to K_i gave an apparent K_i of $1.42 \pm 0.29 \mu\text{M}$ (mean \pm S.E.M. $n = 5$).

Figures 4.6 and 4.7 depict a representative experiment for the inhibition of transporter-mediated dye efflux by CSA in N2a cells. Dye retention by the cells shows saturation

kinetics with an apparent IC_{50} of $0.36 \pm 0.05 \mu\text{M}$. Analysis of the data from 4 independent experiments gave an overall IC_{50} of $0.44 \pm 0.13 \mu\text{M}$. Conversion of the IC_{50} values to K_i gave an apparent K_i of $0.37 \pm 0.10 \mu\text{M}$ (mean \pm S.E.M. $n = 4$).

Differences between the mean K_i values from each cell line, for dye efflux inhibition, by CSA were compared using Student's t-test (Table 4.2). The K_i for inhibition of H33342 dye efflux by CSA in mouse N2a cells ($0.37 \pm 0.10 \mu\text{M}$) was significantly smaller than that for SH-SY5Y ($1.42 \pm 0.29 \mu\text{M}$; $P < 0.05$).

Inhibition of BCRP- and bcrp- mediated H33342 efflux by KO-143

KO-143 was used as a BCRP-specific inhibitor in the H33342 efflux assay in both SH-SY5Y and N2a cell lines over a concentration range 0-5 μM . In four independent experiments, represented by the single experiments in Figures 4.8 and 4.9, there was no significant inhibition of H33342 efflux by KO-143 in either cell line up to 1 μM . The apparent significance of the effect at 2.5 μM and above in SH-SY5Y cells ($P < 0.01$) is likely due to non-specific inhibition at concentrations far above the K_i for KO-143, which is in the sub-micromolar range (Allen *et al.*, 2002; Matsson *et al.*, 2009). In contrast, inhibition by CSA (5 μM) caused a significant increase in intracellular dye retention above control of $215 \pm 17 \%$ and $297 \pm 51 \%$ in SH-SY5Y and N2a cell lines respectively (both $P < 0.01$ versus control), demonstrating a high level of MDR1/mdr1a activity in both cell lines where there was no significant activity of BCRP/bcrp.

As validation, MDCKII-BCRP transfected cells demonstrated concentration-dependent inhibition of dye efflux by Ko143, ($P < 0.01$ at 0.3 μM Ko143 and above; Figure 4.10) K_i values obtained for inhibition of H33342 dye efflux in SH-SY5Y and N2a cells by CSA and avermectins therefore reflect MDR1/mdr1a activity rather than BCRP/bcrp activity.

Functional Assay of MDR1 and mdr1a activity in SH-SY5Y and N2a cells exposed to avermectins

Dose-response curves for the ability of selected avermectins to increase intracellular H33342 dye retention were profiled over the concentration range 0-7 μM , at a constant

H33342 dye concentration of $1\mu\text{M}$. Mean K_i values were for each avermectin were compared between cell lines using Student's t-test (Table 4.2).

Abamectin

Over a concentration range $0\text{-}7\mu\text{M}$ abamectin, there were significant concentration-dependent increases in intracellular dye retention observed in both SH-SY5Y human and N2a mouse cell lines. (both $P < 0.01$ at $5\mu\text{M}$ abamectin and above).

Figure 4.11 shows an individual experiment in SH-SY5Y human cells, representative of 6 similar experiments, exposed to a range of abamectin concentrations ($0\text{-}7\mu\text{M}$). There is a dose-dependent increase in intracellular fluorescence ($P < 0.01$ versus control at $7\mu\text{M}$ abamectin). Figure 4.12 shows the same data as a dose-response curve with an IC_{50} of $0.75 \pm 0.12 \mu\text{M}$.

Figure 4.13 shows a single experiment in N2a mouse cells exposed to a concentration range $0\text{-}7\mu\text{M}$ abamectin, representative of 6 similar experiments. There is a dose-dependent increase in intracellular fluorescence ($P < 0.01$ versus control at $7\mu\text{M}$ abamectin). The same data is expressed as a dose-response curve in Figure 4.14 with an IC_{50} for abamectin of $1.29 \pm 0.21 \mu\text{M}$.

In summary, abamectin inhibited H33342 efflux with a Mean K_i of $0.95 \pm 0.08 \mu\text{M}$ for human SH-SY5Y cells and $0.77 \pm 0.25 \mu\text{M}$ for mouse N2a cells (both mean \pm S.E.M. $n = 6$ experiments). There are no significant differences between the human and mouse cell lines in mean IC_{50} or K_i values for inhibition of H33342 efflux by abamectin ($P > 0.05$; Table 4.2).

Emamectin benzoate

Over a concentration range $0\text{-}7\mu\text{M}$ emamectin benzoate, there were significant concentration-dependent increases in intracellular dye retention observed in both SH-SY5Y human and N2a mouse cell lines (both $P < 0.01$ at $5\mu\text{M}$ emamectin benzoate versus control).

A representative experiment performed in SH-SY5Y cells resulted in a concentration-dependent increase in intracellular fluorescence ($P < 0.01$ at $5\mu\text{M}$ emamectin benzoate; Figure 4.15), with an IC_{50} of $0.65 \pm 0.10 \mu\text{M}$ (Figure 4.16). Figures 4.17 and 4.18 depict a like experiment in N2a cells. The concentration-dependent increase in intracellular fluorescence reached $P < 0.01$ versus control at $5\mu\text{M}$ emamectin benzoate and above, giving an IC_{50} of $0.57 \pm 0.08 \mu\text{M}$.

To summarise, emamectin benzoate inhibited H33342 efflux with a mean K_i of $0.60 \pm 0.07\mu\text{M}$ for human MDR1 in SH-SY5Y cells (mean \pm S.E.M. $n = 6$) and $0.56 \pm 0.02 \mu\text{M}$ for *mdr1a* in mouse N2a cells (mean \pm S.E.M. $n = 5$). There are no significant differences between the human and mouse cell lines in IC_{50} or K_i values for inhibition of H33342 efflux by emamectin benzoate ($P > 0.05$; Table 4.2).

Ivermectin

Over a concentration range $0\text{-}7\mu\text{M}$ ivermectin, there were significant concentration-dependent increases in intracellular dye retention observed in both SH-SY5Y human and N2a mouse cell lines (both $P < 0.01$ at $5\mu\text{M}$ and above versus control).

The individual experiment in Figure 4.19 shows a concentration-dependent increase in intracellular fluorescence in SH-SY5Y cells in the presence of ivermectin, ($P < 0.01$ at $5\mu\text{M}$ ivermectin versus control). The IC_{50} for the same data in Figure 4.20 is $0.49 \pm 0.07 \mu\text{M}$. A parallel experiment for ivermectin in N2a cells also resulted in a concentration-dependent increase in intracellular fluorescence ($P < 0.01$ at $5\mu\text{M}$ ivermectin versus control, Figure 4.21). The IC_{50} for this data is $0.24 \pm 0.05 \mu\text{M}$ (Figure 4.22).

To summarise, ivermectin inhibited H33342 efflux with a K_i of $0.24 \pm 0.06 \mu\text{M}$ in human SH-SY5Y cells (mean \pm S.E.M. $n = 4$) and $0.18 \pm 0.02 \mu\text{M}$ (mean \pm S.E.M. $n = 6$) for mouse N2a cells. There are no significant differences between the human and mouse cell lines in IC_{50} or K_i values for inhibition of H33342 efflux by ivermectin ($P > 0.05$; Table 4.2).

4.4 Discussion

A main objective of this study was to ascertain how relevant data obtained in mouse models are to understanding the handling of avermectins in humans. Further to the positive data on mRNA and protein expression of MDR1/mdr1a in SH-SY5Y human and N2a mouse cells (Chapter 3), the data obtained here shows that both cell lines displayed sensitivity to the MDR1/mdr1 substrate CSA but not the BCRP/bcrp inhibitor Ko-143, and therefore had functionality of MDR1/mdr1a, making them suitable for comparison in this study.

Abamectin, emamectin benzoate and ivermectin all inhibited MDR1-mediated H33342 dye efflux in both SH-SY5Y and N2a cell lines, following Michaelis-Menten-like saturating kinetics, where low K_i values equate to high affinity of the inhibitor for the transporter. All avermectins had potencies in the low micromolar range, similar to the known MDR1 substrate CSA (K_i for CSA in SH-SY5Y cells $1.42 \pm 0.29 \mu\text{M}$; K_i in N2a cells $0.37 \pm 0.10 \mu\text{M}$). The order of affinities for MDR1 in human SH-SY5Y cells was ivermectin ($K_i 0.24 \pm 0.08 \mu\text{M}$) \geq emamectin benzoate ($K_i 0.60 \pm 0.07 \mu\text{M}$) $>$ abamectin ($K_i 0.95 \pm 0.08 \mu\text{M}$). The order of affinities for mdr1a in mouse N2a cells followed a similar trend with ivermectin ($K_i 0.18 \pm 0.02 \mu\text{M}$) $>$ emamectin benzoate ($K_i 0.56 \pm 0.02 \mu\text{M}$) \geq abamectin ($K_i 0.77 \pm 0.25 \mu\text{M}$). Importantly the human SH-SY5Y and mouse N2a neuroblastoma cell lines did not differ significantly in their native MDR1 efflux transport profiles in response to exposure to abamectin, emamectin benzoate or ivermectin ($P > 0.05$ for all comparisons, Table 4.2). These findings indicate that existing kinetic data obtained in mouse models expressing endogenous mdr1a is also applicable to humans. This is a useful observation in the light of the ongoing reliance on existing data obtained in mouse models such as mdr1a (-/-) or CF-1 mice to predict the effects of human exposure (Macdonald & Gledhill, 2007).

Prior to the current work, observations in mouse models *in vivo* found that ivermectin and abamectin accumulate in mdr1-deficient tissues, suggesting that they may be substrates for mdr1 (Schinkel *et al.*, 1994; Lankas *et al.*, 1997). These results suggested that mouse

brain was protected from exposure to ivermectin and vinblastine if MDR1 was present, but did not study the interaction of these compounds with MDR1 at the cellular level.

Ivermectin was identified as a *mdr1* substrate by Pouliot *et al.*, (1997) and Schinkel *et al.*, (1995). Pouliot and co-workers showed that the steady-state accumulation of [³H]-ivermectin was lower in drug-resistant cells than drug-sensitive human lymphoma cells in a similar manner to the known MDR1 substrate [³H]-vinblastine, that the efflux of both drugs was ATP-dependent, and that this efflux could be inhibited by the presence of cyclosporin A or unlabelled ivermectin in molar excess. Schinkel *et al.*, (1995) provided evidence that MDR1-mediated transport of ivermectin, cyclosporin A and digoxin, in a basal to apical direction in bidirectional transfer experiments in porcine kidney epithelial cells transfected with human MDR1 or mouse *mdr1a* (Schinkel *et al.*, 1995).

In the current study, abamectin, emamectin benzoate and ivermectin all inhibited the efflux of H33342 through MDR1 and *mdr1a* with potency in the low micromolar range, similar to that observed with the established MDR1 substrate and inhibitor CSA (Tsuji *et al.*, 1993). The current data adds to other evidence that ivermectin is a potent MDR1 inhibitor (Didier & Loor, 1996) and that ivermectin and the related compound selamectin are MDR1 substrates (Geyer *et al.*, 2009). In another *in vivo* study, both CSA and ivermectin concentrations were found to increase in brains of *mdr1a* (-/-) CF-1 mice exposed to 0.2mg/kg ivermectin and 1mg/kg CSA by the oral and iv routes; CSA accumulated 10- and 15- fold greater after oral and iv dosing respectively in *mdr1a*(-/-) brains compared to *mdr1a*(+/+) brains, whereas ivermectin was 70-fold higher in *mdr1a*(-/-) than in *mdr1a*(+/+) brains 24 hours after oral dosing (Kwei *et al.*, 1999). These authors account for this difference in drug accumulation in mouse brain tissues as being due to the presence or absence of *mdr1a* at the blood-brain barrier. The *in vitro* data in the current study is in agreement with these observations. *Mdr1*-mediated H33342 efflux was modulated by both CSA and ivermectin in mouse neuroblastoma N2a cells. Similar data on the interaction of ivermectin and CSA with *mdr1* were obtained in bovine brain microvessel endothelial cells, where 1µg/ml CSA or 50ng/ml ivermectin were both found to significantly enhance rhodamine-123 uptake compared to control, although the

inhibitory effect of ivermectin was prevented in the presence of serum (Rose *et al.*, 1998). These authors conclude that “unbound ivermectin is at least an inhibitor” of *mdr1* in bovine brain endothelial cells.

Data pertaining to the effect of ivermectin on human MDR1 was obtained by Brayden and Griffin (2008) in MDCKII wild-type monolayers or cells transfected with MDR1, MRP1 or MRP2. Brayden and Griffin found an increase in basolateral-to-apical flux of tritiated ivermectin and selamectin across monolayers of MDCKII-MDR1 cells compared to the other cell lines, and this flux was significantly reduced by the bilateral addition of the MDR1 inhibitor verapamil (100 μ M). This data indicated that both avermectins interacted with human MDR1 in an overexpression cell model. However, flux of the avermectins across the MRP1-, MRP2- transfected and wild-type cell lines were also significantly reduced by the addition of 100 μ M verapamil, apparently due to the background expression of canine *mdr1*. The use of human cells expressing only endogenous levels of human MDR1 in the current study is an advantage since it should more closely resemble physiological expression of MDR1 and other ABC transporters in human brain cells over a limited number of passages and, because the cells are of human origin, background expression of transporters endogenous to a different species does not obscure the data obtained for human MDR1.

The current study strengthens the existing evidence that avermectins are MDR1 inhibitors by adding emamectin benzoate to the list of likely inhibitors of both human MDR1 and mouse *mdr1a*, and extending the pre-existing data in favour of ivermectin and abamectin as inhibitors of human MDR1 (Didier & Loo, 1996; Lespine *et al.*, 2007; Brayden & Griffin, 2008) and mouse *mdr1a* (Schinkel *et al.*, 1994, 1996).

In another in-vitro overexpression system, using the fluorescent MDR1 substrate dye rhodamine-123 (rho-123), Lespine *et al.*, (2007) tested the avermectin insecticides ivermectin, abamectin, doramectin, eprinomectin, selamectin and the structurally related milbemycin moxidectin as putative inhibitors of dye efflux from porcine kidney epithelial cells transfected with either murine *mdr1a* or human MDR1. The IC₅₀ values for

abamectin and ivermectin are similar to those obtained in the current study, at $0.11 \pm 0.01 \mu\text{M}$ and $0.44 \pm 0.07 \mu\text{M}$, respectively, proving them potent inhibitors of rho-123 efflux. The other avermectins had similar effects, but the milbemycin Moxidectin was a weaker inhibitor with a IC_{50} of $4.4 \pm 0.6 \mu\text{M}$ (Lespine *et al.*, 2007). When comparing these values with the current study, it is noted that the H33342 substrate dye binds to a structurally distinct site on MDR1 from that of Rho-123 (Shapiro & Ling, 1997). Hence the assays should be regarded as qualitatively different, since the binding sites will likely have different affinities for their substrates, so the IC_{50} values are not directly comparable. Calculating K_i values takes account of differences in substrate affinities between transporters and different dyes, so overcoming this problem.

Lespine *et al.*, (2006) also used the CSA analogue Valspodar as a positive control to inhibit rhodamine-123 efflux in *mdr1a*-transfected but not untransfected cells with an IC_{50} of $0.11 \pm 0.03 \mu\text{M}$. All the avermectins tested inhibited transport of rhodamine 123 in *mdr1a*-transfected cells. abamectin inhibited transport by $83 \pm 2\%$, and ivermectin by $86 \pm 2\%$ of the effect of Valspodar. Similar trends were observed in the inhibition of MDR1 ATPase activity, with IC_{50} values for abamectin and ivermectin at 0.2 and $2.0 \mu\text{M}$ for basal-, and 0.02 and $0.05 \mu\text{M}$ for verapamil-stimulated ATPase activity, respectively. Abamectin and ivermectin were thus shown to be potent modulators of MDR1 activity in vitro in LLCK-PK1 *mdr1a*-transfected cells. In LLCK-PK1 cells transfected with human MDR1, ivermectin inhibited rhodamine123 efflux with an IC_{50} of $1.0 \pm 0.2 \mu\text{M}$.

Griffin *et al.*, (2005) investigated transepithelial transport of ivermectin, selamectin and moxidectin across human intestinal epithelial Caco-2 cells. All three were transported preferentially in a basolateral to apical direction, although the milbemycin moxidectin was a weaker MDR1 substrate than the avermectins, since the secretory flux of both ivermectin and selamectin, but not moxidectin, was decreased in the presence of the MDR1 inhibitor verapamil ($20 \mu\text{M}$). Ivermectin and selamectin were potent inhibitors of rhodamine-123 secretion, with IC_{50} 's of $0.1 \mu\text{M}$, whereas the IC_{50} for moxidectin of $10.0 \mu\text{M}$ indicates weaker inhibitory activity (Griffin *et al.*, 2005).

In the current study, within each cell line there was an apparent rank order of affinities of the avermectins tested for inhibition of H33342 efflux through human MDR1 and mouse *mdr1a*. In human SH-SY5Y neuroblastoma cells, the order of affinities is ivermectin > emamectin benzoate > abamectin, whereas emamectin benzoate and ivermectin have significantly higher affinity than abamectin ($P < 0.05$ for emamectin and $P < 0.01$ for ivermectin in SH-SY5Y cells (Table 4.3). Affinities for *mdr1a* in mouse N2a neuroblastoma cells follow a similar trend, with ivermectin > emamectin benzoate ($P < 0.05$) \geq abamectin (Table 4.4). This is an interesting observation with respect to the neurotoxicities of ivermectin observed in animal models deficient in *mdr1*; if ivermectin is the most potent inhibitor of MDR1 of the three avermectins tested, it may also have the greatest impact upon cells when its function is inhibited or impaired. It is interesting to look at whether this relatively high affinity of ivermectin for MDR1 compared to emamectin benzoate or abamectin has any other impact on efflux transport or cell health. This idea has been explored in Chapter 6.

Potential role of other transporters in avermectin handling

Data obtained in this study on mRNA and protein expression of BCRP/*bcrp* (Chapter 3) indicates that it is not expressed in human SH-SY5Y or mouse N2a cells, and the absence of functional response to the BCRP/*bcrp* inhibitor KO-143 substantiates this observation. The expression of human BCRP and mouse *bcrp* at the blood-brain barrier of the respective species has been well documented (Eisenblätter *et al.*, 2003; Cisternino *et al.*, 2004; Weksler *et al.*, 2005; Ek *et al.*, 2010), and *bcrp* protein expression was up-regulated in the brain of *mdr1a*(-/-) knockout mice, indicating a potential compensatory mechanism (Cisternino *et al.*, 2004). CSA has been identified as an inhibitor but not a substrate for human BCRP in stably transfected HEK-293 cells (Gupta *et al.*, 2006), with an IC_{50} value of $4.3 \pm 1.9 \mu\text{M}$, but Geyer *et al.* (2008) found that *bcrp*(-/-) mice did not accumulate ivermectin or Selamectin in brain tissue *in vivo* compared to wild-type mice, whereas *mdr1a/b*(-/-) mouse brain accumulated 60x higher ivermectin concentrations; these authors suggest that *bcrp* is therefore not an important efflux carrier for ivermectin or Selamectin at the mouse blood-brain barrier *in vivo* compared to *mdr1a*. Conversely,

Jani *et al.*, (2010) measured H33342 efflux in cells transfected with human BCRP and found that ivermectin inhibited cellular efflux and ATPase activities of BCRP with IC₅₀ values of 1.0- and 1.68 μ M respectively. Taken together this evidence is not conclusive as to the importance of BCRP/bcrp. It is possible that, in situations where P-gp activity is impaired, BCRP/bcrp efflux activity could become important in limiting avermectin accumulation. Since human BCRP and mouse bcrp were not present in the cell lines studied, further work is still required to assess their contribution to the efflux of avermectin insecticides in the CNS in humans and in mice.

In contrast to BCRP, mRNA level expression of MRP transporters by SH-SY5Y cells was observed in this study (Chapter 3) and there is existing evidence to suggest either that MRP transporters do interact with ivermectin (Lespine *et al.*, 2006), or do not (Brayden & Griffin, 2008). As well as being a substrate for MDR1, Lespine *et al.*, (2007) showed that ivermectin can inhibit the ATPase activity of MRPs 1, 2 and 3 with different affinities, and is transported by MRP1. They suggested that, as well as MDR1, the MRP efflux proteins may influence ivermectin transport. In contrast, Brayden and Griffin (2008) found significant basal to apical transport of ivermectin and selamectin, in both MDCK wild-type and MDCK-MDR1, -MRP1 and -MRP2 transfected cell lines. They concluded that background canine *mdr1* expression in all four lines masked transport by the transfected proteins. Transport was indeed inhibited by the MDR1/*mdr1* substrate verapamil, but not by MRP inhibitors. It was therefore claimed that the MRPs have negligible influence if MDR1 is expressed. An awareness of the influence of transporters other than MDR1 is essential though; SH-SY5Y human neuroblastoma cells used in our study are morphologically different from kidney. In the light of this conflict we set out to explore the function of MRP transporters in human and mouse cells in Chapter 5.

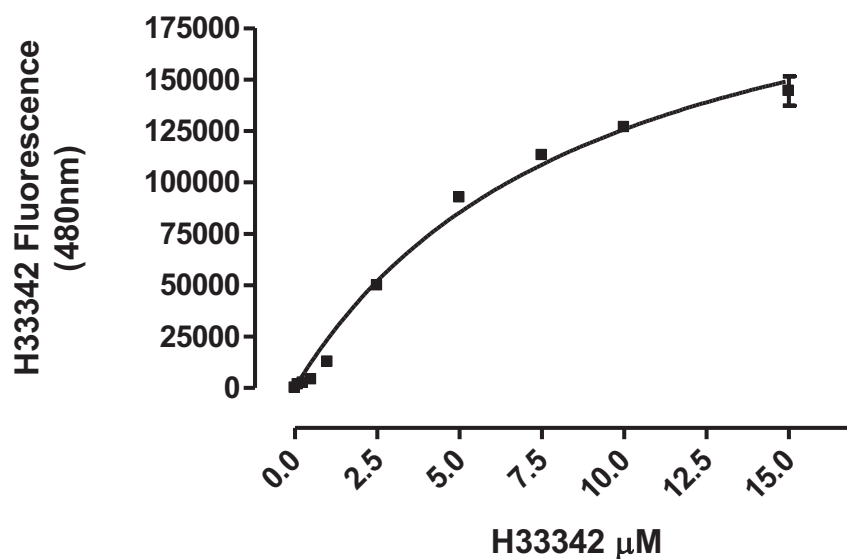


Figure 4.1 Hoechst 33342 dose-response curve (0 - 15 μM) in SH-SY5Y cells.

The data above are mean \pm S.E.M. $n = 6$ wells per concentration from a single experiment representative of 4 experiments, analysed by nonlinear least squares regression with an EC_{50} of $9.00 \pm 1.00 \mu\text{M}$ ($R^2=0.98$). The other individual experiments in SH-SY5Y cells generated EC_{50} values for H33342 retention of $18.30 \pm 12.90 \mu\text{M}$, $10.67 \pm 1.98 \mu\text{M}$, and $3.18 \pm 0.48 \mu\text{M}$, giving an EC_{50} of $10.30 \pm 3.11 \mu\text{M}$ (mean \pm S.E.M. $n = 4$).

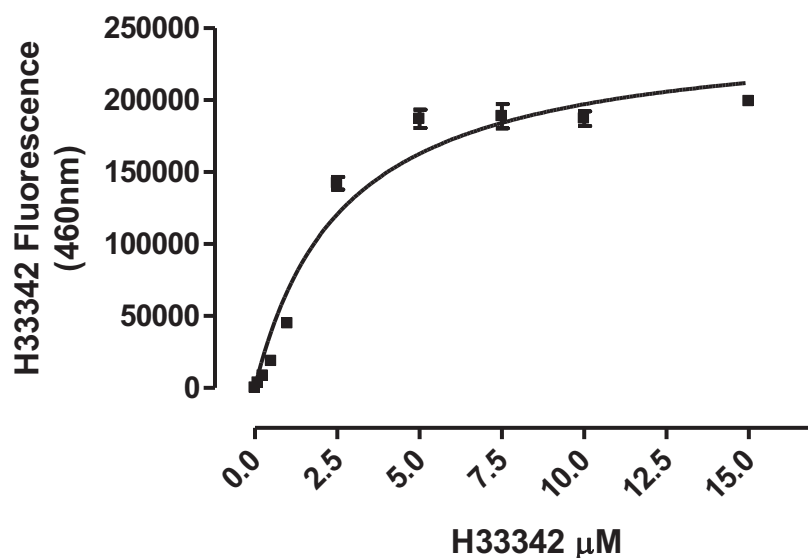


Figure 4.2 Hoechst 33342 dose-response curve (0-15 μM) in N2a cells.

The data above are mean \pm S.E.M. $n = 6$ wells per concentration from a single experiment representative of 4 experiments, analysed by nonlinear least squares regression with an EC_{50} of $2.68 \pm 0.34 \mu\text{M}$ ($R^2=0.95$). The other individual experiments generated EC_{50} values for H33342 retention of $6.97 \pm 2.09 \mu\text{M}$, $4.07 \pm 1.48 \mu\text{M}$ and $7.60 \pm 1.70 \mu\text{M}$, giving an EC_{50} of $5.33 \pm 1.17 \mu\text{M}$ (mean \pm S.E.M. $n = 4$).

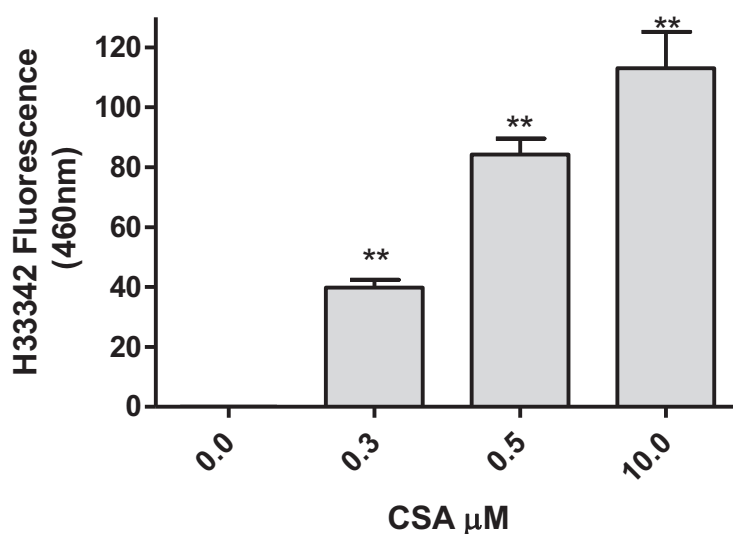


Figure 4.3 Hoechst 33342 dye efflux assay to determine CSA-sensitive transporter expression in SHSY5Y cells at least 1 day after seeding.

Data is mean \pm S.E.M. of $n = 6$ wells per concentration from a single experiment representative of 4 independent experiments, analysed by One-Way ANOVA with Dunnett's post-test; At $1\mu\text{M}$ CSA, the increase in intracellular fluorescence was $42 \pm 8\%$ and at $10\mu\text{M}$ CSA was $74 \pm 11\%$; * $P < 0.05$; ** $P < 0.01$ versus control.

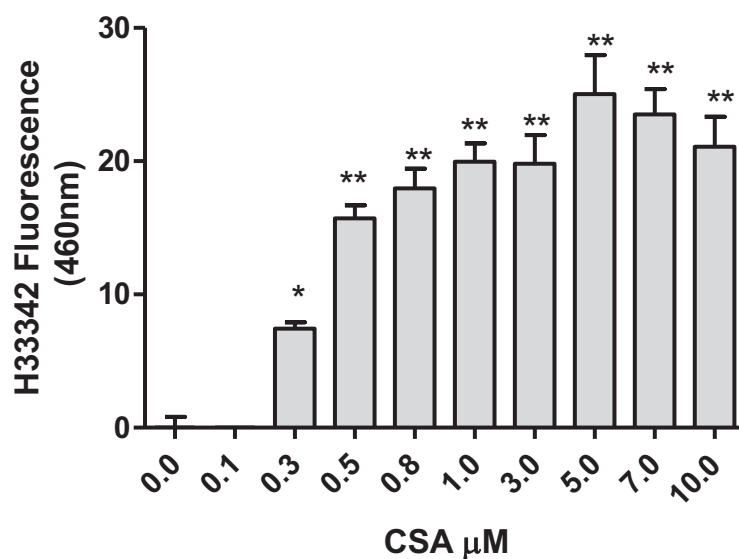


Figure 4.4 Dose-response for the ability of CSA (0-10 μM) to inhibit transporter-mediated efflux of $1\mu\text{M}$ H33342 in SH-SY5Y cells.

Data are mean \pm S.E.M. $n = 6$ wells per concentration from a single experiment, representative of 4 independent experiments, analysed by One-Way ANOVA with Dunnett's post-test; * $P < 0.05$; ** $P < 0.01$ versus control. Owing to apparent, variable cytotoxicity at 7-10 μM CSA, $5\mu\text{M}$ CSA was used as a positive control standard in all further assays.

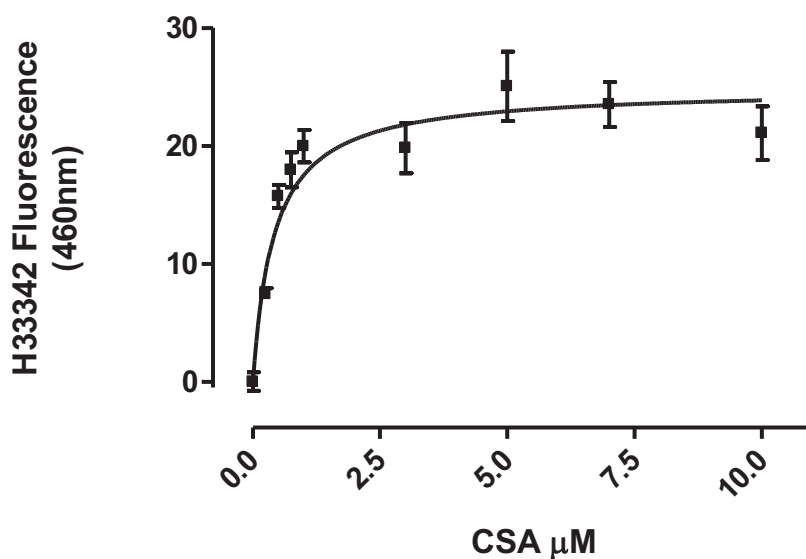


Figure 4.5 Dose-response curve for the ability of CSA (0-10 μM) to inhibit transporter-mediated efflux of 1 μM H33342 in SH-SY5Y cells.

Data are mean \pm S.E.M. $n = 6$ wells per concentration from a single experiment representative of 4 independent experiments, analysed with non-linear least-squares regression. The IC_{50} of the above curve is $0.42 \pm 0.09 \mu\text{M}$ ($R^2=0.77$). The other individual experiments generated IC_{50} values of $2.02 \pm 0.20 \mu\text{M}$, $2.32 \pm 0.30 \mu\text{M}$, $1.82 \pm 0.48 \mu\text{M}$, and $1.73 \pm 0.19 \mu\text{M}$, giving a mean IC_{50} of $1.66 \pm 0.33 \mu\text{M}$ and K_i of $1.42 \pm 0.29 \mu\text{M}$ (mean \pm S.E.M. $n = 5$).

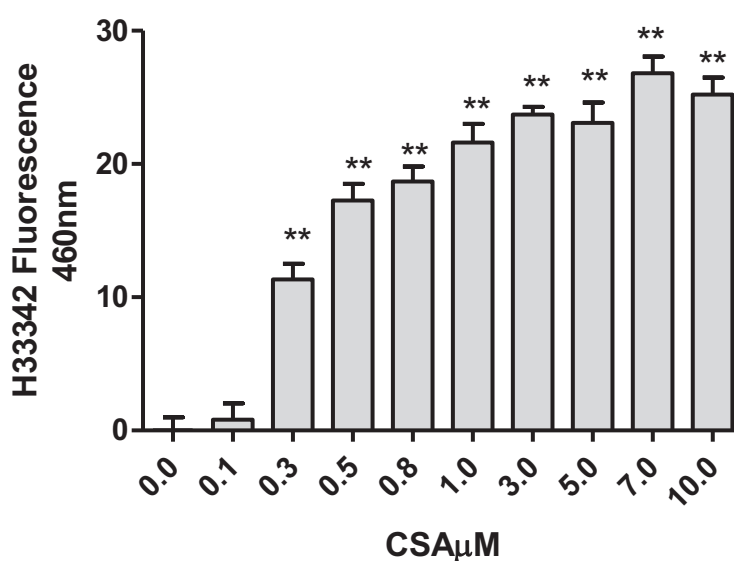


Figure 4.6 Dose-response curve for the ability of CSA (0-10 μM) to inhibit transporter-mediated efflux of 1 μM H33342 in N2a cells.

Data are mean \pm S.E.M. $n = 6$ wells per concentration from a single experiment representative of 4 independent experiments, analysed with One way ANOVA and Dunnett's post test; * $P < 0.05$, ** $P < 0.01$ versus control. Owing to apparent, variable cytotoxicity at 7-10 μM CSA, 5 μM CSA was used as a positive control standard in all further assays.

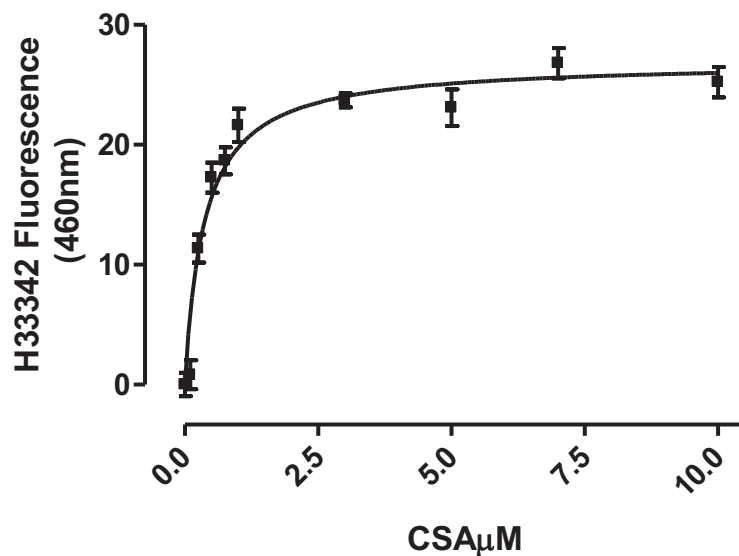


Figure 4.7 Dose-response curve for the ability of CSA (0-10 μM) to inhibit transporter-mediated H33342 efflux in N2a cells, with an H33342 concentration of 1 μM .

Data are mean \pm S.E.M. $n = 6$ wells per concentration from a single experiment representative of 4 independent experiments, analysed with non-linear least-squares regression. The IC_{50} of the above curve is $0.36 \pm 0.05 \mu\text{M}$ ($R^2 = 0.88$). The other individual experiments generated IC_{50} values of $0.39 \pm 0.10 \mu\text{M}$, $0.22 \pm 0.06 \mu\text{M}$ and $0.80 \pm 0.40 \mu\text{M}$, giving a mean IC_{50} of $0.44 \pm 0.13 \mu\text{M}$ and K_i of $0.37 \pm 0.10 \mu\text{M}$ (mean \pm S.E.M. $n = 4$).

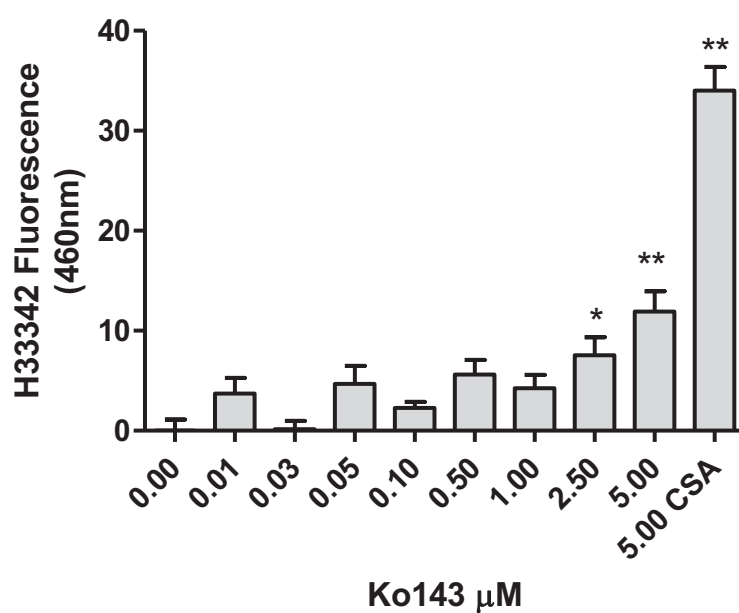


Figure 4.8 Dose-response curve for the ability of KO-143 (0-5 μM) to inhibit BCRP-mediated efflux of 1 μM H33342 in SH-SY5Y cells.

Data are mean \pm S.E.M. $n = 6$ wells per concentration from a single experiment representative of 4 independent experiments. Data were analysed by One way ANOVA and Dunnett's post test; * $P < 0.05$; ** $P < 0.01$ versus control.

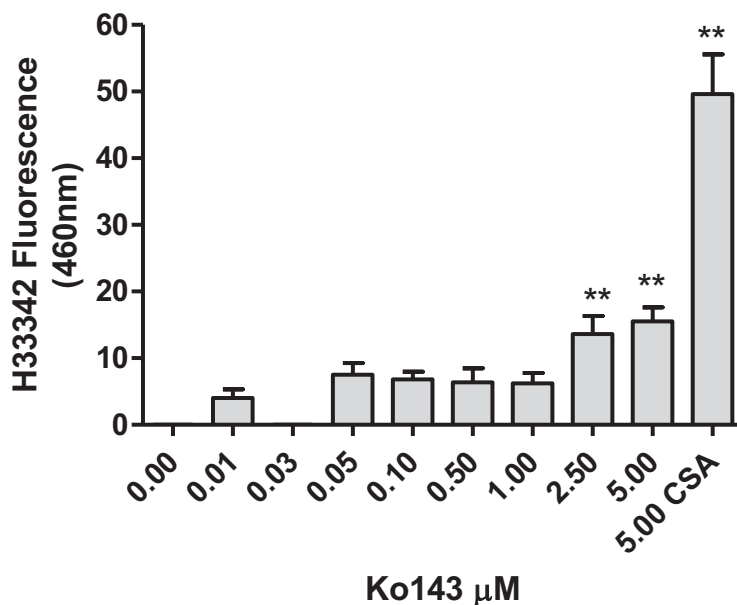


Figure 4.9 Dose-response curve for the ability of KO-143 (0-5 μ M) to inhibit bcrp-mediated efflux of 1 μ M H33342 in N2a cells.

Data are mean \pm S.E.M. $n = 6$ wells per concentration from a single experiment representative of 4 independent experiments, Data were analysed by One way ANOVA and Dunnett's post test; * $P < 0.05$; ** $P < 0.01$ versus control.

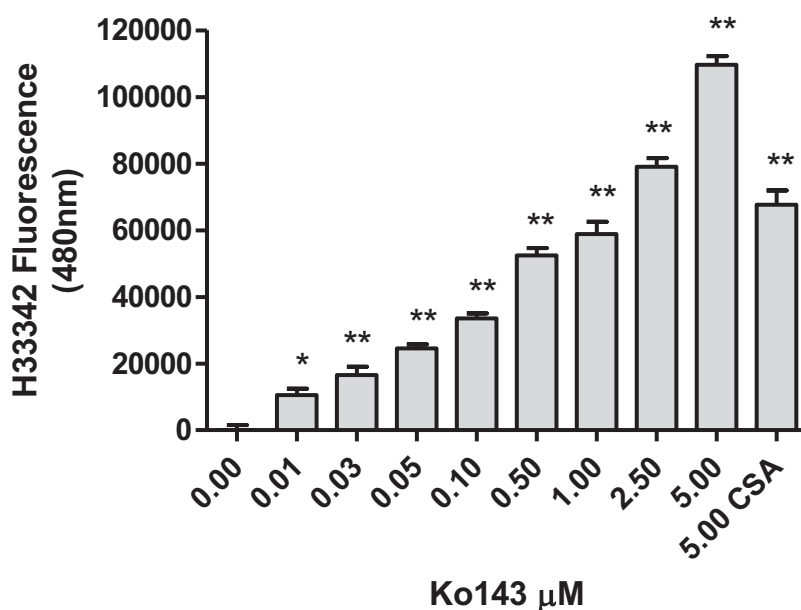


Figure 4.10 Dose-response curve for the ability of KO-143 (0-5 μ M) to inhibit BCRP-mediated efflux of 1 μ M H33342 in MDCKII-BCRP cells.

Data are mean \pm S.E.M. $n = 6$ wells per concentration from a single experiment representative of 2 independent experiments. Data were analysed by One way ANOVA and Dunnett's post test; * $P < 0.05$; ** $P < 0.01$ versus control.

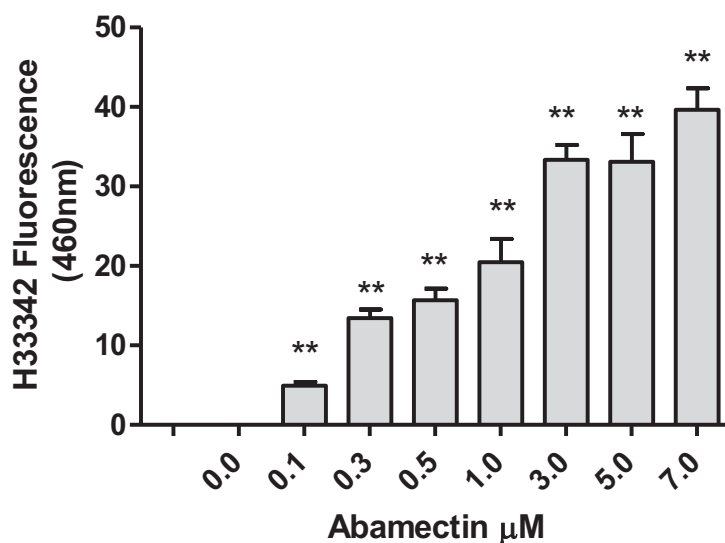


Figure 4.11 Dose-response curve for the ability of abamectin (0-7 μM) to inhibit MDR1-mediated efflux of 1 μM H33342 in SH-SY5Y cells.

Data are mean \pm S.E.M. $n = 6$ wells per concentration from a single experiment representative of 4 independent experiments, Data were analysed with One way ANOVA and Dunnett's post test; * $P < 0.05$, ** $P < 0.01$ versus control.

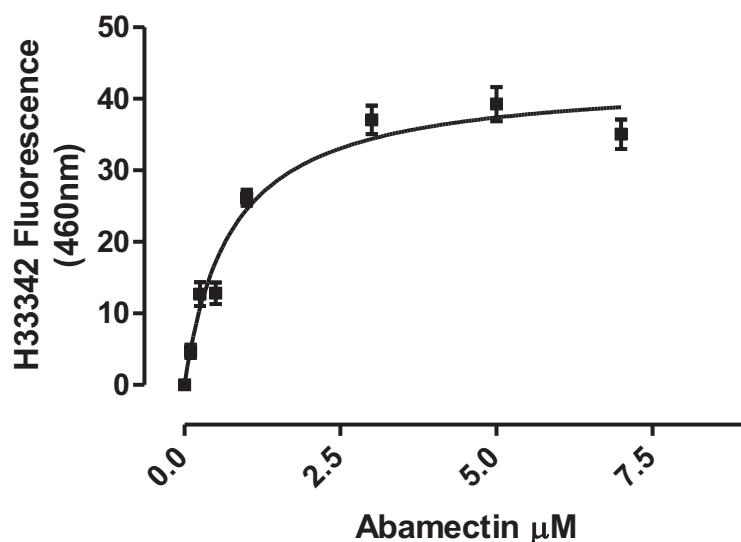


Figure 4.12 Dose-response curve for the ability of abamectin (0-7 μM) to inhibit MDR1-mediated efflux of 1 μM H33342 in SH-SY5Y cells.

Data are mean \pm S.E.M. $n = 6$ wells per concentration from a single experiment representative of 4 independent experiments, analysed with non-linear least-squares regression. The IC_{50} of the above curve is $0.77 \pm 0.11 \mu\text{M}$ ($R^2 = 0.77$). The other individual experiments generated IC_{50} values of $0.85 \pm 0.17 \mu\text{M}$, $1.34 \pm 0.32 \mu\text{M}$, $0.95 \pm 0.15 \mu\text{M}$, $1.19 \pm 0.25 \mu\text{M}$ and $1.18 \pm 0.36 \mu\text{M}$, giving a mean IC_{50} of $1.05 \pm 0.09 \mu\text{M}$ and K_i of $0.95 \pm 0.08 \mu\text{M}$ (mean \pm S.E.M. $n = 6$).

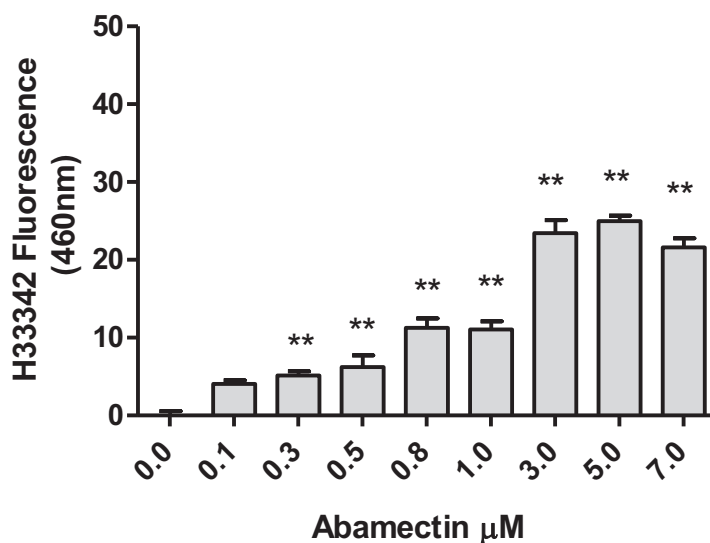


Figure 4.13 Dose-response curve for the ability of abamectin (0-7 μM) to inhibit *mdr1a*-mediated efflux of 1 μM H33342 in N2a cells.

Data are mean \pm S.E.M. $n = 6$ wells per concentration from a single experiment representative of 4 independent experiments, Data were analysed with One way ANOVA and Dunnett's post test; * $P < 0.05$, ** $P < 0.01$ versus control.

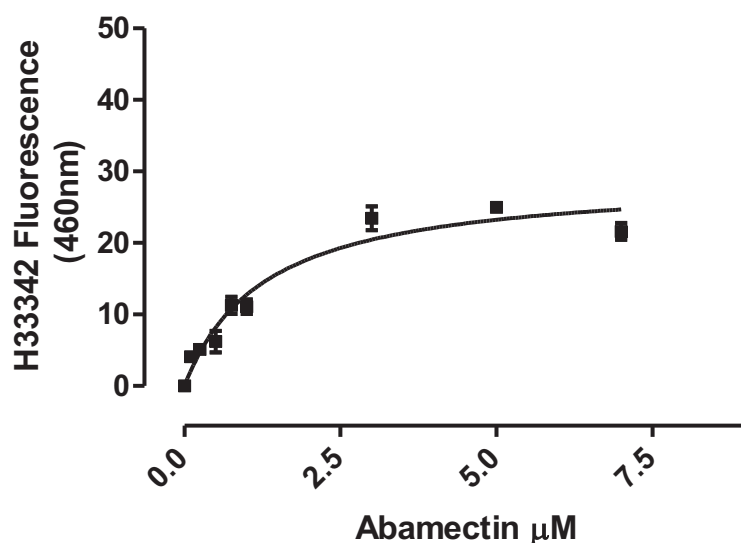


Figure 4.14 Dose-response curve for the ability of abamectin (0-7 μM) to inhibit *mdr1a*-mediated efflux of 1 μM H33342 in N2a cells.

Data are mean \pm S.E.M. $n = 6$ wells per concentration from a single experiment representative of 4 independent experiments, analysed with non-linear least-squares regression. The IC_{50} of the above curve is $1.29 \pm 0.21 \mu\text{M}$. ($R^2=0.87$). The other individual experiments generated IC_{50} values of $1.35 \pm 0.39 \mu\text{M}$, $0.21 \pm 0.08 \mu\text{M}$, $1.94 \pm 0.60 \mu\text{M}$, $0.43 \pm 0.12 \mu\text{M}$ and $0.23 \pm 0.10 \mu\text{M}$ giving a mean IC_{50} of $0.91 \pm 0.29 \mu\text{M}$ and K_i of $0.77 \pm 0.25 \mu\text{M}$ (mean \pm S.E.M. $n = 6$).

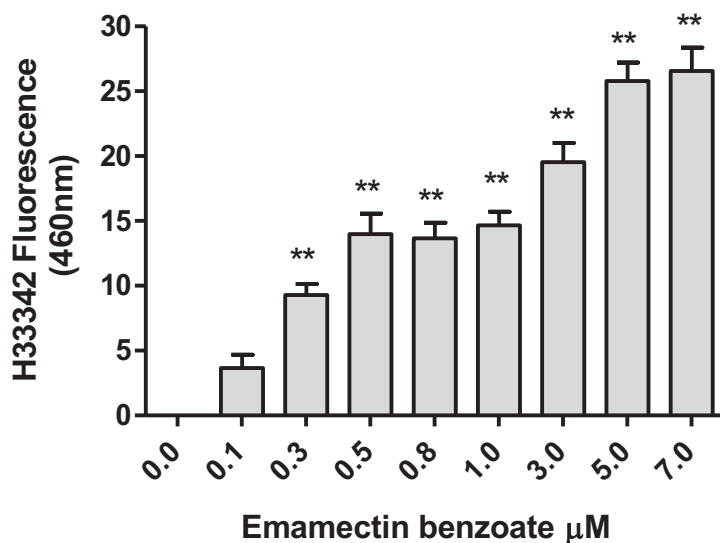


Figure 4.15 Dose-response curve for the ability of emamectin benzoate (0-7μM) to inhibit MDR1-mediated efflux of 1μM H33342 in SH-SY5Y cells.

Data are mean ± S.E.M. $n = 6$ wells per concentration from a single experiment representative of 4 independent experiments, analysed with One way ANOVA and Dunnett's post test; * $P < 0.05$, ** $P < 0.01$ versus control.

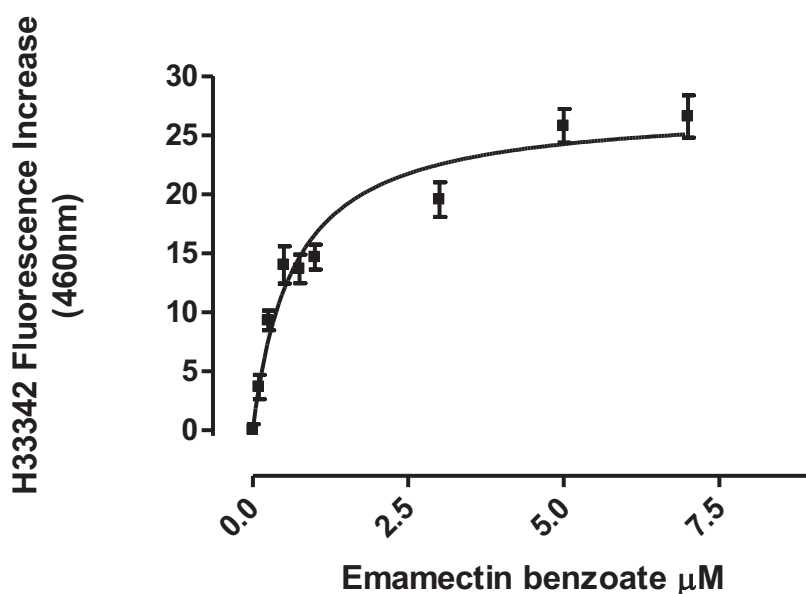


Figure 4.16 Dose-response curve for the ability of emamectin benzoate (0-7μM) to inhibit MDR1-mediated efflux of 1μM H33342 in SH-SY5Y cells.

Data are mean ± S.E.M. $n = 6$ wells per concentration from a single experiment representative of 4 independent experiments, analysed with non-linear least-squares regression. The IC_{50} of the above curve is $0.65 \pm 0.10 \mu M$ ($R^2 = 0.87$). The other individual experiments generated IC_{50} values of $0.75 \pm 0.09 \mu M$, $0.78 \pm 0.11 \mu M$, $0.38 \pm 0.09 \mu M$, $0.86 \pm 0.31 \mu M$ and $0.51 \pm 0.12 \mu M$, giving a mean IC_{50} of $0.66 \pm 0.07 \mu M$ and K_i of $0.60 \pm 0.07 \mu M$ (mean ± S.E.M. $n = 6$).

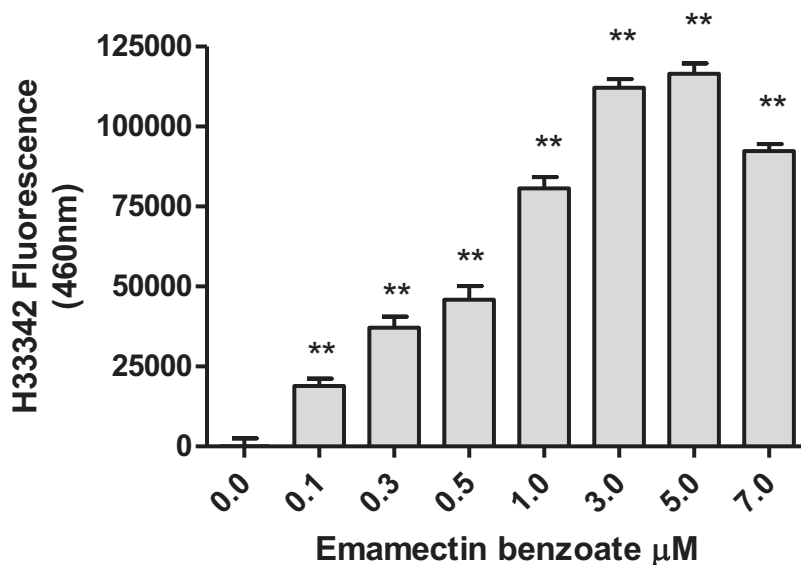


Figure 4.17 Dose-response curve for the ability of emamectin benzoate (0-7 μM) to inhibit *mdr1a*-mediated efflux of 1 μM H33342 in N2a cells.

Data are mean \pm S.E.M. $n = 6$ wells per concentration from a single experiment representative of 4 independent experiments, analysed with One way ANOVA and Dunnett's post test; * $P < 0.05$, ** $P < 0.01$ versus control.

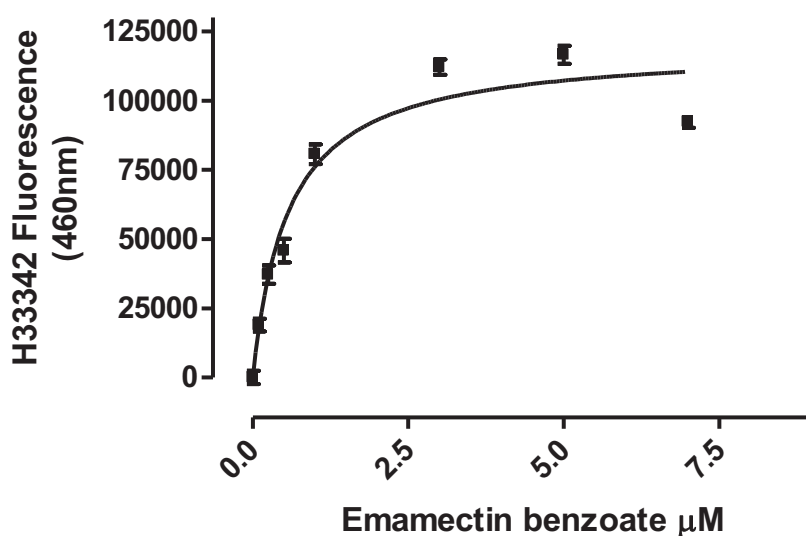


Figure 4.18 Dose-response curve for the ability of emamectin benzoate (0-7 μM) to inhibit *mdr1a*-mediated efflux of 1 μM H33342 in N2a cells.

Data are mean \pm S.E.M. $n = 6$ wells per concentration from a single experiment representative of 4 independent experiments, analysed with non-linear least-squares regression. The IC_{50} of the above curve is $0.57 \pm 0.08 \mu\text{M}$ ($R^2 = 0.92$). The other individual experiments generated IC_{50} values of $0.68 \pm 0.16 \mu\text{M}$, $0.72 \pm 0.22 \mu\text{M}$, $0.64 \pm 0.28 \mu\text{M}$ and $0.70 \pm 0.26 \mu\text{M}$, giving a mean IC_{50} of $0.66 \pm 0.03 \mu\text{M}$ and K_i of $0.56 \pm 0.02 \mu\text{M}$ (mean \pm S.E.M. $n = 5$).

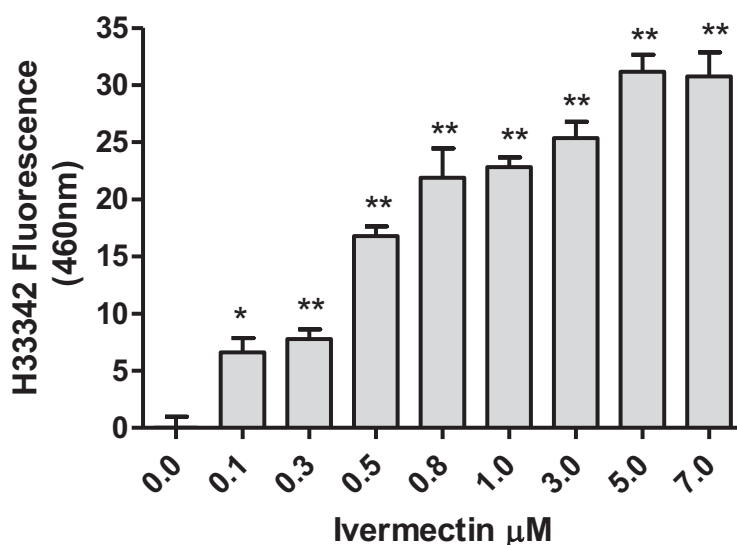


Figure 4.19 Dose-response curve for the ability of ivermectin (0-7 μM) to inhibit MDR1-mediated efflux of 1 μM H33342 in SH-SY5Y cells.

Data are mean \pm S.E.M. $n = 6$ wells per concentration from a single experiment representative of 4 independent experiments, analysed with One way ANOVA and Dunnett's post test; * $P < 0.05$, ** $P < 0.01$ versus control.

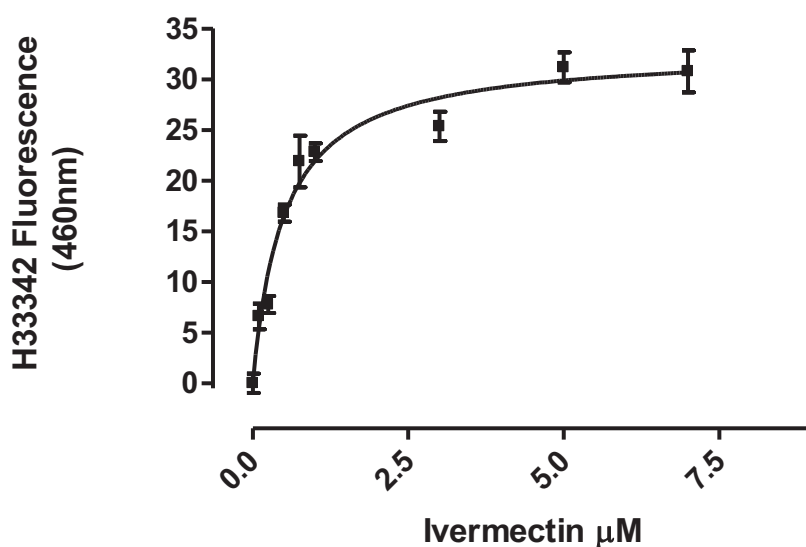


Figure 4.20 Dose-response curve for the ability of ivermectin (0-7 μM) to inhibit MDR1-mediated efflux of 1 μM H33342 in SH-SY5Y cells.

Data are mean \pm S.E.M. $n = 6$ wells per concentration from a single experiment representative of 4 independent experiments, analysed with non-linear least-squares regression. The IC_{50} of the above curve is $0.50 \pm 0.07 \mu\text{M}$ ($R^2 = 0.88$). The other individual experiments generated IC_{50} values of $0.22 \pm 0.05 \mu\text{M}$, $0.23 \pm 0.08 \mu\text{M}$ and $0.11 \pm 0.05 \mu\text{M}$, giving a mean IC_{50} of $0.27 \pm 0.08 \mu\text{M}$ and K_i of $0.24 \pm 0.08 \mu\text{M}$ (mean \pm S.E.M. $n = 4$).

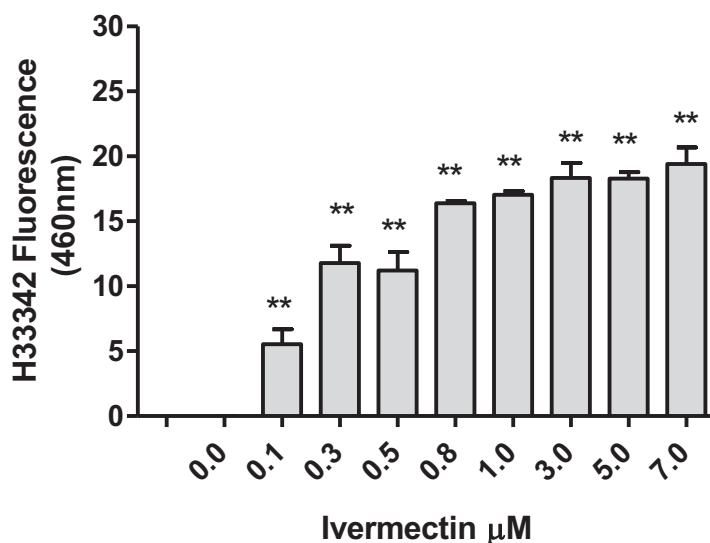


Figure 4.21 Dose-response curve for the ability of ivermectin (0-7 μM) to inhibit *mdr1a*-mediated efflux of 1 μM H33342 in N2a cells.

Data are mean \pm S.E.M. $n = 6$ wells per concentration from a single experiment representative of 4 independent experiments, analysed with One way ANOVA and Dunnett's post test; * $P < 0.05$, ** $P < 0.01$ versus control.

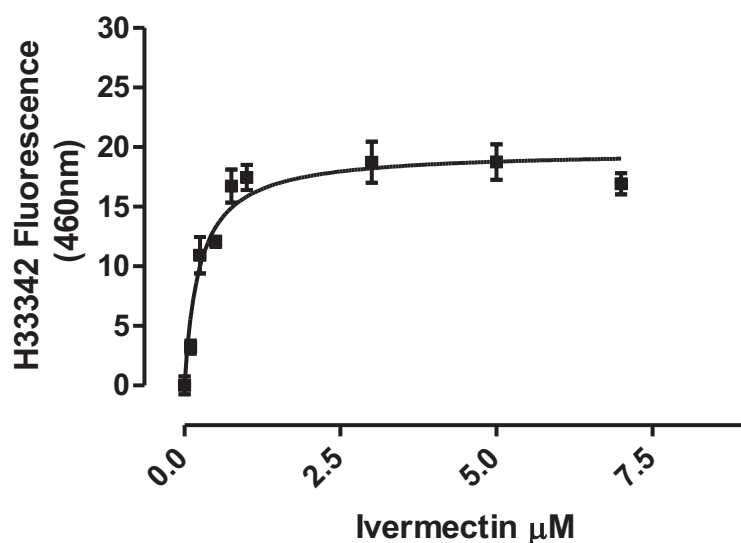


Figure 4.22 Dose-response curve for the ability of ivermectin (0-7 μM) to inhibit *mdr1a*-mediated efflux of 1 μM H33342 in N2a cells.

Data are mean \pm S.E.M. $n = 6$ wells per concentration from a single experiment representative of 4 independent experiments, analysed with non-linear least-squares regression. The IC_{50} of the above curve is $0.24 \pm 0.05 \mu\text{M}$ ($R^2 = 0.82$). The other individual experiments generated IC_{50} values of $0.15 \pm 0.07 \mu\text{M}$, $0.15 \pm 0.09 \mu\text{M}$ and $0.26 \pm 0.05 \mu\text{M}$, $0.17 \pm 0.05 \mu\text{M}$ and $0.31 \pm 0.07 \mu\text{M}$ giving a mean IC_{50} of $0.21 \pm 0.03 \mu\text{M}$ and K_i of $0.18 \pm 0.02 \mu\text{M}$ (mean \pm S.E.M. $n = 6$).

Table 4.1 Affinity constants (EC_{50} values) for H33342 in human SH-SY5Y and mouse N2a neuroblastoma cells.

EC_{50} values measure the affinities of the MDR1 and mdr1a transporters for H33342. Data are mean \pm S.E.M. $n = 4$ independent experiments, analysed with Student's two-tailed T-test ($P > 0.05$ between cell lines).

Mean EC_{50} values/ μ M	SH-SY5Y			N2a			P value
	Mean	SEM	N	Mean	SEM	N	
H33342	10.30	3.12	4	5.33	1.18	4	0.18

Table 4.2 K_i values for avermectin treatments in human and mouse neuroblastoma cells.

Data is K_i from IC_{50} via Cheng & Prusoff's equation (1973) (See Chapter 2 and Tables 4.6 and 4.7), mean \pm S.E.M. $n \geq 4$ independent experiments, analysed with Student's two-tailed T-test.

Mean K_i values/ μ M	SH-SY5Y			N2a			P value
	Mean	SEM	N	Mean	SEM	N	
CSA	1.42	0.29	5	0.37	0.10	4	$P < 0.05$
abamectin	0.95	0.08	6	0.77	0.25	6	$P > 0.05$
emamectin benzoate	0.60	0.07	6	0.56	0.02	5	$P > 0.05$
ivermectin	0.24	0.08	4	0.18	0.02	6	$P > 0.05$

Table 4.3 Mean K_i values of avermectins for MDR1-mediated efflux of H33342 in SH-SY5Y cells, analysed by One-Way ANOVA with Dunnett's post test.

The order of affinities is ivermectin \geq emamectin benzoate $>$ abamectin.

SH-SY5Y $K_i/\mu\text{M}$	Mean	SEM	N	P value
abamectin	0.95	0.08	6	----
emamectin benzoate	0.60	0.07	6	P<0.01
ivermectin	0.24	0.08	4	P<0.01

Table 4.4 Mean K_i values of avermectins for *mdr1a*-mediated efflux of H33342 in N2a cells, from $n \geq 4$ independent experiments, analysed by One-Way ANOVA with Dunnett's post test.

The order of affinities is ivermectin $>$ emamectin benzoate \geq abamectin.

N2a $K_i/\mu\text{M}$	Mean	SEM	N	P value
abamectin	0.77	0.25	6	----
emamectin benzoate	0.56	0.02	5	P>0.05
ivermectin	0.18	0.02	6	P<0.05

Table 4.5 Summary of EC₅₀ values for H33342 (0-15µM) CSA in SH-SY5Y cells and N2a cells. Mean IC₅₀ values were used to convert IC₅₀ values for inhibitors to K_i values (Cheng-Prussoff, 1973).

SH-SY5Y cells EC ₅₀ values/µM								
	Mean EC ₅₀ /µM	Mean	SEM	N				
H33342	18.3±12.90	10.67±1.98	9.00±1.00	3.18±0.48	H33342	10.30	3.12	4
N2a cells EC ₅₀ values/µM								
H33342	6.97±2.09	2.68±0.34	4.07±1.48	7.60±1.70	H33342	5.33	1.17	4

Table 4.6 Summary of IC₅₀ and K_i values and Mean ±SEM of data for the effect of selected avermectins and CSA on MDR1-mediated H33342 efflux in SH-SY5Y cells. IC₅₀ values were converted to K_i values using the Cheng and Prussoff method (1973) using the equation described in Chapter 2. In summary $K_i = [IC_{50}] / (1 + ([substrate] / EC_{50}))$. H33342 substrate concentration was 1µM. $1µM / 10.30 = 0.097 + 1 = 1.097$.

SH-SY5Y IC ₅₀ values/µM								
	IC ₅₀	K _i	Mean	SEM	N			
CSA	0.42±0.09	1.82±0.48	1.73±0.19	2.32±0.3	2.02±0.20	1.66	0.33	5
abamectin	0.85±0.17	1.34±0.32	0.95±0.15	0.77±0.11	1.19±0.25	1.18±0.36	0.09	6
emamectin benzoate	0.38±0.09	0.65±0.10	0.75±0.09	0.78±0.11	0.86±0.31	0.51±0.12	0.07	6
ivermectin	0.22±0.05	0.50±0.07	0.23±0.08	0.11±0.05		0.27	0.08	4
SH-SY5Y K _i values/µM								
	IC ₅₀	K _i	Mean	SEM	N			
CSA	0.38	1.66	1.58	2.11	1.36	1.42	0.29	5
abamectin	0.77	1.22	0.87	0.70	1.08	0.95	0.08	6
emamectin benzoate	0.35	0.59	0.68	0.71	0.78	0.60	0.07	6
ivermectin	0.20	0.46	0.21	0.10		0.24	0.08	4

Table 4.7 Summary of IC₅₀ and K_i values and mean ± S.E.M. of data for the effect of selected avermectins and CSA on mdr1a-mediated H33342 efflux in N2a cells.

IC₅₀ values were converted to K_i values using the Cheng and Prussoff method (1973) using the equation described in Chapter 2. In summary, $K_i = [IC_{50}] / (1 + ([substrate] / EC_{50}))$. H33342 substrate concentration was 1 μM. $1 \mu M / 5.33 = 0.188 + 1 = 1.188$.

		N2a IC ₅₀ values/ μM						Mean	SEM	N
CSA	0.36±0.05	0.39±0.10	0.22±0.06	0.80±0.40			0.44	0.13	4	
abamectin	0.23±0.10	0.21±0.08	1.94±0.60	1.29±0.21	0.43±0.12	1.35±0.49	0.91	0.29	6	
emamectin benzoate	0.72±0.22	0.64±0.28	0.68±0.16	0.57±0.08	0.70±0.26		0.66	0.03	5	
ivermectin	0.15±0.07	0.15±0.09	0.26±0.05	0.24±0.05	0.17±0.05	0.31±0.07	0.21	0.03	6	
		N2a K _i values/μM						Mean	SEM	N
CSA	0.30	0.33	0.19	0.67			0.37	0.10	4	
abamectin	0.19	0.18	1.63	1.09	0.36	1.14	0.77	0.25	6	
emamectin benzoate	0.61	0.54	0.57	0.48	0.59		0.56	0.02	5	
ivermectin	0.13	0.13	0.22	0.20	0.14	0.26	0.18	0.02	6	

Summary Conclusions

The aims of this work were to characterise the dependence of intracellular accumulation of H33342 dye, a fluorescent MDR1 and BCRP substrate, upon avermectin exposure. We set out to compare kinetics in mouse and human cells for the transporter interactions. Abamectin, emamectin benzoate and ivermectin all interacted with human MDR1 and mouse *mdr1a*. Ivermectin had the highest affinity for this interaction with both MDR1 and *mdr1a*. The order of affinities for MDR1 in human SH-SY5Y cells was ivermectin (K_i $0.24 \pm 0.08 \mu\text{M}$) \geq emamectin benzoate (K_i $0.60 \pm 0.07 \mu\text{M}$) $>$ abamectin (K_i $0.95 \pm 0.08 \mu\text{M}$). The order of affinities for *mdr1a* in mouse N2a cells followed a similar trend with ivermectin (K_i $0.18 \pm 0.02 \mu\text{M}$) $>$ emamectin benzoate (K_i $0.56 \pm 0.02 \mu\text{M}$) \geq abamectin (K_i $0.77 \pm 0.25 \mu\text{M}$). Importantly, there were no significant differences in affinities for abamectin, emamectin benzoate or ivermectin between cell lines ($P > 0.05$). These findings indicate that existing kinetic data obtained in mouse models relating to endogenous *mdr1a* is applicable to humans, who express MDR1. Both cell lines were insensitive to Ko-143, indicating that BCRP and *bcrp* were not functionally expressed in human SH-SY5Y or mouse N2a cells.

Chapter 5 Measurement of the interaction of avermectin insecticides with multidrug resistance proteins using a CMFDA fluorescence dye retention assay

5.1 Summary

In view of the comparability of MDR1 kinetics with those of *mdr1a* demonstrated in Chapter 4, and the pre-existing conflict of opinion as to whether avermectins inhibit MRP/mrp transporter activity, this study aimed to characterise avermectin interaction with the MRP proteins.

I. Initial experiments measured intracellular retention of the fluorescent MRP/mrp substrate dye GSMF, an intracellular metabolic product of CMFDA. Intracellular GSMF retention increased significantly above background readings in the absence of dye ($P < 0.01$) with CMFDA concentrations up to $1.5\mu\text{M}$. In both cell lines, exposure to MK571 ($10\mu\text{M}$) caused an increase in intracellular fluorescence above dye-only controls, which was significant at CMFDA concentrations above $0.2\mu\text{M}$ in SH-SY5Y cells and above $0.4\mu\text{M}$ in N2a cells ($P < 0.001$ versus control).

II. In MK-571 concentration-dependence assays up to $15\mu\text{M}$ with a constant CMFDA concentration of $1\mu\text{M}$, significant inhibition of GSMF efflux was observed at $5\mu\text{M}$ MK-571 and above in SH-SY5Y cells ($P < 0.01$) and at $1\mu\text{M}$ and above ($P < 0.01$) in N2a cells compared to $1\mu\text{M}$ CMFDA alone.

III. Inhibition of GSMF efflux through MRP and mrp transporters by $5\mu\text{M}$ abamectin, $5\mu\text{M}$ CSA and $10\mu\text{M}$ MK-571 were all of comparable magnitude (all $P < 0.01$ versus $1\mu\text{M}$ CMFDA only).

IV. Dose-response curves were performed for selected avermectins ($0-7\mu\text{M}$) with $1\mu\text{M}$ CMFDA. Abamectin inhibited GSMF efflux with an IC_{50} of $2.25 \pm <0.01 \mu\text{M}$ ($n = 30$) in SH-SY5Y cells and $1.68 \pm 0.63 \mu\text{M}$ ($n = 24$) in N2a cells; emamectin benzoate with an IC_{50} of $1.87 \pm 0.57 \mu\text{M}$ ($n = 36$) in SH-SY5Y cells and $2.74 \pm 1.01 \mu\text{M}$ ($n = 24$) in N2a cells; and ivermectin with a mean IC_{50} of $1.58 \pm 0.51 \mu\text{M}$ ($n = 24$) in SH-SY5Y cells and $1.94 \pm 0.72 \mu\text{M}$ ($n = 24$) in N2a cells. There were no significant differences in IC_{50} values between cell lines ($P > 0.05$) for each avermectin tested. There were also no significant differences in IC_{50} values between abamectin, emamectin benzoate and ivermectin in either SH-SY5Y or in N2a cell lines (all $P > 0.05$).

5.2 Introduction

In this study it was of interest to assess whether MRP/mrp transporters interacted with avermectins in a similar way to MDR1 and *mdr1a* in the same model cell lines. Human MRP1 is highly expressed in neuroblastoma cell lines including undifferentiated SH-SY5Y cells similar to those used in this study (Bordow *et al.*, 1994).

CMFDA dye was used initially in flow cytometry to measure intracellular glutathione content in melanoma cells (Coates & Tripp, 1995) and to identify inflammatory cells based on its intracellular conjugation with glutathione. Its metabolic product GSMF was identified as a substrate of MRP transporter proteins and used in a fluorescence efflux assay to profile MRP transporter activity by Roelofsen *et al.* (1997). CMFDA diffuses across the cell membrane and is cleaved by non-specific intracellular esterases into CMF which slowly permeates the cell membrane. CMF reacts with intracellular thiol groups including those on glutathione, forming GSMF which is a high-affinity substrate for efflux by MRP transporters (Leier *et al.*, 2000; Lespine *et al.*, 2007; Förster *et al.*, 2008). The CMFDA assay has been used as a fluorescence assay to profile human MRP2 activity in MDCKII-MRP2 transfected cells, using MK-571 as a MRP2 inhibitor at 20 μ M to significantly increase intracellular CMF retention ($P < 0.01$ compared to control; Lindenmaier *et al.* 2005) with an IC_{50} of $21.2 \pm 1.1 \mu$ M in the same cells (Förster *et al.*, 2008). Förster and co-workers showed that inhibition of native BCRP and P-gp had no effect on intracellular fluorescence levels, indicating that the intracellular metabolite of CMFDA, GSMF, is a specific substrate for MRP family members. In the current study, GSMF was used as a substrate for the multidrug resistance proteins human MRP and mouse *mrp*, in a dye retention assay similar to the H33342 assay in Chapter 4 (See Methods Chapter 2). Transport kinetics were assessed as *cis*-inhibition of efflux of GSMF, through MRP/mrp transporters by MK-571 or selected avermectin insecticides.

MK-571 has been shown to selectively inhibit human multidrug resistance proteins at concentrations of the order of 10 μ M (Leier *et al.*, 2000; Lespine *et al.*, 2006). In the current study, MRP/mrp efflux activity was examined over a dye concentration range CMFDA 0-1.5 μ M, in the presence and absence of the MRP/mrp inhibitor MK571 (10 μ M). Concentration-dependence assays over a range of concentrations of MK-571 (0-50 μ M) were then obtained in each cell line at an external CMFDA concentration of 1 μ M. 10 μ M MK571

was included in all assays to confirm function of MRP/mrp transporters. Since CSA was used as a control inhibitor of MDR1/mdr1a in Chapter 4, and it is reported to inhibit the activity of multidrug resistance proteins as well (Matsson *et al.*, 2009), 5 μ M CSA was tested in the CMFDA assay to investigate the specificity of its inhibition of efflux transporters. To assess the interaction of avermectins with the MRP/mrp efflux transporters that are endogenously expressed in these neuroblastoma cells, dose response curves for abamectin, emamectin benzoate and ivermectin (0-7 μ M) were obtained with external CMFDA concentration set at 1 μ M.

5.3 Results

CMFDA dose-response curves

The human and mouse cell lines were exposed to a range of CMFDA concentrations in the presence and absence of the multidrug resistance protein inhibitor MK571 (10 μ M) and intracellular GSMF fluorescence was measured. Incubation of cells with 0-1.5 μ M CMFDA resulted in a significant increase in fluorescence compared with cells not exposed to CMFDA ($P < 0.01$). The increase in GSMF retention was a linear function of the external CMFDA concentration over the concentration range tested. Concentrations higher than 1.5 μ M resulted in cellular toxicity, so it was not possible to achieve saturation and obtain EC_{50} values for GSMF efflux; hence K_i values could not be calculated from IC_{50} values for putative inhibitors. In the presence of MK571 (10 μ M), intracellular retention of fluorescent GSMF was significantly higher than in the absence of MK571 at a given concentration of CMFDA.

Figure 5.1 shows mean data from 4 experiments (in total $n = 12$) in which SH-SY5Y cells were exposed to a range of CMFDA dye concentrations (0 - 1.5 μ M) in the presence or absence of 10 μ M MK571. Data are normalised to background fluorescence (100%). At 1 μ M CMFDA there is an increase of $3500 \pm 310\%$ above background (cells without dye). In the presence of MK571 (10 μ M) intracellular fluorescence is significantly higher - $11040 \pm 369\%$; $P < 0.001$ compared to 1 μ M CMFDA alone. MRP-mediated efflux of GSMF is therefore significantly inhibited by MK571 in SH-SY5Y cells.

Figure 5.2 shows mean data, normalised to background fluorescence (100%), from 4 experiments (in total $n = 12$) in which N2a cells were exposed to a range of CMFDA dye concentrations (0 - 1.5 μ M) in the presence or absence of 10 μ M MK571. At 1 μ M CMFDA

alone the intracellular GSMF fluorescence signal was $3745 \pm 478\%$ higher than background in the absence of dye, which is similar to the response of SH-SY5Y cells. After the addition of MK571 ($10\mu\text{M}$) intracellular fluorescence is significantly higher $-11540 \pm 729\%$; $P < 0.001$ compared to $1\mu\text{M}$ CMFDA alone, which demonstrates that efflux of GSMF mediated by mrp transporters was significantly inhibited by MK571 in N2a cells.

In summary, cells were exposed to a range of CMFDA concentrations to profile MRP and mrp efflux function in human and mouse cell lines and to determine the lowest practical CMFDA dye concentration to use for each cell line to give a measurable distinction in intracellular fluorescence levels between control and inhibitor. Human SH-SY5Y and mouse N2a neuroblastoma cells were both susceptible to inhibition of GSMF efflux by $10\mu\text{M}$ MK571 and responded with increases in intracellular GSMF fluorescence of comparable magnitude; 3.08- and 3.15-fold, respectively ($P > 0.05$). $1\mu\text{M}$ CMFDA was chosen as a suitable concentration for all further assays in both cell lines.

Efflux modulation by MK571 and CSA

The concentration dependence of intracellular GSMF fluorescence upon exposure to MK571 was assessed over a concentration range $0 - 50\mu\text{M}$ MK571 using $1\mu\text{M}$ CMFDA. Due to cellular toxicity in both cell lines at 25 and $50\mu\text{M}$ (data not shown) the analyses were restricted to $0 - 15\mu\text{M}$ MK571. Figures 5.3 and 5.4 show mean data from 4 experiments in SH-SY5Y cells and N2a cells, respectively, normalised to control ($n = 24$). In both sets of experiments there were significant increases in intracellular fluorescence above control at 5 , 10 and $15\mu\text{M}$ in SH-SY5Y cells ($P < 0.01$) and at $1\mu\text{M}$ and above in N2a cells ($P < 0.01$). The IC_{50} for inhibition of GSMF efflux through mrp transporters in N2a cells was $2.67 \pm 0.91\mu\text{M}$ (Figure 5.4). A saturable curve was not obtainable for SH-SY5Y cells in these experiments (Figure 5.3). $10\mu\text{M}$ MK571 was included in all subsequent experiments as an internal control to confirm functional inhibition of MRP/mrp transporters.

To test the specificity of transporter inhibition for the different compounds used, $5\mu\text{M}$ CSA was compared with $10\mu\text{M}$ MK571, $5\mu\text{M}$ abamectin, or control. $10\mu\text{M}$ MK571 and $5\mu\text{M}$ CSA both inhibit CMFDA dye efflux through MRP/ mrp transporters to a similar degree in SH-SY5Y cells (both $P < 0.01$ versus $1\mu\text{M}$ CMFDA only; Figure 5.5) and in N2a cells (both $P < 0.01$ versus $1\mu\text{M}$ CMFDA only; Figure 5.6).

Functional inhibition of CMFDA efflux through MRP and mrp transporters by avermectins

Abamectin, emamectin benzoate and ivermectin were all tested over a concentration range 0 – 7 μM in SH-SY5Y and N2a cell lines at a constant CMFDA concentration of 1 μM to generate dose-response curves, in which data were normalised to solvent only control (0 μM avermectin, 100%) and then 100% control was subtracted and data expressed as % fluorescence increase above control. MK-571 (10 μM) was included in all assays with avermectins as an internal control, where it consistently inhibited CMFDA efflux significantly compared to control ($P < 0.01$ in all experiments). Significant concentration-dependent increases in intracellular dye retention were observed for all insecticides tested in both cell lines ($P < 0.01$ at 5 μM and above). Dose-response curves generated were analysed by non-linear least-squares regression to generate IC_{50} values (summarised in Tables 5.1, 5.2 and 5.3). A drop-off in intracellular fluorescence levels was observed for all three avermectins in both cell lines above 6 μM , so dose-response curves are shown over the concentration range 0 – 6 μM only.

Abamectin

SH-SY5Y human cells were exposed to a range of abamectin concentrations (0 – 6 μM) and fluorescent GSMF retained inside cells was quantified at 520 ± 2.5 nm. Mean data from 5 independent experiments (total $n = 30$) are normalised to % control as above and shown as a dose response curve (Figure 5.7). The IC_{50} from nonlinear regression analysis for inhibition of GSMF efflux by abamectin in SH-SY5Y cells was $2.25 \pm <0.01$ μM .

Figure 5.8 shows mean data normalised to % control from 4 independent experiments ($n = 24$), performed in parallel in N2a mouse cells exposed to a range of abamectin concentrations (0 -6 μM). Analysis by non-linear regression returned an IC_{50} for abamectin of 1.68 ± 0.63 μM for inhibition of GSMF efflux in N2a cells.

To summarise, mean IC_{50} values were $2.25 \pm <0.01$ μM for abamectin in human SH-SY5Y cells and 1.68 ± 0.63 μM for mouse N2a cells. There are no significant differences for inhibition of GSMF efflux by abamectin between the SH-SY5Y human and N2a mouse cell lines (two-tailed t-test; $P = 0.32$, Table 5.1).

Emamectin benzoate

SH-SY5Y human cells were exposed to a range of concentrations of emamectin benzoate (0 - 6 μM). Data from 6 independent experiments (total $n = 36$) are expressed as mean \pm S.E.M. normalised to % control (Figure 5.9). Analysis by nonlinear least squares regression gave a dose-response curve with an IC_{50} for inhibition of GSMF efflux through human MRP transporters by emamectin benzoate of $1.87 \pm 0.57 \mu\text{M}$.

Figure 5.10 shows mean data, normalised to % control, from 4 independent experiments (total $n = 24$) performed in parallel in N2a mouse cells which were exposed to a range of 0 – 6 μM emamectin benzoate concentrations. Nonlinear regression analysis generated an IC_{50} for inhibition of GSMF efflux through mouse mrp transporters by emamectin benzoate of $2.74 \pm 1.01 \mu\text{M}$.

Emamectin benzoate inhibited H33342 efflux with a Mean IC_{50} of $1.87 \pm 0.57 \mu\text{M}$ for human SH-SY5Y cells and $2.74 \pm 1.01 \mu\text{M}$ for mouse N2a cells. There are no significant differences between the human and mouse cell lines in Mean IC_{50} values for inhibition of CMFDA efflux by emamectin benzoate (two-tailed t-test; $P = 0.42$, Table 5.1).

Ivermectin

SH-SY5Y human cells were exposed to a range of ivermectin concentrations (0 - 6 μM). Figure 5.11 shows mean data from 4 individual experiments ($n = 24$), normalised to % control. Data were analysed by nonlinear regression to generate an IC_{50} of $1.58 \pm 0.51 \mu\text{M}$ for the ability of ivermectin to inhibit GSMF efflux through human MRP transporters.

Figure 5.12 shows mean data from 4 independent experiments (total $n = 24$), normalised to % control, in N2a mouse cells exposed to a range of ivermectin concentrations (0 – 6 μM). Nonlinear regression analysis of the dose-response curve gave an IC_{50} of $1.94 \pm 0.72 \mu\text{M}$ for inhibition of GSMF efflux through mouse mrp transporters by ivermectin.

In summary, ivermectin inhibited H33342 efflux with a mean IC_{50} of $1.58 \pm 0.51 \mu\text{M}$ for human SH-SY5Y cells and $1.94 \pm 0.72 \mu\text{M}$ for mouse N2a cells. There are no significant differences between the human and mouse cell lines in Mean IC_{50} values for inhibition of CMFDA efflux by ivermectin (two-tailed T-test; $P = 0.69$, Table 5.1).

Data obtained in this chapter for the interaction of abamectin, emamectin benzoate and ivermectin with MRPs expressed in the neuroblastoma cell line SH-SY5Y, of human origin, and with mrps expressed in N2a cells of mouse origin, indicates that all three avermectins tested significantly inhibit the efflux of CMFDA through both MRP and mrp transporters ($P < 0.01$ vs solvent only control at $5\mu\text{M}$ and above of each avermectin), and that there are no significant species differences in this interaction. Similar data was obtained for MDR1 and *mdr1a* in Chapter 4.

5.5 Discussion

Human MRP2 activity was measured in MDCKII-MRP2 transfected cells by Lindenmaier *et al.*, (2005) using $20\mu\text{M}$ MK571 as a positive control inhibitor to test the interaction of selected progestins with MRP2 in the CMFDA assay. Förster *et al.* (2008) found that MK-571 had an IC_{50} of $21.2 \pm 1.1 \mu\text{M}$ as a MRP2 inhibitor in MDCKII-MRP2 cells using the CMFDA intracellular metabolite GSMF as an MRP substrate. In the current study, there were significant increases in intracellular GSMF fluorescence at $5\mu\text{M}$ MK571 and above in SH-SY5Y cells and $1\mu\text{M}$ MK571 and above in N2a cells, in four independent experiments (all $P < 0.01$ versus $1\mu\text{M}$ CMFDA only). The IC_{50} from these experiments for inhibition of GSMF efflux through mrp transporters in N2a cells was $2.67 \pm 0.91 \mu\text{M}$. An IC_{50} value was not obtainable for SH-SY5Y cells because the cells did not achieve saturation with GSMF. Experiments by others in our lab on the HK2 cell line have yielded similar results (data not shown).

Further support for MK571 as an effective inhibitor of MRP transporters comes from Leier *et al.* (2000), who report specific inhibition of PAH efflux by MK-571 with an IC_{50} of $4 \mu\text{M}$ in HEK293-MRP2 cells. MK-571 also inhibited human MRP1 in an HL60-MRP1 transfected cell line at concentrations up to $30\mu\text{M}$ with an IC_{50} of $2\mu\text{M}$ in a retention assay using Calcein-AM (Lespine *et al.*, 2006). It is apparent that IC_{50} values differ according to the efflux substrate and cell line used, however the value of $2.67 \pm 0.91 \mu\text{M}$ obtained for N2a cells in this study is in agreement with above values obtained in transfected cells using Calcein-AM or PAH (2 and $4 \mu\text{M}$, respectively; Lespine *et al.*, 2006 and Leier *et al.*, 2000). Experiments using $1\mu\text{M}$ CMFDA with MK571 over a concentration range $0 - 15 \mu\text{M}$ need to be repeated to obtain a corresponding IC_{50} for SH-SY5Y cells.

In the current study, abamectin, emamectin benzoate and ivermectin all inhibited efflux of the CMFDA metabolite GSMF through MRP transporters in human SH-SY5Y neuroblastoma cells with respective mean IC_{50} values of $2.25 \pm <0.01 \mu\text{M}$, $1.87 \pm 0.57 \mu\text{M}$ and $1.58 \pm 0.51 \mu\text{M}$; all three avermectins also inhibited GSMF efflux through mrp transporters in N2a neuroblastoma cells with respective mean IC_{50} values of $1.68 \pm 0.63 \mu\text{M}$, $2.74 \pm 1.01 \mu\text{M}$ and $1.94 \pm 0.75 \mu\text{M}$. There were no significant differences in affinities of abamectin ($P=0.32$), emamectin benzoate ($P=0.42$) or ivermectin ($P=0.69$) for MRP or mrp transporters between human SH-SY5Y or mouse N2a cells (Table 5.1). Likewise affinities of the avermectins for MDR1 or *mdr1a* did not differ significantly between the two cell lines (Chapter 4). All avermectins tested had affinities in the low micromolar range for inhibition of efflux of the CMFDA metabolite GSMF through MRP/mrp transporters, similar to the affinities measured for H33342 efflux inhibition through MDR1/*mdr1a* in Chapter 4. This is an important finding in the light of conflicting reports as to the role of MRP/mrp transporters in ivermectin efflux (Lespine *et al.*, 2006; Brayden & Griffin, 2008).

Brayden and Griffin (2008) suggested that ivermectin and selamectin did not undergo flux through MRP2, since the avermectins apparently did not inhibit the flux of the MRP2-specific substrate sulforhodamine 101 through MDCKII-MRP2 cells (data not shown). These authors performed basal-apical and apical-basal flux studies in MDCK II-MDR1, MDCKII-MRP1 and MDCKII-MRP2 transfected cells, as well as MDCKII wild-type cells. Fluxes of radiolabelled ivermectin and selamectin were polarised in the basolateral to apical direction in MDCKII-MDR1 cells. Ivermectin and selamectin were also found to inhibit the flux of Rhodamine-123, an MDR1/*mdr1* substrate (Matsson *et al.*, 2009). The validity of transport assays on MRP- expressing cell lines was limited by two factors; the constitutive expression of functional *mdr1* (most likely canine) across all cell types, and the lack of an MRP1-specific substrate.

Conversely, Lespine *et al.*, (2006) present evidence which supports the data for ivermectin obtained in the current study. These researchers conducted transport assays in two different cell lines in which MRP1 expression is high, using two different dyes. In A459 cells the apparent IC_{50} for ivermectin with Calcein-AM was $1 \mu\text{M}$, and $2.5 \mu\text{M}$ with BCECF; in HL60-MRP1 cells the IC_{50} for ivermectin was $3.8 \mu\text{M}$ with Calcein-AM only. The IC_{50} values for

inhibition of dye efflux by ivermectin in the current study using CMFDA are similar to that for Calcein-AM in A459 cells ($1\mu\text{M}$), at $1.58 \pm 0.51 \mu\text{M}$; however this is for all MRP transporters expressed in the cells, not necessarily reflecting solely MRP1 activity. It should be noted that IC_{50} values obtained using different substrate dyes are not directly comparable; this would require K_i values, however the similar findings in the two assay types by Lespine and co-workers (2007) and in the current study together provide strong support that ivermectin inhibits one or more human MRP transporters, including MRP1. Evidence suggesting interaction of ivermectin with other human MRP transporters indicates lower affinity, with inhibition of the ATPase activity of MRP2 and MRP3 returning IC_{50} values of $18 \pm 5 \mu\text{M}$ and $40 \pm 21 \mu\text{M}$ respectively, compared to MDR1 ($\text{IC}_{50} = 2.5 \pm 2\mu\text{M}$) and MRP1 ($\text{IC}_{50} = 9 \pm 4 \mu\text{M}$) (Lespine *et al.* 2006). The current study has extended this evidence by showing functional activity of MRP- and mrp- type transporters in human and mouse neuronal cells, respectively. This functional activity was likewise inhibited by ivermectin but also by abamectin and emamectin benzoate.

Contrary to the findings for human MDR1 and mouse *mdr1a*, there were no significant differences between affinities of abamectin, emamectin benzoate or ivermectin for MRP transporters (Table 5.2) or mrp transporters (Table 5.3) in either human SH-SY5Y or in mouse N2a cells (all $P > 0.05$ compared to abamectin). In contrast, the order of affinities for human MDR1 was ivermectin $>$ emamectin benzoate $>$ abamectin, and for mouse *mdr1a* was ivermectin $>$ emamectin benzoate \geq abamectin. Brayden and Griffin (2008) suggest that, where there is background expression of MDR1, substrate efflux by MRP proteins is not significant. The similarity of avermectin affinities for MDR1/*mdr1a* as for MRP/mrp transporters found in this study suggests that MRP/mrp proteins may have a complementary interaction with avermectins. The fact that they are inhibited with similar affinity means that the avermectins could affect the efflux of MRP/mrp substrates that are transported less efficiently by MDR1/*mdr1a*, such as unconjugated bilirubin (Corich *et al.* 2009).

There are reports elsewhere of substrate overlap, e.g. Calcein-AM and rhodamine-123 are transported by both MDR1 and MRP-type proteins (McAleer *et al.*, 1999; Brayden & Griffin, 2008); indeed if the substrates are multispecific the presence of multiple transporters may mask the source of observable effects. Due to the use of distinct dyes and specific inhibitors,

substrate overlap was not considered a problem in this study, however. Metabolites of CMFDA are specific substrates for MRP-/mrp- transporters (McAleer *et al.*, 1999; Luna-Tortós *et al.*, 2009; Förster *et al.*, 2008), H33342 is selective for MDR1/mdr1 and BCRP/bcrp at appropriate concentrations (Matsson *et al.*, 2009), and the transporters were responsive to their respective specific inhibitors (Ko-143 for BCRP/bcrp and MK-571 for MRP/mrp) in this study. Accordingly the IC₅₀ values obtained should relate to the specific transporter types under investigation in each assay, MDR1/mdr1 or MRP/mrp.

It is important that, in the current study, 5 μ M CSA was found to inhibit CMFDA efflux significantly compared to control ($P < 0.01$), consistently comparable with inhibition by 10 μ M MK-571. This observation is in agreement with another study which reports that CSA is a multi-specific inhibitor of MDR1, BCRP and MRP2 (Matsson *et al.* 2009). CSA is also capable of inhibiting human BCRP in transfected HEK-BCRP cells with an IC₅₀ of 4.3 \pm 1.9 μ M where there is little endogenous expression of MDR1 or MRP1/MRP2 (Gupta *et al.*, 2006).

In order to clarify the specificity of the two model inhibitors CSA and MK571, dose-response curves should be performed in the model cell lines with the CMFDA assay for MRP/mrp transporters simultaneously with H33342 as an MDR1/mdr1a substrate to quantify relative inhibition of each of the transporter types. The same assays should be performed with the avermectins, since the importance of the two transporter types in avermectin handling will depend not only on the affinity of the interactions, which are similar, but also upon absolute expression and activity levels, which can best be compared in a simultaneous assay. The excitation and emission wavelengths (355nm excitation and 480nm emission for H33342, and 480nm excitation and 520nm emission for CMFDA) are distinct enough that signal overlap was not a problem.

The experiments in the current studies were not flux assays, so although they have identified inhibitory interactions for abamectin, emamectin benzoate and ivermectin with MDR1/mdr1a as well as MRP/mrp transporters, they do not address whether or not these proteins mediate efflux of the avermectins. To address this question, further work is required to ascertain intracellular avermectin concentrations after treatment, using HPLC/MS. Assessment of intracellular concentrations under the same conditions with individual transporters knocked out would then determine which transporters are involved in avermectin efflux.

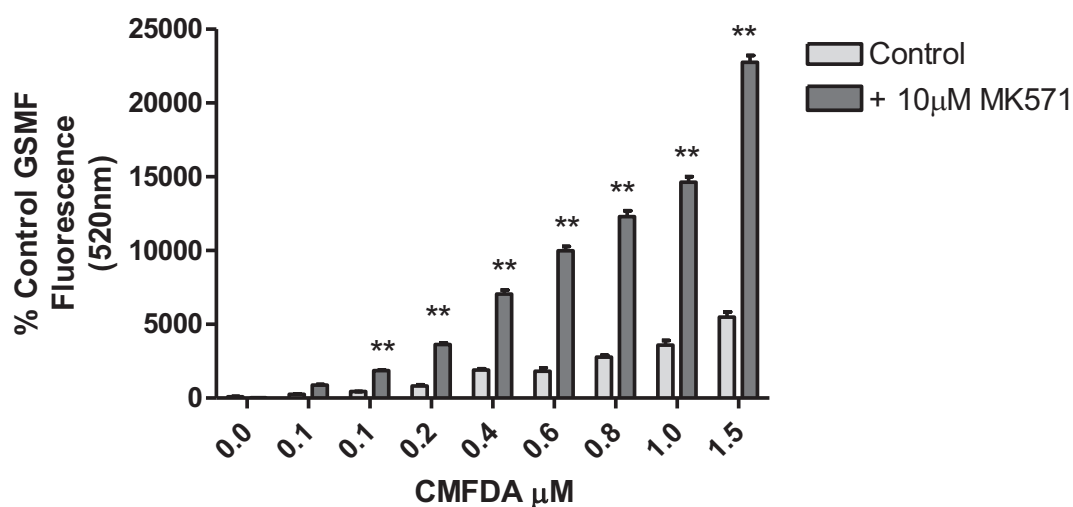


Figure 5.1 Concentration dependence of intracellular GSMF fluorescence after treatment with CMFDA (0-1.5 μM) in SH-SY5Y cells \pm 10 μM MK-571. The data above are mean \pm S.E.M. $n = 12$ wells per concentration from 4 experiments, analysed by One-way ANOVA with Dunnett's post-test; ** $P < 0.01$; At 0.2 μM CMFDA and above, the increases in intracellular fluorescence in the presence of 10 μM MK571 was significant compared to the corresponding control ($P < 0.001$ by Bonferroni's post-test, not shown).

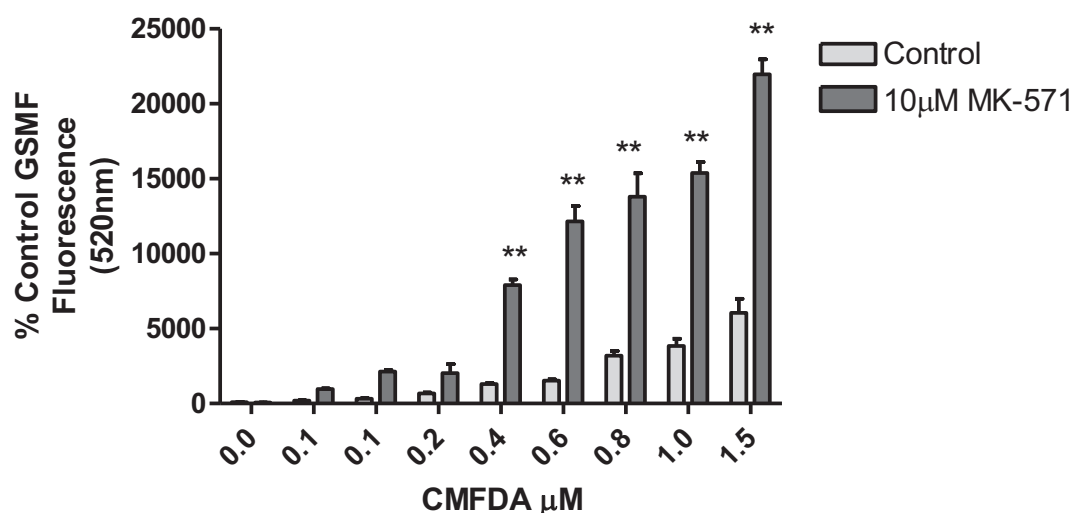


Figure 5.2 Concentration dependence of intracellular GSMF fluorescence after treatment with CMFDA (0-1.5 μM) in N2a cells \pm 10 μM MK-571. Data are mean \pm S.E.M. $n = 12$ wells per concentration from 4 experiments, analysed by One-way ANOVA with Dunnett's post-test; * $P < 0.05$; ** $P < 0.01$. At 0.4 μM CMFDA and above, the increase in intracellular fluorescence in the presence of 10 μM MK571 was significant compared to the corresponding control ($P < 0.001$ by Bonferroni's post-test, not shown).

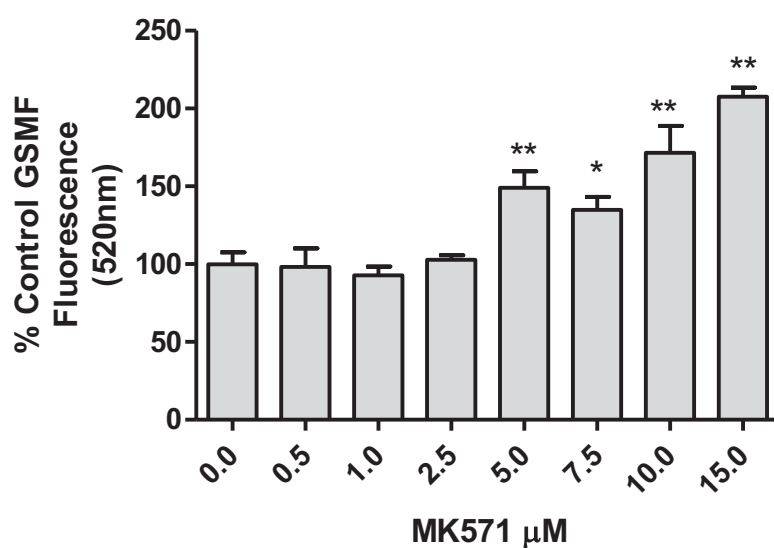


Figure 5.3 Concentration-dependence of MK-571 (0-15 μM) for the ability of to inhibit transporter-mediated efflux of 1 μM CMFDA in SH-SY5Y cells. Data are mean \pm S.E.M. $n = 24$ from 4 independent experiments, analysed by One-Way ANOVA with Dunnett's post-test; * $P < 0.05$; ** $P < 0.01$ versus control.

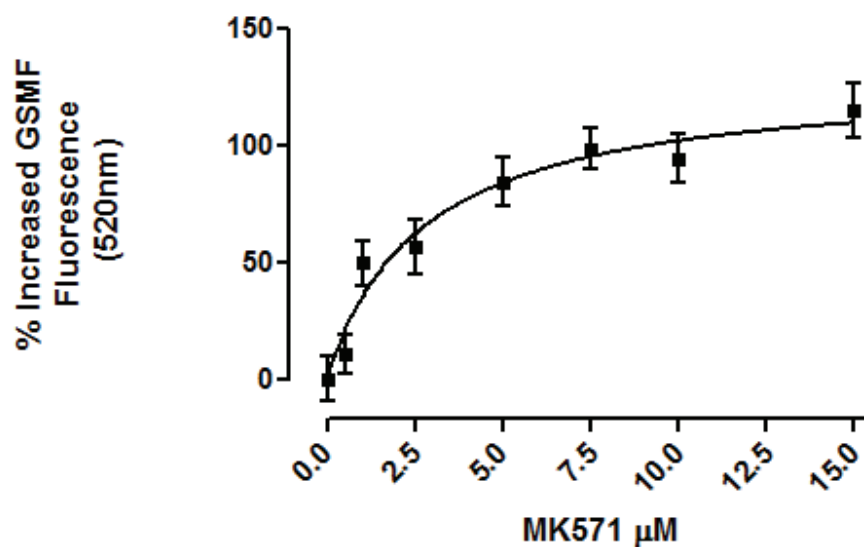


Figure 5.4 Concentration dependence of MK-571 (0-15 μM) for ability to inhibit transporter-mediated efflux of 1 μM CMFDA in N2a cells. Data are mean \pm S.E.M. of $n = 24$ from 4 independent experiments, analysed by nonlinear least-squares regression, One-site binding, Hyperbola. The mean IC_{50} for MK571 from the above curve is $2.67 \pm 0.91 \mu\text{M}$ in N2a cells.

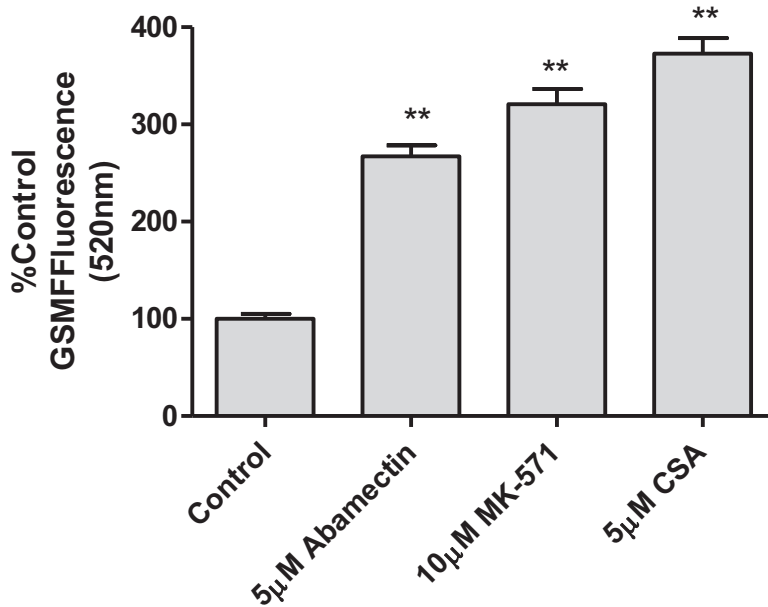


Figure 5.5 Inhibition of transporter-mediated efflux of 1µM CMFDA efflux by 5µM abamectin, 10µM MK571 or 5µM CSA in SH-SY5Y cells compared to control. Data are mean ± S.E.M. $n = 6$ wells from 2 independent experiments, analysed by One-way ANOVA and Dunnett's post test; * $P < 0.05$, ** $P < 0.01$ versus control.

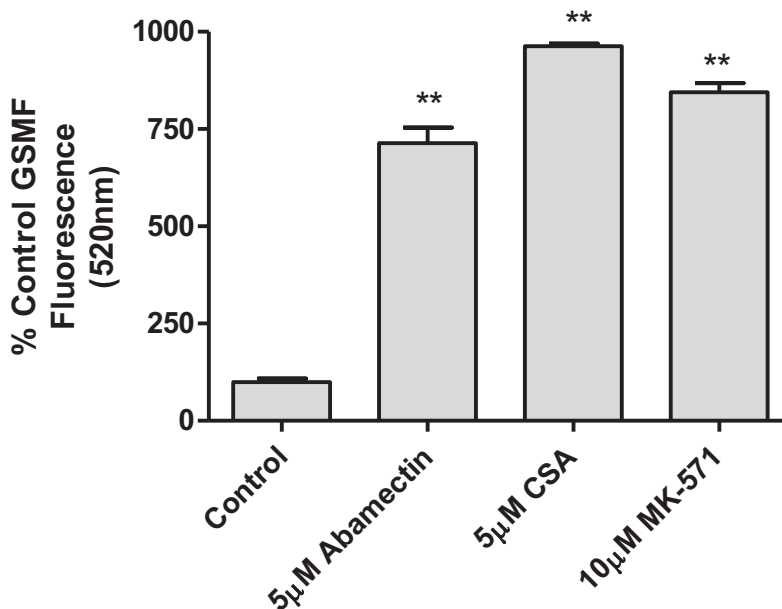


Figure 5.6 Inhibition of transporter-mediated efflux of 1µM CMFDA efflux by 5µM abamectin, 10µM MK571 or 5µM CSA in N2a cells compared to control. Data are mean ± S.E.M. $n = 6$ wells from 2 independent experiments, analysed by One-way ANOVA and Dunnett's post test; * $P < 0.05$, ** $P < 0.01$ versus control.

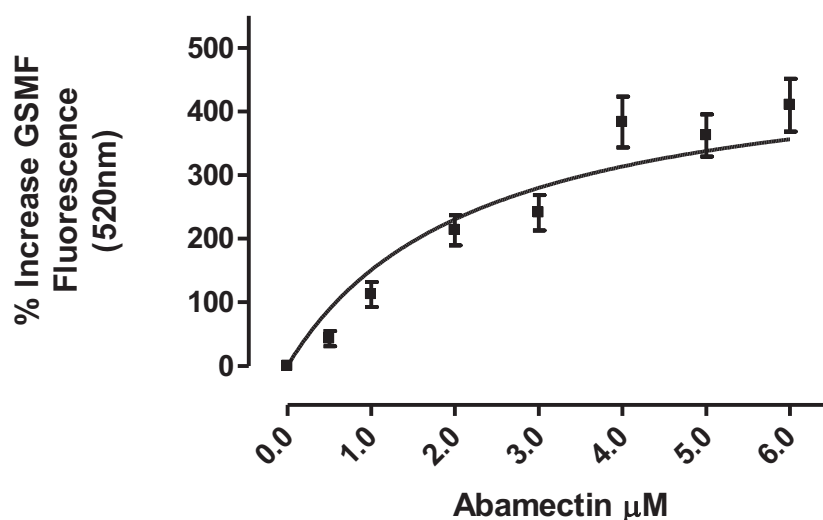


Figure 5.7 Dose-response curve for the ability of abamectin (0-6 μM) to inhibit MRP-mediated efflux of 1 μM CMFDA in SH-SY5Y cells. Data are mean ± S.E.M. $n = 30$ from 5 independent experiments, each $n = 6$ wells per concentration, analysed with non-linear least-squares regression. The IC_{50} of the above curve is $2.25 \pm <0.01 \mu\text{M}$.

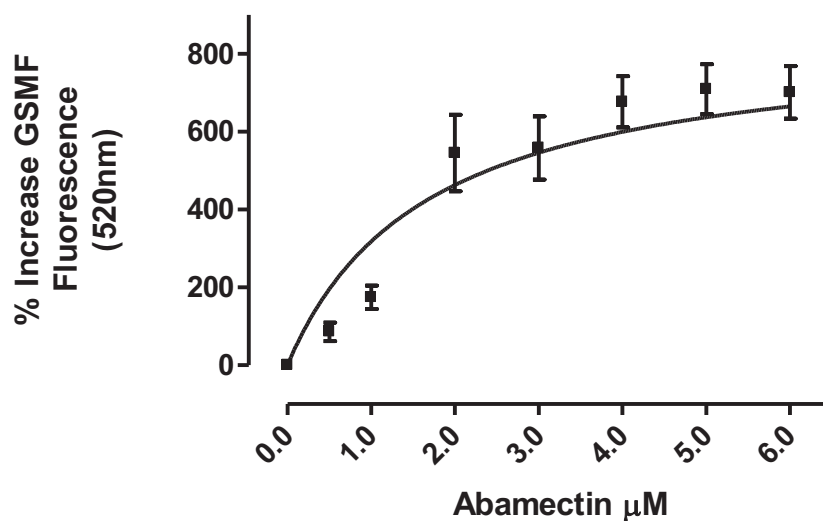


Figure 5.8 Dose-response curve for the ability of abamectin (0-6 μM) to inhibit MRP-mediated efflux of 1 μM CMFDA in N2a cells. Data are mean ± S.E.M. $n = 24$ from 4 independent experiments, analysed with non-linear least-squares regression. The IC_{50} of the above curve is $1.68 \pm 0.63 \mu\text{M}$.

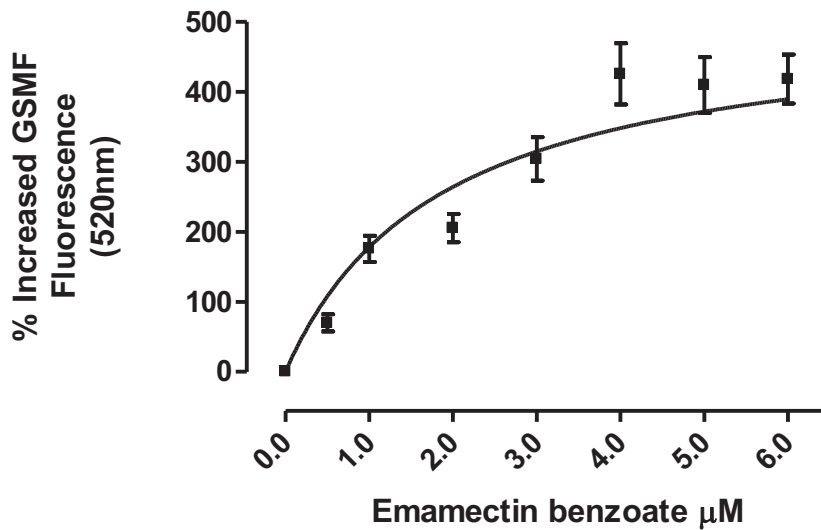


Figure 5.9 Dose-response curve for the ability of emamectin benzoate (0-6 μM) to inhibit MRP-mediated efflux of 1 μM CMFDA in SH-SY5Y cells. Data are mean \pm S.E.M. $n = 36$ from 6 independent experiments, analysed with non-linear least-squares regression. The IC_{50} of the above curve is $1.87 \pm 0.57 \mu\text{M}$.

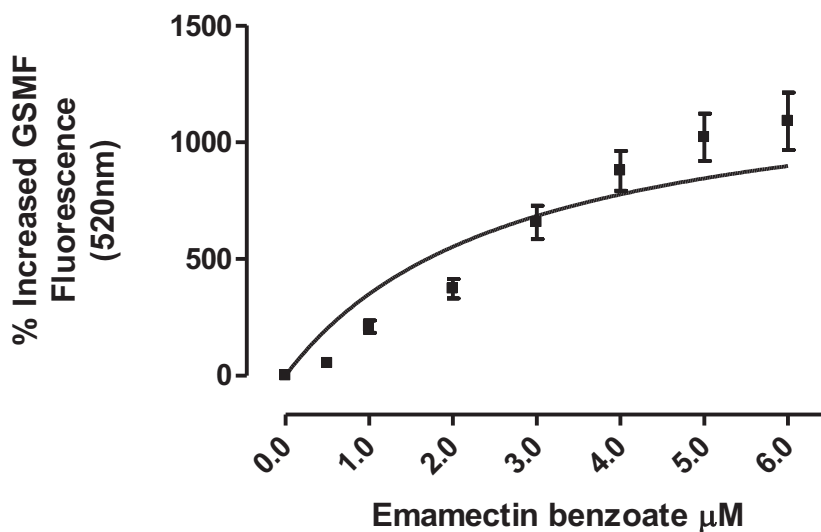


Figure 5.10 Dose-response curve for the ability of emamectin benzoate (0-6 μM) to inhibit mrp-mediated efflux of 1 μM CMFDA in N2a cells. Data are mean \pm S.E.M. $n = 24$ from 4 independent experiments, analysed with non-linear least-squares regression. The IC_{50} of the above curve is $2.74 \pm 1.01 \mu\text{M}$.

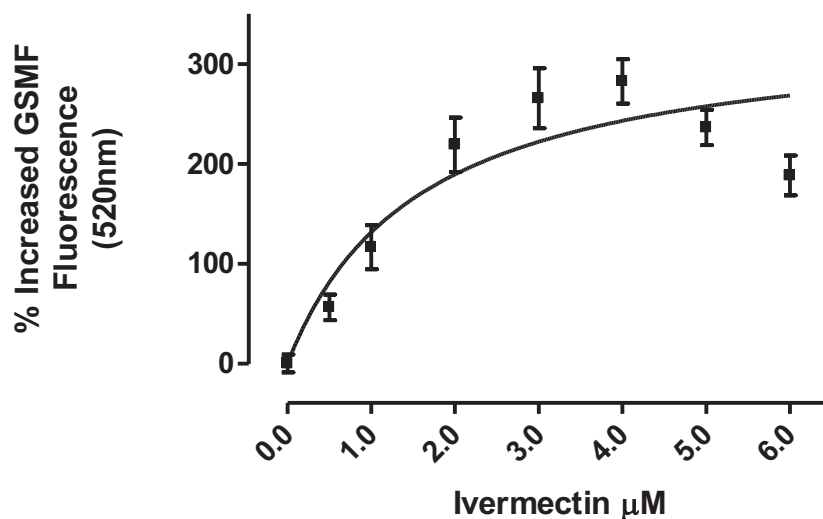


Figure 5.11 Dose-response curve for the ability of ivermectin (0-6 μM) to inhibit MRP-mediated efflux of 1 μM CMFDA in SH-SY5Y cells. Data are mean \pm S.E.M. $n = 24$ from 4 independent experiments, analysed with non-linear least-squares regression. The IC_{50} of the above curve is $1.58 \pm 0.51 \mu\text{M}$.

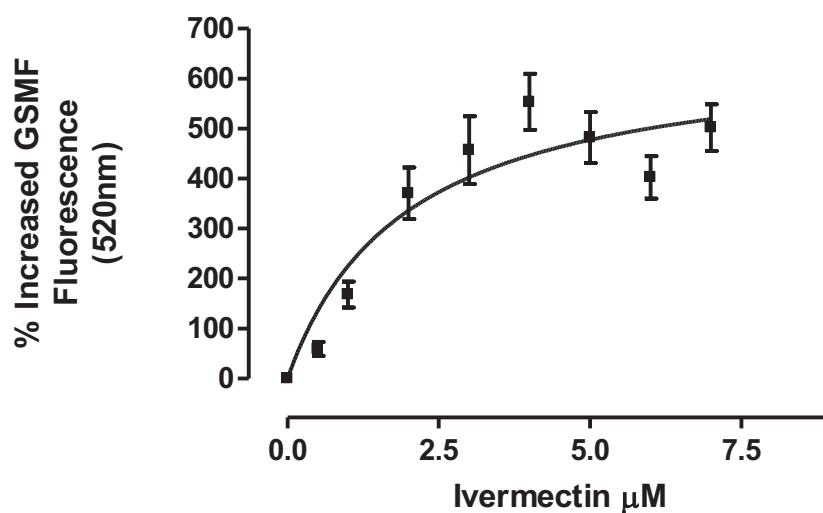


Figure 5.12 Dose-response curve for the ability of ivermectin (0-6 μM) to inhibit mrp-mediated efflux of 1 μM CMFDA in N2a cells. Data are mean \pm S.E.M. $n = 24$ from 4 independent experiments, analysed with non-linear least-squares regression. The IC_{50} of the above curve is $1.94 \pm 0.72 \mu\text{M}$.

Table 5.1 IC₅₀ values for interaction of the avermectin insecticides abamectin, emamectin benzoate and ivermectin with human MRP transporters and mouse mrp transporters in the CMFDA assay. The P values are from a t-test of each compound; all are P>0.05 indicating no significant differences in MRP interaction between the human SH-SY5Y and mouse N2a cell lines.

	SH-SY5Y			N2a			
	Mean	SEM	N	Mean	SEM	N	P value
abamectin	2.25	<0.01	30	1.68	0.63	24	0.32
emamectin benzoate	1.87	0.57	36	2.74	1.01	24	0.42
ivermectin	1.58	0.51	24	1.94	0.72	24	0.69

Table 5.2 Mean IC₅₀ values for interaction of the avermectin insecticides with MRP transporters in SH-SY5Y cells in the CMFDA assay. P values are from One-Way ANOVA with Dunnet's post-test; all are P>0.05 indicating no significant differences in affinity of abamectin, emamectin benzoate or ivermectin for MRP transporters in SH-SY5Y human cells.

Mean IC ₅₀ / μM	SH-SY5Y	SEM	N	P value
abamectin	2.25	<0.01	30	---
emamectin benzoate	1.87	0.57	36	P>0.05
ivermectin	1.58	0.51	24	P>0.05

Table 5.3 IC₅₀ values for interaction of the avermectin insecticides abamectin, emamectin benzoate and ivermectin with mouse mrp transporters in N2a cells in the CMFDA assay. P values are from One-Way ANOVA with Dunnet's post-test; all are P>0.05 indicating no significant differences in affinity of abamectin, emamectin benzoate or ivermectin for mrp transporters in N2a mouse cells.

Mean IC ₅₀ / μM N2a	SEM	N	P value
abamectin	0.63	24	---
emamectin benzoate	1.01	24	P>0.05
ivermectin	0.72	24	P>0.05

Summary Conclusions

To investigate the relevance of MRP/ mrp transporters to avermectin exposure, this study aimed to characterise avermectin interactions with the MRP and mrp transporter proteins. Kinetic data obtained for MDR1 and mdr1a in Chapter 4 could then be placed in the context of other transporters. CMFDA dye retention experiments confirmed the functionality of MRP and mrp transporters and sensitivity to MK-571 in SH-SY5Y and N2a cell lines. Dose response curves with $1\mu\text{M}$ CMFDA and either abamectin, emamectin benzoate and ivermectin at $0-7\mu\text{M}$ returned IC_{50} values that were comparable between cell lines ($P>0.05$) and avermectin compounds ($P>0.05$), ranging from $1.58 \pm 0.51 \mu\text{M}$ (ivermectin, SH-SY5Y cells) to $2.74 \pm 1.01 \mu\text{M}$ (emamectin benzoate, N2a cells). These values do not differ significantly from affinities for MDR1 and mdr1a, and thus abamectin, emamectin benzoate and ivermectin all have important interactions with MDR1 and MRP and their mouse counterparts in human SH-SY5Y and mouse N2a cell lines.

Chapter 6: Cell Viability and Markers of Avermectin Exposure

6.1 Summary

This section of work explores the effects of avermectin exposure upon cell viability, and potential early markers of exposure, such as changes in chemokine gene expression, neurite outgrowth and the expression of transporter genes.

- I. Abamectin and ivermectin exposure for 1 hour up to 10 μ M caused no significant decreases in mitochondrial dehydrogenase activity compared to control in either SH-SY5Y or N2a cell lines using the MTT assay of cell viability ($P > 0.05$).
- II. Exposure of cells to emamectin benzoate up to 5 μ M for 1 hour caused no significant changes in mitochondrial activity in either cell line ($P > 0.05$ compared to control). At 7-10 μ M emamectin benzoate in SH-SY5Y cells there was a significant decrease in conversion of MTT to formazan compared to control ($P < 0.01$), but this did not apply to N2a cells.
- III. From a qPCR array panel of 84 genes, expression of the BDNF, AIMP1, CX3CL1 and the chemokine-related factor SDF2 genes were identified as potential markers of exposure which increased or decreased expression more than 3-fold compared to control after exposure to 1 μ M emamectin benzoate or 1 μ M ivermectin.
- IV. An acute 1 hour exposure to 1 μ M abamectin, emamectin benzoate or ivermectin post-differentiation made no apparent qualitative difference to neurite expression in N2a cells compared with the positive control 0.1mM hydrogen peroxide, in preliminary experiments which need further investigation.
- V. Exposure of SH-SY5Y cells to 1 μ M abamectin, emamectin benzoate or ivermectin for 1 hour brought about no significant changes expression levels for the MDR1 or MRP1 gene compared to solvent control ($P > 0.05$ for both genes).

6.2 Introduction

MTT Assay of cell viability

The MTT assay has been used successfully as a measure of pesticide-induced damage of SH-SY5Y cells and other drug resistant cell lines (Hu *et al.*, 2009; Gao *et al.*, 2010) and N2a cells (Sul *et al.*, 2009). Hu and co-workers studied the cytotoxic effect of 100nM rotenone on SH-SY5Y cells in the presence and absence of a donor of hydrogen sulphide, which was found to

protect against rotenone-induced damage. Gao *et al.*, (2010) assessed the intrinsic cytotoxicity of the macrocyclic lactone sister compounds doramectin and nemadectin to the human breast carcinoma adriamycin-resistant cell line MCF7/adr, and found IC₅₀ values of 14µM and 19.7µM, respectively. 8µM of either compound was insufficient to cause 15% cell death. At concentrations of 1 – 8 µM, though, both compounds were effective at reversing resistance to adriamycin in a concentration-dependent manner. 8µM doramectin rendered these cells up to 50-fold more sensitive to adriamycin, and 8µM nemadectin brought about a 24-fold reversal in adriamycin resistance (Gao *et al.*, 2010). N2a cells were evaluated for their sensitivity to the neurotoxicant 2,3,7,8-tetrachlorodibenzo-p-dioxin (TCDD) from 0 - 1000 nM over 24 hour exposure using MTT by Sul *et al.*, (2009) who found that 100-1000nM TCDD brought about a significant decrease in mitochondrial activity (P < 0.05). Since the MTT method is thus a proven assay for pesticide toxicity in the test cell lines, it was used to measure gross changes in cell viability in response to avermectin exposure in the current study.

Chemokines in the CNS

Chemokines are constitutively expressed in a variety of brain cells including neurons, astrocytes and glial cells and are important in normal brain homeostasis and development; for example SDF1 and its receptor CXCR4 mediate neuronal migration during development (Bajetto *et al.*, 1999; Zhu *et al.*, 2009). Brain-derived neurotrophic factor, BDNF, is involved in regulating dopamine uptake and release in mouse brain (Bosse *et al.*, 2011). Chemokines have the potential to be useful markers of exposure because they are induced under conditions of cell damage e.g. ischemia during stroke, or viral infection and inflammation (Bajetto *et al.* 2001 Review).

Neurite outgrowth

Recently neurite outgrowth in mouse neuroblastoma N2a cells has proved to be a sensitive assay of damage in response to pesticide exposure. Both mouse N2a and human SHSY5Y cells can be induced to produce neurite outgrowths. Differentiated N2a and SH-SY5Y cells have both been used successfully in experiments on pesticide exposure and viral infection (Vesanen *et al.* 1994; Kume *et al.* 2008; Miglio *et al.* 2009; Cheung *et al.* 2009; Sun *et al.* 2010). Since differentiation of the cells affects expression levels of MDR1 (Bates *et al.*, 1989), it stands independently of the transport assays, which were all performed with undifferentiated cells. It is however of burgeoning interest as a quantitative marker of early

effects on cell growth and maintenance and is worth investigating for the avermectins in this study.

Modulation of MDR1 and MRP1 expression by avermectins

Both MDR1 (Bates *et al.*, 1989) and MRP1 (Bordow *et al.*, 1994; Corich *et al.*, 2009) are inducible genes, and both genes have been reported to interact avermectins (Lespine *et al.*, 2006). Furthermore, the related macrocyclic lactone compounds doramectin and nemadectin have been reported to down-regulate MDR1 mRNA and protein expression (Gao *et al.*, 2010). Hence it was of interest to see if the expression of these genes was affected by acute exposure to avermectins.

Aims

This study set out to ascertain the effect of acute avermectin exposure upon cell viability, measured by the MTT assay of mitochondrial dehydrogenase activity. The avermectin concentration range and length of exposure paralleled that of the transporter assays in Chapters 4 and 5. Potential markers of avermectin exposure were also of interest, preferably ones that can be identified earlier in time or at lower avermectin concentrations than those that might affect cell viability.

6.3 Results

MTT Assay

The MTT assay of cell proliferation was used in parallel to the transport assays, to measure the effect of avermectin exposure upon on cell monolayer integrity. The assay was first validated by dosing the cells with a range of concentrations of Triton-X100, which is a detergent that brings about cell lysis. Example experiments are shown in Figures 6.1 and 6.2 in SH-SY5Y and N2a cells respectively. From these validation experiments, 0.01% Triton-X100 was used as a positive control in all experiments to achieve 100% cell lysis with an exposure time of 15 minutes. Figure 6.3 displays the results from SH-SY5Y cells exposed to abamectin 0-10 μ M for 1 hour. In 4 independent assays after exposure to abamectin up to 10 μ M there were no significant differences in the percentage of cells capable of metabolising MTT to formazan compared to control ($P > 0.05$, $n = 4$ experiments, each $n = 6$ wells per concentration). The same was true for N2a cells (Figure 6.4; $P > 0.05$, $n = 4$ experiments).

Emamectin Benzoate was used to dose cells from 0-10 μ M for 1 hour. The results in Figure 6.5 for SH-SY5Y show that at 7 and 10 μ M there were significant decreases in viable cell number compared to control ($P < 0.05$ and $P < 0.01$ respectively, $n = 5$ experiments). To compare the sensitivity of N2a cells as compared to SH-SY5Y cells, cells were exposed to emamectin benzoate for 1 hour in the MTT assay. The mean data is presented and analysed in Figure 6.6. There was no significant trend in cell viability changes in response to any of the treatments compared to control in 4 independent experiments ($P > 0.05$, $n = 4$ experiments, each $n = 6$ wells per concentration), suggesting that the N2a cells may be less sensitive than SH-SY5Y cells to low μ M concentrations of this pesticide.

Figures 6.7 and 6.8 show MTT assays performed on SHSY5Y and N2a cells respectively, performed in parallel to the transporter experiments, to determine the effect of ivermectin upon cell proliferation. Cell viability for all ivermectin concentrations tested (up to 10 μ M) does not vary significantly from control after 1 hour exposure for either SH-SY5Y or N2a cells ($P > 0.05$, $n = 4$ experiments, each $n = 6$ wells per concentration).

Chemokine and receptor gene expression after avermectin exposure

Figures 6.7 A-D show mRNA for chemokines, chemokine receptors and chemokine-like factors expressed at a Ct value > 35 in SH-SY5Y cells exposed to 1 μ M emamectin benzoate (Figure 6.7 A & B) or ivermectin (Figure 6.7 C & D) for 18 hours, plotted against corresponding gene expression in solvent control samples. The 84-gene qPCR array panel used was SABiosciences PAHS-022. Notable expressed genes are shown in red; these are BDNF (Figure 6.7 C), which increased its expression level above control after treatment with Ivermectin; AIMP1 (Figure 6.7 C) whose expression increased approximately 2-fold above control after treatment with both ivermectin and emamectin benzoate. There was decreased mRNA expression of the ligand CX3CL1 after exposure to both emamectin benzoate and ivermectin (Figure 6.7 -B, -C and -D). Of particular interest is SDF2 as a potential marker of exposure, since its expression decreased approximately 6-fold compared to control after exposure to both emamectin benzoate and ivermectin (1 μ M) (Figure 6.7 A & 6.7 C). The data obtained in the current study cannot be conclusive as to a potential, as some of the data conflicts and there were insufficient chemokine array plates available to increase the n number of the data, hence results are plotted individually for each of the two independent samples for each condition against its control; however, BDNF, AIMP1, CX3CL1 and SDF2 are all candidates for further study.

Neurite outgrowth

There are two different approaches to assessing neurite outgrowth, which measure different aspects of neurite health. The first method is to expose the cells to the putative toxin during differentiation. The second is to pre-differentiate the cells, then expose them to toxin post-differentiation, which is a measure of the maintenance of neurite integrity in mature cells. This latter was the method adopted in the current study.

N2a cells were induced to express neurites for 24 hours, then treated with either solvent control (Figure 6.8A), 0.1mM hydrogen peroxide (B) or 1 μ M abamectin(C, D), emamectin benzoate (E) or ivermectin (F) and antibody-stained as detailed in the methods section and figure legends. The cells were then visualised using a x63 oil immersion lens on a Leica TCS-NT confocal microscope, scanned with argon laser at 488 (FITC) and 568 (TRITC) with 4-6 sections in the xy plane (Figure 6.8 A-F). Each figure shown is representative of 6 similar fields for each condition. Qualitatively, treatment with the selected avermectins for 1 hour post neurite induction did not bring about significant reduction neurite expression by N2a cells. Acute exposure of neurite-induced N2a cells to 1 μ M abamectin, emamectin benzoate or ivermectin had no qualitative effect upon neurite expression as assessed in 2-3 independent experiments. The standard accepted for quantitation is 100 neurites per condition when measuring cell length and 100 neurites in control cells when counting neurite number. The current experiments produced too few neurites to meaningfully quantitate the results either by number or length, and these preliminary observations require further work.

Modulation of MDR1 and MRP1 expression by avermectins

To investigate the effect of avermectin exposure upon MDR1 and MRP1 mRNA expression, three independent passages of SH-SY5Y cells were dosed with 1 μ M abamectin, emamectin benzoate or ivermectin for 18 hours in the absence of serum. RNA samples from the cells were assayed by qPCR in triplicate, so that data are mean \pm S.E.M. of $n = 9$. No significant changes in MDR1 mRNA expression were found in SH-SY5Y cells ($P > 0.05$; Figure 6.9), or in expression levels of MRP1 mRNA ($P > 0.05$; Figure 6.10).

6.4 Discussion

MTT assay

As one of a number of measures of toxicity, we initially focussed on the MTT assay as a broad measure of cell proliferation and monolayer integrity in parallel to the transporter assays. The methodology was validated by looking at the impact of a short 1 hour exposure to Triton X100 upon the viability of SH-SY5Y and N2a cells. Triton X 100 proved to be a very effective method of inducing damage with maximal cell death occurring with Triton X100 concentrations as low as 0.01%. Avermectins were much less toxic to both cell lines. In a series of experiments repeated 4-5 times for each avermectin, we found no significant loss of cell viability as measured by MTT after 1 hour exposure of SH-SY5Y cells or N2a cells to either 10 μ M abamectin or ivermectin. In contrast, when the concentration dependence of emamectin benzoate induced cell damage was measured, exposure of SH-SY5Y cells to 10 μ M was associated with significant ($P < 0.01$) decrease in cell viability. The data indicate that exposure for 1 hour to emamectin benzoate concentrations of 7 μ M and above resulted in $\geq 50\%$ cell death. It is noted that it was difficult to obtain data points above 6 μ M for emamectin benzoate in the H33342 assay in Chapter 4; this can now be attributed to cellular toxicity at concentrations above 6 μ M. For comparison, circulating plasma concentrations of avermectins detected in animal models are $\sim 22 - 70$ nM/L (Alvinerie *et al.*, 1999; Gokbulut *et al.*, 2010).

Chemokines and receptors as potential biomarkers of avermectin exposure

Of all the chemokines and receptors whose expression was assayed in the array, the genes of particular interest as potential markers of avermectin exposure are BDNF, AIMP1 and SDF-2. BDNF (Brain-Derived Neurotrophic Factor) increased its mRNA expression levels compared to control in response to treatment with 1 μ M ivermectin. The expression of BDNF is induced by cortical neurons and it is necessary for the survival of striatal neurons in the human brain (NCBI Gene database, Dec 2008). The AIMP1 gene is specifically induced during apoptosis, and is likely to be responsible for modulating the activity of tRNA synthetase in normal cells, but renders vasculature sensitive to tumour necrosis factor during inflammation. (NCBI Gene Database, information dated Dec. 2008). AIMP1 increased its expression compared to control after treatment with both emamectin benzoate and ivermectin (Figure 6.9C) in 1 out of 2 samples and is worth further investigation as a potential marker.

CX3CL1 also decreased its expression in response to exposure to both avermectins tested (Figures 6.9 B, C & D) and has been found to suppress the activation of microglia in Parkinson's Disease, after insult with 6-hydroxydopamine (6-OHDA) and thus protect against neuronal cell damage; its expression is constitutively suppressed but low doses of 3ng/day to Sprague-Dawley rats resulted in neuroprotection (Pabon *et al.*, 2011). Also, CX3CL1 knockout mice are susceptible to autonomous neurotoxicity caused by microglial activation (Cardona *et al.*, 2006).

In contrast, the mRNA expression level of SDF-2 decreased compared to control after 18hr exposure to both avermectins. SDF2 (stromal-cell derived factor 2) is a secretory protein induced in the endoplasmic reticulum under stressed conditions, highly conserved in animals and plants. Mutations result in abortive growth and seedling development in the *Arabidopsis thaliana* plant, as it promotes the accumulation of unfolded proteins to facilitate growth and development (Schott *et al.* 2010). The data obtained in the current study cannot be conclusive as to a potential, as some of the data conflicts and there were insufficient chemokine array plates available to increase the *n* number of the data, however, BDNF, AIMP1, CX3CL1 and SDF2 are all candidates for further study.

Neurite outgrowth

Although there are a number of reports of successful quantitative measurement of neurite outgrowth in N2a cells and in SH-SY5Y cells, either by length or by number, it proved difficult to induce neurites in either cell line on a sufficiently large scale to obtain meaningful quantitative data ($n \geq 100$ neurites per condition). SH-SY5Y cells were a particularly difficult cell type to induce neurite expression in, since they tended to produce short, highly branched neurites, and the outgrowth of these was inhibited upon contact with the adjacent cells (data not shown). Different densities and time profiles were tested, but further work is required with other differentiation agents in order to make this data quantifiable and to compare both cell lines. The N2a cells tended to clump when seeded at a suitable density for neurite outgrowth, and unsuccessful variations in cell seeding density, this problem was overcome by low-level sonication of the cells in suspension for 30 seconds before seeding. It is important to note that this procedure may have had an effect upon transporter expression, itself, since it may have subjected the cells to mild stress, but this was not ascertained.

It is pertinent to compare the results of Sun *et al.*, (2010) who did quantitate a dose-dependent decrease in neurite expression with abamectin and the related compound doramectin in N2a cells at concentrations as low as 0.5 μ M up to 4 μ M. This was achieved by co-incubation of the avermectin compounds with the differentiation agent dibutyryl cAMP for 48hr, which is a much longer exposure time than that tested in this study. The measurements are also different; the work of Sun *et al.*, (2010) looked at the effects of avermectin exposure upon initiating differentiation, where as the current study looked at the maintenance of established neurites after an acute 1hr exposure. The longer exposure during differentiation is of interest and should be investigated in further work.

Modulation of MDR1 and MRP1 mRNA expression by avermectins

Exposure to abamectin, emamectin benzoate or ivermectin at 1 μ M for 18 hours resulted in no significant changes to the expression levels of mRNA for either MDR1 or MRP1 over 3 independent passages of SH-SY5Y cells. 18 hours is a short exposure time for the turnover of mRNA to protein and it is of interest to extend the time-span of these experiments to 24 and 48 hours. It would also be illuminating to incubate cells with a specific inhibitor of MDR1 or the MRP transporters, e.g. MK571, and assess whether exposure to avermectins brought about modulation of gene and protein expression of the transporter type whose activity was not inhibited. This would shed light on whether or not other transporters can compensate for loss of efflux function of the avermectins by a given transporter.

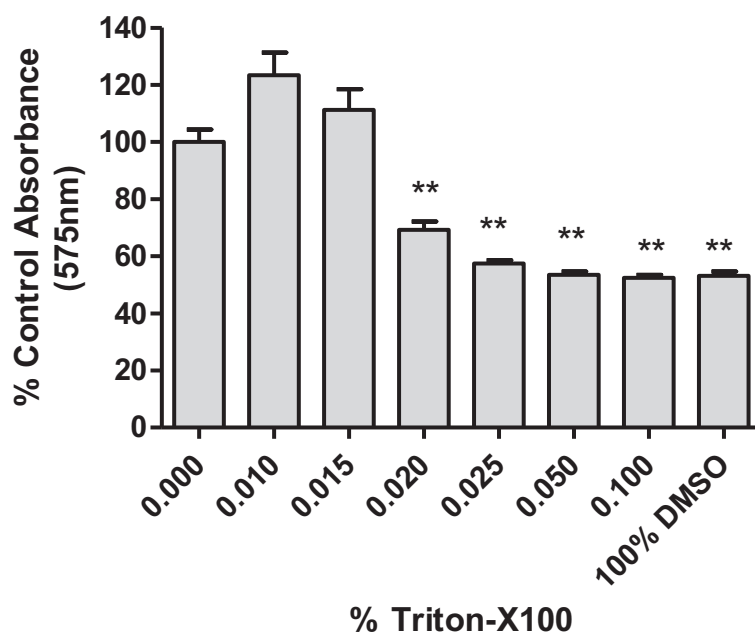


Figure 6.1 SH-SY5Y cells were exposed to a range of concentrations of Triton-X100. Data in the above experiment is mean \pm S.E.M. $n = 8$, representative of 3 similar experiments at different concentrations of detergent within the range 0 – 1.0 %. ** $P < 0.01$.

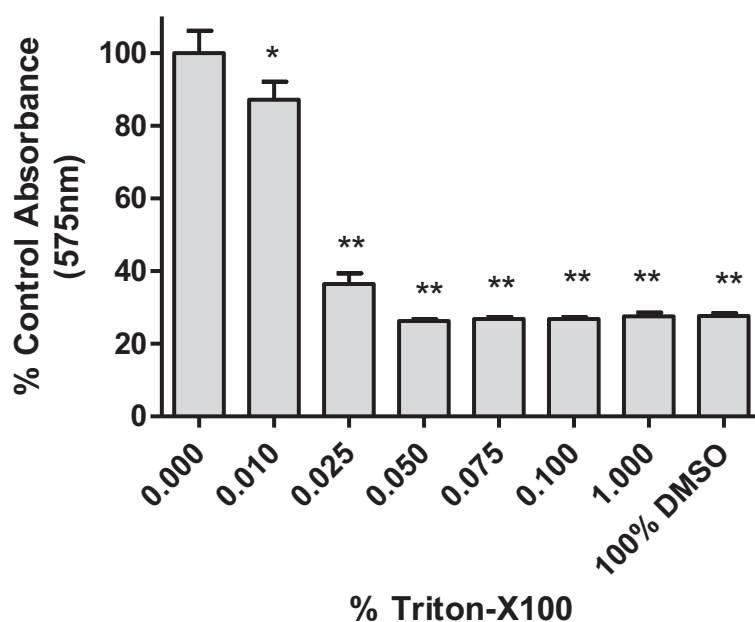


Figure 6.2 N2a cells were exposed to a range of concentrations of Triton-X100. Data in the above experiment is mean \pm S.E.M. $n = 8$, representative of 3 similar experiments at different concentrations of detergent within the range 0 – 1.0 % ** $P < 0.01$.

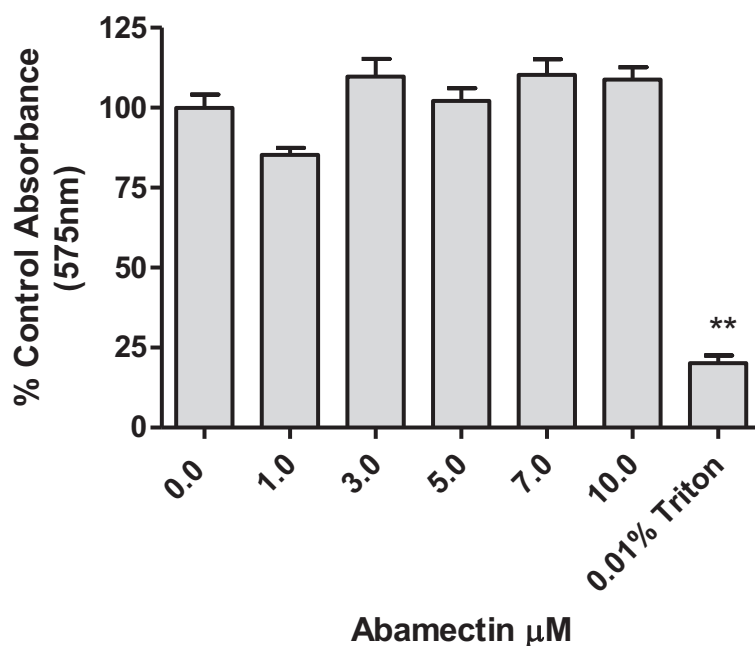


Figure 6.3 SH-SY5Y cells grown to a sub-confluent monolayer were exposed to abamectin at a concentration range 0-10µM for 1 hr, or to 0.01% triton-X-100 for 15 minutes and then incubated in the dark with MTT reagent dissolved in Krebs buffer for 2 hours at 37 °C, after which absorbance of intracellular formazan, solubilised in 100% DMSO, was read at 575 ± 5 nm, against a background of cells exposed to 100% DMSO but not MTT. The background absorbance was subtracted, and the readings were normalised to 100% for cells exposed to solvent control and MTT reagent. Data are mean \pm S.E.M. $n = 4$ experiments, each $n = 6$ wells per concentration. Data are analysed by One-Way ANOVA with Dunnett's post test compared to solvent control; ** $P < 0.01$.

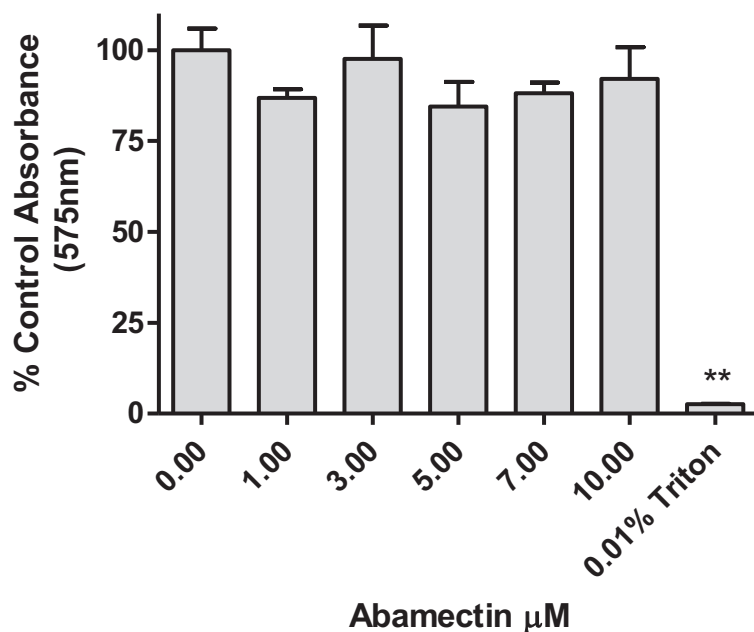


Figure 6.4 N2a cells grown to a sub-confluent monolayer were exposed to abamectin at a concentration range 0-10µM for 1 hr, or to 0.01% triton-X-100 for 15 minutes and then incubated in the dark with MTT reagent dissolved in Krebs buffer for 2 hours at 37 °C, after which absorbance of intracellular formazan, solubilised in 100% DMSO, was read at 575 ± 5 nm, against a background of cells exposed to 100% DMSO but not MTT. The background absorbance was subtracted, and the readings were normalised to 100% for cells exposed to solvent control and MTT reagent. Data are mean \pm S.E.M. $n = 4$ independent experiments, each $n = 6$ wells per concentration. Data are analysed by One-Way ANOVA with Dunnett's post test compared to solvent control; ** $P < 0.01$.

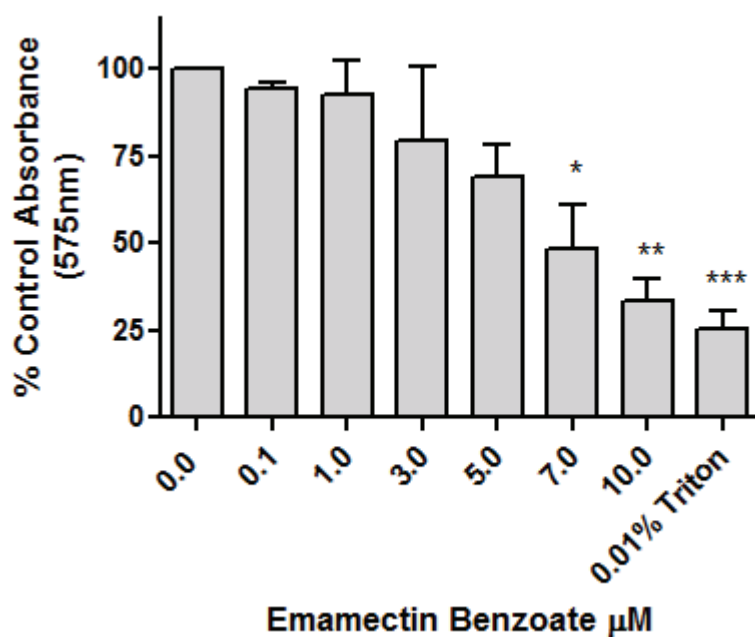


Figure 6.5 SH-SY5Y cells grown to a sub-confluent monolayer were exposed to emamectin benzoate at a concentration range 0-10 μM for 1hr or to 0.01% triton-X-100 for 15 minutes and then incubated with MTT reagent for 2 hours, after which absorbance of intracellular formazan, solubilised in 100% DMSO was read at 575nm against a background of cells without MTT exposed to the solubilisation agent DMSO (100%). The background absorbance was subtracted, and the readings were normalised to that for cells exposed to solvent control then MTT reagent. Data are mean \pm S.E.M. $n = 5$ independent experiments, each $n = 6$ wells per concentration. Data are analysed by One-Way ANOVA with Dunnett's post test compared to solvent control; * $P < 0.05$, ** $P < 0.01$, *** $P < 0.001$

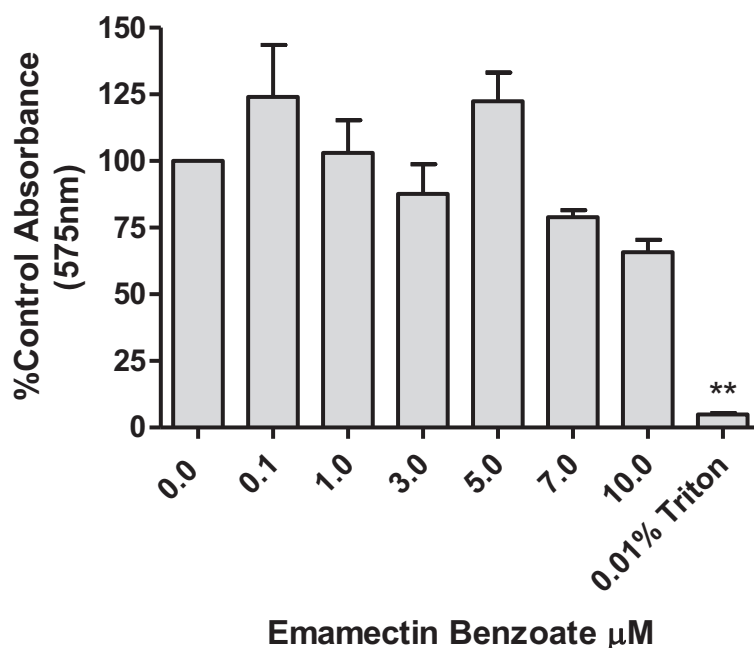


Figure 6.6 N2a cells grown to a sub-confluent monolayer were exposed to emamectin benzoate at a concentration range 0-10 μM for 1hr or to 0.01% triton-X-100 for 15 minutes and then incubated with MTT reagent for 2 hours, after which absorbance of intracellular formazan, solubilised in 100% DMSO was read at 575nm against a background of cells without MTT exposed to the solubilisation agent DMSO (100%). The background absorbance was subtracted, and the readings were normalised to that for cells exposed to solvent control then MTT reagent. Data are mean \pm S.E.M. of $n = 4$ independent experiments, each $n = 6$ wells per concentration. Data are analysed by One-Way ANOVA with Dunnett's post test compared to solvent control; ** $P < 0.01$.

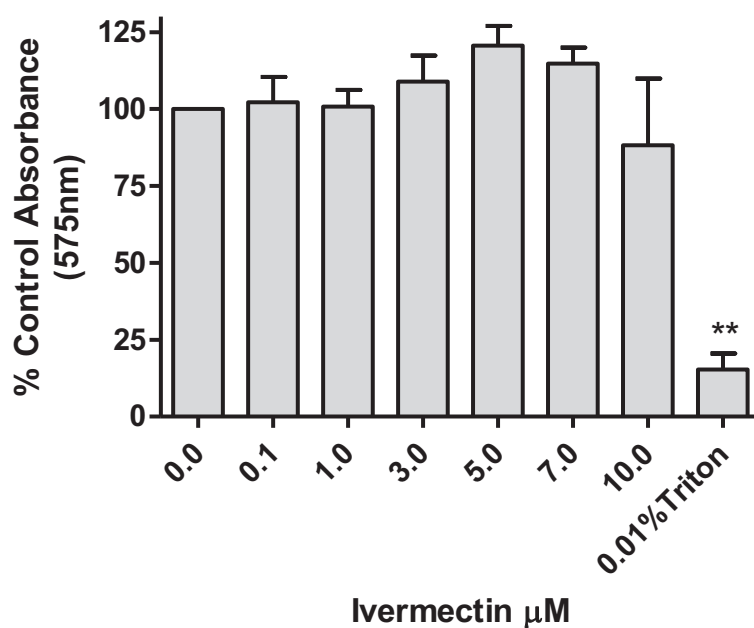


Figure 6.7 SH-SY5Y cells grown to a sub-confluent monolayer were exposed to ivermectin at a concentration range 0-10μM for 1hr or to 0.01% triton-X-100 for 15 minutes and then incubated with MTT reagent for 2 hours, after which absorbance of intracellular formazan, solubilised in 100% DMSO was read at 575nm against a background of cells without MTT exposed to the solubilisation agent DMSO (100%). The background absorbance was subtracted, and the readings were normalised to that for cells exposed to solvent control then MTT reagent. Data are mean \pm S.E.M $n = 4$ independent experiments, each $n = 6$ wells per concentration. Data are analysed by One-Way ANOVA with Dunnett's post test compared to solvent control; ** $P < 0.01$.

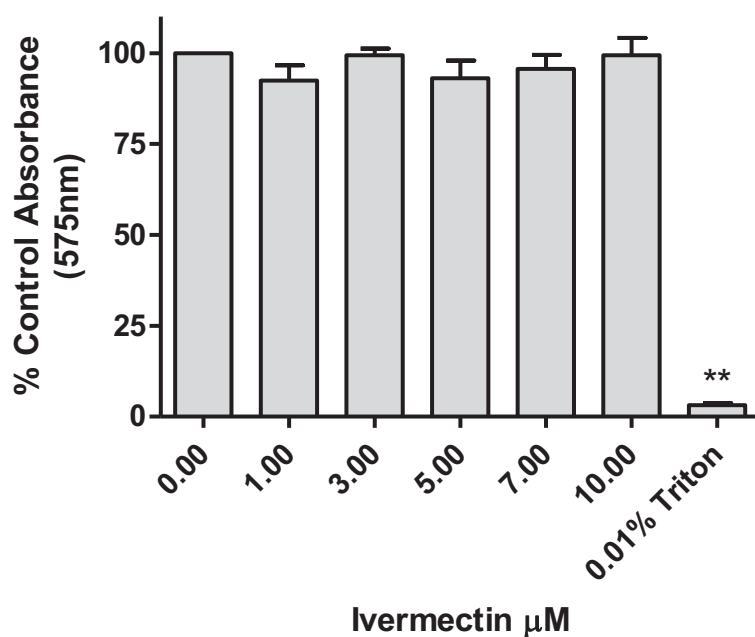


Figure 6.8 N2a cells grown to a sub-confluent monolayer were exposed to ivermectin at a concentration range 0-10μM for 1hr or to 0.01% triton-X-100 for 15 minutes and then incubated with MTT reagent for 2 hours, after which absorbance of intracellular formazan, solubilised in 100% DMSO was read at 575nm against a background of cells without MTT exposed to the solubilisation agent DMSO (100%). The background absorbance was subtracted, and the readings were normalised to that for cells exposed to solvent control then MTT reagent. Data are mean \pm S.E.M. of $n = 4$ independent experiments, each $n = 6$ wells per concentration. Data are analysed by One-Way ANOVA with Dunnett's post test compared to solvent control; ** $P < 0.01$.

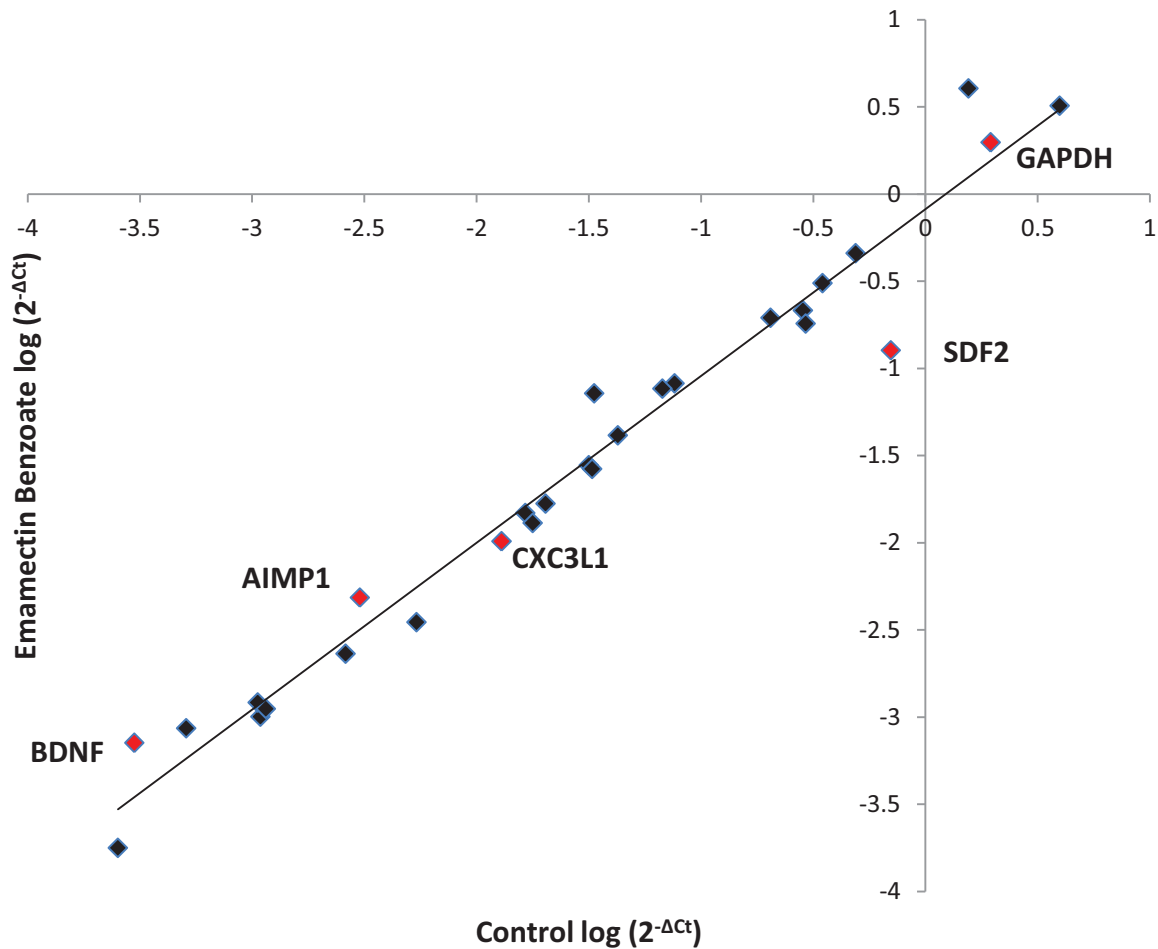


Figure 6.9 A Emamectin benzoate Sample 1

Chemokine and chemokine receptor mRNA expression was detected in a 96 well qPCR array (SABiosciences PAHS-022) after exposure of independent SH-SY5Y cells samples to SH-SY5Y cells to 1 μ M emamectin benzoate, 1 μ M ivermectin or solvent control for 18 hours in the absence of serum. Figure 6.7 A and B show gene expression for 2 independent RNA samples from cells exposed to emamectin benzoate versus control. Genes that returned a $C_t < 35$ are expressed as $\log(2^{-\Delta C_t})$. Housekeeping gene expression is included for comparison. Of interest as potential markers of emamectin benzoate and ivermectin exposure are BDNF (Brain-Derived Neurotrophic Factor), AIMP1 (aminoacyl tRNA synthetase complex-interacting multifunctional protein 1), CX3CL1 (chemokine (C-X3-C motif) ligand 1) and SDF2 (stromal cell-derived factor 2), whose data points are highlighted in red.

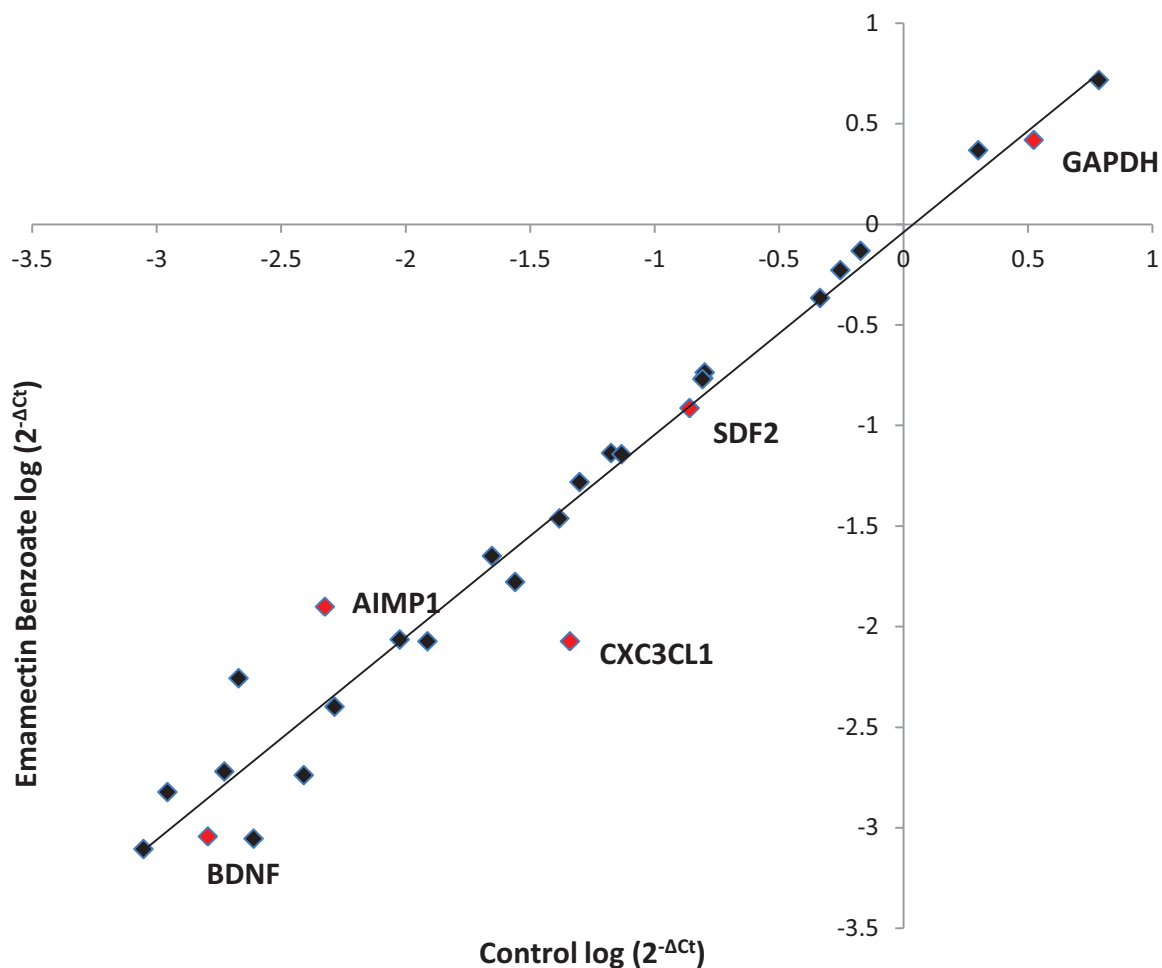


Figure 6.9 B Emamectin benzoate Sample 2

Chemokine and chemokine receptor mRNA expression was detected in a 96 well qPCR array (SABiosciences PAHS-022) after exposure of independent SH-SY5Y cells samples to SH-SY5Y cells to 1 μ M emamectin benzoate, 1 μ M ivermectin or solvent control for 18 hours in the absence of serum. Figure 6.7 A and B show gene expression for 2 independent RNA samples from cells exposed to emamectin benzoate versus control. Genes that returned a $C_t < 35$ are expressed as $\log(2^{-\Delta C_t})$. Housekeeping gene expression is included for comparison. Of interest as potential markers of emamectin benzoate and ivermectin exposure are BDNF (Brain-Derived Neurotrophic Factor), AIMP1 (aminoacyl tRNA synthetase complex-interacting multifunctional protein 1), CX3CL1 (chemokine (C-X3-C motif) ligand 1) and SDF2 (stromal cell-derived factor 2), whose data points are highlighted in red.

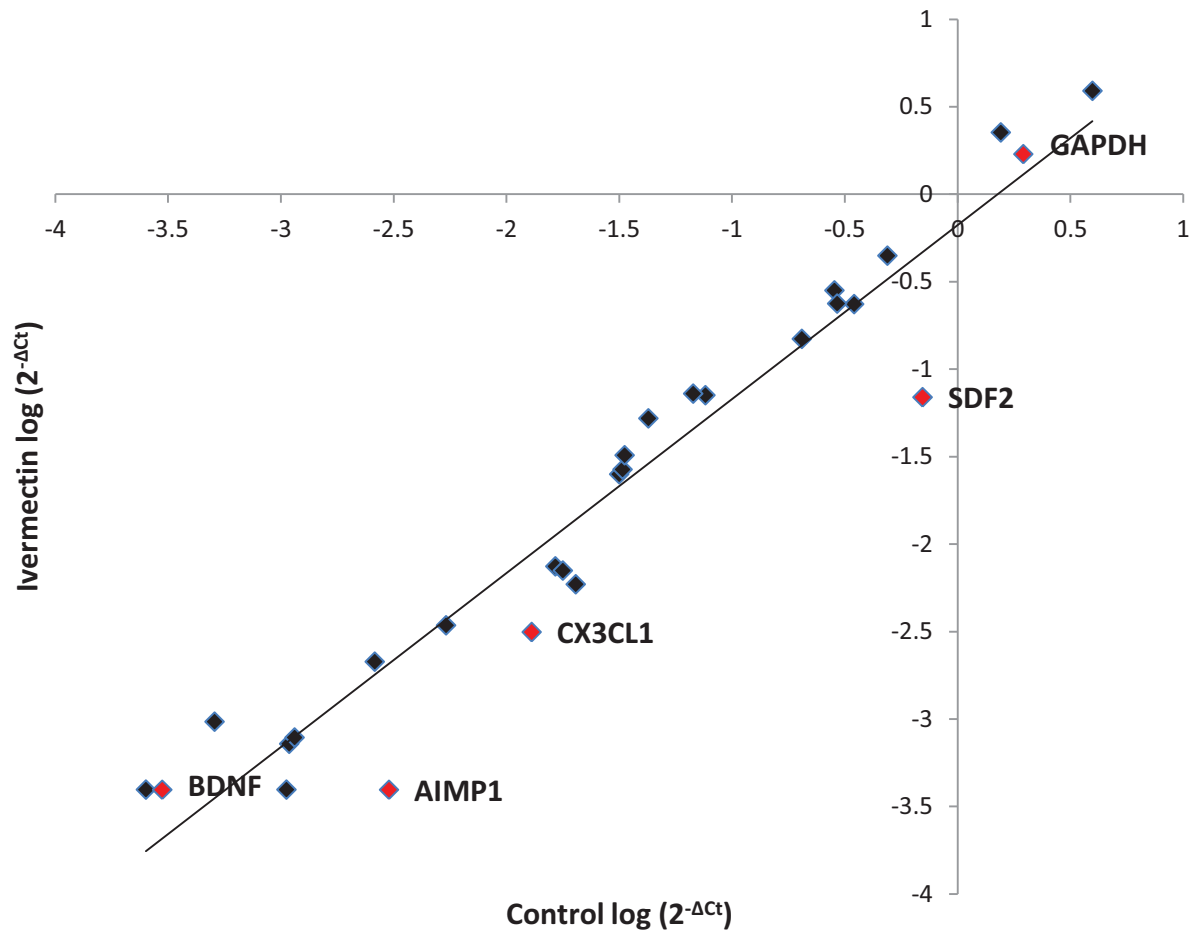


Figure 6.9 C Ivermectin Sample 1

Chemokine and chemokine receptor mRNA expression was detected in a 96 well qPCR array (SABiosciences PAHS-022) after exposure of independent SH-SY5Y cells samples to SH-SY5Y cells to 1 μ M emamectin benzoate 1 μ M ivermectin or solvent control for 18 hours in the absence of serum. Figure 6.7 C and D show gene expression for 2 independent RNA samples from cells exposed to ivermectin versus control. Genes that returned a $C_t < 35$ are expressed as $\log(2^{-\Delta C_t})$. Housekeeping gene expression is included for comparison. Of interest as potential markers of emamectin benzoate and ivermectin exposure are BDNF (Brain-Derived Neurotrophic Factor), AIMP1 (aminoacyl tRNA synthetase complex-interacting multifunctional protein 1), CX3CL1 (chemokine (C-X3-C motif) ligand 1) and SDF2 (stromal cell-derived factor 2), whose data points are highlighted in red.

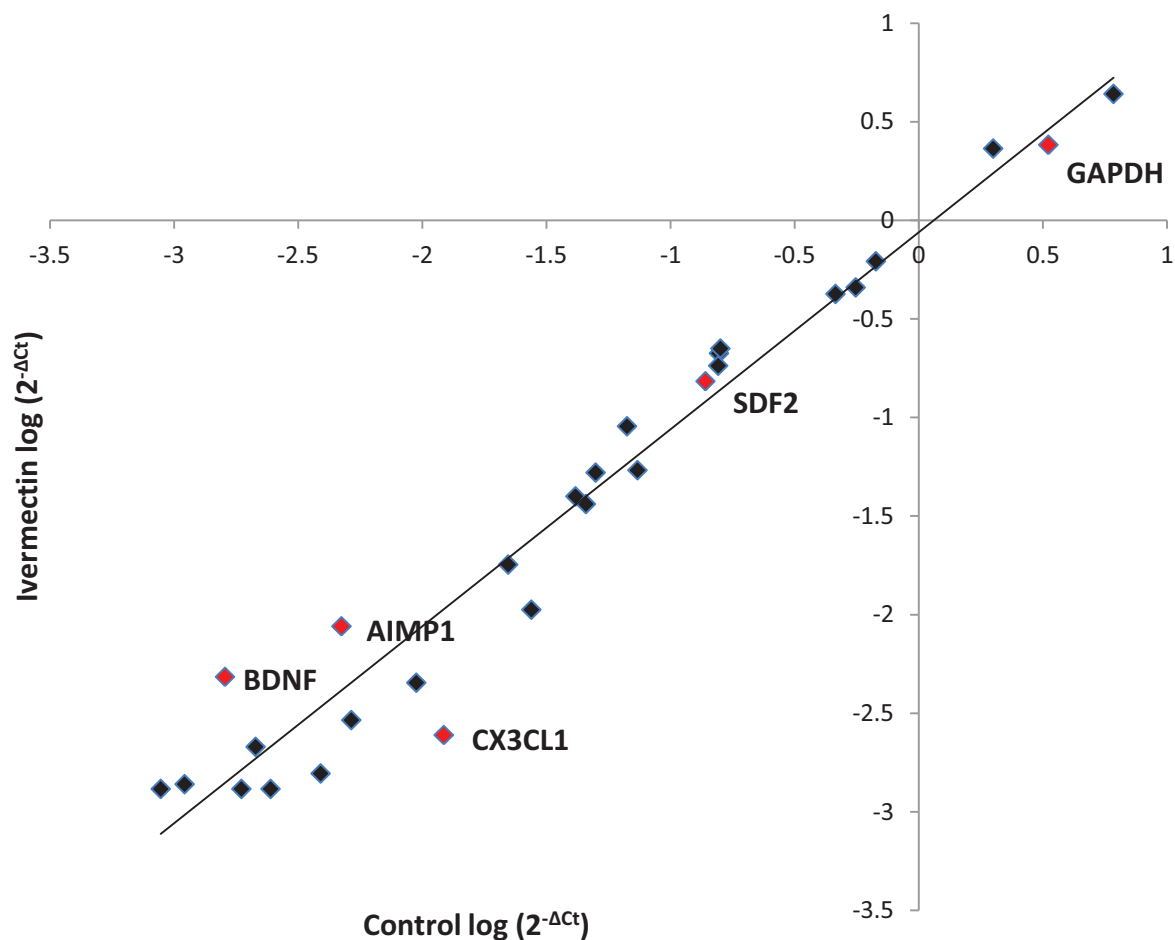
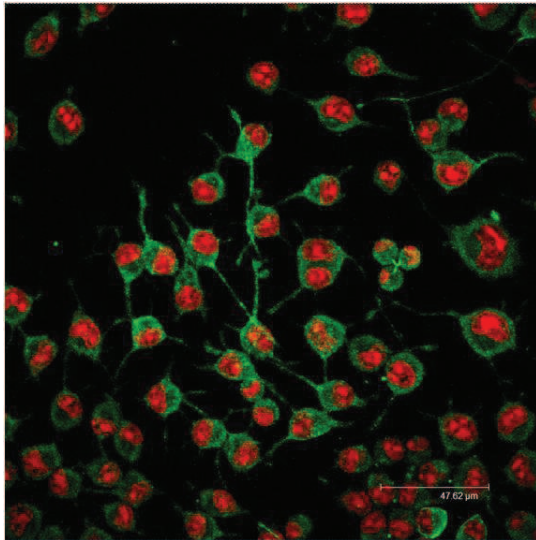


Figure 6.9 D Ivermectin Sample 2

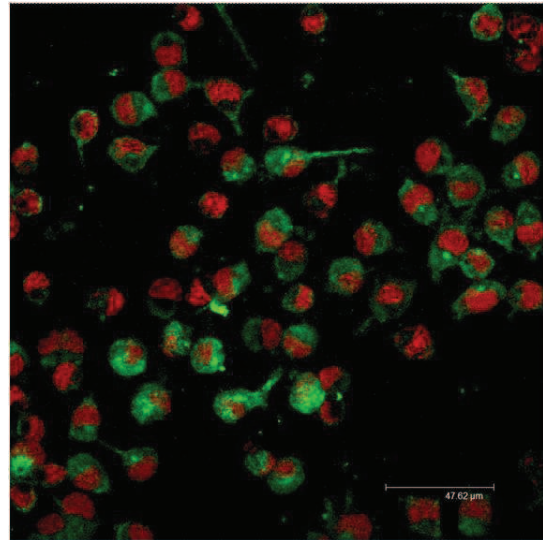
Figure 6.9 Chemokine and chemokine receptor mRNA expression was detected in a 96 well qPCR array (SABiosciences PAHS-022) after exposure of independent SH-SY5Y cells samples to SH-SY5Y cells to 1 μ M emamectin benzoate, 1 μ M ivermectin or solvent control for 18 hours in the absence of serum. Figure 6.7 C and D show gene expression for 2 independent RNA samples from cells exposed to ivermectin versus control. Genes that returned a $C_t < 35$ are expressed as $\log(2^{-\Delta C_t})$. Housekeeping gene expression is included for comparison. Of interest as potential markers of emamectin benzoate and ivermectin exposure are BDNF (Brain-Derived Neurotrophic Factor), AIMP1 (aminoacyl tRNA synthetase complex-interacting multifunctional protein 1), CX3CL1 (chemokine (C-X3-C motif) ligand 1) and SDF2 (stromal cell-derived factor 2), whose data points are highlighted in red.

Figure 6.10 Neurite outgrowths in N2a cells visualised by confocal microscopy (A-D) and light contrast microscopy (E-F) at x63 magnification. Cells were stained with anti- α -tubulin antibody and FITC conjugated rabbit anti-mouse IgG as described in methods (A-D). Alternatively cells were viewed under a light contrast microscope (Leica) as live cells without fixation or staining (E-F). Test conditions prior to visualisation were 60 min exposure to: solvent control (A); 0.01M hydrogen peroxide (positive control for ablation of neurite outgrowth -B); 1 μ M abamectin (C); 1 μ M abamectin (D); 1 μ M emamectin benzoate (E); 1 μ M ivermectin (F). The images are representative of 6 similar fields in each experiment and the experiments were replicated 3 times.

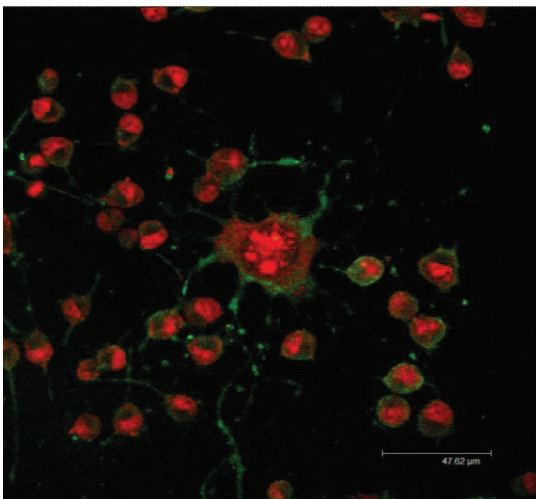
A



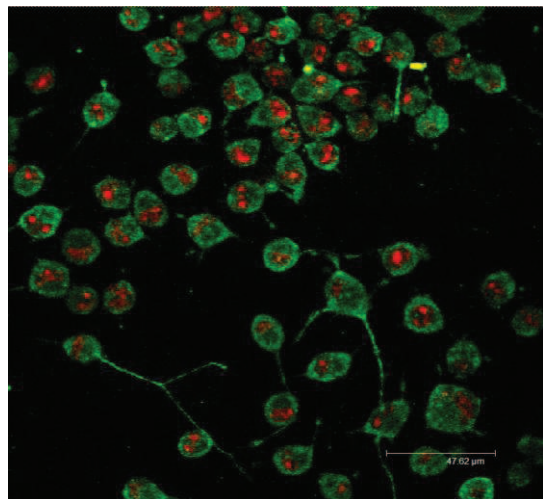
B



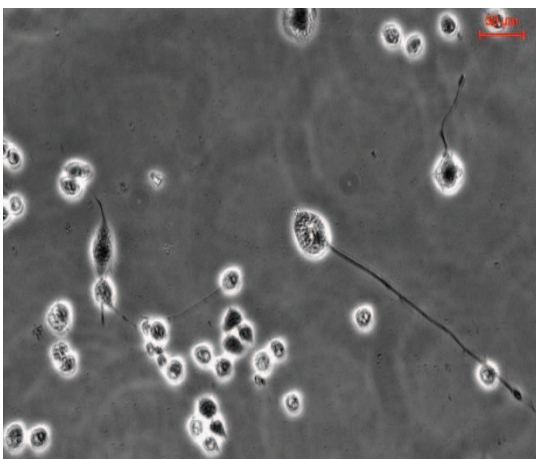
C



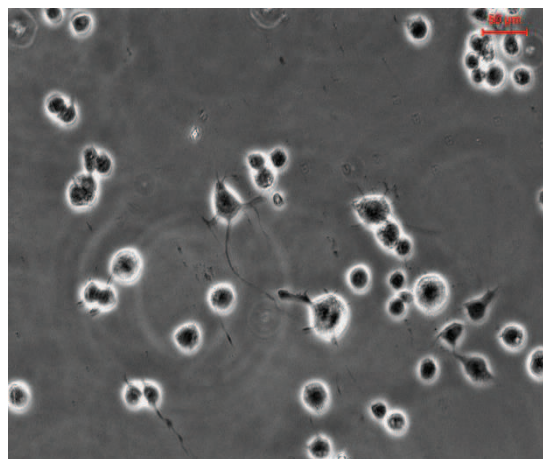
D



E



F



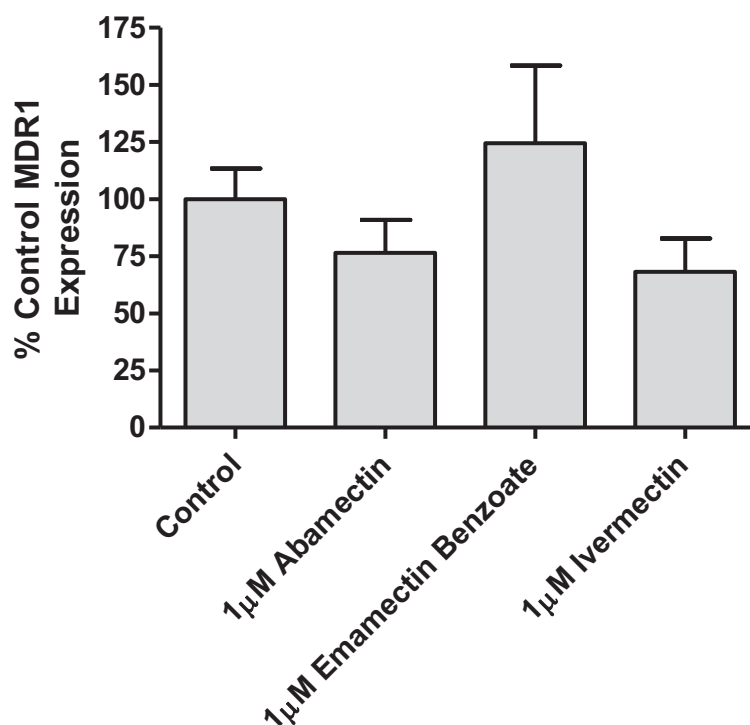


Figure 6.11 MDR1 mRNA expression in SH-SY5Y cells after exposure to 1µM abamectin, emamectin benzoate, ivermectin or solvent control for 18 hours in the absence of serum, normalised to GAPDH expression. Data are mean \pm S.E.M. $n = 9$ using total RNA from 3 independent passages of cells, each performed in triplicate, tested for statistical significance by One-Way ANOVA with Dunnett's post-test. There were no significant differences between treatments ($P > 0.05$)

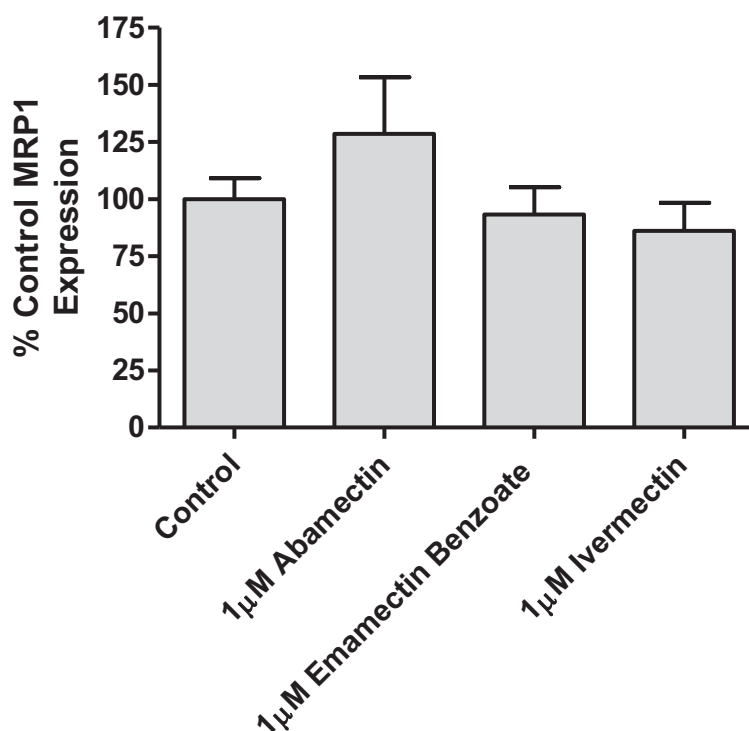


Figure 6.12 Expression of MRP1 mRNA in SH-SY5Y cells after exposure to 1 μM abamectin, emamectin benzoate, ivermectin or solvent control for 18 hours in the absence of serum, normalised to GAPDH expression. Data are mean ± S.E.M. $n = 9$, using RNA from 3 independent passages of cells, each performed in triplicate. Data were tested for statistical significance using One-Way ANOVA with Dunnett's post-test. There were no significant differences between treatments ($P > 0.05$).

Summary Conclusions

There were no gross effects on cell viability, assessed using the MTT assay, for abamectin or emamectin benzoate up to 10 μM in SH-SY5Y or N2a cells exposed for 1 hour, conditions comparable to the transport assays in Chapters 4 and 5. Emamectin benzoate at 7 μM and above caused a 50% decrease in SH-SY5Y cell viability ($P < 0.01$) but not for N2a cells. Neurite outgrowth did not qualitatively change after 1hr exposure to 1 μM abamectin, emamectin benzoate or ivermectin in N2a cells. Expression of MDR1 and MRP1 transporter mRNA was not significantly changed compared to control over 3 passages of SH-SY5Y cells after 18hr exposure to 1 μM concentrations of abamectin, emamectin benzoate or ivermectin. The chemokine genes BDNF, AIMP1 CX3CL1 and SDF2 either increased or decreased mRNA expression versus control after 18hr exposure to emamectin benzoate or ivermectin at 1 μM and therefore were all identified as candidate markers of emamectin benzoate and ivermectin exposure. BDNF and SDF2 are important chemokines in neural cells.

Chapter 7: General Discussion, Conclusions and Future Work

This study has shown that the macrocyclic lactone insecticides abamectin, emamectin benzoate and ivermectin interact with both MDR1 and MRP transporters in both human and mouse neuroblastoma cells SH-SY5Y and N2a. It has explored the quantitative aspects of this interaction and discovered that the avermectins tested inhibit the efflux of substrate dyes through the MDR1/mdr1a and MRP/mrp transporters with similar affinities in the low μM range. It is yet to be determined whether the insecticides themselves are substrates for these transporters, but it is likely that they compete for efflux as the interaction does not increase toxicity. The concentrations used are well in excess of the peak plasma concentrations found for ivermectin in cattle after therapeutic doses ($20\text{ng/mL} = 22\text{nM/L}$) (Alvinerie *et al.*, 1999). As insecticides the avermectins have very low application rates on crops (e.g. 6g per hectare), as well as short half-lives under conditions of light and moisture, so occupational exposure would result in lower plasma concentrations.

SH-SY5Y cells have already proven a useful model for investigating neurotoxicity. Although their origin is from peripheral bone marrow, PCR array studies showed that they expressed a similar array of uptake and efflux transporters to that in the blood-brain barrier, except that BCRP was not expressed. Functional expression of the key efflux transporters MDR1 and MRP1 was maintained over three sequential passages. Uptake and efflux transporter expression in SH-SY5Y cells was similar to that at the BBB and also closely resembles transporter expression in other CNS cell models such as the endothelial cell line hCMEC/D3 (Carl *et al.*, 2010). N2a cells also sustained the expression of mRNA for mdr1a but not for bcrp over three passages, although the full profile of mouse transporters was not investigated.

Until now, transporter affinity data has mostly been obtained in cell lines into which the transporter of interest was transfected, resulting in overexpression, e.g. (Griffin *et al.*, 2005; Lespine *et al.*, 2007; Brayden & Griffin, 2008; Geyer *et al.*, 2009). Arguably these studies may skew the results, returning a higher affinity for the overexpressed transporter than that measurable when the transporter is constitutively expressed. The current study is the first to compare the interaction of avermectins with endogenously expressed transporters in both

human and mouse neuroblastoma cell lines. Data obtained in the current study indicates that the affinity profiles for the two efflux transporter types MDR1 and *mdr1a* as well as MRP and *mrp* are similar between cell lines. This confirms the usefulness of data from mouse model cell lines to predict human exposure and suggests that affinity data from *in vivo* mouse models expressing functional *mdr1* may be used to draw useful comparisons too.

MDR1 dye retention assays performed in the current study confirmed the existing evidence indicating that ivermectin and abamectin are inhibitors of MDR1-mediated substrate dye efflux and show that emamectin benzoate was also an inhibitor. All three avermectins returned K_i values for MDR1 and *mdr1a* inhibition in the low μM range but ivermectin was the most potent MDR1 inhibitor. In MRP dye retention assays that all three avermectins also inhibited human MRP- and mouse *mrp* transporter efflux activity with affinities in the low μM range that were similar to those for MDR1 and *mdr1a*, and avermectin affinities for MRP versus *mrp* transporters were similar for all three compounds. The interaction of MRP transporters with avermectins has been in dispute due to the conflicting findings of Lespine *et al* (2006) and Brayden and Griffin (2008), but the data in the current study has confirmed that abamectin, emamectin benzoate and ivermectin inhibit MRP- and *mrp*-mediated efflux. However, their importance in avermectin disposition relative to MDR1 or *mdr1a* was not determined, and is dependent upon absolute protein expression levels as well as affinities.

Interspecies variation in mRNA expression of efflux transporters has been reported, with MRP5 being most highly expressed in human BMECs but MRP4 detected at the highest level in mouse, and mRNA levels of BCRP being higher in mouse than human. However mRNA MDR1 was expressed at equally high levels in all species examined (Warren *et al.*, 2009). It is important to note that Warren and colleagues did not conclusively quantitate transporter protein expression levels. To investigate the functional consequences of differences in absolute transporter expression levels between human and mouse brain cells, it will be necessary to perform simultaneous assays of MDR1 and *mdr1a* in our model cell lines alongside the MRP and *mrp* transporters. The dyes H33342 and CMFDA should be used simultaneously in the presence and absence of specific inhibitors (see future work).

Avermectins exhibited low toxicity to SH-SY5Y and N2a neuroblastoma cells in culture. Toxicity only occurred for emamectin above $6\mu\text{M}$; this is 100-fold higher than concentrations of ivermectin observed after administration of doses within the therapeutic range (Alvinerie *et al.*, 1999). It is important to explore whether toxicity can be increased by exposing the cells to mixtures of therapeutic drugs such as cyclosporin and avermectins at therapeutic concentrations.

Chemokine genes are induced in the CNS under conditions of chemical stress. Induction of these genes might be an early marker of CNS exposure and were explored in cells exposed to avermectins. Although the studies produced inconclusive results because of low sample size, SDF2, BDNF and AIMP1 were the chemokine genes most affected and these emerge as candidates for further study as biomarkers, using a larger sample size and perhaps longer avermectin exposure times than 18 hours.

18 hours' acute exposure to abamectin, emamectin benzoate and ivermectin did not result in changes to MDR1 or mrp1 mRNA expression levels in the current study, however the related compounds doramectin and nemadectin have been shown to reverse adriamycin resistance by 7-fold and 3-fold, respectively, at $1\mu\text{M}$. They also significantly down-regulated MDR1 mRNA protein and protein after 24 hours' exposure by 30-40% at concentrations of $5\mu\text{M}$ (Gao *et al.*, 2010). In future studies, it would be of interest to increase the exposure to avermectins by lengthening the exposure times, increasing the concentrations or repeat dosing, to assess the effect on expression of these transporter genes. It would also be of interest to expose the cells to avermectins and simultaneously inhibit or silence MDR1 using siRNA to see whether MRP1, or other transporters, up-regulate their gene and protein expression levels in response.

SH-SY5Y cells and N2a cells are both neuronal precursor cell types that exist in a relatively stable state. It is possible to induce neurite expression in both cell types as they begin to differentiate into neural cells, by the application of differentiation agents including retinoic acid, dibutyryl cAMP and sodium butyrate. All of these agents may be expected to have an influence upon efflux transporter expression levels; retinoic acid treatment has been reported

to increase MDR1 expression in SH-SY5Y cells (Bates *et al.* 1989). For this reason the cells were maintained in an undifferentiated state throughout the transporter and proliferation experiments (Chapters 3-5) but the potential to assess neurite outgrowth as a quantitative marker of avermectin exposure was worth exploiting independently here, since differentiated N2a and SH-SY5Y cells have both been used successfully in experiments on pesticide exposure and viral infection (Vesanen *et al.* 1994; Kume *et al.* 2008; Miglio *et al.* 2009; Cheung *et al.* 2009; Sun *et al.* 2010).

Assays of neurite outgrowth in differentiated cells suggest that the cells maintain outgrowths after 1 hours' exposure to 1 μ M avermectins. Further work is necessary to quantitate effects of avermectin exposure on neurite length and rate of growth; it would be worth exploring differences in their response when they are cultured with avermectins during or after differentiation. The reversibility of any effects on neurite outgrowth should be investigated.

Other avermectins and the milbemycins

The new generation avermectins and milbemycins are all derivatives of ivermectin. They may take over eventually due to better potency and/or lower toxicity in veterinary or human uses (e.g. selamectin) but for the foreseeable future the natural compound abamectin and its semi-synthetic derivatives emamectin benzoate and ivermectin are in use and will remain of global importance, so a greater understanding of mechanisms of avermectin exposure is pertinent.

Conclusions

These studies have confirmed that avermectins are substrates for efflux pumps MDR1 and MRP, and that the counterpart mouse transporters have similar kinetics to human. Variation in expression of the efflux pumps between cells in the CNS and between individuals may contribute to variation in levels of exposure. Although the molecules are relatively non-toxic at therapeutic doses, reduced efflux from the CNS has led to toxicity in *mdr1* knockout animals. It is unlikely that such non-functional MDR1 polymorphisms will be identified in humans, but variability in the transport of individual substrates due to SNPs, or competition with other efflux inhibitors or substrate drugs such as CSA or adriamycin (Gao *et al.*, 2010)

might still occur in humans; indeed the effects of some polymorphisms are substrate-specific in animals (Shilling *et al.*, 2006).

Future work

1. Measure intracellular avermectin levels by HPLC after experiments with inhibitors to establish whether or not MDR1/mdr1a and MRP/mrp efflux the avermectins directly (e.g. Sams *et al.*, 1993).
2. Assay transporter activity with both H33342 and CMFDA simultaneously, in the presence of avermectins with and without inhibitors, to explore the relative contributions of the two transporter types MDR1/mdr1a and MRP/mrp when both are present and functional.
3. Conduct assays with avermectins in a BCRP-expressing cell line e.g. hMEC/D3 cells to explore the contributions of BCRP/ bcrp not studied here but important at the blood-brain barrier.
4. Further investigate changes in chemokine expression for SDF2, AIMP1 and BDNF.
5. Perform siRNA knockdown to confirm importance of individual transporter types.
6. The co-culture of SH-SY5Y and N2a cells with astrocytes may more closely approximate physiology of CNS barrier sites.
7. Assay the influence of polymorphisms upon avermectin exposure in a suitable cell type e.g. HEK293.

Chapter 8: References

- Allen JD, van Loevezijn A, Lakhai JM, van der Valk M, van Tellingen O, Reid G, Schellens JHM, Koomen G-J & Schinkel AH (2002). Potent and specific inhibition of the breast cancer resistance protein multidrug transporter in vitro and in mouse intestine by a novel analogue of fumitremorgin C. *Mol Cancer Ther* **1**, 417–425.
- Alvinerie M, Sutra JF, Galtier P, Lifschitz A, Virkel G, Sallovitz J & Lanusse C (1999). Persistence of ivermectin in plasma and faeces following administration of a sustained-release bolus to cattle. *Res Vet Sci* **66**, 57–61.
- Armstrong R, MacPhee D, Katz T & Endris R (2000). A field efficacy evaluation of emamectin benzoate for the control of sea lice on Atlantic salmon. *Can Vet J* **41**, 607–612.
- Bain LJ & LeBlanc GA (1996). Interaction of structurally diverse pesticides with the human MDR1 gene product P-glycoprotein. *Toxicol Appl Pharmacol* **141**, 288–298.
- Bajetto A, Bonavia R, Barbero S, Florio T & Schettini G (2001). Chemokines and their receptors in the central nervous system. *Front Neuroendocrinol* **22**, 147–184.
- Bajetto A, Bonavia R, Barbero S, Piccioli P, Costa A, Florio T & Schettini G (1999). Glial and neuronal cells express functional chemokine receptor CXCR4 and its natural ligand stromal cell-derived factor 1. *J Neurochem* **73**, 2348–2357.
- Barragry TB (1987). A Review of the Pharmacology and Clinical Uses of Ivermectin. *Can Vet J* **28**, 512–517.
- Bates SE, Mickley LA, Chen YN, Richert N, Rudick J, Biedler JL & Fojo AT (1989). Expression of a drug resistance gene in human neuroblastoma cell lines: modulation by retinoic acid-induced differentiation. *Mol Cell Biol* **9**, 4337–4344.
- Biedler JL, Helson L & Spengler BA (1973). Morphology and Growth, Tumorigenicity, and Cytogenetics of Human Neuroblastoma Cells in Continuous Culture. *Cancer Research* **33**, 2643–2652.
- Blot A, Billups D, Bjørkmo M, Quazi AZ, Uwechue NM, Chaudhry FA & Billups B (2009). Functional expression of two system A glutamine transporter isoforms in rat auditory brainstem neurons. *Neuroscience* **164**, 998–1008.
- Bordow SB, Haber M, Madafiglio J, Cheung B, Marshall GM & Norris MD (1994). Expression of the multidrug resistance-associated protein (MRP) gene correlates with amplification and overexpression of the N-myc oncogene in childhood neuroblastoma. *Cancer Res* **54**, 5036–5040.
- Bosse KE, Maina FK, Birbeck JA, France MM, Roberts JJP, Colombo ML & Mathews TA (2011). Aberrant striatal dopamine transmitter dynamics in brain-derived neurotrophic factor-deficient mice. *Journal of Neurochemistry*; DOI: 10.1111/j.1471-4159.2011.07531.x.
- Brayden DJ & Griffin J (2008). Avermectin transepithelial transport in MDR1- and MRP-transfected canine kidney monolayers. *Vet Res Commun* **32**, 93–106.

- Bröer A, Wagner CA, Lang F & Bröer S (2000). The heterodimeric amino acid transporter 4F2hc/y+LAT2 mediates arginine efflux in exchange with glutamine. *Biochem J* **349 Pt 3**, 787–795.
- Bronger H, König J, Kopplow K, Steiner H-H, Ahmadi R, Herold-Mende C, Keppler D & Nies AT (2005). ABCC drug efflux pumps and organic anion uptake transporters in human gliomas and the blood-tumor barrier. *Cancer Res* **65**, 11419–11428.
- Brunner M, Langer O, Sunder-Plassmann R, Dobrozemsky G, Müller U, Wadsak W, Krcal A, Karch R, Mannhalter C, Dudczak R, Kletter K, Steiner I, Baumgartner C & Müller M (2005). Influence of functional haplotypes in the drug transporter gene ABCB1 on central nervous system drug distribution in humans. *Clin Pharmacol Ther* **78**, 182–190.
- Campbell, W C ed. (1989). *Ivermectin and Abamectin*. Springer-Verlag, NY.
- Cardona AE, Pioro EP, Sasse ME, Kostenko V, Cardona SM, Dijkstra IM, Huang D, Kidd G, Dombrowski S, Dutta R, Lee J-C, Cook DN, Jung S, Lira SA, Littman DR & Ransohoff RM (2006). Control of microglial neurotoxicity by the fractalkine receptor. *Nat Neurosci* **9**, 917–924.
- Carl SM, Lindley DJ, Couraud PO, Weksler BB, Romero I, Mowery SA & Knipp GT (2010). ABC and SLC transporter expression and pot substrate characterization across the human CMEC/D3 blood-brain barrier cell line. *Mol Pharm* **7**, 1057–1068.
- Cheung Y-T, Lau WK-W, Yu M-S, Lai CS-W, Yeung S-C, So K-F & Chang RC-C (2009). Effects of all-trans-retinoic acid on human SH-SY5Y neuroblastoma as in vitro model in neurotoxicity research. *Neurotoxicology* **30**, 127–135.
- Cisternino S, Mercier C, Bourasset F, Roux F & Scherrmann J-M (2004). Expression, up-regulation, and transport activity of the multidrug-resistance protein Abcg2 at the mouse blood-brain barrier. *Cancer Res* **64**, 3296–3301.
- Coates A & Tripp E (1995). Comparison of two fluorochromes for flow cytometric assay of cellular glutathione content in human malignant melanoma. *Melanoma Res* **5**, 107–111.
- Cole SP, Bhardwaj G, Gerlach JH, Mackie JE, Grant CE, Almquist KC, Stewart AJ, Kurz EU, Duncan AM & Deeley RG (1992). Overexpression of a transporter gene in a multidrug-resistant human lung cancer cell line. *Science* **258**, 1650–1654.
- Cordon-Cardo C, O'Brien JP, Casals D, Rittman-Grauer L, Biedler JL, Melamed MR & Bertino JR (1989). Multidrug-resistance gene (P-glycoprotein) is expressed by endothelial cells at blood-brain barrier sites. *Proc Natl Acad Sci USA* **86**, 695–698.
- Corich L, Aranda A, Carrassa L, Bellarosa C, Ostrow JD & Tiribelli C (2009). The cytotoxic effect of unconjugated bilirubin in human neuroblastoma SH-SY5Y cells is modulated by the expression level of MRP1 but not MDR1. *Biochem J* **417**, 305–312.
- Crissman HA & Steinkamp JA (1987). A new method for rapid and sensitive detection of bromodeoxyuridine in DNA-replicating cells. *Exp Cell Res* **173**, 256–261.
- Dallas S, Miller DS & Bendayan R (2006). Multidrug resistance-associated proteins: expression and function in the central nervous system. *Pharmacol Rev* **58**, 140–161.

- Daood M, Tsai C, Ahdab-Barmada M & Watchko JF (2008). ABC transporter (P-gp/ABCB1, MRP1/ABCC1, BCRP/ABCG2) expression in the developing human CNS. *Neuropediatrics* **39**, 211–218.
- Daurio CP, Gilman MR, Pulliam JD & Seward RL (1987). Reproductive evaluation of male beagles and the safety of ivermectin. *Am J Vet Res* **48**, 1755–1760.
- Didier A & Loor F (1996). The abamectin derivative ivermectin is a potent P-glycoprotein inhibitor. *Anticancer Drugs* **7**, 745–751.
- Drexler G & Sieghart W (1984). Properties of a high affinity binding site for [3H]ivermectin B1a. *Eur J Pharmacol* **99**, 269–277.
- Drożdżik M, Białecka M, Myśliwiec K, Honczarenko K, Stankiewicz J & Sych Z (2003). Polymorphism in the P-glycoprotein drug transporter MDR1 gene: a possible link between environmental and genetic factors in Parkinson's disease. *Pharmacogenetics* **13**, 259–263.
- Eisenblätter T, Hüwel S & Galla H-J (2003). Characterisation of the brain multidrug resistance protein (BMDP/ABCG2/BCRP) expressed at the blood-brain barrier. *Brain Res* **971**, 221–231.
- Ek CJ, Wong A, Liddel SA, Johansson PA, Dziegielewska KM & Saunders NR (2010). Efflux mechanisms at the developing brain barriers: ABC-transporters in the fetal and postnatal rat. *Toxicol Lett* **197**, 51–59.
- Flaskos J, Fowler MJ, Teurtre C & Hargreaves AJ (1999). The effects of carbaryl and trichlorphon on differentiating mouse N2a neuroblastoma cells. *Toxicology Letters* **110**, 79–84.
- Flaskos J, Harris W, Sachana M, Muñoz D, Tack J & Hargreaves AJ (2007). The effects of diazinon and cypermethrin on the differentiation of neuronal and glial cell lines. *Toxicology and Applied Pharmacology* **219**, 172–180.
- Flaskos J, McLean WG, Fowler MJ & Hargreaves AJ (1998). Tricresyl phosphate inhibits the formation of axon-like processes and disrupts neurofilaments in cultured mouse N2a and rat PC12 cells. *Neurosci Lett* **242**, 101–104.
- Förster F, Volz A & Fricker G (2008). Compound profiling for ABCC2 (MRP2) using a fluorescent microplate assay system. *Eur J Pharm Biopharm* **69**, 396–403.
- Fotakis G & Timbrell JA (2006). In vitro cytotoxicity assays: comparison of LDH, neutral red, MTT and protein assay in hepatoma cell lines following exposure to cadmium chloride. *Toxicol Lett* **160**, 171–177.
- Furuno T, Landi M-T, Ceroni M, Caporaso N, Bernucci I, Nappi G, Martignoni E, Schaeffeler E, Eichelbaum M, Schwab M & Zanger UM (2002). Expression polymorphism of the blood-brain barrier component P-glycoprotein (MDR1) in relation to Parkinson's disease. *Pharmacogenetics* **12**, 529–534.
- Gao A, Wang X, Xiang W, Liang H, Gao J & Yan Y (2010). Reversal of P-glycoprotein-mediated multidrug resistance in vitro by doramectin and nemadectin. *J Pharm Pharmacol* **62**, 393–399.

- Geyer J, Gavrilova O & Petzinger E (2009). Brain penetration of ivermectin and selamectin in *mdr1a,b* P-glycoprotein- and *bcrp*- deficient knockout mice. *J Vet Pharmacol Ther* **32**, 87–96.
- Gokbulut C, Cirak VY, Senlik B, Aksit D, Durmaz M & McKellar QA (2010). Comparative plasma disposition, bioavailability and efficacy of ivermectin following oral and pour-on administrations in horses. *Vet Parasitol* **170**, 120–126.
- Goodell MA, Brose K, Paradis G, Conner AS & Mulligan RC (1996). Isolation and functional properties of murine hematopoietic stem cells that are replicating *in vivo*. *J Exp Med* **183**, 1797–1806.
- Gow JM, Hodges LM, Chinn LW & Kroetz DL (2008). Substrate-dependent effects of human ABCB1 coding polymorphisms. *J Pharmacol Exp Ther* **325**, 435–442.
- Griffin J, Fletcher N, Clemence R, Blanchflower S & Brayden DJ (2005). Selamectin is a potent substrate and inhibitor of human and canine P-glycoprotein. *J Vet Pharmacol Ther* **28**, 257–265.
- Guerrini I, Thomson AD, Cook CCH, McQuillin A, Sharma V, Kopelman M, Reynolds G, Jauhar P, Harper C & Gurling HMD (2005). Direct genomic PCR sequencing of the high affinity thiamine transporter (SLC19A2) gene identifies three genetic variants in Wernicke Korsakoff syndrome (WKS). *Am J Med Genet B Neuropsychiatr Genet* **137B**, 17–19.
- Gupta A, Dai Y, Vethanayagam RR, Hebert MF, Thummel KE, Unadkat JD, Ross DD & Mao Q (2006). Cyclosporin A, tacrolimus and sirolimus are potent inhibitors of the human breast cancer resistance protein (ABCG2) and reverse resistance to mitoxantrone and topotecan. *Cancer Chemother Pharmacol* **58**, 374–383.
- Hartkoorn RC, Kwan WS, Shallcross V, Chaikan A, Liptrott N, Egan D, Sora ES, James CE, Gibbons S, Bray PG, Back DJ, Khoo SH & Owen A (2010). HIV protease inhibitors are substrates for OATP1A2, OATP1B1 and OATP1B3 and lopinavir plasma concentrations are influenced by SLCO1B1 polymorphisms. *Pharmacogenet Genomics* **20**, 112–120.
- Hendrikse NH, de Vries EG, Eriks-Fluks L, van der Graaf WT, Hospers GA, Willemsen AT, Vaalburg W & Franssen EJ (1999). A new *in vivo* method to study P-glycoprotein transport in tumors and the blood-brain barrier. *Cancer Res* **59**, 2411–2416.
- Hoffmann K & Löscher W (2007). Upregulation of brain expression of P-glycoprotein in MRP2-deficient TR(-) rats resembles seizure-induced up-regulation of this drug efflux transporter in normal rats. *Epilepsia* **48**, 631–645.
- Hoffmeyer S, Burk O, von Richter O, Arnold HP, Brockmöller J, John A, Cascorbi I, Gerloff T, Roots I, Eichelbaum M & Brinkmann U (2000). Functional polymorphisms of the human multidrug-resistance gene: multiple sequence variations and correlation of one allele with P-glycoprotein expression and activity *in vivo*. *Proc Natl Acad Sci USA* **97**, 3473–3478.
- Hsiao P, Bui T, Ho RJY & Unadkat JD (2008). *In vitro*-to-*in vivo* prediction of P-glycoprotein-based drug interactions at the human and rodent blood-brain barrier. *Drug Metab Dispos* **36**, 481–484.
- Hu L-F, Lu M, Wu Z-Y, Wong PT-H & Bian J-S (2009). Hydrogen sulfide inhibits rotenone-induced apoptosis via preservation of mitochondrial function. *Mol Pharmacol* **75**, 27–34.

- Jani M, Makai I, Kis E, Szabó P, Nagy T, Krajcsi P & Lespine A (2011). Ivermectin interacts with human ABCG2. *J Pharm Sci* **100**, 94–97.
- Juliano RL & Ling V (1976). A surface glycoprotein modulating drug permeability in Chinese hamster ovary cell mutants. *Biochim Biophys Acta* **455**, 152–162.
- Jung JE, Moon JY, Ghil SH & Yoo BS (2009). 2,3,7,8-Tetrachlorodibenzo-p-dioxin (TCDD) inhibits neurite outgrowth in differentiating human SH-SY5Y neuroblastoma cells. *Toxicol Lett* **188**, 153–156.
- Kelsell DP *et al.* (2005). Mutations in ABCA12 underlie the severe congenital skin disease harlequin ichthyosis. *Am J Hum Genet* **76**, 794–803.
- Kimchi-Sarfaty C, Oh JM, Kim I-W, Sauna ZE, Calcagno AM, Ambudkar SV & Gottesman MM (2007). A “silent” polymorphism in the MDR1 gene changes substrate specificity. *Science* **315**, 525–528.
- Klaassen CD & Aleksunes LM (2010). Xenobiotic, bile acid, and cholesterol transporters: function and regulation. *Pharmacol Rev* **62**, 1–96.
- Klebe RR (1969). Neuroblastoma: Cell culture analysis of a differentiating stem cell system. *J Cell Biol* **43**, 69A.
- Kodaira H, Kusuhara H, Ushiki J, Fuse E & Sugiyama Y (2010). Kinetic analysis of the cooperation of P-glycoprotein (P-gp/Abcb1) and breast cancer resistance protein (Bcrp/Abcg2) in limiting the brain and testis penetration of erlotinib, flavopiridol, and mitoxantrone. *J Pharmacol Exp Ther* **333**, 788–796.
- Kokoz YM, Tsyganova VG, Korystova AF, Grichenko AS, Zenchenko KI, Drinyaev VA, Mosin VA, Kruglyak EB, Sterlina TS & Victorov AV (1999). Selective cytostatic and neurotoxic effects of avermectins and activation of the GABA α receptors. *Biosci Rep* **19**, 535–546.
- Korystov YN, Ermakova NV, Kublik LN, Levitman MK, Shaposhnikova VV, Mosin VA, Drinyaev VA, Kruglyak EB, Novik TS & Sterlina TS (2004). Avermectins inhibit multidrug resistance of tumor cells. *Eur J Pharmacol* **493**, 57–64.
- Krishnamurthy PC, Du G, Fukuda Y, Sun D, Sampath J, Mercer KE, Wang J, Sosa-Pineda B, Murti KG & Schuetz JD (2006). Identification of a mammalian mitochondrial porphyrin transporter. *Nature* **443**, 586–589.
- Kume T, Kawato Y, Osakada F, Izumi Y, Katsuki H, Nakagawa T, Kaneko S, Niidome T, Takada-Takatori Y & Akaike A (2008). Dibutyryl cyclic AMP induces differentiation of human neuroblastoma SH-SY5Y cells into a noradrenergic phenotype. *Neurosci Lett* **443**, 199–203.
- Kwei GY, Alvaro RF, Chen Q, Jenkins HJ, Hop CE, Keohane CA, Ly VT, Strauss JR, Wang RW, Wang Z, Pippert TR & Umbenhauer DR (1999). Disposition of ivermectin and cyclosporin A in CF-1 mice deficient in mdr1a P-glycoprotein. *Drug Metab Dispos* **27**, 581–587.
- Lalande ME, Ling V & Miller RG (1981). Hoechst 33342 dye uptake as a probe of membrane permeability changes in mammalian cells. *Proc Natl Acad Sci USA* **78**, 363–367.

- Lankas GR, Cartwright ME & Umbenhauer D (1997). P-glycoprotein deficiency in a subpopulation of CF-1 mice enhances avermectin-induced neurotoxicity. *Toxicol Appl Pharmacol* **143**, 357–365.
- Lasota JA & Dybas RA (1990). Abamectin as a pesticide for agricultural use. *Acta Leiden* **59**, 217–225.
- Lawton M, Iqbal M, Kontovraki M, Lloyd Mills C & Hargreaves AJ (2007). Reduced tubulin tyrosination as an early marker of mercury toxicity in differentiating N2a cells. *Toxicology in Vitro* **21**, 1258–1261.
- Lee CGL, Tang K, Cheung YB, Wong LP, Tan C, Shen H, Zhao Y, Pavanni R, Lee EJD, Wong M-C, Chong SS & Tan EK (2004). MDR1, the blood-brain barrier transporter, is associated with Parkinson's disease in ethnic Chinese. *J Med Genet* **41**, e60.
- Lees F, Baillie M, Gettinby G & Revie CW (2008). The efficacy of emamectin benzoate against infestations of *Lepeophtheirus salmonis* on farmed Atlantic salmon (*Salmo salar* L) in Scotland, 2002-2006. *PLoS ONE* **3**, e1549.
- Leggas M, Zhuang Y, Welden J, Self Z, Waters CM & Stewart CF (2004). Microbore HPLC method with online microdialysis for measurement of topotecan lactone and carboxylate in murine CSF. *J Pharm Sci* **93**, 2284–2295.
- Leier I, Hummel-Eisenbeiss J, Cui Y & Keppler D (2000). ATP-dependent para-aminohippurate transport by apical multidrug resistance protein MRP2. *Kidney Int* **57**, 1636–1642.
- Leslie EM, Deeley RG & Cole SPC (2005). Multidrug resistance proteins: role of P-glycoprotein, MRP1, MRP2, and BCRP (ABCG2) in tissue defense. *Toxicol Appl Pharmacol* **204**, 216–237.
- Lespine A, Dupuy J, Orłowski S, Nagy T, Glavinas H, Krajcsi P & Alvinerie M (2006). Interaction of ivermectin with multidrug resistance proteins (MRP1, 2 and 3). *Chem Biol Interact* **159**, 169–179.
- Lespine A, Martin S, Dupuy J, Roulet A, Pineau T, Orłowski S & Alvinerie M (2007). Interaction of macrocyclic lactones with P-glycoprotein: structure-affinity relationship. *Eur J Pharm Sci* **30**, 84–94.
- Li Q-Y, Wang H-M, Wang Z-Q, Ma J-F, Ding J-Q & Chen S-D (2010). Salidroside attenuates hypoxia-induced abnormal processing of amyloid precursor protein by decreasing BACE1 expression in SH-SY5Y cells. *Neurosci Lett* **481**, 154–158.
- Liguori R, Correia R, Thomas C, Decaudin B, Cisneros J & Lopez A (2010). Emamectin benzoate (Affirm). a modern insecticide for the control of lepidoptera larvae on fruits, grapes and vegetables crops. *Commun Agric Appl Biol Sci* **75**, 247–253.
- Lindenmaier H, Becker M, Haefeli WE & Weiss J (2005). Interaction of progestins with the human multidrug resistance-associated protein 2 (MRP2). *Drug Metab Dispos* **33**, 1576–1579.
- Loo TW & Clarke DM (2005). Recent progress in understanding the mechanism of P-glycoprotein-mediated drug efflux. *J Membr Biol* **206**, 173–185.

- Löscher W & Potschka H (2005). Drug resistance in brain diseases and the role of drug efflux transporters. *Nat Rev Neurosci* **6**, 591–602.
- Luna-Tortós C, Rambeck B, Jürgens UH & Löscher W (2009). The antiepileptic drug topiramate is a substrate for human P-glycoprotein but not multidrug resistance proteins. *Pharm Res* **26**, 2464–2470.
- Macdonald N & Gledhill A (2007). Potential impact of ABCB1 (p-glycoprotein) polymorphisms on avermectin toxicity in humans. *Arch Toxicol* **81**, 553–563.
- Matsson P, Pedersen JM, Norinder U, Bergström CAS & Artursson P (2009). Identification of novel specific and general inhibitors of the three major human ATP-binding cassette transporters P-gp, BCRP and MRP2 among registered drugs. *Pharm Res* **26**, 1816–1831.
- McAlear MA, Breen MA, White NL & Matthews N (1999). pABC11 (also known as MOAT-C and MRP5), a member of the ABC family of proteins, has anion transporter activity but does not confer multidrug resistance when overexpressed in human embryonic kidney 293 cells. *J Biol Chem* **274**, 23541–23548.
- Mealey KL, Bentjen SA, Gay JM & Cantor GH (2001). Ivermectin sensitivity in collies is associated with a deletion mutation of the *mdr1* gene. *Pharmacogenetics* **11**, 727–733.
- Miglio G, Rattazzi L, Rosa AC & Fantozzi R (2009a). PPARgamma stimulation promotes neurite outgrowth in SH-SY5Y human neuroblastoma cells. *Neurosci Lett* **454**, 134–138
- Miglio G, Rosa AC, Rattazzi L, Collino M, Lombardi G & Fantozzi R (2009b). PPARgamma stimulation promotes mitochondrial biogenesis and prevents glucose deprivation-induced neuronal cell loss. *Neurochem Int* **55**, 496–504.
- Miller DS (2010). Regulation of P-glycoprotein and other ABC drug transporters at the blood-brain barrier. *Trends Pharmacol Sci* **31**, 246–254.
- Müller H, Klinkhammer W, Globisch C, Kassack MU, Pajeva IK & Wiese M (2007). New functional assay of P-glycoprotein activity using Hoechst 33342. *Bioorg Med Chem* **15**, 7470–7479.
- Morita N, Yasumori T & Nakayama K (2003). Human MDR1 polymorphism: G2677T/A and C3435T have no effect on MDR1 transport activities. *Biochem Pharmacol* **65**, 1843–1852.
- Mutoh K, Mitsuhashi J, Kimura Y, Tsukahara S, Ishikawa E, Sai K, Ozawa S, Sawada J-ichi, Ueda K, Katayama K & Sugimoto Y (2006). A T3587G germ-line mutation of the MDR1 gene encodes a nonfunctional P-glycoprotein. *Mol Cancer Ther* **5**, 877–884.
- Nies AT, Jedlitschky G, König J, Herold-Mende C, Steiner HH, Schmitt H-P & Keppler D (2004). Expression and immunolocalization of the multidrug resistance proteins, MRP1-MRP6 (ABCC1-ABCC6), in human brain. *Neuroscience* **129**, 349–360.
- Novotny M., Krautmann M., Ehrhart J., Godin C., Evans E., McCall J., Sun F, Rowan T. & Jernigan A. (2000). Safety of selamectin in dogs. *Veterinary Parasitology* **91**, 377–391.
- Ose A, Kusuhara H, Endo C, Tohyama K, Miyajima M, Kitamura S & Sugiyama Y (2010). Functional characterization of mouse organic anion transporting peptide 1a4 in the uptake and efflux of drugs across the blood-brain barrier. *Drug Metab Dispos* **38**, 168–176.

- Pabon MM, Bachstetter AD, Hudson CE, Gemma C & Bickford PC (2011). CX3CL1 reduces neurotoxicity and microglial activation in a rat model of Parkinson's disease. *J Neuroinflammation* **8**, 9.
- Pabon MM, Bachstetter AD, Hudson CE, Gemma C & Bickford PC (n.d.). CX3CL1 reduces neurotoxicity and microglial activation in a rat model of Parkinson's disease. *J Neuroinflammation* **8**, 9–9.
- Poller B, Drewe J, Krähenbühl S, Huwyler J & Gutmann H (2010). Regulation of BCRP (ABCG2) and P-glycoprotein (ABCB1) by cytokines in a model of the human blood-brain barrier. *Cell Mol Neurobiol* **30**, 63–70.
- Potschka H, Fedrowitz M & Löscher W (2003). Brain access and anticonvulsant efficacy of carbamazepine, lamotrigine, and felbamate in ABCC2/MRP2-deficient TR- rats. *Epilepsia* **44**, 1479–1486.
- Pouliot JF, L'Heureux F, Liu Z, Prichard RK & Georges E (1997). Reversal of P-glycoprotein-associated multidrug resistance by ivermectin. *Biochem Pharmacol* **53**, 17–25.
- Price RD, Oe T, Yamaji T & Matsuoka N (2006). A simple, flexible, nonfluorescent system for the automated screening of neurite outgrowth. *J Biomol Screen* **11**, 155–164.
- Roelofsen H, Vos TA, Schippers IJ, Kuipers F, Koning H, Moshage H, Jansen PL & Müller M (1997). Increased levels of the multidrug resistance protein in lateral membranes of proliferating hepatocyte-derived cells. *Gastroenterology* **112**, 511–521.
- Ronaldson PT, Bendayan M, Gingras D, Piquette-Miller M & Bendayan R (2004). Cellular localization and functional expression of P-glycoprotein in rat astrocyte cultures. *J Neurochem* **89**, 788–800.
- Rose JM, Peckham SL, Scism JL & Audus KL (1998). Evaluation of the role of P-glycoprotein in ivermectin uptake by primary cultures of bovine brain microvessel endothelial cells. *Neurochem Res* **23**, 203–209.
- Ross RA (1983). Coordinate morphological and biochemical interconversion of human neuroblastoma cells. *J Natl Cancer Inst* **71**, 741–747.
- Sachana M, Flaskos J, Alexaki E, Glynn P & Hargreaves A. (2001). The toxicity of chlorpyrifos towards differentiating mouse N2a neuroblastoma cells. *Toxicology in Vitro* **15**, 369–372.
- Sadée W, Yu VC, Richards ML, Preis PN, Schwab MR, Brodsky FM & Biedler JL (1987). Expression of neurotransmitter receptors and myc protooncogenes in subclones of a human neuroblastoma cell line. *Cancer Res* **47**, 5207–5212.
- Sams R (1993). Chemical assay of avermectins by high performance liquid chromatography with fluorescence detection. *Vet Parasitol* **48**, 59–66.
- Sanghera MF (2008). An Investigation of the Neurotoxic and Genotoxic Effects of Chlorpyrifos In N2a Cells. *The FASEB Journal*.
- Schaefer M, Roots I & Gerloff T (2006). In-vitro transport characteristics discriminate wild-type ABCB1 (MDR1) from ALA893SER and ALA893THR polymorphisms. *Pharmacogenet Genomics* **16**, 855–861.

- Schinkel AH, Smit JJ, van Tellingen O, Beijnen JH, Wagenaar E, van Deemter L, Mol CA, van der Valk MA, Robanus-Maandag EC & te Riele HP (1994). Disruption of the mouse *mdr1a* P-glycoprotein gene leads to a deficiency in the blood-brain barrier and to increased sensitivity to drugs. *Cell* **77**, 491–502.
- Schinkel AH, Wagenaar E, van Deemter L, Mol CA & Borst P (1995). Absence of the *mdr1a* P-Glycoprotein in mice affects tissue distribution and pharmacokinetics of dexamethasone, digoxin, and cyclosporin A. *J Clin Invest* **96**, 1698–1705.
- Schinkel AH, Wagenaar E, Mol CA & van Deemter L (1996). P-glycoprotein in the blood-brain barrier of mice influences the brain penetration and pharmacological activity of many drugs. *J Clin Invest* **97**, 2517–2524.
- Schott A, Ravaut S, Keller S, Radzimanowski J, Viotti C, Hillmer S, Sinning I & Strahl S (2010). Arabidopsis stromal-derived Factor2 (SDF2) is a crucial target of the unfolded protein response in the endoplasmic reticulum. *J Biol Chem* **285**, 18113–18121.
- Shapiro AB & Ling V (1997). Positively cooperative sites for drug transport by P-glycoprotein with distinct drug specificities. *Eur J Biochem* **250**, 130–137.
- Shea TB, Perrone-Bizzozero NI, Beermann ML & Benowitz LI (1991). Phospholipid-mediated delivery of anti-GAP-43 antibodies into neuroblastoma cells prevents neuritogenesis. *J Neurosci* **11**, 1685–1690.
- Shilling RA, Venter H, Velamakanni S, Bapna A, Woebking B, Shahi S & van Veen HW (2006). New light on multidrug binding by an ATP-binding-cassette transporter. *Trends Pharmacol Sci* **27**, 195–203.
- Shoop WL, Mrozik H & Fisher MH (1995). Structure and activity of avermectins and milbemycins in animal health. *Veterinary Parasitology* **59**, 139–156.
- Siddiqui A, Kerb R, Weale ME, Brinkmann U, Smith A, Goldstein DB, Wood NW & Sisodiya SM (2003). Association of multidrug resistance in epilepsy with a polymorphism in the drug-transporter gene ABCB1. *N Engl J Med* **348**, 1442–1448.
- Sidiropoulou E, Sachana M, Flaskos J, Harris W, Hargreaves AJ & Woldehiwet Z (2009). Diazinon oxon affects the differentiation of mouse N2a neuroblastoma cells. *Arch Toxicol* **83**, 373–380.
- Soontornmalai A, Vlaming MLH & Fritschy J-M (2006). Differential, strain-specific cellular and subcellular distribution of multidrug transporters in murine choroid plexus and blood-brain barrier. *Neuroscience* **138**, 159–169.
- Sreeramulu K, Liu R & Sharom FJ (2007). Interaction of insecticides with mammalian P-glycoprotein and their effect on its transport function. *Biochim Biophys Acta* **1768**, 1750–1757.
- Sul D, Kim H-S, Cho E-K, Lee M, Kim HS, Jung W-W, Hwang KW & Park S-Y (2009). 2,3,7,8-TCDD neurotoxicity in neuroblastoma cells is caused by increased oxidative stress, intracellular calcium levels, and tau phosphorylation. *Toxicology* **255**, 65–71.
- Sun Y-J, Long D-X, Li W, Hou W-Y, Wu Y-J & Shen J-Z (2010). Effects of avermectins on neurite outgrowth in differentiating mouse neuroblastoma N2a cells. *Toxicol Lett* **192**, 206–211.

- Sunder-Plassmann R, Rieger S, Endler G, Brunner M, Müller M & Mannhalter C (2005). Simultaneous analysis of MDR1 C3435T, G2677T/A, and C1236T genotypes by multiplexed mutagenically separated PCR. *Clin Chem Lab Med* **43**, 192–194.
- Sweet DH, Miller DS, Pritchard JB, Fujiwara Y, Beier DR & Nigam SK (2002). Impaired organic anion transport in kidney and choroid plexus of organic anion transporter 3 (Oat3 (Slc22a8)) knockout mice. *J Biol Chem* **277**, 26934–26943.
- Takano A, Kusuhara H, Suhara T, Ieiri I, Morimoto T, Lee Y-J, Maeda J, Ikoma Y, Ito H, Suzuki K & Sugiyama Y (2006). Evaluation of in vivo P-glycoprotein function at the blood-brain barrier among MDR1 gene polymorphisms by using ¹¹C-verapamil. *J Nucl Med* **47**, 1427–1433.
- Tan E-K, Chan DK-Y, Ng P-W, Woo J, Teo YY, Tang K, Wong L-P, Chong SS, Tan C, Shen H, Zhao Y & Lee CGL (2005). Effect of MDR1 haplotype on risk of Parkinson disease. *Arch Neurol* **62**, 460–464.
- Taub ME, Podila L, Ely D & Almeida I (2005). Functional assessment of multiple P-glycoprotein (P-gp) probe substrates: influence of cell line and modulator concentration on P-gp activity. *Drug Metab Dispos* **33**, 1679–1687.
- Taylor MJ, Hoerauf A & Bockarie M (2010). Lymphatic filariasis and onchocerciasis. *The Lancet* **376**, 1175–1185.
- Thiebaut F, Tsuruo T, Hamada H, Gottesman MM, Pastan I & Willingham MC (1987). Cellular localization of the multidrug-resistance gene product P-glycoprotein in normal human tissues. *Proc Natl Acad Sci USA* **84**, 7735–7738.
- Tsuji A, Tamai I, Sakata A, Tenda Y & Terasaki T (1993). Restricted transport of cyclosporin A across the blood-brain barrier by a multidrug transporter, P-glycoprotein. *Biochem Pharmacol* **46**, 1096–1099.
- Uhr M, Ebinger M, Rosenhagen MC & Grauer MT (2005). The anti-Parkinson drug budipine is exported actively out of the brain by P-glycoprotein in mice. *Neurosci Lett* **383**, 73–76.
- Uhr M, Grauer MT, Yassouridis A & Ebinger M (2007). Blood-brain barrier penetration and pharmacokinetics of amitriptyline and its metabolites in p-glycoprotein (abcb1ab) knock-out mice and controls. *J Psychiatr Res* **41**, 179–188.
- Umbenhauer DR, Lankas GR, Pippert TR, Wise LD, Cartwright ME, Hall SJ & Beare CM (1997). Identification of a P-glycoprotein-deficient subpopulation in the CF-1 mouse strain using a restriction fragment length polymorphism. *Toxicol Appl Pharmacol* **146**, 88–94.
- Vesonen M, Salminen M, Wessman M, Lankinen H, Sistonen P & Vaheri A (1994). Morphological differentiation of human SH-SY5Y neuroblastoma cells inhibits human immunodeficiency virus type 1 infection. *J Gen Virol* **75** (Pt 1), 201–206.
- Vialou V, Amphoux A, Zwart R, Giros B & Gautron S (2004). Organic cation transporter 3 (Slc22a3) is implicated in salt-intake regulation. *J Neurosci* **24**, 2846–2851.
- Warren MS, Zerangue N, Woodford K, Roberts LM, Tate EH, Feng B, Li C, Feuerstein TJ, Gibbs J, Smith B, de Morais SM, Dower WJ & Koller KJ (2009). Comparative gene expression profiles of ABC transporters in brain microvessel endothelial cells and brain in five species including human. *Pharmacol Res* **59**, 404–413.

- Weksler BB, Subileau EA, Perrière N, Charneau P, Holloway K, Leveque M, Tricoire-Leignel H, Nicotra A, Bourdoulous S, Turowski P, Male DK, Roux F, Greenwood J, Romero IA & Couraud PO (2005). Blood-brain barrier-specific properties of a human adult brain endothelial cell line. *FASEB J* **19**, 1872–1874.
- Wijnholds J, Mol CA, van Deemter L, de Haas M, Scheffer GL, Baas F, Beijnen JH, Scheper RJ, Hatse S, De Clercq E, Balzarini J & Borst P (2000). Multidrug-resistance protein 5 is a multispecific organic anion transporter able to transport nucleotide analogs. *Proc Natl Acad Sci USA* **97**, 7476–7481.
- Wise LD, Allen HL, Hoe CM, Verbeke DR & Gerson RJ (1997). Developmental neurotoxicity evaluation of the avermectin pesticide, emamectin benzoate, in Sprague-Dawley rats. *Neurotoxicol Teratol* **19**, 315–326.
- Yousif S, Marie-Claire C, Roux F, Scherrmann J-M & Declèves X (2007). Expression of drug transporters at the blood-brain barrier using an optimized isolated rat brain microvessel strategy. *Brain Res* **1134**, 1–11.
- Zhao R, Raub TJ, Sawada GA, Kasper SC, Bacon JA, Bridges AS & Pollack GM (2009). Breast cancer resistance protein interacts with various compounds in vitro, but plays a minor role in substrate efflux at the blood-brain barrier. *Drug Metab Dispos* **37**, 1251–1258.
- Zhu Y, Matsumoto T, Mikami S, Nagasawa T & Murakami F (2009). SDF1/CXCR4 signalling regulates two distinct processes of precerebellar neuronal migration and its depletion leads to abnormal pontine nuclei formation. *Development* **136**, 1919–1928.

Primer	Sequence	Primer Melting Temp, T _m /°C	Annealing Temp//°C	Expected Product Size/bp
hMDR1F	5'-TTCACCTCAGTTACCCATCTCG-3'	58.4	58	82
hMDR1R	5'-GTCTGCCCACTCTGCACCTTC-3'	63.7		
hBCRPF	5'-CAGGTGGAGGCAAATCTTCG-3'	59.4	55	59
hBCRPR	5'-TTGGATCTTTCCTTGCAGCTAA-3'	56.5		
hMRP1F	5'-TGGCATCACCTTCTCCATCC-3'	59.4	58	86
hMRP1R	5'-GAGAGCAGGACGACTTCCCG-3'	63.7		
mMdr1aF	5'-CTTACAGCCAGCATTCTCCG-3'	55.8	55	87
mMdr1aR	5'-CTGTTCTGCCCGCTGGGTTTC-3'	59.1		
mBcrpF	5'-GGTTATGTGGTTCAAGATGAC-3'	53.7	53	86
mBcrpR	5'-GTTGGAAGTCGAAGAGCTGCT-3'	58.2		

Human MDR1 primer alignment Appendix B

NCBI Reference Sequence: NM_000927.3

Homo sapiens ATP-binding cassette, sub-family B (MDR/TAP), member 1 (ABCB1), mRNA

ORIGIN

```
1  tattcagata ttctccagat tcctaaagat tagagatcat ttctcattct cctaggagta
61  ctcaactcag gaagcaacca gataaaagag aggtgcaacg gaagccagaa cattcctcct
121 ggaaattcaa cctgtttcgc agtttctcga ggaatcagca ttcagtcaat cggggccggg
181 agcagtcatc tgtggtgagg ctgattggct gggcaggaac agcgccgggg cgtgggctga
241 gcacagccgc ttcgctctct ttgccacagg aagcctgagc tcattcgagt agcggctctt
301 ccaagctcaa agaagcagag gccgctgttc gtttccttta ggtcctttcca ctaaagtcgg
361 agtatcttct tccaaaattt cacgtcttgg tggccgttcc aaggagcgcg aggtcggaat
421 ggatcttgaa ggggaccgca atggaggagc aaagaagaag aactttttta aactgaacaa
481 taaaagtga aaagataaga aggaaaagaa accaactgtc agtgtattht caatgthtctg
541 ctattcaaat tggcttgaca agttgtatat ggtggtggga actthtggctg ccatcatcca
601 tggggctgga cttcctctca tgatgctggg gthtggagaa atgacagata tctthtgaaa
661 tgcaggaaat ttagaagatc tgatgtcaaa catcactaat agaagtgata tcaatgatac
721 agggthtctt atgaatctgg aggaagacat gaccaggat gcctattatt acagtggaat
781 tgggtgctgg gtgctggtht ctgcttacct tcaggthtca thtthtggthtcc tggcagctgg
841 aagacaaata cacaaaatta gaaaacagtht thtthtcatgct ataatgthtcc aggagatagtht
901 ctggthttht gatgthtccagat thtggggagct taacaccgca thtaccagatg atgthtctccaa
961 gattaatgaa ggaathtggtht acaaaathtgg aathtthtcttht cagthtcaatgg caacathttht
1021 cactgggtht atagthttagg thtaccagthtgg thtggaaagct accctthtthtga thtthtggccat
1081 cagthtctgtht cthtggactgtht cagthtctgtht ctgggcaaaag atactatcttht cattthtactga
1141 taaagaactc thttagcgtatg caaaagctgg agcagthttagct gaagagthtct thtggcagcaat
1201 tagaactgtht atthtgcathttht gaggacaaaa gaaagaacttht gaaagthtaca acaaaathttht
1261 agaagaagct aaaagaathttht ggataaaagaa agctathtthtaca gccaatathttht ctatagthtthtgc
1321 tgctthtctctg ctgathtctatg catctthtthtgc thtctggccttht thtggthtthtggga ccacctthtggtht
1381 cctctcaggg gaathtthtctca thtggacaagtht actcactgtht thtctthtthtctg thtthtthtthtgg
1441 ggctthtthttagtht gthtggacagtht catctccaag cattgaaagca thtthtgcaaatg caagagthtggagc
1501 agctthtthtga atctthtcaaga thtathtthtgataa thttagccaagtht atthtgacagct atthtthtgaagag
1561 tgggcacaaa ccagataata thttagggaaa thtthtggaaatht agaaathttht ttc actthtcaagtht
1621 cccatctcga aaagaagtht agathtctthtga gggthtctgaac ctgaagthtthtgc agagthtgggca
1681 gacggthtggcc ctggthtthtggaa acagthtggctg thtggaaagagc acaacagthtcc agctgathtthtgc
1741 gagthtctctat gacccacag aggggagthtggtht cagthtthtthtga thtggacagthtata thttaggacatht
1801 aathtthtgaag thtthtctacggg aathtthtctthtgg thtthtggthtthtga thtggaaacctg thtthtggthtthtgc
1861 caccacgata gctgaaaaca thtctgctatgg ccgthtggaaaat gthtccacathtgg atgagathtthtga
1921 gaaagctgtht aaggaaagcca atgctctatga cthtthtthtctatg aaactgthtctc athtthtthtthtga
1981 caccctggtht ggagagagag gggcccagtht gagthtggthtggtht cagaagcagata ggathtthtggccat
```

Human MDR1 primer alignment Appendix B

2041 tgcacgtgcc ctggttcgca accccaagat cctcctgctg gatgaggcca cgtcagcctt
2101 ggacacagaa agcgaagcag tggttcaggt ggctctggat aaggccagaa aaggtcggac
2161 caccattgtg atagctcatc gtttgtctac agttcgtaat gctgacgtca tgcgtggttt
2221 cgatgatgga gtcattgtgg agaaaggaaa tcatgatgaa ctcatgaaag agaaaggcat
2281 ttacttcaaa cttgtcacia tgcagacagc aggaaatgaa gttgaattag aaaatgcagc
2341 tgatgaatcc aaaagtgaaa ttgatgcctt ggaaatgtct tcaaatgatt caagatccag
2401 tctaataaga aaaagatcaa ctcgtaggag tgtccgtgga tcacaagccc aagacagaaa
2461 gcttagtacc aaagaggctc tggatgaaag tatacctcca gtttcctttt ggaggattat
2521 gaagctaaat ttaactgaat ggccttattt tgttgttggg gtattttgtg ccattataaa
2581 tggaggcctg caaccagcat ttgcaataat attttcaaaag attatagggg tttttacaag
2641 aattgatgat cctgaaacaa aacgacagaa tagtaacttg ttttcaactat tgtttctagc
2701 ccttgggaatt atttctttta ttacattttt ccttcagggg ttcacatttg gcaaagctgg
2761 agagatcctc accaagcggc tccgatacat ggttttccga tccatgctca gacaggatgt
2821 gagttgggtt gatgacccta aaaacaccac tggagcattg actaccaggc tcgccaatga
2881 tgctgctcaa gttaaagggg ctataggttc caggcttgct gtaattacc agaatatagc
2941 aatccttggg acaggaataa ttatatcctt catctatggg tggcaactaa cactgttact
3001 cttagcaatt gtaccatca ttgcaatagc aggagtgtt gaaatgaaaa tgttgtctgg
3061 acaagcactg aaagataaga aagaactaga aggttctggg aagatcgcta ctgaagcaat
3121 agaaaacttc cgaaccgttg tttctttgac tcaggagcag aagtttgaac atatgtatgc
3181 tcagagtttg caggtaccat acagaaactc tttgaggaaa gcacacatct ttggaattac
3241 attttcttcc acccaggcaa tgatgtattt ttcctatgct ggatgtttcc ggtttggagc
3301 ctacttggtg gcacataaac tcatgagctt tgaggatgtt ctgttagtat tttcagctgt
3361 tgtctttggg gccatggccg tggggcaagt cagttcattt gtcctgact atgccaaagc
3421 caaaatatca gcagcccaca tcatcatgat cattgaaaaa acccctttga ttgacagcta
3481 cagcacggaa ggcctaattc cgaacacatt ggaaggaaat gtcacatttg gtgaagttgt
3541 attcaactat cccacccgac cggacatccc agtgcttcag ggactgagcc tggaggtgaa
3601 gaagggccag acgctggctc tgggtggcag cagtggctgt gggaagagca cagtggcca
3661 gctcctggag cggttctacg accccttggc agggaaaagt ctgcttgatg gcaaagaaat
3721 aaagcgactg aatgttcagt ggctccgagc acacctgggc atcgtgtccc aggagcccat
3781 cctgtttgac tgcagcattg ctgagaacat tgcctatgga gacaacagcc ggggtgtgtc
3841 acaggaagag attgtgaggg cagcaaagga ggccaacata catgccttca tcgagtcact
3901 gcctaataaa tatagcacta aagtaggaga caaaggaact cagctctctg gtggccagaa
3961 acaacgcatt gccatagctc gtgcccttgt tagacagcct catattttgc ttttggatga
4021 agccacgtca gctctggata cagaaagtga aaagggtgtc caagaagccc tggacaaagc
4081 cagagaaggc cgcacctgca ttgtgattgc tcaccgctg tccaccatcc agaatgcaga
4141 cttaatagtg gtgtttcaga atggcagagt caaggagcat ggcacgcatc agcagctgct
4201 ggcacagaaa ggcattctatt tttcaatggg cagtgtccag gctggaacaa agcgcagctg
4261 aactctgact gtatgagatg ttaaataactt tttaatattt gtttagatat gacatttatt
4321 caaagttaaa agcaaacact tacagaatta tgaagaggta tctgtttaac atttctcag
4381 tcaagttcag agtcttcaga gacttcgtaa ttaaaggaac agagtgagag acatcatcaa
4441 gtggagagaa atcatagttt aaactgcatt ataaatttta taacagaatt aaagtagatt

Human MDR1 primer alignment Appendix B

4501 ttaaaagata aaatgtgtaa ttttgtttat attttcccat ttggactgta actgactgcc
4561 ttgctaaaag attatagaag tagcaaaaag tattgaaatg tttgcataaa gtgtctataa
4621 taaaactaaa ctttcatgtg actggagtca tcttgtccaa actgcctgtg aatatactt
4681 ctctcaattg gaatattgta gataacttct gctttaaaaa agttttcttt aaatatacct
4741 actcattttt gtgggaatgg ttaagcagtt taaataattc ctgttgata tgtctattca
4801 cattgggtct tacagaacca tctggcttca ttcttcttgg acttgatcct gctgattctt
4861 gcatttccac at

//

Homo sapiens ATP-binding cassette, sub-family G (WHITE), member 2 (ABCG2), mRNA

NCBI Reference Sequence: NM_004827.2

ORIGIN

```
1 gtcagcgcctg cctgagctcg tcccctggat gtccgggtct ccccaggcgg ccacccgccc
61 gctcccacatc tgacctccag ccgcagcggc tcccacgccc gccgcccggc gaggggagcg
121 ctccgggcgcg ccgggtgtgg ttgggggaag gggttgtgcc gcgcgcgggc tgcgtgctgt
181 gccactcaa aaggttccgg gcgcgcagga ggaagaggc agtgcccgcc actcccactg
241 agattgagag acgcggcaag gaggcagcct gtggaggaac tggtaggat ttaggaacgc
301 accgtgcaca tgcttgggtg tcttgtaag tggaaactgc tgctttagag tttgtttgga
361 aggtccgggt gactcatccc aacatttaca tccttaattg ttaaagcgc gctcccgagc
421 gcacgcaccc tgagatcctg agcctttggt taagaccgag ctctattaag ctgaaaagat
481 aaaaactctc cagatgtctt ccagtaatgt cgaagttttt atcccagtgt cacaaggaaa
541 caccaatggc ttccccgcga cagcttccaa tgacctgaag gcatttactg aaggagctgt
601 gttaagtgtt cataacatct gctatcgagt aaaactgaag agtggccttc tacctgtctg
661 aaaaccagtt gagaaagaaa tattatcgaa tatcaatggg atcatgaaac ctgggtctcaa
721 cgccatcctg ggaccacag gtggaggcaa atcttcgttta ttagatgtct tagctgcaag
781 gaaagatcca agtggattat ctggagatgt tctgataaat ggagcaccgc gacctgccaa
841 tttcaaagt aattcagggt acgtgtgata agatgatggt gtgatgggca ctctgacggt
901 gagagaaaac ttacagttct cagcagctct tcggcttgca acaactatga cgaatcatga
961 aaaaaacgaa cggattaaca gggtcattca agagttaggt ctggataaag tggcagactc
1021 caaggttggg actcagttta tccgtgggtg gtctggagga gaaagaaaaa ggactagtat
1081 agaatggag cttatcactg atccttccat cttgttcttg gatgagccta caactggctt
1141 agactcaagc acagcaaagt ctgtcctttt gctcctgaaa aggatgtcta agcagggagc
1201 aacaatcacc ttctccattc atcagcctcg atattccatc ttcaagttgt ttgatagcct
1261 caccttattg gcctcaggaa gacttatggt ccacgggcct gctcaggagg ccttgggata
1321 ctttgaatca gctggttatc actgtgaggc ctataataac cctgcagact tcttcttgga
1381 catcattaat ggagattcca ctgctgtggc attaaacaga gaagaagact ttaaagccac
1441 agagatcata gagccttcca agcaggataa gccactcata gaaaaattag cggagattta
1501 tgtcaactcc tccttctaca aagagacaaa agctgaatta catcaacttt ccgggggtga
1561 gaagaagaag aagatcacag tcttcaagga gatcagctac accacctcct tctgtcatca
1621 actcagatgg gtttccaagc gttcattcaa aaacttgctg ggtaatcccc aggctctat
1681 agctcagatc attgtcacag tcgtactggg actggttata ggtgccattt actttgggct
1741 aaaaaatgat tctactggaa tccagaacag agctgggggt ctcttcttcc tgacgaccaa
1801 ccagtgtttc agcagtgttt cagccgtgga actctttgtg gtagagaaga agctcttcat
1861 acatgaatac atcagcggat actacagagt gtcacttat ttccttggaa aactgttatc
1921 tgatttatta cccatgagga tgttaccaag tattatattt acctgtatag tgtacttcat
1981 gttaggattg aagccaaagg cagatgcctt ctctgttatg atgtttacc ttatgatggg
2041 ggcttattca gccagttcca tggcactggc catagcagca ggtcagagtg tggtttctgt
2101 agcaacactt ctcagacca tctgtttgt gtttatgatg atttttcag gtctgttggg
2161 caatctcaca accattgcat cttggctgtc atggcttcag tacttcagca ttccagata
2221 tggatttacg gctttgcagc ataatagaatt tttgggacaa aacttctgcc caggactcaa
```

Human BCRP primer Alignment Appendix B

2281 tgcaacagga aacaatcctt gtaactatgc aacatgtact ggcaagaat atttggtaaa
2341 gcagggcatc gatctctcac cctggggcct gtggaagaat cacgtggcct tggcttgtat
2401 gattgttatt ttctcaciaa ttgcctacct gaaattgtta tttcttaaaa aatattctta
2461 aatttcccct taattcagta tgatttatcc tcacataaaa aagaagcact ttgattgaag
2521 tattcaatca agtttttttg ttgttttctg ttcccttgcc atcacactgt tgcacagcag
2581 caattgtttt aaagagatac attttttagaa atcacacaaa actgaattaa acatgaaaga
2641 acccaagaca tcatgtatcg catattagtt aatctcctca gacagtaacc atggggaaga
2701 aatctgggtct aatttattaa tctaaaaaag gagaattgaa ttctggaaac tctgacaag
2761 ttattactgt ctctggcatt tgtttcctca tctttaaaaat gaataggtag gttagtagcc
2821 cttcagtctt aatactttat gatgctatgg tttgccatta ttttaataaat gacaaatgta
2881 ttaatgctat actggaaatg taaaattgaa aatatgttgg aaaaaagatt ctgtcttata
2941 gggtaaaaaa agccaccgtg atagaaaaaa aatctttttg ataagcacat taaagttaat
3001 agaacttact gatattcctg tctagtggta taatatctca ggaatcttgg ctgagggttt
3061 ggaactgtgg gtagagtaga gggccaggag tccagtaata gaattcttgc accatttctg
3121 gaacattcta gctctgggag gtcacgtaac cttcttgggg tagttcagtg gtttagtggt
3181 ttataatcca ggtgtgctgc agaatcatct gaggaacttt gctaaaatac aaaaatctgg
3241 cctaagtagc tccagatcta ccttcataaa ggaatctgac cactcctgga tttggtaatt
3301 tccaagttct gaaaatttta cttaggattt aataactatt aacatctgct cctacatagg
3361 ttttctttcc tacttatata cttatgttct tcttcattct aaccttcac agtaataggg
3421 aatgttttta attttatttt tttagttgaa gggtaaatgta ccaaaaaata tagttcagtg
3481 aattaaaatg aacacacatg tgcaaccatc aattcaggtc aagaaataga agattgtagc
3541 acacaaaagc ctactcagcc attctcccag tcaactactc cttccttacc cctgggttat
3601 ttttgaaatg acacttgatg tatttccctc tgttgctggt atgagaacat tgctacagcc
3661 aagtgttgtg tttctgtgtg cataggttga tacttaatta tctccccact ttttaataaa
3721 cttttaattt ggaaataatt ttagattgac agaaaagttg caaagatagt gaggaaagtt
3781 cctgtctact ctttgctcag cttcccttaa tgttaacatt ttatatagca agatgcattt
3841 gtcaaagcta acaagttaac attggtacaa tcaactgtta ttaaactgca cacaatattc
3901 agatttcacc acttttccac taatattctt tcattgttct aggattcaat tcaggagacc
3961 acatttcac tagccctctt ttttaaaaagt aaatactttt cagcacttac aggagttaac
4021 tgagctgggg catcatgggtg tatagacgcc ctgacactgg tcatcttggg attcatttag
4081 tttgtcagtg ggtgccctga cattctgtca caacatcaat ttgggaacat ggcatatat
4141 ttttatcttt gaactttttt ctttttggat gacatttgat taatgctgca tcttggaaac
4201 cattatcttt tttcttgggt atgtgatcag gaagattaat cagtttttcc tgttcttggg
4261 ataattcctg cttttcacat acctgtccct tacagttctc tataataacc cttcccttat
4321 tacacagaga gaaatatcta tctatacttt ttacacaaaa tatacttcaa aagaaacaaa
4381 acagccacaa ttattaactt tttaaataaa tgagaattta attatatacct aaaaaaaaaa
4441 aaaaa

//

Human MRP1 primer alignment Appendix B

Homo sapiens ATP-binding cassette, sub-family C (CFTR/MRP), member 1 (ABCC1), transcript variant 1, mRNA

NCBI Reference Sequence: NM_004996.3

ORIGIN

```
1 ccaggcggcg ttgcggcccc ggccccggct ccctgcgccg ccgcccgcgc cgcgcgcagc
61 gctagcgcca gcagccgggc ccgatcaccg gccgcccggg gcccgccgcc gcccgcgcca
121 gcaaccgggc ccgatcaccg gccgcccggg gcccgccgcc gcccgcgcca ccggcatggc
181 gctccggggc ttctgcagcg ccgatggctc cgaccgcgctc tgggactgga atgtcacgtg
241 gaataccagc aaccccgact tcaccaagtg ctttcagaac acggtcctcg tgtgggtgcc
301 ttgtttttac ctctgggcct gtttcccctt ctacttcctc tatctctccc gacatgaccg
361 aggctacatt cagatgacac ctctcaacaa aaccaaaaact gccttgggat ttttgcgtg
421 gatcgtctgc tgggcagacc tcttctactc tttctgggaa agaagtcggg gcatattcct
481 ggccccagtg tttctggta gcccaactct cttgggcatc accatgctgc ttgctacctt
541 ttttaattcag ctggagagga ggaaggagtg tcagtcttca gggatcatgc tcactttctg
601 gctggtagcc ctagtgtgtg ccctagccat cctgagatcc aaaattatga cagcctaaa
661 agaggatgcc caggtggacc tgtttcgtga catcactttc tacgtctact tttccctctt
721 actcattcag ctcgtcttgt cctgtttctc agatcgctca cccctgttct cggaaacctat
781 ccacgacctt aatccctgcc cagagtcacg cgcttccttc ctgtcgagga tcacctctg
841 gtggatcaca gggttgattg tccggggcta ccgccagccc ctggagggca gtgacctctg
901 gtccttaaac aaggaggaca cgtcggaaac agtcgtgcct gttttggtaa agaactggaa
961 gaaggaatgc gccaaagacta ggaagcagcc ggtgaagggt gtgtactcct ccaaggatcc
1021 tgcccagccg aaagagagtt ccaagtgga tgcgaatgag gagtgaggg ctttgatcgt
1081 caagtcccca cagaaggagt ggaaccctc tctgtttaag gtgtataca agaccttgg
1141 gccctacttc ctcatgagct tcttcttcaa ggccatccac gacctgatga tgttttccgg
1201 gccgcagatc ttaaagttgc tcatcaagtt cgtgaatgac acgaaggccc cagactggca
1261 gggctacttc tacaccgtgc tgctgtttgt cactgcctgc ctgcagacct tcgtgctgca
1321 ccagtacttc cacatctgct tcgtcagtgg catgaggatc aagaccgctg tcattggggc
1381 tgtctatcgg aaggccctgg tgatcaccaa ttcagccaga aaatcctcca cggtcgggga
1441 gattgtcaac ctcatgtctg tggacgctca gaggttcatg gacttggcca cgtacattaa
1501 catgatctgg tcagcccccc tgcaagtcac ccttgctctc tacctcctgt ggctgaatct
1561 gggcccttcc gtccctggctg gagtggcggt gatggctctc atggtgccc tcaatgctgt
1621 gatggcgatg aagaccaaga cgtatcaggt ggccacatg aagagcaaag acaatcggat
1681 caagctgatg aacgaaatc tcaatgggat caaagtgcta aagctttatg cctgggagct
1741 ggcattcaag gacaaggtgc tggccatcag gcaggaggag ctgaaggtgc tgaagaagtc
1801 tgctacctg tcagccgtgg gcacctcac ctgggtctgc acgcccttct tgggtggcctt
1861 gtgcacattt gccgtctacg tgaccattga cgagaacaac atcctggatg cccagacagc
1921 cttcgtgtct ttggccttgt tcaacatcct ccggtttccc ctgaacattc tccccatggt
1981 catcagcagc atcgtgcagg cgagtgtctc cctcaaacgc ctgaggatct ttctctccca
2041 tgaggagctg gaacctgaca gcatcgagcg acggcctgtc aaagacggcg ggggcacgaa
2101 cagcatcacc gtgaggaatg ccacattcac ctgggcccagg agcgcacctc ccacactgaa
2161 tggcatcacc ttctccatcc ccgaagggtc tttggtggcc gtggtgggccc aggtgggctg
2221 cggaaagtct tccctgctct cagccctctt ggctgagatg gacaaagtgg aggggcacgt
2281 ggctatcaag ggctccgtgg cctatgtgcc acagcaggcc tggattcaga atgattctct
```

Human MRP1 primer alignment Appendix B

2341 ccgagaaaaac atcctttttg gatgtcagct ggaggaacca tattacaggt cctgataca
 2401 ggcctgtgcc ctccctccag acctggaaat cctgcccagt ggggatcgga cagagattgg
 2461 cgagaagggc gtgaacctgt ctgggggcca gaagcagcgc gtgagcctgg cccggggcct
 2521 gtactccaac gctgacattt acctcttcga tgatcccctc tcagcagtgg atgccatgt
 2581 gggaaaaacac atctttgaaa atgtgattgg cccaagggg atgctgaaga acaagacgcg
 2641 gatcttggtc acgcacagca tgagctactt gccgcaggtg gacgtcatca tcgtcatgag
 2701 tggcggcaag atctctgaga tgggctccta ccaggagctg ctggctcgag acggcgcctt
 2761 cgctgagttc ctgctacct atgccagcac agagcaggag caggatgcag aggagaacgg
 2821 ggtcacgggc gtcagcggtc cagggaaagga agcaaagcaa atggagaatg gcatgctggg
 2881 gacggacagt gcagggaagc aactgcagag acagctcagc agctcctcct cctatagtgg
 2941 ggacatcagc aggcaccaca acagcaccgc agaactgcag aaagctgagg ccaagaagga
 3001 ggagacctgg aagctgatgg aggtgacaa ggcgcagaca gggcaggtca agctttcct
 3061 gtactgggac tacatgaagg ccatcggact cttcatctcc ttctcagca tcttctttt
 3121 catgtgtaac catgtgtccg cgctggcttc caactattgg ctcagcctct ggactgatga
 3181 ccccatcgtc aacgggactc aggagcacac gaaagtccgg ctgagcgtct atggagccct
 3241 gggcatttca caagggatcg cctgttttg ctactccatg gccgtgtcca tcggggggat
 3301 cttggcttcc cgctgtctgc acgtggacct gctgcacagc atcctgcggt caccatgag
 3361 cttctttgag cggacccccca gtgggaacct ggtgaaccgc ttctccaagg agctggacac
 3421 agtggactcc atgatcccgg aggtcatcaa gatgttcatg ggctccctgt tcaacgtcat
 3481 tggtgectgc atcgttatcc tgctggccac gccatcgcc gccatcatca tcccgccct
 3541 tggcctcacc tacttcttcg tccagagggt ctacgtggct tcctcccggc agctgaagcg
 3601 cctcgagtcg gtcagccgct ccccggtcta ttcccatttc aacgagacct tgctgggggt
 3661 cagcgtcatt cgagccttcg aggagcagga gcgcttcatc caccagagtg acctgaaggt
 3721 ggacgagAAC cagaaggcct attaccccag catcgtggcc aacaggtggc tggcctgctg
 3781 gctggagtgt gtgggcaact gcatcgttct gtttgcctgc ctgtttgctg tgatctccag
 3841 gcacagcctc agtgcctggct tgggtggcct ctacgtgtct tactcattgc aggtcaccac
 3901 gtacttgaac tggctgggtc ggatgtcatc tgaaatggaa accaacatcg tggcctgga
 3961 gaggtcaag gactattcag agactgagaa ggaggcgccc tggcaaatcc aggagacagc
 4021 tccgccagc agctggcccc aggtgggccc agtggaaattc cggaactact gctgctgcta
 4081 ccgagaggac ctggacttcg ttctcaggca catcaatgtc acgatcaatg ggggagaaaa
 4141 ggtcggcacc gtggggcgga cgggagctgg gaagtcgtcc ctgaccctgg gcttatttcg
 4201 gatcaacgag tctgcccgaag gagagatcat catcgtatggc atcaacatcg ccaagatcgg
 4261 cctgcacgac ctccgcttca agatcaccat catccccag gaccctgttt tgttttcggg
 4321 ttccctccga atgaacctgg acccattcag ccagtactcg gatgaagaag tctggacgtc
 4381 cctggagctg gccacactga aggacttcgt gtcagccctt cctgacaagc tagaccatga
 4441 atgtgcagaa ggcgggggaga acctcagtgt cgggcagcgc cagcttgtgt gcctagcccg
 4501 ggcctgctg aggaagacga agatccttgt gttggatgag gccacggcag cctggacct
 4561 ggaacggac gacctcatcc agtccaccat ccggacacag ttcgaggact gcaccgtcct
 4621 caccatcgcc caccggtca acaccatcat ggactacaca aggtgatcg tcttggacaa
 4681 aggagaaatc caggagtacg gcgccccatc ggacctcctg cagcagagag gtcttttcta
 4741 cagcatggcc aaagacgccc gcttgggtgt agccccagag ctggcataatc tggtcagaac
 4801 tgcagggcct atatgccagc gcccaggggag gagtcagtac ccctggtaaa ccaagcctcc
 4861 cacactgaaa ccaaacata aaaaccaaacc ccagacaacc aaaacatatt caaagcagca
 4921 gccaccgcca tccggtcccc tgcttggaac tggctgtgaa gaccaggag agacagagat

Human MRP1 primer alignment Appendix B

4981 gcgaaccacc caaacacgc acaccctgcc cctggtgccc tgagacagac acacagcctc
5041 acgccccagc gaatgcaagt ggtttcctgg tgcttcccac ggaggagttt tggcagccag
5101 acttctggag gaattggttg tatagaagat cctagtgacc aaattcagcc tactgcctcg
5161 gatctctcca gccgaagtct gtggactgca agtctttgag atgcttctgg ctcccatcac
5221 ctctaacatc cttgtctggg tctaccagga acgcttcatt tccttggggc tgcagttttg
5281 tggttgaggg gcctggagaa aatcattttc tccccttggc agtgtcccag ggccttgat
5341 ggtcctctta ccaacatctg gtcttccagc cactcaaaaag ctgggaacca gcctctcagc
5401 gccagctcta ccagttctcg ttttgggcca gaggcagcct ctgactccc acgcctgtcc
5461 tcctggaagg gacctgggtg gactaacggc taacctggac ctggaactgt agggccaggg
5521 gattgtctca gggccgacgt tccacctggg gcttccctcc ccaccacccc cgactccagg
5581 ctttcccttt tttcttttgt tcaacattgt aagaacaatc aatgctgtta ttactgttcc
5641 caccatgatt gatgtgggtt aaatattaag gagatggcct catgggaatt tgacctgac
5701 tagaaataga gactgagagt gagcaaccag ctggaaggta ctatgccagt cctagcagaa
5761 aaatgtgtta ggggcctggc ccaaagcagt gttggttgct tacagtgttg attgattttg
5821 ttcttttttc ttaccacctc ttttctttcc ctctcatggt acctgctcat ggttatgaag
5881 ctttcaaagt aaagaacacg aaatacctcc caagtattac cagtgggtac caaaaaatg
5941 tccccttgag tcttttcctt gtttttagat gttaattctc tcccttggca tccggttagc
6001 cccccagggg gggcagcatt gtggagaact tgatatttag ttactgatgc tcttccagga
6061 cacgaaaaga acccatcttt gaatatcaat gatttttttt ttttaagtac tgttccgggg
6121 agaaaaacag tctcaaaact tgaacttctt gggaaatagaa gtgttgggct gagaagtaac
6181 attcccagga aatagtgaga agctcgccct gtgtttgaaa ccgtgttggc ctctgtgttc
6241 ctggaagaaa acaggggaagc agcatctttt aaagcctgtt ctttaagggtg tctcgttaga
6301 gcccaaagtg gaatccggaa ggcagccaga gctgaggctg cccaagact cagacttgct
6361 aagaattacg ccgccgactt caaacccaga gagcatcttt cttttaggcg aaaacgcata
6421 tatttatttt ttgtaagtta taccattctt tcacattaga taaactaagt tttgggggat
6481 ccttttgtaa tgacttacac tggaaatgcg aacatttgca gtaaaaaaat atatatatat
6541 ctatatatatt tatttctttc taaa

//

Mus musculus ATP-binding cassette, sub-family B (MDR/TAP), member 1A (*Abcb1a*), mRNA

NCBI Reference Sequence: NM_011076.2 red highlight = human MDR1 primer

ORIGIN

```

1  acagtggaac agcggtttcc aggagctgct ggtcccatct tccaaggctc tgctcaactc
61  agagccgctt cttccaaagt ctacatcttg gtggactttg cagaggaaac cgggaggtag
121 agacacgtga ggtcgtgatg gaacttgaag aggaccttaa ggaagagca gacaagaact
181 tctcaaagat gggcaaaaag agtaaaaagg agaagaaaga aaagaaacca gcagtcagtg
241 tgcttacaat gtttcgttat gcaggttggc tggacagggt gtacatgctg gtgggaactc
301 tggctgctat tatccatgga gtggcgctcc cacttatgat gctgatcttt ggtgacatga
361 cagatagctt tgcaagtgta ggaaacgtct ctaaaaacag tactaatatg agtgaggccg
421 ataaaagagc catgtttgcc aaactggagg aagaaatgac cacgtacgcc tactattaca
481 ccgggattgg tgctggtgtg ctcatagttg cctacatcca ggtttcattt tggtgccctg
541 cagctggaag acagatacac aagatcaggc agaagttttt tcatgctata atgaatcagg
601 agataggctg gtttgatgtg catgacgttg gggagctcaa caccggctc acagatgatg
661 tttccaaaat taatgaagga attggtgaca aaatcggaat gttcttccag gcaatggcaa
721 ctttttttgg tggttttata ataggattta cccgtggctg gaagctaacc cttgtgattt
781 tggccatcag ccctgttctt ggactgtcag ctggtatttg ggcaaagata ttgtcttcat
841 ttactgataa ggaactccat gcttatgcaa aagctggagc agttgctgaa gaagtcttag
901 cagccatcag aactgtgatt gcgtttggag gacaaaagaa ggaacttgaa aggtacaata
961 acaacttgga agaagctaaa aggctgggga taaagaaagc tatcacggcc aacatctcca
1021 tgggtgcagc ttttctcctt atctatgcat catatgctct ggcattctgg tatgggactt
1081 ccttgggtcat ctccaaagaa tactctattg gacaagtgct cactgtcttc tttccgtgt
1141 taattggagc attcagtggt ggacaggcat ctccaaatat tgaagccttc gccaatgcac
1201 gaggagcagc ttatgaagtc ttcaaaataa ttgataataa gcccagtata gacagcttct
1261 caaagagtgg gcacaaacca gacaacatac aaggaaatct ggaatttaag aatattcact
1321 tcagttaccc atctcgaaaa gaagttcaga tcttgaaggg cctcaatctg aaggtgaaga
1381 gcggacagac ggtggccctg gttggcaaca gtggctgtgg aaaaagcaca actgtccagc
1441 tgatgcaaag gctctacgac cccctagatg gcatggtcag tatcgacgga caggacatca
1501 gaaccatcaa tgtgaggtat ctgagggaga tcattggtgt ggtgagtcag gaacctgtgc
1561 tgtttgccac cacgatcgcc gagaacattc gctatggccg agaagatgtc accatggatg
1621 agattgagaa agctgtcaag gaagccaatg cctatgactt catcatgaaa ctgccccacc
1681 aatttgacac cctggttggg gagagagggg cgcagctgag tgggggacag aacagagaa
1741 tcgccattgc ccgggcccctg gtccgcaatc ccaagatcct tttgttggac gaggccacct
1801 cagccctgga tacagaaagt gaagctgtgg ttcaggccgc actggataag gctagagaag
1861 gccggaccac cattgtgata gctcatcgct tgtctaccgt tcgtaatgct gacgtcattg
1921 ctggttttga tgggtgtgtc attgtggagc aaggaaatca tgatgagctc atgagagaaa
1981 agggcattta cttcaaaactt gtcatgacac agacagcagg aatgaaatt gaattaggaa
2041 atgaagcttg taaatctaag gatgaaattg ataattttaga catgtcttca aaagattcag
2101 gatccagtct aataagaaga agatcaactc gcaaaagcat ctgtggacca catgaccaag
2161 acaggaagct tagtaccaaa gagggcccctg atgaagatgt acctccagct tccttttggc
2221 ggatcctgaa gttgaattca actgaaatggc cttattttgt ggttgggtata ttctgtgcca

```

2281 taataaatgg aggcttacag ccagcattct ccgtaatat ttcaaaagtt gtaggggttt
 2341 ttacaaatgg tggccccct gaaacccagc ggcagaaacag caacttgttt tccttgttgc
 2401 ttctgatcct tgggatcatt tctttcatta cattttttct tcagggcttc acatttggca
 2461 aagctggaga gatcctcacc aagcgactcc gatacatggt tttcaaatcc atgctgagac
 2521 aggatgtgag ctggtttgat gaccctaaaa acaccaccgg agcactgacc accaggctcg
 2581 ccaacgatgc tgctcaagtg aaaggggcta cagggcttag gcttgctgtg attttccaga
 2641 acatagcaaa tcttgggaca ggaatcatca tatccctaata ctatggctgg caactaacac
 2701 ttttactctt agcaattgta cccatcattg cgatagcagg agtggttgaa atgaaaatgt
 2761 tgtctggaca agcactgaaa gataagaagg aactagaagg ttctggaaa attgctacgg
 2821 aagcaattga aaacttccgc actgttgtct ctttgactcg ggagcagaag tttgaaacca
 2881 tgtatgcca gagcttgacg ataccataca gaaatgcgat gaagaaagca cacgtgtttg
 2941 ggatcacggt ctccctcacc caggccatga tgtatttttc ttatgctgct tgtttccggg
 3001 tcggtgccta cttggtgaca caacaactca tgacttttga aaatgttctg ttagtattct
 3061 cagctattgt ctttgggtgcc atggcagtgg ggcaggtcag ttcatcgcct cctgactatg
 3121 cgaaagccac agtgtcagca tcccacatca tcaggatcat tgagaaaacc cccgagattg
 3181 acagctacag cacgcaaggc ctaaagccga atatgttggg aggaaatgtg caatttagtg
 3241 gagtcgtggt caactatccc acccgacca gcatcccagt gcttcagggg ctgagccttg
 3301 aggtgaagaa gggccagacg ctggccctgg tgggcagcag tggctgcggg aagagcacag
 3361 tgggtccagct gctcgagcgc ttctacgacc ccatggctgg atcagtgttt ctagatggca
 3421 aagaaataaa gcaactgaat gtccagtggc tccgagcaca gctgggcatt gtgtcccaag
 3481 agcccattct ctttgactgc agcatcgcag agaacattgc ctacggagac aacagccggg
 3541 tcgtgtctta tgaggagatt gtgagggcag ccaaggaggc caacatccac cagttcatcg
 3601 actcgtacc tgataaatac aacaccagag taggagacaa aggcactcag ctgtcgggtg
 3661 ggcagaagca gcgcacgcgc atcgcacgcg ccctcgtcag acagcctcac attttacttc
 3721 tggacgaagc aacatcagct ctggatacag aaagtgaaaa ggttgtccag gaagcgtg
 3781 acaaagccag ggaaggccgc acctgcattg tgatcgtcct ccgcctgtcc accatccaga
 3841 acgcgactt gatcgtggtg attcagaacg gcaaggtcaa ggagcacggc acccaccagc
 3901 agctcgtggc gcagaagggc atctacttct caatggtcag tgtgcaggct ggagcaaagc
 3961 gctcatgaac tgtgaccatg taagatgtta agtattttta ttgtttgtat tcatatatgg
 4021 tgtttaatcc aagtcaaaag gaaaacactt actaaaatag ccagttatct attttctgcc
 4081 acagtggaaa gcatttagtt tggtttagag tcttcagagg ctttgttaatt aaaaaaaca
 4141 aatagatac agcatcaaat ggagattaat gctttaaaat gcactataaa atttataaaa
 4201 gggttaaaag tgaatgtttg ataatatata cttttattta tactttctca tttgtaacta
 4261 taactgattt ctgcttaaca aattatgtat gtatcaaaaa ttactgaaat gtttgtataa
 4321 agtatatata gtgaaactga gcattcatat ttttgagtta ttttgctcaa aatgcatg
 4381 aaattatata ttgtcccaac tggaaatattg tacataattt tagccttaa aaaacagtcc
 4441 attactgggg ggagggggca tcaactatg ggcacaagtgt tactcagaca tgggcacctg
 4501 agttcagatc cctaccacct aagtaagcag caaggtgtgg tgtttttgta atgccagtgc
 4561 tagaggcaga aacagacaga tcctgcaggc tcagtggctg gccaaacagc ctagccaaca
 4621 tagcgcgttc caggttcagt gagaaaactt gtctcaaaaa tcagagggaa aagcaaatga
 4681 ggggtgcagc catgtgcact catgcaaatg ccatacatgc agaagtatgt gcacacacac
 4741 gcacacatta accaacgact agcaaggaaa atgaaggtgg ataagagggg tgggactggg
 4801 acaaaggagg gtacctggat gaatatgact gaaggacgtt atgtacacat atgaaaacgt
 4861 cgtactgaaa ctcaactaaa tgtatactta atatatgcta ataaaatatt tttaaaagaa

4921 aaaaatatcc ataattgtaa ataagaggat cttataatta aaagacccta aggattc

//

Mus musculus ATP-binding cassette, sub-family G (WHITE), member 2 (Abcg2), mRNA

NCBI Reference Sequence: NM_011920.3

ORIGIN

```

1 atataaaaag atctctctgt ctggatttcc tctttttccaa tctccttgcc agataagagg
61 ggtaggttg tcttgagttg gaaccacat ttctttcttg attcaggata accagctaac
121 agatattcac tactgtcgtc ctgaaattaa ctgaggatat tcattaatth cctggaagct
181 agatthttga aaagtcttga ttttgctgt ctcttgaggc aaaacttagc aactttgggg
241 attgataaat cttctgtctt cctggctctc tccctgcttt ttctcaactc cactgcaagc
301 aagagtggac atactcttag ggtggctttt gtggcaggca tggatcctag ctgaactctt
361 tctccagtgt acaacattgc tgcattctac tgaggcctga cagttctcct tttgacacct
421 cattacacat agcagagaaa ggcataaatc ctaaagatgt cttccagtaa tgaccacgtg
481 ttagtaccaa tgtcgcagag aaacaacaac ggccttctta ggatgaactc cagagccgtt
541 aggacgctcg cagaaggaga tgtgttgagt tttcatcaca tcacctatcg agtgaaagta
601 aagagtgggt ttctagtccg gaaaacagtt gagaaaagaaa tactatcaga tatcaatggg
661 atcatgaaac ctggccttaa tgctattctg ggaccacag gcggaggcaa gtcttcgttg
721 ctagatgtct tagcagcaag gaaagatcca aagggattat ctggagatgt tttgataaat
781 ggagcacctc aacctgccc tttcaaagtc tgttcaaggtt atgtggttca agatgacggt
841 gtgatgggca ccctgacagt gagagaaaaac ttacagttct cagcagctct tcgacttcca
901 acaactatga agaatcatga aaaaaatgaa cggattaaca caatcattaa agagttaggt
961 ctggaaaaag tagcagattc taaggctcga actcagttta tccgtggcat ctctggagga
1021 gaaagaaaaa ggacaagcat agggatggag ctgatcactg acccttccat cctcttctg
1081 gatgagccca cgactggttt ggactcaagc acagcgaatg ctgtcctttt gctcctgaaa
1141 aggatgtcta aacagggctg aacaatcatt ttctccattc atcagcctcg gtattccatc
1201 tttaaagttgt ttgacagcct caccttactg gcttccggga aactcgtggt ccatgggcca
1261 gcacagaagg ccttggagta ctttgcatca gcaggttacc actgtgagcc ctacaacaac
1321 cctgcggtatt ttttcttga tgtcatcaat ggagattctt ctgctgtgat gttaaataga
1381 gaggaacaag acaatgaagc aaacaagact gaagagcctt ccaagggaga gaagccagta
1441 atagaaaatt tatctgagtt ttatatcaac tctgccatct atggagaaac aaaagctgaa
1501 ttagatcaac ttccaggagc tcaggaaaag aaaggaacat cggccttcaa agagccagtc
1561 tatgttacct ctttctgtca ccagctccga tggattgcca ggcgctcatt taaaaacttg
1621 ctcggaacc ctcaagcttc tgttgctcag ttaattgtta cagtcatact ggggcttatt
1681 attggtgcca tttactttga tctgaaatat gatgccgctg gaatgcaaaa tagagctgga
1741 gttttgtttt tctgactac caaccagtgt ttttccagtg tgcagctgt ggagctgttc
1801 gtagtggaga agaaactctt catacatgag tacatcagtg gatattacag agtgtcttct
1861 tacttctttg gaaaggtgat gtctgattta ctccccatga ggttcttgcc aagtgttata
1921 ttcacttgta tattatactt catgttagga ctgaagaaga cgggtggatgc ttttttcatc
1981 atgatgttta cccttataat ggtggcttat acggccagtt ccatggcact ggccatagcc
2041 acaggccaaa gtgtgggtgc tgtagcaaca cttctcatga caatcgcttt tgtatthtag
2101 atgctctttt ctggcctctt ggtgaatctc agaaccattg ggccttggct gtcctggctt
2161 cagtacttta gcattcctcg atatggcttc acagctttgc agtataatga attcttggga
2221 caagagtttt gtccaggatt caatgtaacg gacaacagca cttgtgttaa cagctatgca

```

```
2281 atatgtactg gtaacgagta cttgataaat cagggcatcg aactgtcacc ttggggactg
2341 tggaagaatc atgtggccct ggcttgtatg attattatct tcctcacaat tgctacctg
2401 aaattgttgt ttcttaaaaa gtattcttaa tttccccttt aacggactat taattgtact
2461 ccaattaaat atgggcactt tgattaccat aaa
```

//

RT² Profiler™ PCR Array Human Drug Transporters (PAHS-070A)

Need more information about PCR Array products? Please Visit [PCR Array Home](#) or [Email Technical Support](#).
Array Layout

ABCA1 A01	ABCA12 A02	ABCA13 A03	ABCA2 A04	ABCA3 A05	ABCA4 A06	ABCA9 A07	ABCB1 A08	ABCB11 A09	ABCB4 A10	ABCB5 A11	ABCB6 A12	*
ABCC1 B01	ABCC10 B02	ABCC11 B03	ABCC12 B04	ABCC2 B05	ABCC3 B06	ABCC4 B07	ABCC5 B08	ABCC6 B09	ABCD1 B10	ABCD3 B11	ABCD4 B12	Applicable to plate-based arrays. For "R" plate arrays, please refer to the gene
ABCF1 C01	ABCG2 C02	ABCG8 C03	AQP1 C04	AQP7 C05	AQP9 C06	ATP6V0C C07	ATP7A C08	ATP7B C09	MVP C10	SLC10A1 C11	SLC10A2 C12	
SLC15A1 D01	SLC15A2 D02	SLC16A1 D03	SLC16A2 D04	SLC16A3 D05	SLC19A1 D06	SLC19A2 D07	SLC19A3 D08	SLC22A1 D09	SLC22A2 D10	SLC22A3 D11	SLC22A6 D12	
SLC22A7 E01	SLC22A8 E02	SLC22A9 E03	SLC28A1 E04	SLC28A2 E05	SLC28A3 E06	SLC29A1 E07	SLC29A2 E08	SLC2A1 E09	SLC2A2 E10	SLC2A3 E11	SLC31A1 E12	
SLC38A2 F01	SLC38A5 F02	SLC3A1 F03	SLC3A2 F04	SLC5A1 F05	SLC5A4 F06	SLC25A13 F07	SLC7A11 F08	SLC7A5 F09	SLC7A6 F10	SLC7A7 F11	SLC7A8 F12	
SLC7A9 G01	SLCO1A2 G02	SLCO1B1 G03	SLCO1B3 G04	SLCO2A1 G05	SLCO2B1 G06	SLCO3A1 G07	SLCO4A1 G08	TAP1 G09	TAP2 G10	VDAC1 G11	VDAC2 G12	
B2M H01	HPRT1 H02	RPL13A H03	GAPDH H04	ACTB H05	HGDC H06	RTC H07	RTC H08	RTC H09	PPC H10	PPC H11	PPC H12	

table.

Gene Table

Position	Unigene	GeneBank	Symbol	Description	Gene Name
A01	Hs.429294	NM_005502	ABCA1	ATP-binding cassette, sub-family A (ABC1), member 1	ABC-1, ABC1, CERP, FLJ14958, HDLDT1, MGC164864, MGC165011, TGD
A02	Hs.134585	NM_173076	ABCA12	ATP-binding cassette, sub-family A (ABC1), member 12	DKFZp434G232, FLJ41584, ICR2B, LI2
A03	Hs.226568	NM_152701	ABCA13	ATP-binding cassette, sub-family A (ABC1), member 13	DKFZp313D2411, FLJ16398, FLJ33876, FLJ33951

A04	Hs.421202	NM_001606	ABCA2	ATP-binding cassette, sub-family A (ABC1), member 2	ABC2, MGC129761
A05	Hs.26630	NM_001089	ABCA3	ATP-binding cassette, sub-family A (ABC1), member 3	ABC-C, ABC3, EST111653, LBM180, MGC166979, MGC72201, SMDP3
A06	Hs.416707	NM_000350	ABCA4	ATP-binding cassette, sub-family A (ABC1), member 4	ABC10, ABCR, ARMD2, CORD3, DKFZp781N1972, FFM, FLJ17534, RMP, RP19, STGD, STGD1
A07	Hs.131686	NM_080283	ABCA9	ATP-binding cassette, sub-family A (ABC1), member 9	DKFZp686F2450, EST640918, MGC75415
A08	Hs.489033	NM_000927	ABCB1	ATP-binding cassette, sub-family B (MDR/TAP), member 1	ABC20, CD243, CLCS, GPI70, MDR1, MGC163296, P- GP, PGY1
A09	Hs.658439	NM_003742	ABCB11	ATP-binding cassette, sub-family B (MDR/TAP), member 11	ABC16, BRIC2, BSEP, PFIC-2, PFIC2, PGY4, SPGP
A10	Hs.654403	NM_000443	ABCB4	ATP-binding cassette, sub-family B (MDR/TAP), member 4	ABC21, GBD1, MDR2, MDR2, 3, MDR3, PFIC-3, PGY3
A11	Hs.658821	NM_178559	ABCB5	ATP-binding cassette, sub-family B (MDR/TAP), member 5	ABCB5alpha, ABCB5beta,

A12	Hs.107911	NM_005689	ABCB6	ATP-binding cassette, sub-family B (MDR/TAP), member 6	EST422562 ABC, ABC14, FLJ22414, MTABC3, PRP, umat
B01	Hs.709181	NM_004996	ABCC1	ATP-binding cassette, sub-family C (CFTR/MRP), member 1	ABC29, ABCC, DKFZp686N04233, DKFZp781G125, GS-X, MRP, MRP1
B02	Hs.55879	NM_033450	ABCC10	ATP-binding cassette, sub-family C (CFTR/MRP), member 10	EST182763, MRP7, SIMRP7
B03	Hs.652267	NM_032583	ABCC11	ATP-binding cassette, sub-family C (CFTR/MRP), member 11	EWWD, MRP8, WW
B04	Hs.410111	NM_033226	ABCC12	ATP-binding cassette, sub-family C (CFTR/MRP), member 12	MGC27071, MRP9
B05	Hs.368243	NM_000392	ABCC2	ATP-binding cassette, sub-family C (CFTR/MRP), member 2	ABC30, CMOAT, DJS, KIAA1010, MRP2, cMRP
B06	Hs.463421	NM_003786	ABCC3	ATP-binding cassette, sub-family C (CFTR/MRP), member 3	ABC31, DKFZp686E22157, EST90757, MLP2, MOAT-D, MRP3, cMOAT2
B07	Hs.508423	NM_005845	ABCC4	ATP-binding cassette, sub-family C (CFTR/MRP), member 4	EST170205, MOAT-B, MOATB, MRP4
B08	Hs.728765	NM_005688	ABCC5	ATP-binding cassette, sub-family C (CFTR/MRP), member 5	ABC33, DKFZp686C1782, EST277145, MOAT-C, MOATC, MRP5, SMRP, pABC11
B09	Hs.442182	NM_001171	ABCC6	ATP-binding cassette, sub-family C (CFTR/MRP), member 6	ABC34, ARA,

B10	Hs.159546	NM_000033	ABCD1	ATP-binding cassette, sub-family D (ALD), member 1	EST349056, MLP1, MOATE, MRP6, PXE, PXE1, URG7
B11	Hs.700576	NM_002858	ABCD3	ATP-binding cassette, sub-family D (ALD), member 3	ABC42, ALD, ALDP, AMN
B12	Hs.94395	NM_005050	ABCD4	ATP-binding cassette, sub-family D (ALD), member 4	ABC43, PMP70, PXMP1, ZWS2
C01	Hs.655285	NM_001090	ABCF1	ATP-binding cassette, sub-family F (GCN20), member 1	ABC41,
C02	Hs.480218	NM_004827	ABCG2	ATP-binding cassette, sub-family G (WHITE), member 2	EST352188, P70R, P79R, PMP69, PXMP1L
C03	Hs.413931	NM_022437	ABCG8	ATP-binding cassette, sub-family G (WHITE), member 8	ABC27, ABC50
C04	Hs.76152	NM_198098	AQP1	Aquaporin 1 (Colton blood group)	ABC15, ABCP, BCRP, BCRP1, BMDP, CD338, CDw338, EST157481, MGC102821, MRX, MXR, MXR1
C05	Hs.455323	NM_001170	AQP7	Aquaporin 7	GBD4, MGC142217, STSL
C06	Hs.104624	NM_020980	AQP9	Aquaporin 9	AQP-CHIP, CHIP28, CO, MGC26324
					AQP7L, AQP9, AQPap, MGC149555, MGC149556
					AQP-9, HsT17287, SSC1

C07	Hs.389107	NM_001694	ATP6V0C	ATPase, H ⁺ transporting, lysosomal 16kDa, V0 subunit c	ATP6C, ATP6L, ATPL, VATL, VPPC, Vma3
C08	Hs.496414	NM_000052	ATP7A	ATPase, Cu ⁺⁺ transporting, alpha polypeptide	DSMAX, FLJ17790, MK, MNK, SMAX3
C09	Hs.492280	NM_000053	ATP7B	ATPase, Cu ⁺⁺ transporting, beta polypeptide	PWD, WCI, WD, WND
C10	Hs.632177	NM_017458	MVP	Major vault protein	LRP, VAULT1
C11	Hs.952	NM_003049	SLC10A1	Solute carrier family 10 (sodium/bile acid cotransporter family), member 1	NTCP
C12	Hs.194783	NM_000452	SLC10A2	Solute carrier family 10 (sodium/bile acid cotransporter family), member 2	ASBT, IBAT, ISBT, NTCP2, PBAM
D01	Hs.436893	NM_005073	SLC15A1	Solute carrier family 15 (oligopeptide transporter), member 1	HPECT1, HPEPT1, PEPT1
D02	Hs.518089	NM_021082	SLC15A2	Solute carrier family 15 (H ⁺ /peptide transporter), member 2	FLJ33407, PEPT2
D03	Hs.75231	NM_003051	SLC16A1	Solute carrier family 16, member 1 (monocarboxylic acid transporter 1)	FLJ36745, HHF7, MCT, MCT1, MGC44475
D04	Hs.75317	NM_006517	SLC16A2	Solute carrier family 16, member 2 (monocarboxylic acid transporter 8)	AHDS, DXS128, DXS128E, MCT 7, MCT 8, MCT7, MCT8, MRX22, XPCT
D05	Hs.500761	NM_004207	SLC16A3	Solute carrier family 16, member 3 (monocarboxylic acid transporter 4)	MCT 3, MCT 4, MCT-3, MCT-4, MCT3, MCT4, MGC138472, MGC138474
D06	Hs.84190	NM_194255	SLC19A1	Solute carrier family 19 (folate transporter), member 1	CHMD, FOLT,

D07	Hs.30246	NM_006996	SLC19A2	Solute carrier family 19 (thiamine transporter), member 2	IFC1, REFC, RFC1 TC1, THT1, THTR1, TRMA
D08	Hs.221597	NM_025243	SLC19A3	Solute carrier family 19, member 3	THTR2
D09	Hs.117367	NM_003057	SLC22A1	Solute carrier family 22 (organic cation transporter), member 1	HOCT1, OCT1, oct1_cds
D10	Hs.436385	NM_003058	SLC22A2	Solute carrier family 22 (organic cation transporter), member 2	MGC32628, OCT2
D11	Hs.567337	NM_021977	SLC22A3	Solute carrier family 22 (extraneuronal monoamine transporter), member 3	EMT, EMTH, OCT3
D12	Hs.369252	NM_004790	SLC22A6	Solute carrier family 22 (organic anion transporter), member 6	FLJ55736, HOAT1, MGC45260, OAT1, PAHT, ROAT1
E01	Hs.485438	NM_006672	SLC22A7	Solute carrier family 22 (organic anion transporter), member 7	MGC24091, MGC45202, NLT, OAT2
E02	Hs.266223	NM_004254	SLC22A8	Solute carrier family 22 (organic anion transporter), member 8	MGC24086, OAT3
E03	Hs.502772	NM_080866	SLC22A9	Solute carrier family 22 (organic anion transporter), member 9	FLJ23666, HOAT4, OAT4, OAT7, UST3H, ust3
E04	Hs.459187	NM_004213	SLC28A1	Solute carrier family 28 (sodium-coupled nucleoside transporter), member 1	CNT1, HCNT1
E05	Hs.367833	NM_004212	SLC28A2	Solute carrier family 28 (sodium-coupled nucleoside transporter), member 2	CNT2, FLJ21468, HCNT2, HsT17153, MGC138252, SPNT1
E06	Hs.591877	NM_022127	SLC28A3	Solute carrier family 28 (sodium-coupled nucleoside transporter), member 3	CNT3
E07	Hs.25450	NM_004955	SLC29A1	Solute carrier family 29 (nucleoside transporters), member 1	ENT1, MGC1465, MGC3778
E08	Hs.569017	NM_001532	SLC29A2	Solute carrier family 29 (nucleoside transporters), member 2	DER12, ENT2,

E09	Hs.473721	NM_006516	SLC2A1	Solute carrier family 2 (facilitated glucose transporter), member 1	HNP36 DYT17, DYT18, GLUT, GLUT1, GLUT1DS, MGC141895, MGC141896, PED
E10	Hs.167584	NM_000340	SLC2A2	Solute carrier family 2 (facilitated glucose transporter), member 2	GLUT2
E11	Hs.419240	NM_006931	SLC2A3	Solute carrier family 2 (facilitated glucose transporter), member 3	FLJ90380, GLUT3
E12	Hs.532315	NM_001859	SLC31A1	Solute carrier family 31 (copper transporters), member 1	COPT1, CTR1, MGC75487, hCTR1
F01	Hs.221847	NM_018976	SLC38A2	Solute carrier family 38, member 2	ATA2, KIAA1382, PRO1068, SAT2, SNAT2
F02	Hs.195155	NM_033518	SLC38A5	Solute carrier family 38, member 5	JM24, SN2, SNAT5, pp7194
F03	Hs.112916	NM_000341	SLC3A1	Solute carrier family 3 (cystine, dibasic and neutral amino acid transporters, activator of cystine, dibasic and neutral amino acid transport), member 1	ATR1, CSNU1, D2H, FLJ34681, NBAT, RBAT
F04	Hs.502769	NM_002394	SLC3A2	Solute carrier family 3 (activators of dibasic and neutral amino acid transport), member 2	4F2, 4F2HC, 4T2HC, CD98, CD98HC, MDU1, NACAE
F05	Hs.1964	NM_000343	SLC5A1	Solute carrier family 5 (sodium/glucose cotransporter), member 1	D22S675, NAGT, SGLT1
F06	Hs.130101	NM_014227	SLC5A4	Solute carrier family 5 (low affinity glucose cotransporter), member 4	DJ90G24.4, SAAT1, SGLT3
F07	Hs.489190	NM_014251	SLC25A13	Solute carrier family 25, member 13 (citric)	ARALAR2, CITRIN, CTLN2

F08	Hs.390594	NM_014331	SLC7A11	Solute carrier family 7 (anionic amino acid transporter light chain, xc- system), member 11	CCBR1, xCT
F09	Hs.513797	NM_003486	SLC7A5	Solute carrier family 7 (amino acid transporter light chain, L system), member 5	4F2LC, CD98, D16S469E, E16, LAT1, MPE16, hLAT1
F10	Hs.653193	NM_003983	SLC7A6	Solute carrier family 7 (amino acid transporter light chain, y+L system), member 6	DKFZp686K15246, KIAA0245, LAT-2, LAT3, y+LAT-2
F11	Hs.513147	NM_003982	SLC7A7	Solute carrier family 7 (amino acid transporter light chain, y+L system), member 7	LAT3, LPI, MOP-2, Y+LAT1, y+LAT-1
F12	Hs.632348	NM_182728	SLC7A8	Solute carrier family 7 (amino acid transporter light chain, L system), member 8	LAT2, LPI-PC1
G01	Hs.408567	NM_014270	SLC7A9	Solute carrier family 7 (glycoprotein-associated amino acid transporter light chain, bo,+ system), member 9	BAT1, CSNU3, FLJ94301
G02	Hs.46440	NM_021094	SLCO1A2	Solute carrier organic anion transporter family, member 1A2	OATP, OATP-A, OATP1A2, SLC21A3
G03	Hs.449738	NM_006446	SLCO1B1	Solute carrier organic anion transporter family, member 1B1	LST-1, LST1, MGC133282, OATP-C, OATP1B1, OATP2, OATPC, SLC21A6
G04	Hs.504966	NM_019844	SLCO1B3	Solute carrier organic anion transporter family, member 1B3	LST-3TM13, LST3, OATP1B3, OATP8, SLC21A8
G05	Hs.518270	NM_005630	SLCO2A1	Solute carrier organic anion transporter family, member 2A1	MATR1, OATP2A1, PGT, SLC21A2
G06	Hs.7884	NM_007256	SLCO2B1	Solute carrier organic anion transporter family, member 2B1	DKFZp686E0517,

G07	Hs.311187	NM_013272	SLCO3A1		Solute carrier organic anion transporter family, member 3A1	KIAA0880, OATP-B, OATP2B1, OATPB, SLC21A9 FLJ40478, OATP-D, OATP3A1, OATPD, SLC21A11
G08	Hs.235782	NM_016354	SLCO4A1		Solute carrier organic anion transporter family, member 4A1	OATP-E, OATP1, OATP4A1, OATPE, OATPRP1, POAT, SLC21A12
G09	Hs.352018	NM_000593	TAP1		Transporter 1, ATP-binding cassette, sub-family B (MDR/TAP)	ABC17, ABCB2, APT1, D6S114E, FLJ26666, FLJ41500, PSF1, RING4, TAP1*0102N, TAPIN
G10	Hs.502	NM_000544	TAP2		Transporter 2, ATP-binding cassette, sub-family B (MDR/TAP)	ABC18, ABCB3, APT2, D6S217E, PSF2, RING11
G11	Hs.519320	NM_003374	VDAC1		Voltage-dependent anion channel 1	MGC111064, PORIN, VDAC-1
G12	Hs.355927	NM_003375	VDAC2		Voltage-dependent anion channel 2	FLJ23841, POR
H01	Hs.534255	NM_004048	B2M		Beta-2-microglobulin	-
H02	Hs.412707	NM_000194	HPRT1		Hypoxanthine phosphoribosyltransferase 1	HGPRT, HPRT
H03	Hs.728776	NM_012423	RPL13A		Ribosomal protein L13a	L13A, TSTA1
H04	Hs.592355	NM_002046	GAPDH		Glyceraldehyde-3-phosphate dehydrogenase	G3PD, GAPD, MGC88685
H05	Hs.520640	NM_001101	ACTB		Actin, beta	PS1TP5BP1

H06	N/A	SA_00105	HGDC	Human Genomic DNA Contamination	HIGX1A
H07	N/A	SA_00104	RTC	Reverse Transcription Control	RTC
H08	N/A	SA_00104	RTC	Reverse Transcription Control	RTC
H09	N/A	SA_00104	RTC	Reverse Transcription Control	RTC
H10	N/A	SA_00103	PPC	Positive PCR Control	PPC
H11	N/A	SA_00103	PPC	Positive PCR Control	PPC
H12	N/A	SA_00103	PPC	Positive PCR Control	PPC

RT² Profiler™ PCR Array Human Chemokines & Receptors (PAHS-022A)

Need more information about PCR Array products? Please Visit [PCR Array Home](#) or [Email Technical Support](#).

Array Layout

APLNR A01	BDNF A02	CXCR5 A03	C5 A04	C5AR1 A05	CCBP2 A06	CCL1 A07	CCL11 A08	CCL13 A09	CCL15 A10	CCL16 A11	CCL17 A12	*
CCL18 B01	CCL19 B02	B03	B04	CCL4 B05	CCL5 B06	CCL7 B07	CCL8 B08	CCR1 B09	CCR10 B10	CCR2 B11	CCR3 B12	Applicable to plate-based arrays. For "R" plate arrays, please refer to the gene
CCR4 C01	CCR5 C02	CCR6 C03	CCR7 C04	CCR8 C05	CCR1 C06	CCR2 C07	CKLF C08	CMTM1 C09	CMTM2 C10	CMTM3 C11	CMTM4 C12	
CMKLR1 D01	CSF3 D02	CX3CL1 D03	CX3CR1 D04	CXCL1 D05	CXCL10 D06	CXCL11 D07	CXCL12 D08	CXCL13 D09	CXCL2 D10	CXCL3 D11	CXCL5 D12	
CXCL6 E01	CXCL9 E02	CXCR3 E03	CXCR4 E04	CXCR6 E05	CYFIP2 E06	TYMP E07	GDF5 E08	GPR31 E09	HCAR1 E10	HIF1A E11	IL13 E12	
IL16 F01	IL18 F02	IL1A F03	IL4 F04	IL8 F05	CXCR1 F06	LTB4R F07	MMP2 F08	MMP7 F09	MYD88 F10	NFKBI F11	AIMP1 F12	
SDF2 G01	SLIT2 G02	TCPI0 G03	TLR2 G04	TLR4 G05	TNF G06	TNFRSF1A G07	TNFSF14 G08	TREM1 G09	VHL G10	XCL1 G11	XCR1 G12	
B2M H01	HPRT1 H02	RPL13A H03	GAPDH H04	ACTB H05	HGDC H06	RTC H07	RTC H08	RTC H09	PPC H10	PPC H11	PPC H12	

table.

Gene Table

Position	Unigene	GeneBank	Symbol	Description	Gene Name
A01	Hs.438311	NM_005161	APLNR	Apelin receptor	AGTRL1, APJ, APJR, FLJ90771, FLJ96609, HG11, MGC45246
A02	Hs.502182	NM_001709	BDNF	Brain-derived neurotrophic factor	MGC34632
A03	Hs.113916	NM_001716	CXCR5	Chemokine (C-X-C motif) receptor 5	BLR1, CDI185, MDR15, MGC117347
A04	Hs.494997	NM_001735	C5	Complement component 5	CPAMD4, FLJ17816, FLJ17822, MGC142298

PAHS-022 Human Chemokines and Receptors SABiosciences PCR array Appendix D

A05	Hs.2161	NM_001736	C5AR1	Complement component 5a receptor 1	C5A, C5AR, C5R1, CD88
A06	Hs.146346	NM_001296	CCBP2	Chemokine binding protein 2	CCR10, CCR9, CMKBR9, D6, MGC126678, MGC138250, hD6
A07	Hs.72918	NM_002981	CCL1	Chemokine (C-C motif) ligand 1	I-309, P500, SCYA1, SISE, TCA3
A08	Hs.54460	NM_002986	CCL11	Chemokine (C-C motif) ligand 11	MGC22554, SCYA11
A09	Hs.414629	NM_005408	CCL13	Chemokine (C-C motif) ligand 13	CKb10, MCP-4, MGC17134, NCC-1, NCC1, SCYA13, SCYL1
A10	Hs.272493	NM_032965	CCL15	Chemokine (C-C motif) ligand 15	HCC-2, HMRP-2B, LKN-1, LKN1, MIP-1D, MIP-5, MRP-2B, NCC-3, NCC3, SCYA15, SCYL3, SY15
A11	Hs.10458	NM_004590	CCL16	Chemokine (C-C motif) ligand 16	CKb12, HCC-4, ILINCK, LCC-1, LEC, LMC, MGC117051, Mtn-1, NCC-4, NCC4, SCYA16, SCYL4
A12	Hs.546294	NM_002987	CCL17	Chemokine (C-C motif) ligand 17	A-152E5.3, ABCD-2, MGC138271, MGC138273, SCYA17, TARC
B01	Hs.143961	NM_002988	CCL18	Chemokine (C-C motif) ligand 18 (pulmonary and activation-	AMAC-1,

PAHS-022 Human Chemokines and Receptors SABiosciences PCR array Appendix D

					regulated)	AMAC1, CKb7, DC-CK1, DCCK1, MIP-4, PARC, SCYA18
B02	Hs.50002	NM_006274	CCL19		Chemokine (C-C motif) ligand 19	CKb11, ELC, MGC34433, MIP-3b, MIP3B, SCYA19
B03	Hs.303649	NM_002982	CCL2		Chemokine (C-C motif) ligand 2	GDCF-2, HC11, HSMCR30, MCAF, MCP-1, MCP1, MGC9434, SCYA2, SMC-CF
B04	Hs.514107	NM_002983	CCL3		Chemokine (C-C motif) ligand 3	G0S19-1, LD78ALPHA, MIP-1-alpha, MIP1A, SCYA3
B05	Hs.75703	NM_002984	CCL4		Chemokine (C-C motif) ligand 4	ACT2, AT744.1, G-26, LAG1, MGC104418, MGC126025, MGC126026, MIP-1-beta, MIP1B, MIP1B1, SCYA2, SCYA4
B06	Hs.514821	NM_002985	CCL5		Chemokine (C-C motif) ligand 5	D17S136E, MGC17164, RANTES, SCYA5, SISd, TCP228
B07	Hs.251526	NM_006273	CCL7		Chemokine (C-C motif) ligand 7	FIC, MARC, MCP-3, MCP3, MGC138463,

PAHS-022 Human Chemokines and Receptors SABiosciences PCR array Appendix D

							MGC138465, NC28, SCYA6, SCYA7
B08	Hs.271387	NM_005623	CCL8		Chemokine (C-C motif) ligand 8		HC14, MCP-2, MCP2, SCYA10, SCYA8
B09	Hs.301921	NM_001295	CCR1		Chemokine (C-C motif) receptor 1		CD191, CKR-1, CKR1, CMKBR1, HM145, MIP1aR, SCYAR1
B10	Hs.278446	NM_016602	CCR10		Chemokine (C-C motif) receptor 10		GPR2
B11	Hs.511794	NM_001123396	CCR2		Chemokine (C-C motif) receptor 2		CC-CKR-2, CCR2A, CCR2B, CD192, CKR2, CKR2A, CKR2B, CMKBR2, FLJ78302, MCP-1- R, MGC103828, MGC111760, MGC168006
B12	Hs.506190	NM_001837	CCR3		Chemokine (C-C motif) receptor 3		CC-CKR-3, CD193, CKR3, CMKBR3, MGC102841
C01	Hs.184926	NM_005508	CCR4		Chemokine (C-C motif) receptor 4		CC-CKR-4, CD194, CKR4, CMKBR4, ChemR13, HGNC:14099, K5- 5, MGC88293
C02	Hs.450802	NM_000579	CCR5		Chemokine (C-C motif) receptor 5		CC-CKR-5, CCCKR5, CD195,

PAHS-022 Human Chemokines and Receptors SABiosciences PCR array Appendix D

C03	Hs.46468	NM_004367	CCR6	Chemokine (C-C motif) receptor 6	CKR-5, CKR5, CMKBR5, FLJ78003, IDDM22
C04	Hs.370036	NM_001838	CCR7	Chemokine (C-C motif) receptor 7	BN-1, C-C CKR-6, CC-CKR-6, CCR-6, CD196, CKR-L3, CKRL3, CMKBR6, DCR2, DRY6, GPR29, GPRCY4, STRL22
C05	Hs.113222	NM_005201	CCR8	Chemokine (C-C motif) receptor 8	BLR2, CD197, CDw197, CMKBR7, EB11
C06	Hs.729361	NM_016557	CCRL1	Chemokine (C-C motif) receptor-like 1	CC-CKR-8, CCR-8, CDw198, CKRL1, CMKBR8, CMKBRL2, CY6, GPRCY6, MGC129966, MGC129973, TER1
C07	Hs.535713	NM_003965	CCRL2	Chemokine (C-C motif) receptor-like 2	CC-CKR-11, CCBP2, CCR-11, CCR10, CCR11, CCX CKR, CCX-CKR, CKR-11, PPR1, VSHK1
					CKRX, CRAM, CRAM-A, CRAM-B, FLJ55815,

PAHS-022 Human Chemokines and Receptors SABiosciences PCR array Appendix D

C08	Hs.15159	NM_181641	CKLF	Chemokine-like factor	HCR, MGC116710, MGC34104 C32, CKLF1, CKLF2, CKLF3, CKLF4, UCK-1
C09	Hs.549232	NM_181269	CMTM1	CKLF-like MARVEL transmembrane domain containing 1	CKLFH, CKLFH1, CKLFSF1, MGC71870
C10	Hs.195685	NM_144673	CMTM2	CKLF-like MARVEL transmembrane domain containing 2	CKLFSF2, MGC39436
C11	Hs.298198	NM_144601	CMTM3	CKLF-like MARVEL transmembrane domain containing 3	BNAS2, CKLFSF3, FLJ31762, MGC51956
C12	Hs.643961	NM_178818	CMTM4	CKLF-like MARVEL transmembrane domain containing 4	CKLFSF4
D01	Hs.197143	NM_004072	CMKLR1	CHEMOKINE-LIKE RECEPTOR 1	CHEMERINR, ChemR23, DEZ, MGC126105, MGC126106
D02	Hs.2233	NM_000759	CSF3	Colony stimulating factor 3 (granulocyte)	C17orf33, CSF3OS, GCSF, MGC45931
D03	Hs.531668	NM_002996	CX3CL1	Chemokine (C-X3-C motif) ligand 1	ABCD-3, C3Xkine, CXC3, CXC3C, NTN, NTT, SCYD1, fractalkine, neurotactin
D04	Hs.78913	NM_001337	CX3CR1	Chemokine (C-X3-C motif) receptor 1	CCRL1, CMKBRL1, CMKDRI, GPRI3,

PAHS-022 Human Chemokines and Receptors SABiosciences PCR array Appendix D

D05	Hs.789	NM_001511	CXCL1	Chemokine (C-X-C motif) ligand 1 (melanoma growth stimulating activity, alpha)	GPRV28, V28 FSP, GRO1, GROa, MGSA, MGSA-a, NAP-3, SCYB1
D06	Hs.632586	NM_001565	CXCL10	Chemokine (C-X-C motif) ligand 10	C7, IFI10, INP10, IP-10, SCYB10, crg-2, gIP-10, mob- 1
D07	Hs.632592	NM_005409	CXCL11	Chemokine (C-X-C motif) ligand 11	H174, I-TAC, IP-9, IP9, MGC102770, SCYB11, SCYB9B, b-R1
D08	Hs.522891	NM_000609	CXCL12	Chemokine (C-X-C motif) ligand 12	IRH, PBSF, SCYB12, SDF1, SDF1A, SDF1B, TLSF, TPAR1
D09	Hs.100431	NM_006419	CXCL13	Chemokine (C-X-C motif) ligand 13	ANGIE, ANGIE2, BCA-1, BCA1, BLC, BLR1L, SCYB13
D10	Hs.590921	NM_002089	CXCL2	Chemokine (C-X-C motif) ligand 2	CINC-2a, GRO2, GROb, MGSA-b, MIP-2a, MIP2, MIP2A, SCYB2
D11	Hs.89690	NM_002090	CXCL3	Chemokine (C-X-C motif) ligand 3	CINC-2b, GRO3, GROg, MIP-2b, MIP2B, SCYB3
D12	Hs.89714	NM_002994	CXCL5	Chemokine (C-X-C motif) ligand 5	ENA-78, SCYB5
E01	Hs.164021	NM_002993	CXCL6	Chemokine (C-X-C motif) ligand 6 (granulocyte chemotactic protein 2)	CKA-3, GCP-2, GCP2, SCYB6
E02	Hs.77367	NM_002416	CXCL9	Chemokine (C-X-C motif) ligand 9	CMK, Humig,

PAHS-022 Human Chemokines and Receptors SABiosciences PCR array Appendix D

E03	Hs.198252	NM_001504	CXCR3		Chemokine (C-X-C motif) receptor 3	MIG, SCYB9, crg-10 CD182, CD183, CKR-L2, CMKAR3, GPR9, IP10-R, Mig-R, MigR
E04	Hs.593413	NM_003467	CXCR4		Chemokine (C-X-C motif) receptor 4	CD184, D2S201E, FB22, HM89, HSY3RR, LAP3, LCRI, LESTR, NPY3R, NPYR, NPYRL, NPYY3R, WHIM
E05	Hs.34526	NM_006564	CXCR6		Chemokine (C-X-C motif) receptor 6	BONZO, CD186, STRL33, TYMSTR
E06	Hs.519702	NM_014376	CYFIP2		Cytoplasmic FMR1 interacting protein 2	PIR121
E07	Hs.592212	NM_001953	TYMP		Thymidine phosphorylase	ECGF, ECGF1, MEDPS1, MNGIE, MTDPS1, PDECGF, TP, hPD-ECGF
E08	Hs.1573	NM_000557	GDF5		Growth differentiation factor 5	BMP14, CDMP1, LAP4, OS5, SYNS2
E09	Hs.248124	NM_005299	GPR31		G protein-coupled receptor 31	-
E10	Hs.610873	NM_032554	HCAR1		Hydroxycarboxylic acid receptor 1	GPR104, GPR81, HCA1, LACR1, TA-GPCR
E11	Hs.597216	NM_001530	HIF1A		Hypoxia inducible factor 1, alpha subunit (basic helix-loop-helix transcription factor)	HIF-1alpha, HIF1, HIF1-ALPHA, MOP1, PASD8,

PAHS-022 Human Chemokines and Receptors SABiosciences PCR array Appendix D

E12	Hs.845	NM_002188	IL13	Interleukin 13	bHLHe78 ALRH, BHR1, IL-13, MGC116786, MGC116788, MGC116789, P600
F01	Hs.459095	NM_004513	IL16	Interleukin 16	FLJ16806, FLJ42735, FLJ44234, LCF, NIL16, PRIL16, prIL-16
F02	Hs.83077	NM_001562	IL18	Interleukin 18 (interferon-gamma-inducing factor)	IGIF, IL-18, IL-1g, IL1F4, MGC12320
F03	Hs.1722	NM_000575	IL1A	Interleukin 1, alpha	IL-1A, IL1, IL1- ALPHA, IL1F1
F04	Hs.73917	NM_000589	IL4	Interleukin 4	BCGF-1, BCGF1, BSF-1, BSF1, IL-4, MGC79402
F05	Hs.624	NM_000584	IL8	Interleukin 8	CXCL8, GCP-1, GCP1, LECT, LUCT, LYNAP, MDNCF, MONAP, NAF, NAP-1, NAP1
F06	Hs.194778	NM_000634	CXCR1	Chemokine (C-X-C motif) receptor 1	C-C, C-C-CKR-1, CD128, CD181, CDw128a, CKR-1, CMKAR1, IL8R1, IL8RA, IL8RBA
F07	Hs.655431	NM_181657	LTB4R	Leukotriene B4 receptor	BLT1, BLTR, CMKRL1, GPR16, LTB4R1, LTBR1, P2RY7, P2Y7

PAHS-022 Human Chemokines and Receptors SABiosciences PCR array Appendix D

F08	Hs.513617	NM_004530	MMP2	Matrix metalloproteinase 2 (gelatinase A, 72kDa gelatinase, 72kDa type IV collagenase)	CLG4, CLG4A, MMP-II, MONA, TBE-1
F09	Hs.2256	NM_002423	MMP7	Matrix metalloproteinase 7 (matrilysin, uterine)	MMP-7, MPSSL1, PUMP-1
F10	Hs.82116	NM_002468	MYD88	Myeloid differentiation primary response gene (88)	MYD88D
F11	Hs.654408	NM_003998	NFKB1	Nuclear factor of kappa light polypeptide gene enhancer in B-cells 1	DKFZp686C01211, EBP-1, KBF1, MGC54151, NF-kappa-B, NF-kappaB, NFKB-p105, NFKB-p50, NFkappaB, p105, p50
F12	Hs.591680	NM_004757	AIMP1	Aminoacyl tRNA synthetase complex-interacting multifunctional protein 1	EMAP2, EMAPII, SCYE1, p43
G01	Hs.514036	NM_006923	SDF2	Stromal cell-derived factor 2	-
G02	Hs.29802	NM_004787	SLIT2	Slit homolog 2 (Drosophila)	FLJ14420, SLIL3, Slit-2
G03	Hs.351	NM_004610	TCP10	T-complex 10 homolog (mouse)	MGC34049, TCP10A
G04	Hs.519033	NM_003264	TLR2	Toll-like receptor 2	CD282, TIL4
G05	Hs.174312	NM_138554	TLR4	Toll-like receptor 4	ARM10, CD284, TOLL, hToll
G06	Hs.241570	NM_000594	TNF	Tumor necrosis factor	DIF, TNF-alpha, TNFA, TNFSF2
G07	Hs.279594	NM_001065	TNFRSF1A	Tumor necrosis factor receptor superfamily, member 1A	CD120a, FPF, MGC19588, TBPI, TNF-R, TNF-R-I, TNF-R55, TNFAR, TNFR1, TNFR55,

PAHS-022 Human Chemokines and Receptors SABiosciences PCR array Appendix D

G08	Hs.129708	NM_003807	TNFSF14	Tumor necrosis factor (ligand) superfamily, member 14	TNFR60, p55, p55-R, p60
G09	Hs.283022	NM_018643	TREM1	Triggering receptor expressed on myeloid cells 1	CD258, HVEM, LIGHT, LTg, TR2
G10	Hs.517792	NM_000551	VHL	Von Hippel-Lindau tumor suppressor	TREM-1 HRCAL, RCA1, VHL1
G11	Hs.546295	NM_002995	XCL1	Chemokine (C motif) ligand 1	ATAC, LPTN, LTN, SCM-1, SCM-1a, SCMI, SCMIa, SCYC1
G12	Hs.248116	NM_005283	XCR1	Chemokine (C motif) receptor 1	CCXCR1, GPR5
H01	Hs.534255	NM_004048	B2M	Beta-2-microglobulin	-
H02	Hs.412707	NM_000194	HPRT1	Hypoxanthine phosphoribosyltransferase 1	HGPRT, HPRT
H03	Hs.728776	NM_012423	RPL13A	Ribosomal protein L13a	L13A, TSTAI
H04	Hs.592355	NM_002046	GAPDH	Glyceraldehyde-3-phosphate dehydrogenase	G3PD, GAPD, MGC88685
H05	Hs.520640	NM_001101	ACTB	Actin, beta	PS1TP5BP1
H06	N/A	SA_00105	HGDC	Human Genomic DNA Contamination	HIGX1A
H07	N/A	SA_00104	RTC	Reverse Transcription Control	RTC
H08	N/A	SA_00104	RTC	Reverse Transcription Control	RTC
H09	N/A	SA_00104	RTC	Reverse Transcription Control	RTC
H10	N/A	SA_00103	PPC	Positive PCR Control	PPC
H11	N/A	SA_00103	PPC	Positive PCR Control	PPC
H12	N/A	SA_00103	PPC	Positive PCR Control	PPC